Friends of the Pleistocene Annual Fieldtrip 2008

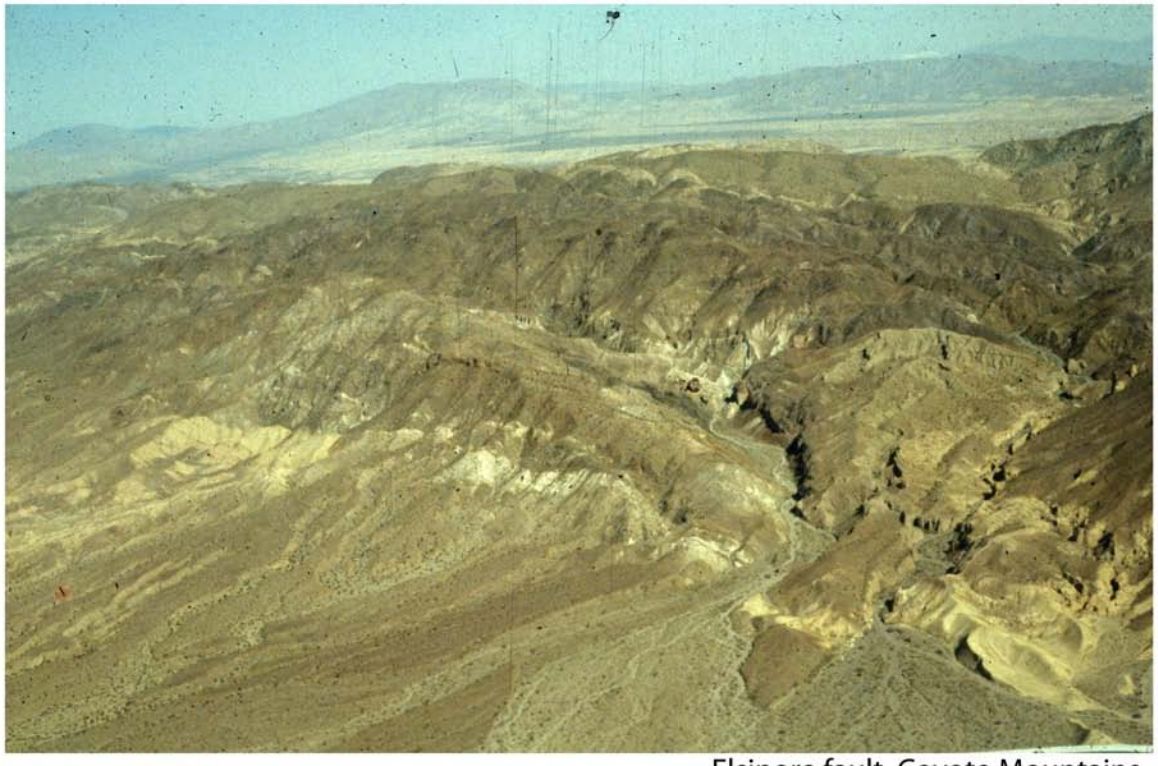

Elsinore fault, Coyote Mountains

Cross-correlation of Quaternary dating techniques, slip rates, and tectonic models in the western Salton Trough

Guidebook and Roadlog

Friends of the Pleistocene

2008 Annual Fieldtrip

Cross-Correlation of Quaternary Dating Techniques, Slip Rates and Tectonic Models in the Western Salton Trough

Leaders:	Day 1	Kim Le, Tom Rockwell, Mike Oskin
	Day 2	Susanne Janecke, Becky Dorsey
	Day 3	Kathryn Fletcher, Kim Le, Mike Oskin, Tom Rockwell, Becky Dorsey, Caitlin Lippincott, Lewis Owen

Camping Coordinator - George Jefferson

Beer and Wine Coordinators - Eldon Gath, Esteban Bowles-Martinez, Tom Rockwell

FOP 2008 Web Master - Tony Carasco, SDSU

T-Shirt Production - Tom Rockwell, Katie Anderson, Neta Wechsler

Clark fault: Day 1

Late Quaternary slip rate gradient constrained from LiDAR imagery and ^{10}Be dating of offset landforms on the southern San Jacinto Fault, California

Kimberly Le[1],Thomas Rockwell[2],Lewis A. Owen[3],Michael Oskin[1],Caitlin Lippincott[2], Marc W. Caffee[4],Jason Dortch[3]

[1]Department of Geological Sciences, University of California, Davis, CA 95616 USA
[2]Department of Geological Sciences, San Diego State University, San Diego, CA 92182, USA
[3]Department of Geology, University of Cincinnati, Cincinnati, OH 45221, USA
[4]Department of Physics, Purdue University, West Lafayette, IN 47906, USA

The right-lateral San Andreas and San Jacinto faults are the two principle structures accommodating Pacific-North America plate motion in southern California. Recent studies across the plate boundary in southern California suggest the San Jacinto fault may be the dominate plate boundary structure accommodating this motion. However, because the late Quaternary slip history of this fault system is insufficiently understood, it difficult to determine the partitioning of deformation across the plate boundary and how it may have changed over time. Landforms displaced by the Clark fault strand of the southern San Jacinto fault zone were mapped using aerial photography and LiDAR imagery, and dated using in-situ terrestrial cosmogenic nuclide ^{10}Be methods. Beheaded channels at Rockhouse Canyon, displaced by 430 ± 40 m and 150 ± 30 m, have been dated to 47.3 ± 7.7 ka and 27.8 ± 8.8 ka, respectively. Farther south, adjacent to the southern Santa Rosa mountains, an alluvial deposit displaced by 51 ± 5 m has been dated to 34.5 ± 6.6 ka. From these sites we determine that the slip rate of the Clark fault diminishes southward from 8.4 ± 1.7 to 1.5 ± 0.3 mm/yr. These rates are lower than those for the central and northern stretches of the San Jacinto fault zone, and imply a slip-rate decrease along the Clark fault from Anza southeastward to its surface termination. Our data suggest that since ~30 to 50 ka, slip along the southern San Jacinto fault zone has been slower than the rate along the southernmost San Andreas fault. This implies that either the slip rate of the San Jacinto fault has substantially decreased since fault initiation, or that fault slip began earlier than previously suggested.

INTRODUCTION

To the south of the big bend at approximately 34°5'N latitude in southern California, the San Andreas fault system consists of the southern San Andreas, the San Jacinto, and the Elsinore fault zones (Fig. 1). The San Andreas and San Jacinto faults zones are the two principle structures accommodating Pacific-North America plate motion in this region (Fig. 1) [Bennett et al., 2004; Fialko et al., 2006]. Geodetically derived slip rates estimates for both, the San Andreas and the San Jacinto fault zones, are on the order of 15-20 mm/yr, whereas the slip rate on the Elsinore fault is only 3-6 mm/yr [Bennett et al, 1996; Fay and Humphreys, 2005].

The San Jacinto fault zone (SJFZ) has historically been more active seismically than the southern San Andreas fault zone [Thatcher et al., 1975; Richards-Dinger and Shearer, 2006], but its longer-term history is controversial. Although many previous studies across the fault system have provided evidence for well-preserved offsets of Quaternary landforms [e.g Sharp, 1967; Sharp, 1981; Morton and Matti, 1993; Rockwell et al., 1990], fault slip rates are often more poorly constrained due to the inherent difficulties of dating Quaternary landforms. Moreover, previous studies have been carried out in many different localities along the fault system and spanning highly variable time intervals, complicating direct comparision of slip rates between the San Jacinto and the San Andreas faults [Sharp, 1981; Weldon and Sieh, 1985; Morton and Matti,, 1986; Harden and Matti, 1989; Rockwell et al, 1990].

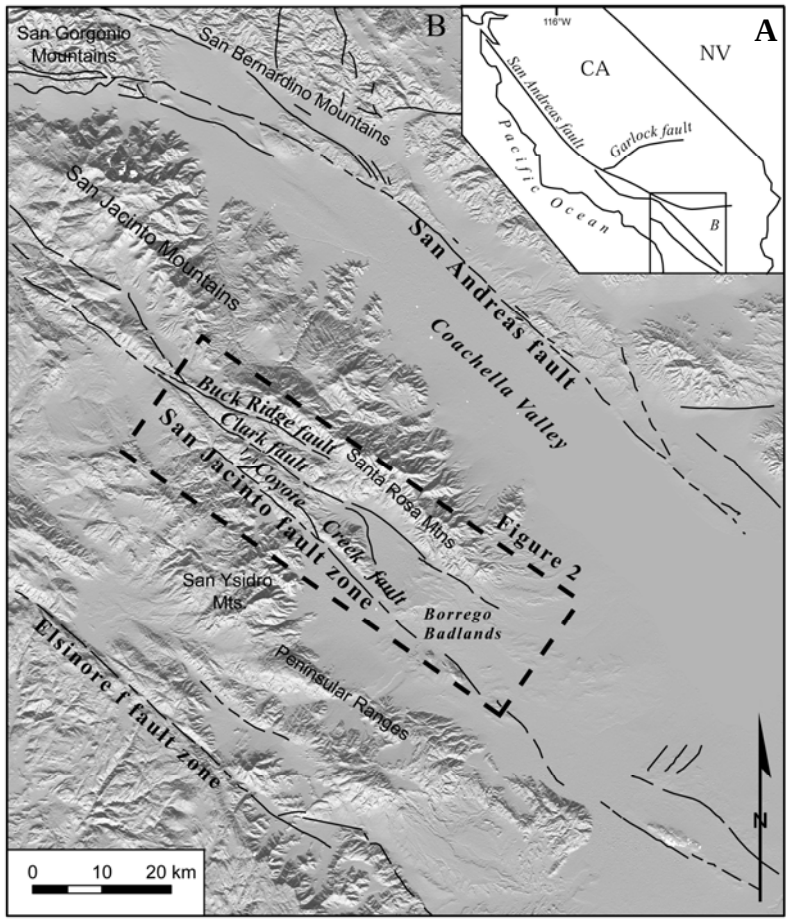

Figure 1. Location map showing [A] the major faults for southern California, and [B] the location the study area along the southern San Jacinto fault.

Presently, there are no slip rate estimates from ^{10}Be exposure dating of offset landforms, but the utility of this method has been demonstrated by recent work along the San Andreas fault [van der Woerd et al., 2003]. Due to the excellent preservation of landforms and offsets in the arid climate of Southern California, the SJFZ provides an ideal location for surface exposure dating. In this study, we present the first Late Quaternary slip rates from ^{10}Be dating of offset landforms along the central and southern stretch of the Clark fault of the southern SJFZ, at Rockhouse Canyon and the southern Santa Rosa Mountains, respectively (Fig. 1). We integrate these newly determined slip rates with previously estimated rates along the northern segment and with total bedrock displacement to make inferences about the long-term slip rate history of the SJFZ and its implication to earthquake

recurrence models used in assessing seismic hazards in southern California.

TECTONIC SETTING

The ~230 km long SJFZ extends from the Big Bend of the San Andreas fault southwards with an average strike of ~N45°W, cutting through Cretaceous and Tertiary plutonic and metamorphic rocks of the Peninsular Ranges (Figs. 1 and 2) [Sharp, 1967].

Total bedrock displacement along the SJFZ at Anza is ~22 to 24 km based on offset of the Thomas Mountain sill in contact with metamorphic rocks of the Bautista Complex (Fig. 2) [Sharp, 1967]. Farther south toward Rockhouse Canyon and the southern Santa Rosa Mountains, Cretaceous tonalite, metamorphic rocks, and the eastern Peninsular Ranges mylonite zone are displaced by ~14.5 km (Fig. 2) [Sharp, 1967]. The same mylonite zone is displaced ~5 km by the adjacent Coyote Creek fault strand (Fig.2) [Sharp, 1967].

Evolution of the SJFZ as a major right-lateral strike slip fault zone has been suggested to occur as early as 2.4 Ma [Rockwell et al., 1990] to 1.5 Ma [Morton and Matti, 1993] to as recently as ~1.1 Ma [Dorsey, 2002; Lutz et al, 2006; Kirby et al.; 2007]. Based on an early Quaternary initiation age of 1.1-1.5 Ma and 22 to 24 km of total slip

[Sharp, 1967], several studies have suggested that the SJFZ is the dominant plate boundary structure with slip rates of >20 mm/yr across the San Jacinto fault since its initiation [Morton and Matti, 1993; Kirby et al., 2007; Lutz et al., 2006].

Quaternary rate estimates along the San Jacinto fault zone may vary from northwest to the southeast. Along the northern section of the SJF, in the San Timoteo badlands, a slip rate of at least 20 mm/yr is suggested based on modeling of vertical displacements of fan deposits and assuming a constant horizontal to vertical slip ratio [Kendrick et al., 2002]. The only other slip rate along the northern SFJZ is from Wesnousky et al. [1991]. These authors provide a minimum latest Holocene rate of 1.7-3.3 mm/yr from what is considered the main strand of multiple fault strands. Published slip rate estimates to the south along the Coyote Creek fault indicate a mid-Quaternary to present rate of 10 ± 3 mm/yr [Dorsey, 2002] and a mid-Holocene slip rate of 1-2 mm/yr along the Coyote Creek fault [Sharp, 1981]. The only published late Quaternary slip rate for the Clark fault is located at Anza (Fig. 2). These slip rates are based on soil ages, which have large uncertainties but nevertheless provide best-estimated slip rates between 11-17 mm/yr. Similarly, Sharp [1981] estimates a minimum mid-Quaternary to present slip rate by reconstructing monolithic alluvial fan deposits to their source, suggesting a slip rate of 8-12 mm/yr (Figure 2). A long paleoseismic record from Anza at Hog Lake indicates that

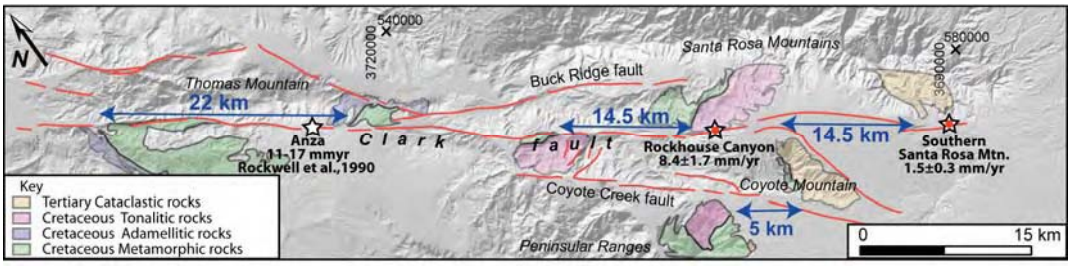

Figure 2. Geologic map of the southern San Jacinto fault zone. The blue arrows show the amount of displacement of plutonic, metamorphic and mylonitic rocks mapped by Sharp [1967]. The white star indicates the location of previously studied localities along the Clark fault segment discussed in the text. The white stars with a red dot indicate new slip rates determined in this study.

earthquakes recur frequently and are strongly clustered in time [Rockwell et al., 2007]. Based on C-14 ages and trenching, these authors estimate a late Holocene slip rate of 15 mm/yr by combining an average return period of ~230 years over the past 4000 years with surface displacement from the last two ruptures at Anza (3-4 m per event). These data imply the mid-Holocene slip rate along the Clark fault at Anza ranges from 12-15 mm/yr.

The ambiguity in the slip rate budget and initiation age for what might be the main plate boundary structure has implications for understanding the tectonic evolution of transform plate boundaries, and for kinematic fault models used to assess earthquake hazards in southern California. Most kinematic fault models assume a constant slip rate along the entire length of a fault, however mechanical models imply a systematic relationship between fault length and displacement with displacement decreasing towards the fault tip [Cowie and Scholz, 1992]. The discrepancy in these long-term slip rate estimates averaged over 10 ka to 1 Ma suggests that 1) the slip rate of the SJFZ has decreased since its initiation, 2) faulting may have initiated before the Quaternary and/or 3) a slip gradient exists along the SJFZ.

Geomorphologic features along the ~120 km long Clark fault suggest that it is the dominant strand in accommodating slip of the San Jacinto fault [Sharp, 1967]. Displacement along the Clark fault from Anza to its surface termination is documented by numerous offset contacts of Cretaceous tonalites, granites, meta-granites, Tertiary mylonites, and Quaternary surfaces along the fault and adjacent to the fault (Figs. 2,3 and 5) [Sharp, 1967, Morton and Matti, 1975, Rockwell et al., 1991]. The right-lateral strike-slip behavior of the Clark fault diffuses southeast of the Santa Rosa Mountains into a zone of faulting and folding toward Imperial Valley [Sharp, 1981]. Quaternary features along the Clark fault indicate youthful activity that include folds, offset and deformed terraces, deflected channels, beheaded channels, offset surfaces, fault scarps, and linear ridges.

METHODS

In the field, landforms along the Clark fault strand were mapped on the basis of LiDAR imagery from the 'B4' Airborne Laser Swath Mapping [ALSM] data set, using 1:5000 and 1:10,000 scale maps at the 10 m contour interval [Bevis et al., 2005]. Following an initial reconnaisance survey, two sites where displaced landforms exhibit little post-depositional degradation, offsets are relatively well constrained, and suitable lithologies for ^{10}Be dating are present were selected for a more detailed study. At Rockhouse Canyon, the northwestern site, we sampled the modern channel and two older beheaded channels for ^{10}Be dating. From each channel, we typically collected ~600g from the top 2 cm of 7-9 quartz-bearing boulders lodged within debris flow bars. In the southern Santa Rosa Mountains, the southeastern site, we collected six ~1000 g of quartz-bearing gravels and pebbles along a 2 m depth profile from a recently incised natural exposure in an offset alluvial fan deposit.

In the lab, the 250 to 500 μm size fraction of the samples was chemically leached by a minimum of four acid leaches: one aqua regia leach of >9 hours; two 5% HF/HNO_3 leaches of ~ 24 hours; and one or more 1% HF/HNO_3 leaches of ~ 24 hours. To remove acid resistant and mafic minerals, heavy liquid [density 2.7 g/cm^3] separations with lithium heteropolytungstate [LST] were used after the first 5% HF/HNO_3 leach. Low background ^{9}Be carrier [^{10}Be/^{9}Be ~ 1 x 10^{-15}] was added to pure quartz, which was then dissolved in concentrated HF and fumed with perchloric acid to remove fluoride atoms. Fifteen to fifty grams of quartz was assumed for determining acid volumes used in the processing of chemical blanks. Next, the samples were passed through anion and cation exchange columns to remove Fe and Ti and to separate the ^{10}Be fraction. Ammonium hydroxide was added to the ^{10}Be fractions to precipitate beryllium hydroxide gel. The beryllium hydroxide was oxidized by ignition at 750^{o}C for 5 minutes in quartz crucibles to produce beryllium oxide. Beryllium oxide was then mixed with Niobium powder and loaded in steel targets for the measurement of the ^{10}Be/^{9}Be ratios by accelerator mass

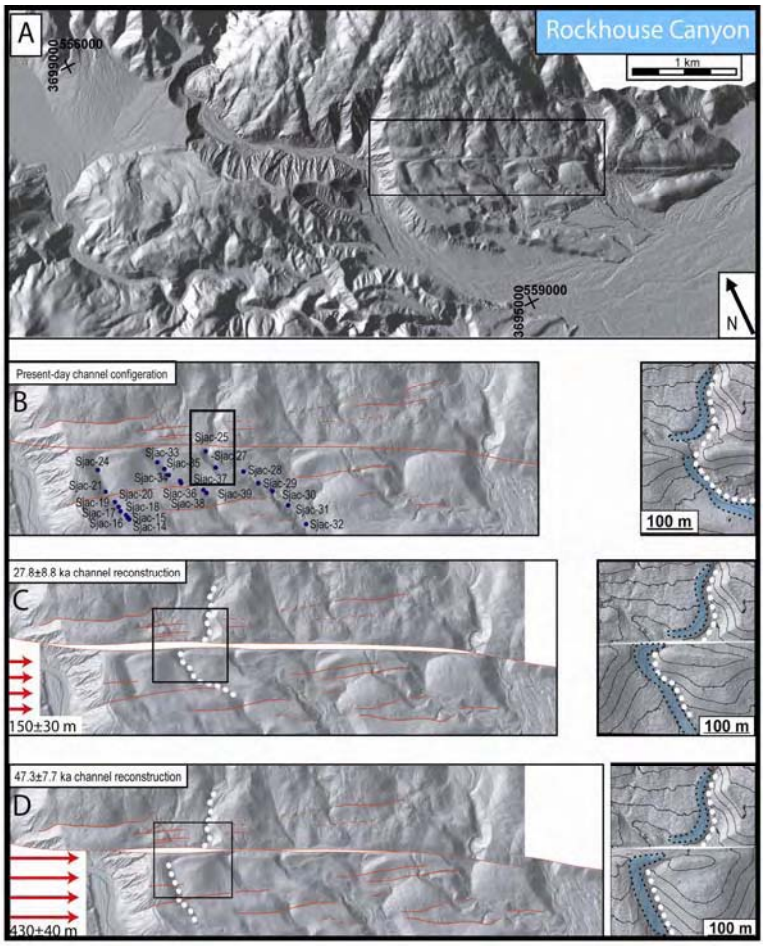

Figure 3. [A] LiDAR image of the Rockhouse Canyon site. [B] Shows the location of beheaded and deflected channels at Rockhouse Canyon is the present configuration of Channels 1, 2 and 3; [C] reconstruction of Channel 2 immediately before beheading; and [D] reconstruction of Channel 1 immediately before beheading. The blue dots in panel B indicate the location of boulder samples collected for ^{10}Be exposure age dating. See Fig. 2 for location.

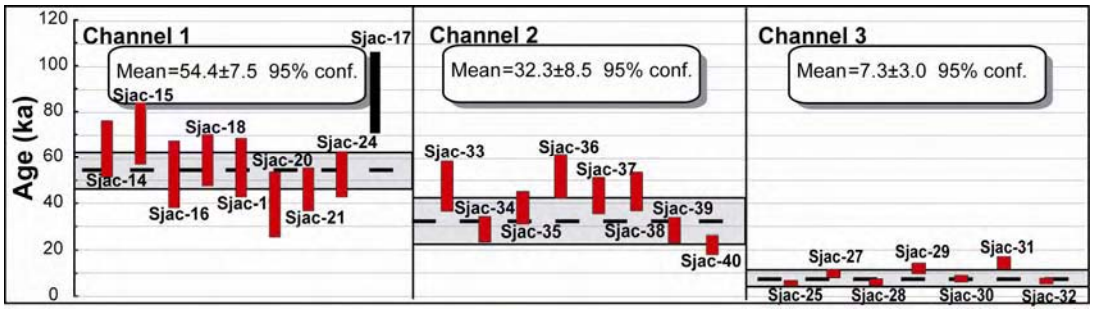

Figure 4. Chart shows the error weighted mean age of Channel 1, Channel 2 and Channel 3. Bouder ages include inheritance from Channel 3. The gray bars are error weighted mean ages [2 σ] used in calculating the age. The black bar is an outlier that is outside the 95% confidence interval of the remaining 8 samples from Channel 1.

spectrometry at CAMS at the Lawrence Livermore National Laboratory or at the PRIME Laboratory at Purdue University. All ^{10}Be ages for boulders samples were calculated using the CRONUS Age Calculator [Balcoetal.,2008;http://hess.ess.washington.edu/math/; Appendix 1].

No correction was made for geomagnetic field variations due to the ongoing debate regarding which, if any correction factors are most appropriate. There also is considerable debate regarding the use of appropriate scaling models [see Balco et al. 2008] and we choose to use the time independent model of Lal [1991] and Stone [2000] to calculate our ages. However, we note that the different scaling models may produce age differences of up to 11%.

RESULTS

ROCKHOUSE CANYON

The Rockhouse Canyon site is located along the western range front of the Santa Rosa Mountains at the northernmost end of Clark Valley in the Anza Borrego desert (Fig. 2). At Rockhouse Canyon, strike-slip fault activity is highly localized onto a single strand displaying channels in various stages of capture (Fig. 3). Two channels (Channel 1 and Channel 2) are completely beheaded from their source and no longer transporting large boulders (Fig. 3).

Contained within these channels are debris flow boulder bar deposits which can only have originated from the present-day drainage area located to the northeast of the fault. Realignment of Channel 1 and Channel 2 indicates displacement of 430 ± 40 m and 150 ± 30 m, respectively (Fig. 3c,d) after accounting for channel deflection prior to beheading (and capture and/or avulsion of the subsequent channel). To realign the beheaded channels along the fault, we used 2 m and 10 m contours to assess the channel wall curvature of the source drainage area. We then applied this procedure to the displaced and beheaded channels on the southwest side of the fault to assess the final form of these channels prior to complete beheading and abandonment (Fig. 3). The curvature of the source drainage indicates at least 70 m of deflection prior to beheading. Combining this curvature distance to the channel curvature distance from the southwest side of the fault for Channel 1 and Channel 2 indicates 430 ± 40 m and 150 ± 30 m, respectively. The uncertainties associated with the displacement is based on the maximum and minimum distance permitted to realign the contour curvature of the channel walls along both sides of the fault (Fig. 3c,d).

To constrain the ages of these displacements, we determined ^{10}Be exposure ages of 9 boulders in each of the beheaded channels, and of 7 boulders in the active channel; the resulting 25 sample ages are presented in Appendix 1 and Figure 4. The weighted mean of the individual boulder ages from the active channel, 7.3 ±3.0 ka, was used to infer the inheritance of ^{10}Be produced during exposure and transport prior to deposition. The age of the last depositional event for each of the two beheaded channels was estimated as the weighted mean age of the individual boulder ages from the channel minus the 7.3 ±3.0 ka inheritance age obtained from the active channels. This yielded an age of 47.3 ±7.7 ka for channel 1, and 27.8 ± 8.8 ka for channel 2 (age uncertainties given as the 95% confidence interval; Appendix 1). The age of one sample from channel 1 (Sjac-17) was discarded because it is outside the 95% confidence interval of the remaining 8 exposure ages determined for this channel (Appendix 1; Figs. 3 and 4).

Fitting a single slip rate through both channel offsets versus their age yields a late Quaternary average slip rate of 8.4 ± 1.7 mm/yr for the Clark fault at Rockhouse Canyon. Because minor erosion of the boulder surface is permissible from field observations, we also calculated ages assuming 2 m/Myr and 5 m/Myr of boulder surface erosion, yielding lower slip rates of 7.4 ± 1.7 mm/yr, and 6.0 ± 1.6 mm/yr, respectively. Differencing the raw mean boulder ages and displacements of Channel 1 from Channel 2 yields a significantly faster slip rate of 12.7 ± 5.5 mm/yr from ~30-50 ka. This could indicate significant variability in slip rate on the Clark fault over the Late Quaternary.

SOUTHERN SANTA ROSA MOUNTAINS

The southern Santa Rosa Mountains site is located just northwest of Smoke Tree Canyon on the southwestern range front of the Santa Rosa Mountains, here the Clark fault displaces a late Quaternary alluvial fan. At this locality, the Clark fault terminates into a fan of smaller faults that curve ˜80° southwards away from the main fault, these smaller faults display a normal component of slip south of this bend (Fig. 5). Geomorphic mapping of the Clark fault at the Santa Rosa Mountains imply alluvial fan deposition originating from the Santa Rosa pluton and cataclastic zone which predominately comprises tonalites, marbles and mylonites. Using the nomenclature of Bull

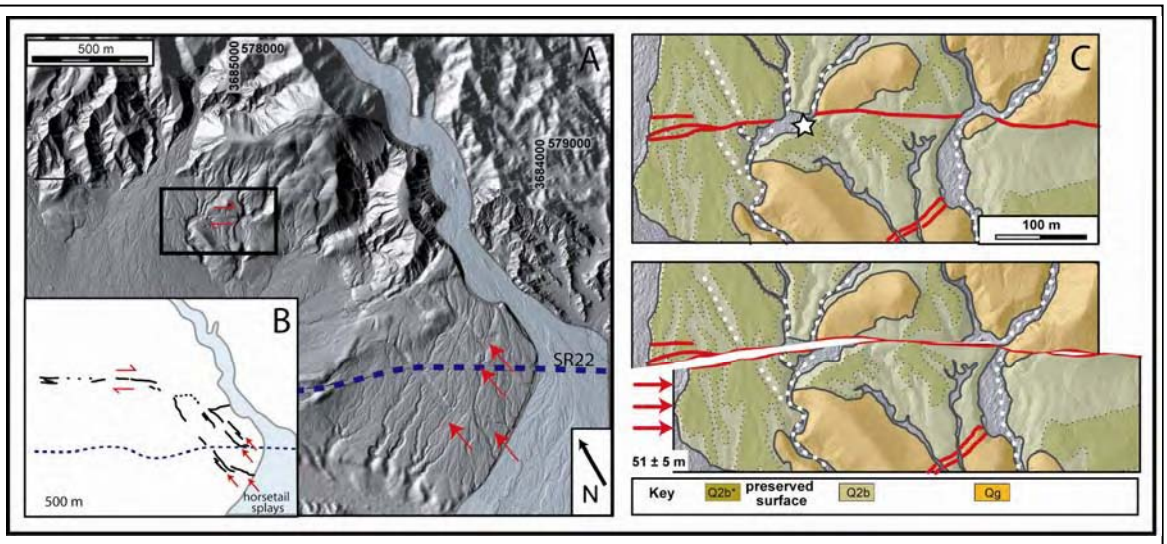

Figure 5. ALSM image of the southern Santa Rosa Mountains site. [A] the present configuration of 3 channels incised into the Q2b surface; [B] Inset showing mapped faults in [A]. [C] reconstruction of two deflected and one beheaded channel. The white star is the location of the 2 m deep depth profile sampled for exposure age dating. See text and Appendix 1 for details.

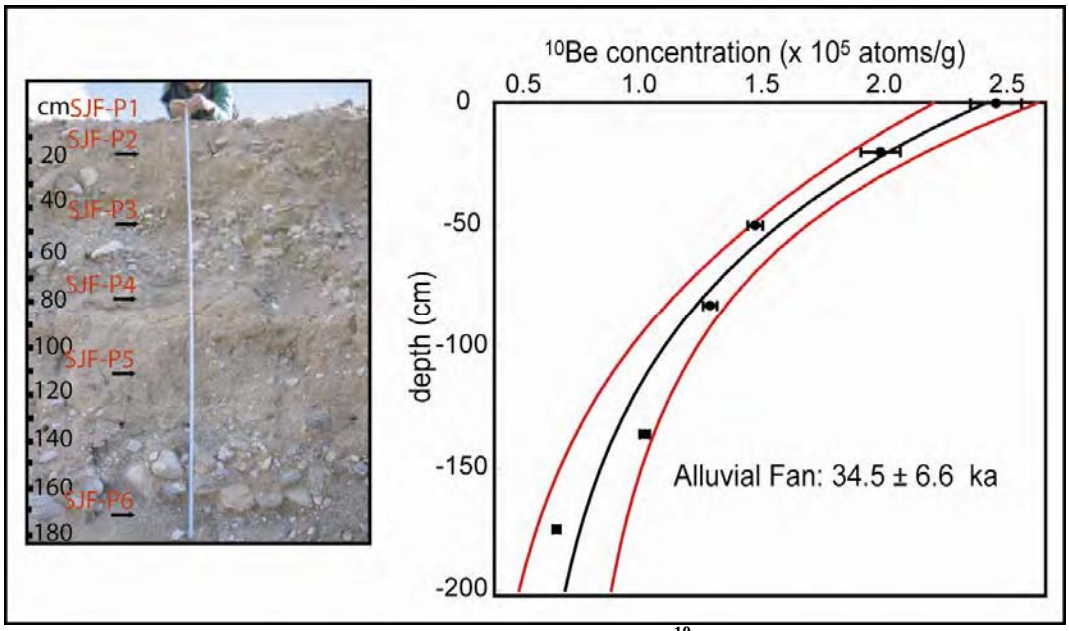

Figure 6. Exponential decrease in the concentration of ^{10}Be with depth from an alluvial surface cut by the Clark fault at the southern Santa Rosa Mountain locality. The stippled gray lines indicate the 95% confidence interval around the black regression line. Dotted lines represent the inheritance and its associated errors. The regression line indicates a surface age of 34.5 ± 6.6 ka.

this site exhibits moderate desert pavement and moderate to strong desert varnish development and a slightly undulating to (1991) this surface can be classified as a Q2b alluvial fan surface. The alluvial fan surface at planar surface morphology. Surface clast exhibits strong rubification on the underside of surface clasts,

The fault displacement at this site is determined using a beheaded channel and two deflected channels as piercing lines (Fig. 5). We note that several other fault strands cut the Q2b surface, but only the one studied here shows significant dextral offset (Fig. 5). Realignment of three channels incised into the alluvial surface implies displacement of 51 ± 5 m (Fig. 5). The uncertainty associated with the offset is based on the maximum and minimum distance permitted to relign all three channels. This distance is best determined by the channel thalweg (5 m length) of Channel 1, which is incised into the Q2b surface (Fig. 5).

To constrain the age of this displacement we dated the alluvial fan using ^{10}Be concentrations from a 2 m-deep exposure using the depth profile methods of Anderson et al. [1996]. The age determined from the depth profile at our Santa Rosa locality is a linear least square fit that produces uncertainty estimates for fit values of ^{10}Be concentrations collected from

a 2 m depth profile exposed from a natural channel incision (Fig. 6). Depth-profiles constrain the inheritance concentration at depth, but are still subject to erosion that may reduce the apparent surface age. A ^{10}Be depth profile defines a model age of 34.5 ± 6.6 ka for the displaced fan surface. Combined with the 51 ±5 m displacement yields a slip rate of 1.5 ± 0.3 mm/yr. The error associated with the slip rate is the RMS error of both age and offset.

DISCUSSION

We compare our slip rates determinations with rates determined over the same time interval (30-50 ka) along the Clark fault from Anza to the southern Santa Rosa Mountains. Our results show a pronounced late-Quaternary southward slip-rate gradient along the Clark fault segment of the SJFZ. The ~11-17 mm/yr Late Quaternary slip rate along the Clark fault segment at Anza [Rockwell et al., 1990] decreases southeastward to 8.4 ± 1.7 mm/yr at Rockhouse Canyon, to 1.5 ± 0.3 mm/yr at the southern Santa Rosa mountains locality (Figs. 1 and 3). This southward decrease in slip rate along the Clark segment is consistent with a similar decrease in slip per event for the past several events, as documented from small channel offsets [Middleton, 2006], but is only consistent with the decrease in total bedrock displacement [Sharp, 1967] from Anza to Rockhouse Canyon. Farther southeast, the total displacement remains at about 14.5 km to the southern Santa Rosa Mountains, whereas the slip rate and the magnitude of slip per event decline by ~80%. The decrease in total offset and slip rate between Anza and Rockhouse Canyon can be attributed to transfer of slip onto the adjacent Coyote Creek fault via the Coyote Mountain fault (located on the east side of Coyote Mountain) and to a group of sinistral faults in Salton Trough (Fig. 2) [Sharp, 1967] and/or absorbed by distributed folding and thrust faulting within the Borrego Badlands [Lutz et al., 2006; Kirby et al., 2006; Belgarde and Janecke, 2007]. However, it is less clear that the total offset of 14.5 km can be absorbed in such a fashion (Belgarde and Janecke, 2007). Outcrop patterns of folded Pleistocene sediments that onlap the southern end of the surface trace of the fault are largely intact (Kirby et al., 2006), indicating dextral offset far less than the basement rock. An alternative explanation is that a significant proportion of slip on the southernmost Clark fault had already accrued prior to deposition of the Brawley formation in the middle Quaternary. By whichever mechanism strain is absorbed, the Clark fault exemplifies how slip-rates are not maintained along the entire length of faults and that considerable strain may be accommodated by adjacent structures near the fault tip [Cowie and Scholz, 1992].

The Late Quaternary slip rate averaged over the past 30 to 50 ka is insufficient to accrue all of the observed displacement across the SJFZ since the 1.1 Ma age of initiation proposed by Lutz et al. [2005] and Kirby et al. [2006]. Either the slip rate of the SJFZ has decreased significantly in the late Quaternary, or slip on the Clark fault strand in the bedrock uplands of the Peninsular Ranges initiated earlier than 1.1 Ma.

Taking our Late Quaternary rate from Rockhouse Canyon (8.4 ± 1.7 mm/yr) as representative of the current slip rate of the Clark fault strand, and combining this with previously published Holocene rates for the Coyote Creek fault [~2-5 mm/yr: Clark et al.,

1972; Sharp, 1981; Pollard and Rockwell, 1995], suggests that the southern SJFZ accommodates ~10-15 mm/yr of plate boundary motion. This rate is similar to the combined rates of the Superstition Mountain fault [5-9 mm/yr: Gurrola and Rockwell, 1996] and Superstition Hills fault [3-6 mm/yr: Hudnut and Sieh, 1989] as well as the rate determined near Anza where there is essentially a single strand [Rockwell et al., 1990]. This rate is also consistent with the strain rates inferred for the southern SJFZ from GPS [Bennett, 2004; Fay and Humphreys, 2005], but is slower than the 21 ± 3 mm/yr suggested from InSAR [Fialko, 2006]. In comparison to the slip rate of the San Andreas fault [van der Woerd et al., 2002], it appears that the SJFZ has been slower during the Late Quaternary.

[20] Our data document considerable spatial variability, and possible temporal variability, along the southern San Andreas-Gulf of California transform plate margin during the Quaternary, which suggests a complex fault system kinematic evolution. Seismic hazard studies commonly rely on long-term Quaternary rates to infer short term hazard. Our observations suggest that we need information over multiple time frames, along with current (geodetic) and Late Holocene slip rates to adequately address earthquake hazards along evolving plate margins. Our slower Late Quaternary slip rate estimates of 8.4 ± 1.7 mm/yr at Rockhouse Canyon and 1.5 ± 0.3 mm/yr for the southern Santa Rosa Mountains, if representative for the life of the fault, suggest that 1) the SJFZ initiated ~1.5-1.7 Ma and 2) it is currently subordinate to the SAF in accommodating plate margin strain. Alternatively, if the stratigraphic data are correct and the fault initiated closer to 1 Ma, then the SJF has slowed down considerably since its' early history.

CONCLUSION

The Clark fault strand of the San Jacinto fault zone displays a pronounced southeastward decrease in Late Quaternary slip rate. ^{10}Be exposure ages of 47.3 ± 7.7 ka and 27.8 ± 8.8 ka for two beheaded channels and 34.5 ± 6.6 ka for a displaced alluvial deposit, imply slip rates of 8.4 ± 1.7 mm/yr at Rockhouse Canyon and 1.5 ± 0.3 mm/yr for the southern Santa Rosa Mountains. This gradient in slip rate must be largely accommodated by distributed deformation within the Salton Trough and ultimately transferred onto the Superstition Hills fault and Superstition Mountains fault. However, it is uncertain that such deformation is sufficient to absorb all 14.5 km of the slip observed from offset bedrock markers. Alternatively, some early slip on the Clark fault may not be expressed in the Salton Trough, perhaps instead being absorbed by blind strike-slip faulting or simply obscured by Plio-Quaternary sedimentation [Belgrade and Janecke, 2007]. Such a mechanism could also account for the total offset along the SJFZ without the need for significant decrease of its slip rate in the Late Quaternary. Our results suggest that, at least for the past ~30-50 kyr, the SJFZ has been subordinate to the San Andreas fault in accommodating plate margin strain.

ACKNOWLEDGEMENTS

This research was supported by a NEHRP grant awarded to T. Rockwell and L.A. Owen and a Southern California Earthquake Center [SCEC] grant awarded to M. Oskin. Special thanks to Alana Wilson and Eitan Shelef for field assistance, Peter Blisniuk for helpful discussions, George Hilley for use of the cosmogenic nuclide extraction laboratory at Stanford University and George Jefferson and all the Rangers at the Anza Borrego State Park for their help throughout the field season. We also thank Dr. Robert Finkel and Dylan Rood for AMS measurements at the Lawrence Livermore National Laboratory.

References

Anderson, R. S., Repka, J.L., Dick, G.S. [1996]. Explicit treatment of inheritance in dating depositional surfaces using in situ ^{10}Be and ^{26}Al. Geology, v. 24[1]: 47-51.

Balco G., Stone J., Lifton N., Dunai T. [2008]. A simple, internally consistent, and easily accessible means of calculating surface exposure ages and erosion rates from Be-10 and Al-26 measurements. Quaternary Geochronology, v. 3]: 174-195.

Bennett, R. A., Friedrich, A, M., Furlong, K. P. [2004]. Codependent histories of the San Andreas and San Jacinto fault zones from inversion of fault displacement rates. Geology, v. 32[11]: 961-964.

Bevis, M., Hudnut, K.; Sanchez, R., Toth, C.; Grejner-Brzezinska, D., Kendrick, E.; Caccamise, D., Raleigh, D.; Zhou, H.; Shan, S.; Shindle, W.; Yong, A.; Harvey, J.; Borsa, A.; Ayoub, F.; Shrestha, R.; Carter, B.; Sartori, M.; Phillips, D.; Coloma, F. [2005]. The B4 Project: Scanning the San Andreas and San Jacinto Fault Zones. American Geophysical Union, Fall Meeting: abstract #H34B-01.

Bull, W.(1991). Geomorphic Responses to Climate Change, Oxford University Press.

Clark, M. M. [1972]. Surface Rupture Along the Coyote Creek Fault. USGS Professional Papers, v. 787: 55-86.

Cowie, P., Scholz, C. [1992]. Physical explanation for the displacement-length relationship of faults using a post-yield fracture mechanics model. Journal of Structural Geology, v. 14[10]: 1133-1148.

Dorsey, R. J. [2002]. Stratigraphic record of Pleistocene initiation and slip on the Coyote Creek fault, Lower Coyote Creek, southern California. Geological Society of America Special Paper, v. 365: 251-269.

Fay, N., Humphreys, E. D. [2005]. Fault slip rates, effects of elastic heterogeneity on geodetic data, and the strength of the lower crust in the Salton Trough region, southern California. Journal of Geophysical Research, v. 110: 1-14.

Fialko, Y. [2006]. Interseismic strain accummulation and the earthquake potential on the southern San Andreas fault system. Nature, v. 441: 968-971.

Gurrola, Larry D. and Rockwell, Thomas K. [1996], Timing and slip for prehistoric earthquakes on the Superstition Mountain fault, Imperial Valley, southern California: Journal of Geophysical Research, v. 101, B3: 5977-5985.

Kendrick, K. J., Morton, D.M., Wells, S.G., Simpson, R.W. [2002]. Spatial and Temporal Deformation along the Northern San Jacinto Fault, Southern California: Implications for Slip Rates. Bulletin of the Seismological Society of America, v. 92[7]: 2782-2802.

Kirby, S., Janecke, S., Dorsey, R., Housen, B., Langenheim, V., McDougall, K., Steely, A. [2007]. Pleistocene Brawley and Ocotillo Formations: Evidence for Initial Strike-Slip Deformation along the San Felipe and San Jacinto Fault Zones, Southern California. The Journal of Geology. v. 115: 43-62.

Lal, D. [1991]. Cosmic ray labeling of erosion surfaces: in situ nuclide production rates and erosion models. Earth and Planetary Science Letters, v. 104: 424-439.

Langenheim, V. E., Jachens, R.C., Morton, D.M., Kistler, R.W. Matti, J.C. [2004]. Geophysical and isotopic mapping of preexisting crustal structures that influence the location and development of the San Jacinto fault zone, southern California. Geological Society of America Bulletin, v. 116[9/10]: 1143-1157.

Li, Y., Vernon, F.L. [2001]. Characterization of the San Jacinto fault zone near Anza, California, by fault zone trapped waves. Journal of Geophysical Research, v. 106: 30671-30688.

Lutz, A. D., R. Housen, B; Janecke, S. [2006]. Stratigraphic record of Pleistocene faulting and basin evolution in the Borrego Badlands, San Jacinto fault, southern California. Geological Society of America Bulletin, v. 118: 1377-1397.

Matmon, A., Schwartz, D.P., Finkel, R., Clemmens, S., Hanks, T [2005]. Dating offset fans along the Mojave section of the San

Andreas fault using cosmogenic 26Al and 10Be. Geological Society of America Bulletin, v. 117: 795-807.

Middleton, T. [2006]. Tectonic Geomorphology of the Southern Clark Fault from Anza Southeast to the San Felipe Hills: Implications of Slip Distribution for Recent Past Earthquakes. Master's Thesis., San Deigo State University, 95 p.

Morton, D. M., and Matti, J.C. [1993]. Extension and Contraction within an evolving divergent strike-slip fault complex: The San Andreas and San Jacinto fault zones at their convergence in Southern California. Boulder, Geological Society of America Memoir, v. 178:107-159.

Pollard, W.J. and Rockwell, T.K., [1995]. Late Holocene slip rate for the Coyote Creek fault, Imperial County, California: Geological Society of America, v. 27, no.5, p.72.

Richards-Dinger, K. and Shearer, P [2006]. Earthquake locations in southern California obtained from source specific location terms. JGR-Solid Earth, v. 105: 10939-10960.

Rockwell, T., Loughman, C., Merifield, P. [1990]. Late Quaternary Rate of Slip along the San Jacinto fault zone near Anza, Southern California. Journal of Geophysical Research, v. 95[B6]: 8593-8605.

Rockwell, T.K., Seitz, G., Dawson, T., Young, J. [2006]. The long record of San Jacinto fault paleoearthquakes at Hog Lake: Implications for regional patterns of strain release in the southern San Andreas fault system: Seismological Research Letters, v. 77: 270.

Sanders, C. O. [1993]. Interaction of the San Jacinto and San Andreas fault zones, southern California: Triggered earthquake migration and coupled recurrence intervals. Science, v 260: 973-975.

Sanders, C. O., Magistrale, H. [1997]. Segmentation of the northern San Jacinto fault zone, southern California. JGR-Solid Earth, v 102: 27, 453-27.

Sharp, R.V. [1967]. San Jacinto fault zone in the Peninsular Ranges of Southern California. Geological Society of America Bulletin, v. 78: 705-729.

Sharp, R. V. [1981]. Variable Rates of Late Quaternary Strike Slip on the San Jacinto Fault Zone, Southern California. Journal of Geophysical Research, v 86[B3]: 1754-1762.

Stone, J.O. [2000] Air pressure and cosmogenic isotope production: Journal of Geophysical Research, v. 105: 23,753-23,759.

Thatcher, W., Hileman, J.A., Hanks, T.C. [1975]. Seismic Slip Distribution along the San Jacinto Fault Zone, Southern California, and Its Implications. Geological Society of America Bulletin, v 86: 1140-1146.

van der Woerd, J., Klinger, Y., Sieh, K., Tapponier, P., Ryerson, F., Meriaux, A [2006]. Long-term slip rate of the southern San Andreas Fault from 10Be-26Al surface exposure dating of an offset alluvial fan. JGR 111. B04407, doi:10.1029/2004JB003559.

Table 1. SUMMARY OF SAN JACINTO FAULT ^{10}Be MODEL AGES

Sample name	Thickness (cm)	Shielding correction	Altitude (m)	Latitude (DD)	Longitude (DD)	^{10}Be measured (10^6 atom g^{-1})	^{10}Be age (ka) 0m/Myr	Error* ± (ka)	^{10}Be age (ka) 2m/Myr	Error* ± (ka)	^{10}Be age (ka) 5m/Myr
Channel 1											
Sjac-14	1	1.000	561	33.4052	-116.3708	0.4352 ± 0.0155	63.7	6.1	71.5	7.7	90.2
Sjac-15	3	1.000	561	33.4052	-116.3707	0.4734 ± 0.0163	70.6	6.7	80.3	8.8	105.4
Sjac-16	4	1.000	560	33.4051	-116.3707	0.3521 ± 0.0363	52.7	7.2	57.9	8.7	69.1
Sjac-17†	2	1.000	563	33.4054	-116.3708	0.5900 ± 0.0346	87.5	9.3	103.2	13.3	153.9
Sjac-18	2	1.000	564	33.4056	-116.3709	0.4002 ± 0.0137	58.9	5.6	65.5	6.9	80.4
Sjac-19	4	1.000	566	33.4058	-116.3709	0.3735 ± 0.0268	55.7	6.4	61.6	7.8	74.5
Sjac-20	2	1.000	572	33.4061	-116.3710	0.2727 ± 0.0406	39.7	6.9	42.6	8.0	48.0
Sjac-21	5	1.000	589	33.4066	-116.3712	0.3130 ± 0.0143	46.2	4.6	50.1	5.4	58.0
Sjac-24	5	1.000	614	33.4076	-116.3710	0.3639 ± 0.0106	52.8	4.9	58.0	5.9	69.1
Weighted mean of sample ages ± error							**54.4 ± 7.5**		**59.4 ± 8.9**		**69.1 ± 10.4**
Inheritance corrected sample ages ± error							**47.3 ± 7.7**		**52.3 ± 9.3**		**62.1 ± 13.0**
Channel 2											
Sjac-33	3	0.977	587	33.4061	-116.3657	0.3169 ± 0.0222	47.6	5.4	51.8	6.4	60.3
Sjac-34	3	0.979	577	33.4053	-116.3656	0.1930 ± 0.0048	29.0	2.6	30.5	2.9	33.1
Sjac-35	4	0.985	573	33.4046	-116.3644	0.2523 ± 0.0059	38.2	3.5	40.9	4.0	45.9
Sjac-36	3	0.988	567	33.4039	-116.3640	0.3433 ± 0.0078	51.8	4.7	56.8	5.7	67.5
Sjac-37	3	0.989	561	33.4033	-116.3635	0.2884 ± 0.0052	43.5	3.9	46.9	4.6	53.7
Sjac-38	5	0.975	545	33.4025	-116.3631	0.2867 ± 0.0067	45.3	4.1	49.0	4.8	56.5
Sjac-39	2	0.976	546	33.4017	-116.3630	0.1871 ± 0.0049	28.7	2.6	30.1	2.9	32.7
Sjac-40	2	0.977	527	33.4039	-116.3664	0.1435 ± 0.0039	22.3	2.0	23.1	2.2	24.6
Weighted mean of sample ages ± error							**32.3 ± 8.5**		**36.6 ± 9.5**		**41.1 ± 10.7**
Inheritance corrected sample ages ± error							**27.8 ± 8.8**		**29.3 ± 9.9**		**31.4 ± 11.9**
Channel 3											
Sjac-25	4	1.000	587	33.4067	-116.3681	0.0333 ± 0.0039	4.9	1.3			
Sjac-27	3	1.000	577	33.4063	-116.3680	0.0715 ± 0.0044	10.5	1.8			
Sjac-28	3	1.000	573	33.4060	-116.3679	0.0370 ± 0.0049	5.5	1.6			
Sjac-29	3	1.000	567	33.4055	-116.3675	0.0893 ± 0.0055	13.6	2.3			
Sjac-30	4	1.000	561	33.4055	-116.3675	0.0486 ± 0.0038	7.5	1.5			
Sjac-31	4	1.000	545	33.4046	-116.3666	0.0991 ± 0.0067	15.6	2.8			
Sjac-32	1	1.000	546	33.4048	-116.3667	0.0397 ± 0.0036	6.2	1.3			

Weighted mean of sample ages ± error						**7.3 ± 3.0**
	Depth (cm)					
SJF-P1	0	1.000	314	33.2967	-116.1677	0.2437 ± 0.0104
SJF-P2	20	1.000	314	33.2967	-116.1677	0.1967 ± 0.0080
SJF-P3	50	1.000	314	33.2967	-116.1677	0.1456 ± 0.0030
SJF-P4	83	1.000	314	33.2967	-116.1677	0.1272 ± 0.0029
SJF-P5	136	1.000	314	33.2967	-116.1677	0.1006 ± 0.0020
SJF-P6	175	1.000	314	33.2967	-116.1677	0.0667 ± 0.0001
Model age ± error						**34.5 ± 6.6**

Notes: ^{10}Be model ages calculated using the CRONUS calculator at Rockhouse Canyon (see Fig. 1 for sample locations).
Abbreviations: DD is decimal degrees,

*External error associated with ^{10}Be model exposure ages.

†Boulder samples that are not used in the calculation of the weighted mean age. See Appendix for details

DAY 2: 2008 FRIENDS OF THE PLEISTOCENE FIELD TRIP, CORDILLERA SECTION

AGE AND STRUCTURE OF THE SAN JACINTO AND SAN FELIPE FAULT ZONES, AND THEIR LIFETIME SLIP RATES

LEADERS:
Susanne U. Janecke
Utah State University
and
Becky J. Dorsey
University of Oregon
Five stops in the northern part of Anza-Borrego State park

Field Trip Guide

EARLY PLEISTOCENE INITIATION AND STRUCTURAL COMPLEXITIES OF THE SAN JACINTO AND SAN FELIPE FAULT ZONES, WESTERN SALTON TROUGH: PART I

Susanne Janecke[1], Becky Dorsey[2], and Benjamin Belgarde[1]
[1]Utah State University and [2]University of Oregon

Contributors:
D. Forand, B. Housen, S. Kirby, V. Langenheim, A. Lutz, T. Rittenhour, and A. Steely

Supporting papers

Dorsey, R. J., Fluette, A., McDougall, K. A., Housen, B. A., Janecke, S. U., Axen, G. A., and Shirvell, C. R., 2007, Chronology of Miocene-Pliocene deposits at Split Mountain Gorge, southern California: A record of regional tectonics and Colorado River evolution: Geology, v. 35, p. 57-60.

Dorsey, R.J., 2006, Stratigraphy, tectonics, and basin evolution in the Anza-Borrego Desert region. In: Jefferson, G.T. and Lindsay, L.E. (eds.) Fossil Treasures of Anza-Borrego Desert. Sunbelt Publications, San Diego, CA, p. 89-104.

Kirby, S. M., Janecke, S. U., Dorsey, R. J., Housen, B. A., McDougall, K., Langenheim, V., and Steely, A., 2007, Pleistocene Brawley and Ocotillo formations: Evidence for initial strike-slip deformation along the San Felipe and San Jacinto fault zones, California: Journal of Geology. v. 115 (1), p. 43-62.

Lutz A.T., Dorsey, R.J., Housen, B.A., Janecke, S.U. (2006) Stratigraphic record of Pleistocene faulting and basin evolution in the Borrego Badlands, San Jacinto fault zone, Southern California. Geological Society of America Bulletin: v. 118, No. 11 pp. 1377–139.

Steely, A.N., Janecke, S.U., Dorsey, R.J., and Axen, G.J. (in press) Early Pleistocene initiation of the San Felipe fault zone, SW Salton Trough, during reorganization of the San Andreas fault system: Geological Society of America Bulletin, 2009. 25 p.

Road log

EARLY PLEISTOCENE INITIATION AND STRUCTURAL COMPLEXITIES OF THE SAN JACINTO AND SAN FELIPE FAULT ZONES, WESTERN SALTON TROUGH: PART II

EARLY PLEISTOCENE INITIATION AND STRUCTURAL COMPLEXITIES OF THE SAN JACINTO AND SAN FELIPE FAULT ZONES, WESTERN SALTON TROUGH: PART I

Susanne Janecke[1], Becky Dorsey[2], and Benjamin Belgarde[1]
[1]Utah State University and [2]University of Oregon

Contributors:

D. Forand, B. Housen, S. Kirby, V. Langenheim, A. Lutz, T. Rittenhour, and A. Steely

BACKGROUND AND STATEMENT OF PROBLEM

The San Jacinto and San Felipe dextral strike-slip fault zones are important for understanding plate-boundary dynamics, regional slip partitioning, and seismic hazards in southern California (Fig. 1). However, their age of initiation and long-term average slip-rates are controversial, and little is known about the structural evolution of these fault zones during their short geologic history. Research by our group over the past ~6 years has addressed these questions with the goal of understanding the age and geological evolution of these fault zones, and their influence on Plio-Pleistocene regional stratigraphy and basin development in the western Salton Trough. A second major question concerns the distribution of strain within the evolving fault zones, particularly in the basinal deposits where prior studies found limited evidence for a significant displacement on the southeastward extension of the Clark fault (Figs 3, 4 and 6).

The age of the San Jacinto and San Felipe fault zones was controversial. One popular model concluded that the San Jacinto zone formed ca. 2-2.5 Ma, based on late Quaternary slip rates of ~9-12 mm/yr at Anza (Sharp, 1967; Rockwell et al., 1990). This rate requires about 2 to 2.5 m.y. to produce the 24-29 km of right slip on the fault (e.g. Sharp, 1967; Hill, 1984). Indirect support for this age was derived from an anticline in the western San Bernardino Mountains that was originally thought to have initiated ~ 2-2.5 Ma near the subsurface branch point between the San Andreas and San Jacinto fault (Table 1)(Meisling and Weldon, 1989; Weldon et al., 1993; Morton and Matti, 1993; Rockwell et al., 1990; Rockwell, pers. comm., 2003; Weldon pers. comm., 2002).

In contrast, stratigraphic and structural studies in the San Timoteo Badlands near San Bernardino concluded that contraction and structural complexities in San Gorgonio Pass resulted in initiation of the San Jacinto fault zone between 1.4 and 1.2 Ma, to partially bypass the eastern 55 km of the Big Bend in the San Andreas fault (Matti and Morton, 1993; Morton and Matti, 1993; Albright, 1999). The faster implied slip rate was subsequently supported by a study in the San Timoteo Badlands by Kendrick et al. (2002), in which a Pleistocene slip rate of ca. 20 mm/yr over the past ~100 k.y. was deduced from rates of active uplift and erosion adjacent to the San Jacinto fault (Table 1). In addition, a recent integrated GPS and InSar inversion study by Fialko (2006) yielded a modern slip rate of 19-21 mm/yr across the San Jacinto fault zone in the Salton Trough. These results could reflect changing slip rates over time but also raise the possibility that there may be no significant or resolvable differences between geologic, Holocene, and modern slip rates in the San Jacinto fault zone.

The large disparity between slip rates derived from different data sets for different timescales has motivated our study to determine the age of initiation and long-term slip rates for the San Jacinto and San Felipe fault zones in the western Salton Trough (Tables 1 and 2). We emphasize that the age of these fault zones must be deduced from stratigraphic, structural, and other

geologic data in and adjacent to the fault zones. Their ages cannot be assumed from extrapolation of young slip rates over geologic timescales, because it is well known that slip rates can and commonly do vary over time. This is a geological problem that must be solved with field-based geologic studies.

Our research has also considered whether there is significant off-fault displacement in the damage zone of strike-slip faults that might explain the discrepancies between higher GPS-based slip rates and slower slip rates based on paleoseismic studies and offset geomorphic features (Belgarde, 2007; D. Forand, in prep.)(Table 1 and Le et al., this volume). One objective of this field trip is to illustrate the extremely distributed strain of the southeastern two structural segments of the Clark fault, and to show that there is significant hidden strain on these structures that is both Quaternary in age and coseismic.

SUMMARY OF RESULTS

Since 2002, S. Janecke, R. Dorsey, and their students and colleagues have carried out a series of detailed mapping, stratigraphic, structural, and paleomagnetic studies of Plio-Pleistocene sedimentary and older crystalline rocks in the San Jacinto and San Felipe fault zones. These studies produced four completed masters theses (Belgarde, 2007; Kirby, 2005; Lutz, 2005; Steely, 2006), one in progress (Forand, in prep.), three papers published or in press (Lutz et al., 2006; Kirby et al., 2007; Steely et al., in press GSA Bulletin, 2009), and one synthesis paper that is close to submission (Janecke et al., in prep). The main results and highlights of these studies are briefly summarized below with an emphasis on the newer and unpublished results in Janecke et al. (in prep.) and two prepublication manuscripts by Janecke and Belgarde in Belgarde (2007). Please refer to the papers themselves for additional detail and figures.

Stratigraphic Studies

The Pleistocene Ocotillo Formation and its eastern distal equivalent, the Brawley Formation, make up a widespread unit of conglomerate and sandstone that rests on older lacustrine deposits of the Borrego Formation in the western Salton Trough (Figs. 3, 5, and 6). Magnetostratigraphic analysis shows that the base of the Ocotillo Formation in the western Borrego Badlands is 1.05 ± 0.03 Ma (Lutz et al., 2006), and the base of the Brawley Formation in the eastern San Felipe Hills is ~1.07 Ma, coincident with the base of the Jaramillo subchron (Kirby et al., 2007). The correlative base of the Ocotillo and Brawley formations varies from a slight hiatus marked by soil development in the Borrego Badlands, to a sharp disconformity in the San Felipe Hills, to a prominent angular unconformity roughly coinciding with the San Felipe anticline in the western San Felipe Hills. The Ocotillo Formation reveals an up-section increase in calcite-cemented, quartz-rich sandstone clasts derived from the Pliocene Arroyo Diablo Formation, a widespread unit derived from the Colorado River that accumulated during slip on the West Salton detachment fault.

The above data show clearly that the laterally equivalent Ocotillo and Brawley formations record rapid, nearly simultaneous progradation of coarse alluvial and fluvial clastic sediments ~25-30 km to the east and NE across a former large perennial lake represented by mud-rich lacustrine deposits of the Borrego Formation. We have considered and rejected a climatic explanation for progradation of the Borrego-Brawley unit because: (1) the age is too young to be the result of global climate change that resulted from onset of northern hemisphere glaciation at ~2.5-3 Ma; (2) climate change cannot explain the angular unconformity that is locally developed at the base of the Ocotillo Formation; and (3) climate forcing also cannot explain the presence of

sandstone clasts reworked from the older Arroyo Diablo Formation, which requires structural inversion uplift and erosion of a basin that previously formed in the hanging wall of the West Salton detachment fault. The Ocotillo and Brawley formations accumulated in a large subsiding depocenter influenced by basin-bounding faults and intrabasinal structures between ~1.1 and 0.5-0.6 Ma (Lutz et al., 2006). Subsidence ended at 0.5-0.6 Ma, resulting in deposition of the thin Fonts Point Sandstone starting at ~0.6 Ma. The Fonts Point Sandstone was possibly the oldest pediment deposit to form in this region after widespread subsidence and deposition ceased. It was subsequently uplifted and now serves as a useful strain marker for active faulting and folding that has been ongoing for the past ~ 500 ka.

Based on the points summarized above, we conclude that rapid progradation of the Ocotillo and Brawley formations was driven by a dramatic increase in sediment flux from the eastern Peninsular Ranges, including inverted parts of the former supradetachment basin of the West Salton detachment fault. Relationships in the San Felipe fault zone provide a record of strike-slip fault initiation at the same time as this major progradational event. Because the San Felipe anticline is related to early slip in the San Jacinto fault zone, the angular unconformity provides another link between this major progradation event and the structural driving forces (Kirby et al., 2007). Clasts reworked from the Arroyo Diablo Formation provide a clear signal of basin inversion and uplift, which itself requires a major structural reorganization at about 1.1 Ma. Recognizing a possible short lag time between earliest fault initiation and resultant erosion and progradation of coarse clastics, we assign an age of about 1.1-1.3 Ma for initiation of the San Jacinto and San Felipe fault zones (Janecke et al., in prep.).

Structural Studies

The structural geology of the San Jacinto and San Felipe fault zones is exceedingly complex and contains many right and left lateral strike-slip, normal and oblique-slip faults, a few reverse faults, scarps, active folds, and other structures. Our work has focused on geologic mapping of the fault zones, interpreting faults and folds, assessing the late Quaternary activity levels (when possible) of these structures, developing and refining segmentation models of the fault zones, and interpreting the cross-sectional geometry of the faults and folds using microseismic data when it is available. Our key findings are summarized below in order of (1) structural geology, (2) dextral displacements, (3) evolution and growth of the new strike-slip faults, and (4) implications of our work.

1. Structural Geology:

a. The structural geology of the San Jacinto, Buck Ridge, and San Felipe fault zones is more interconnected and continuous than prior mapping showed. Neither the Clark nor the Buck Ridge faults dies out to the southeast, in contrast to Sharp (1972) and most subsequent studies. Instead, they intersect with other structures in the SE and are linked to one another by numerous crossing faults that strike in every direction (Belgarde, 2007; Kirby, 2005; Lutz, 2005; Steely, 2006; D. Forand, in prep.; Lutz et al., 2006; Kirby et al., 2007; Steely et al., in press GSA Bulletin, 2009). NE- and E-striking cross faults are most common.

b. The southeast parts of the Clark fault and the San Felipe fault are strongly segmented, with adjacent structural segments having different structural styles, orientations, and fault widths. The Coyote Creek fault zone is much less variable along strike and has more simple traces and fairly simple transitions between structural segments (Belgarde, 2007)(Fig. 3).

c. The Clark fault persists for an additional 25 km SE of its previously defined termination point near Palo Verde Wash (Sharp (1972), continuing SE to the NE-striking left-lateral Extra fault zone (Kirby et al., 2007 Kirby 2005; Belgarde, 2007). The Clark fault zone becomes broader and far more dispersed to the SE, and much of its significant strain is "hidden" within the mud-rich sedimentary basin deposits (Belgarde, 2007). Detailed mapping, however, clearly shows that a large amount of right lateral strain has accumulated there (Fig. 10, 11,15,16,17,18,19) (Kirby et al., 2007; Belgarde, 2007).

d. The Buck Ridge fault curves to the SE north of Clark Lake and becomes the Santa Rosa normal oblique-slip fault (Janecke and Forand, unpublished mapping; Belgarde, 2007). Several strands of the Santa Rosa fault connect with the Clark fault near Lute Ridge (Figs. 3, 4, 9, 10, and 11)(Belgarde and Janecke, in Belgarde, 2007).

e. Folding accommodates dextral strains and block rotation (?) at the SE end of the Clark fault zone (in the last 2-2.5 km)(Kirby et al., 2007; Janecke, unpublished mapping). There is no surface connection between the SE tip of a fault within the Clark fault zone and the Extra fault. A blind structure at depth might persist to the intersection (Kirby, 2005; Janecke, unpublished mapping).

f. Strike-slip faults have "atypical" geometries in mud rich sedimentary rocks, including ramps and flats (Figs. 11, 13 14, 19) dipping "thrust-like" geometries, pitchfork structures (Fig. 19) crossing faults at the same structural levels (Figs. 10, 12), crossing faults that pass over and under one another at different structural levels (Figs. 15, 18), fault-parallel fault-bend folds (Fig. 15 and Steely et al., in press 2009), and pooch structures. These tend to distribute strain over large areas and transfer large strains to distant locations (Figs. 1, 3, 4,10, 12, 15, 16, 17) (Kirby, 2005; Belgarde, 2007).

In general, we find that there are many linkages between adjacent dextral faults. Dozens of additional faults with trace lengths up to 25 km connect the Coyote Creek and Clark faults to one another, to adjacent faults, and likely transfer strain back and forth between them. Similar fault networks connect the San Felipe fault north to the Coyote Creek fault and south to the Earthquake Valley fault zone. It is challenging to parse this interconnected web of faults into discrete fault zones, to precisely quantify the strain in rotating blocks, damage zones, and on subsidiary structures, despite clear signs of localized dextral faults in many areas.

2. Dextral Displacements and Lifetime Slip Rates

a. The Clark fault has about 14.4 km of right separation across Clark Valley (Sharp, 1967), and may have a few kilometers of additional slip after mapping between the Clark and Coyote Creek fault traces is completed. (Janecke and Forand, unpublished mapping)(Figures 4 and 7).

b. The Coyote Creek fault at Coyote Mountain has 3.5±1.3 km of right slip, not the ca. 6 km of prior estimates that were based on Sharp's (1967) map of the base of the Cretaceous Eastern Peninsular Ranges mylonite zone (Dorsey, 2002). The new estimate measures displacement of a distinctive and steeply dipping suite of crystalline rocks across the fault zone. (Janecke et al., in prep.)(Figs. 7 and 8).

c. More than 6 km of right slip on the Clark fault accrued in the Tarantula Wash fault segment on the San Felipe Hills since about 0.55 ± 0.2 Ma. This is a **minimum** slip rate of at least 10.2 (+6.9/-3.3) mm/yr (Kirby, 2005; Janecke et al., in prep.).

d. The San Felipe fault zone is a more important Quaternary fault zone than previously recognized. It offsets planar features 4-13 km with a preferred slip estimate of 6.5 km since ~1.1 to 1.3 Ma (Steely et al., in press; Janecke et al., in prep.)(Fig. 3).

e. Using new total offsets of 17.9±1.3 km across the Clark, Buck Ridge and Coyote Creek faults and the initiation ages for the relevant fault segments between 0.8-0.3 Ma, the combined lifetime slip rate across the San Jacinto fault zone is approximately 17.8 +2.6 -2.3 mm/yr (Janecke et al., in prep.)(Fig. 5). Incompletely known strains in the damage zone of the major faults are likely to increase this estimate slightly, but are too preliminary to include here (Forand and Janecke, in prep.)(Fig. 7).

f. The San Felipe fault zone has a lifetime average slip rate of ~5.4 +6.9 -2.3 mm/yr that is based on its 6.5 km of slip and the range of possible displacements and ages. This exceeds the lifetime slip rate of the southern Elsinore and Coyote Creek faults (Janecke et al., in prep.).

g. Overall, our data sets suggest that lifetime slip rates are fairly high (Fig. 8 and Table 2). Together the San Jacinto and San Felipe fault zones appear to have accumulated roughly half the plate rate since they formed in the early Pleistocene (17.8 + 5.4=23.2 +9.5/-4.6 mm/yr).

3. Evolution and Growth of New Strike-Slip Faults:

a. The faults did not emerge in their present form at 1.1-1.3 Ma. Instead, major structures like the basement-cored San Felipe anticline developed in the San Jacinto fault zone during its early history and have been deactivated, cut, and displacement during its later history (Lutz et al., 2006; Kirby et al., 2007; Steely, 2006).

b. Another example of an evolving fault zone is the San Felipe fault zone. During the first half of its existence near Sunset Wash, over 600 m of conglomerate and pebbly sandstone accumulated within the fault zone. During the second half of its history, as a contractional stepover tightened, these deposits were folded, uplifted and exhumed (Steely et al., in press).

c. In general folding related to the dextral faults was broad and widely spaced during the early history of deformation, producing disconformities, progressive unconformities, and lateral thickness changes across many-kilometer-wide tilt panels (e.g. Fig. 15A-C). Later (after about 0.5 Ma) folding strains increased, became more localized and folds with mappable hinges are spaced roughly 750-100 m apart (Fig. 15D)(Kirby, 2005; Kirby et al., 2007; Lutz, 2005; Steely et al., in press).

d. Despite the very young age of the fault zones (1.1 to 1.3 Ma) they have already been reorganized structurally and the main strands have shifted laterally (Kirby, 2005; Kirby et al., 2007; Lutz, 2005; Lutz et al., 2006; Steely, 2006; Steely et al., in press; Belgarde, 2007).

4. Implications of This Work:

a. It is very unlikely that the slip rates of the San Jacinto and San Felipe fault zones were constant over their life spans because the fault zones changed their geometry and principal faults so much during that time. Models that assume steady-state behavior in such a complex fault zone (with rapidly evolving links and a complex fault mesh) are unlikely to be correct (Janecke et al., in prep.).

b. Displacements and ages of fault segments vary from place to place and therefore slip rates vary along the strike of the fault zones. Care must be taken when comparing slip rates at different time scales, from different segments, and across different faults.

c. Some fault zones have so much strain in their damage zone that it is difficult to accurately measure total displacements in their central strands. The Clark fault in the Arroyo Salada and Tarantula Wash segments display this character (Belgarde, 2007) (Figs. 10-19). We are also finding additional strain in crystalline rocks between the Coyote Creek and Clark fault at Coyote Mountain.

CONCLUDING REMARKS

Recent and ongoing studies by our group show that the San Jacinto and San Felipe fault zones initiated at ca. 1.1-1.3 Ma, during a tectonic reorganization that profoundly changed and widened the distribution of plate-boundary strain in the southern San Andreas fault system. This tectonic event deactivated most of the West Salton detachment fault – though some parts continued to slip in the south – and quickly inverted western parts of the supradetachment basin. This drove rapid uplift and erosion of uplifting fault blocks along the San Felipe and San Jacinto fault zone and progradation of coarse alluvial and fluvial deposits (Ocotillo and Brawley formations) across the western Salton Trough, and completely changed the landscape. Another, less profound change at ~0.5-0.6 Ma caused basins that had collected the Ocotillo and Brawley formations to stop subsiding, resulting in deposition of the first of many pediment deposits, the Fonts Point Sandstone, over a large area. This change initiated the current phase of fault-zone deformation, uplift and erosion that has been active over the past ~ 500 kyrs.

We conclude that slip rates in these fault zones likely vary along the strike, and probably varied significantly over time. The geologic lifetime rate that we calculate for the San Jacinto fault zone – approximately 17.8 +2.6 -2.3 mm/yr – is closer to rates derived from GPS and InSAR inversions than those based on paleoseismic studies and dating of offset Quaternary to Holocene geomorphic features (Table 1 and Le et al., this volume). We suggest that slip rates determined from paleoseismic and neotectonic methods may be incomplete in settings, like the southeast half of the San Jacinto fault zone, where large amounts of strain are taken up outside the main central fault strands. The broad distribution of strain in the damage zones of major faults may hinder attempts to reconcile different timescales of slip rates in this and other active fault zones.

REFERENCES CITED

Albright, L.B., 1999, Magnetostratigraphy and biochronology of the San Timoteo Badlands, southern California, with implications for local Pliocene-Pleistocene tectonic and depositional patterns: Geological Society of America Bulletin, v. 111, p. 1265-1293.

Anderson, G., Agnew, D.C., and Johnson, H.O., 2003, Salton Trough regional deformation estimated from combined trilateration and survey-mode GPS data: Bulletin of the Seismological Society of America, 93, 2402-2414.

Axen, G.J., and Fletcher, J.M., 1998, Late Miocene-Pleistocene extensional faulting, northern Gulf of California, Mexico and Salton Trough, California. International Geology Review 40:217-244.

Becker, T.W., Hardebeck, J.L., and Anderson, G., 2005, Constraints on fault slip rates of the southern California plate boundary from GPS velocity and stress inversions: Geophysical Journal International, 160, 634–650 doi: 10.1111/j.1365-246X.2004.02528.x

Belgarde, B.E., 2007, Structural characterization of the three southeast segments of the Clark fault, Salton Trough, California [M.S thesis]: Utah State University: 4 plates, map scale 1:24,000. 216 p.

Bennett, R. A., Rodi, W., and Reilinger, R. E., 1996, Global Positioning System constraints on fault slip rates in southern California and northern Baja, Mexico: Journal of Geophysical Research,v. 101, p. 21,943–21,960.

Dibblee, T.W., Jr., 1954, Geology of the Imperial Valley region, California. Geology of Southern California, California Division of Mines Bulletin 170, p. 21-28.

Dibblee, T.W., 1984, Stratigraphy and tectonics of the San Felipe Hills, Borrego Badlands, Superstition Hills, and vicinity. In Rigsby, C. A. (ed.), The Imperial Basin - Tectonics, Sedimentation, and Thermal Aspects. Los Angeles, California, Pacific Section S.E.P.M., p. 31-44.

Dibblee. T.W., Jr., 1996, Stratigraphy and tectonics of the Vallecito-Fish Creek Mountains, Vallecito Badlands, Coyote Mountains and Yuha Desert, southwestern Imperial basin, California, in Abbott, P.L., and Seymore, D. C., eds., Sturzstroms and detachment faults, Anza-Borrego Desert State Park, California: South Coast Geological Society, Santa Ana, California, Annual Field Trip Guidebook 24, p. 59-79.

Dorsey, R.J., 2002, Stratigraphic record of Pleistocene initiation and slip on the Coyote Creek fault, lower Coyote Creek, southern California, In Barth, A., ed., Contributions to Crustal Evolution of the Southwestern United States: Geological Society of America Special Paper 365:251–269.

Dorsey, R.J., 2006, Stratigraphy, tectonics, and basin evolution in the Anza-Borrego Desert region. In: Jefferson, G.T. and Lindsay, L.E. (eds.) Fossil Treasures of Anza-Borrego Desert. Sunbelt Publications, San Diego, CA, p. 89-104.

Dorsey, R. J., Fluette, A., McDougall,. K. A., Housen, B. A., Janecke, S. U., Axen, G. A., and Shirvell, C. R., 2007, Chronology of Miocene-Pliocene deposits at Split Mountain Gorge, southern California: A record of regional tectonics and Colorado River evolution: Geology, v. 35, p. 57-60.

Fay, N.P., and Humphreys E.D., 2006, Dynamics of the Salton block: Absolute fault strength and crust-mantle coupling in Southern California. Geology, 34, 261-264.

Fialko, Y., 2006, Interseismic strain accumulation and the earthquake potential on the southern San Andreas fault System: Nature 441: 968-971.

Forand, D., in prep., Structural geology of two crystalline damage zones, southern California [MS thesis]: Utah State University.

Hill, R.I., 1984, Petrology and petrogenesis of batholithic rocks, San Jacinto Mountains, southern California: Pasadena, California Institute of Technology [Ph.D. dissertation]: 660 p.

Hudnut, K., L. Seeber, and T. Rockwell (1989). Slip on the Elmore Ranch fault during the past 330 years and its relation to slip on the Superstition Hills fault, Bull. Seismol. Soc. Amer. 79, no. 2, 330–341.

Janecke, S. U., Dorsey, R. J., Steely, A. N., Kirby, Andrew Lutz, S. M., Housen, B. A., Belgarde, B., and Langenheim, V., Rittenhour, T. and Forand, D., in prep. High Geologic Slip Rates since Early Pleistocene initiation of the San Jacinto and San Felipe Fault Zones in the San Andreas fault system: Southern California, USA: to be submitted to Lithosphere.

o

Janecke, S. U., Belgarde, B. E., 2007, The width of dextral fault zones and shallow decollements of the San Jacinto fault zone, southern California: Annual meeting of the Southern California Earthquake Center, Palm Springs, CA, v. 17. http://www.scec.org/meetings/2007am/index.html

Janecke, S. U., and Belgarde, B. E., 2008, Detecting hidden, high-slip rate faults: S. San Jacinto fault zone; Final Report for NEHRP Grant 06HQGR0031, 96 p. http://earthquake.usgs.gov/research/external/research.php?yearID=2006&pi=janecke&regionID=&award=&keyword=&submit=Find+Projects

Janecke, S. U., Steely, A. N., and Evans, J.P., 2008, Seismic Slip on an Oblique Detachment Fault at Low Angle: Eos Trans. AGU, 89(53), Fall Meet. Suppl., Abstract T53F-06.

Janecke, S.U., Kirby, S.M., Langenheim, V.E., Housen, B.A., Dorsey, R.J., Crippen, R.E., Blom, R.G., 2004, Kinematics and evolutions of the San Jacinto fault zone in the Salton Trough: Progress Report from the San Felipe Hills area: Geological Society of America Abstracts with Programs, v. 37, no. 5, p. 317. http://gsa.confex.com/gsa/2004AM/finalprogram/abstract_78180.htm

Jennings, C.W., 1994, Fault activity map of California and adjacent areas, with locations and ages of recent volcanic eruptions: California Division of Mines and Geology, Geologic Data Map No. 6, map scale 1:750,000.

Jennings, C.W., compiler, 1977, Geologic map of California: California Division of Mines and Geology Geologic Data Map 2, scale 1:750,000.

Kairouz, M.E., 2005, Geology of the Whale Peak Region of the Vallecito Mountains: Emphasis on the Kinematics and Timing of the West Salton Detachment fault, Southern California, [M.S. Thesis]: University of California, Los Angeles. 156 p.

Kendrick, K.J., Morton, D.M., Wells, S.G., and Simpson, R.W., 2002, Spatial and Temporal Deformation along the Northern San Jacinto Fault, Southern California: Implications for Slip Rates: Bulletin of the Seismological Society of America, 92, 2782 - 2802.

Rockwell, T.K., Seitz, G., Dawson, T., and Young, J, 2006, The long record of San Jacinto fault paleoearthquakes at Hog Lake: Implications for regional patterns of strain release in the southern San Andreas fault system: Seismological Research Letters, v 77, p. 270.

Kennedy, M.P., 2000, Preliminary geologic map of the Pechanga 7.5' quadrangle, San Diego and Riverside Counties, California. http://www.consrv.ca.gov/cgs/rghm/rgm/preliminary_geologic_maps.htm

Kennedy, M.P., 2003, Preliminary geologic map of the Vail Lake 7.5' quadrangle, San Diego and Riverside Counties, California. http://www.consrv.ca.gov/cgs/rghm/rgm/preliminary_geologic_maps.htm

Kennedy, M.P., and Morton, D.M., 2003, Preliminary geologic map of the Murrieta 7.5' quadrangle, Riverside County, California. U.S. Geological Survey Open-File Report 03-189, 17 p., scale 1:24,000, http://geopbs.wr.usgs.gov/open-file/of03-189/.

King, N.E., and Savage, J.C., 1983, Strain-rate profile across the Elsinore, San Jacinto and the San Andreas faults near Palm Springs, California, 1973-81: Geophysical Research Letters, v. 10, p. 55-37.

Kirby, S.M., 2005, The Quaternary tectonic and structural evolution of the San Felipe Hills, California, [M.S. Thesis]: Logan, Utah State University, 182 p.

Kirby, S.M., Janecke, S.U., Dorsey, R.J., Housen, B.A., McDougall, K., Langenheim, V., and Steely, A. Jan 2007, Pleistocene Brawley and Ocotillo formations: Evidence for initial strike-slip deformation along the San Felipe and San Jacinto fault zones, California: Journal of Geology, v. 115, p. 43-62.

Lutz, A.T., 2005, Tectonic controls on Pleistocene basin evolution in the central San Jacinto fault zone, southern California, [M.S. thesis]: Eugene, University of Oregon, 136 p.

Lutz, A.T., Dorsey, R.J., Housen, B.A., and Janecke, S.U., 2006, Stratigraphic record of Pleistocene faulting and basin evolution in the Borrego Badlands, San Jacinto fault zone, southern California: Geological Society of America Bulletin, v. 118, p. 1377-1397; DOI: 10.1130/B25946.1.

Magistrale, H., 2002, The relation of the southern San Jacinto fault zone to the Imperial and Cerro Prieto faults. Special Paper 365: Contributions to Crustal Evolution of the Southwestern United States: Vol. 365, pp. 271–278.

Matti, J.C., and Morton D.M., 1993, Paleogeographic evolution of the San Andreas Fault in Southern California: A reconstruction based on a new cross-fault correlation. In: Powell, R.E., Weldon, R J., and Matti, J.C. Eds., The San Andreas Fault System: Displacement, Palinspastic Reconstruction, and Geologic Evolution. Geological Society of America Memoir 178, p. 107-159.

McCaffrey R., 2005, Block kinematics of the Pacific-North America plate boundary in the southwestern United States from inversion of GPS, seismological, and geologic data: Journal of Geophysical Research,110, B07401, doi:10.1029/2004JB003307.

Meade, B. J., and B. H. Hager, 2005, Block models of crustal motion in southern California constrained by GPS measurements: Journal of Geophysical Research, VOL. 110, B03403, doi:10.1029/2004JB003209.

Meisling, R., and Weldon, K., 1989, Late Cenozoic tectonics of the northwestern San Bernardino Mountains, Southern California: Geological Society of America Bulletin, 101, p. 106-128.

Morton, D.M., 1999, Preliminary digital geologic map of the Santa Ana 30'x60' quadrangle, southern California, version 1.0. : U.S. Geological Survey Open-File Report 99-172, U.S. Geological Survey, California.

Morton, D.M., and Matti, J.C., 1993, Extension and contraction in an evolving divergent strike-slip fault complex: the San Andreas and San Jacinto fault zones at their convergence in Southern California, in Powell, R.E., Weldon, R.J., and Matti, J.C., eds., The San Andreas fault system: displacement, palinspastic reconstruction, and geologic evolution: Geological Society of America Memoir v. 178, p. 217-230.

Morton, D.M., and Kennedy, M.P., 2003, Geologic Map of the Bachelor Mountain 7.5' Quadrangle, Riverside County, California: U.S. Geological Survey Open-File Report 03-103.

Rockwell, T., Loughman, C., and Merifield, P., 1990, Late Quaternary rate of slip along the San Jacinto fault zone near Anza, Southern California: Journal of Geophysical Research, v. 95, p. 8593-8605.

Rockwell, T.K., Seitz, G., Dawson, T., Young, J., 2006, The long record of San Jacinto fault paleoearthquakes at Hog Lake: Implications for regional patterns of strain release in the southern San Andreas fault system: Seismological Research Letters, v. 77, no. 2, p. 270.

Rogers, T.H., 1965, Santa Ana sheet: California Division of Mines and Geology Geologic Map of California, scale, 1:250,000.

Sanders, C.O., 1989, Fault segmentation and earthquake occurrence in the strike-slip San Jacinto fault zone, California. In: Schwartz, D. P.; Sibson, R. H. (eds.) Proceedings of Conference XLV; a workshop on Fault segmentation and controls of rupture initiation and termination, U. S. Geological Survey Open-File Report OF 89-0315, p. 324-349.

Savage, J. C., and W. H. Prescott, 1973, Precision of Geodolite distance measurements for determining fault movements: Journal of Geophysical Research, 78, 6001–6008.

Savage, J. C., Prescott, W.H., 1976, Strain accumulation on the San Jacinto Fault near Riverside, California: Bulletin of the Seismological Society of America, vol.66, no.5, pp.1749-1754, Oct 1976

Savage, J.C., Prescott, W.H., Lisowski, M., and King, N., 1979, Deformation across the Salton Trough, California 1973-1977: Journal of Geophysical Research, 84, p. 3069-3079.

Sharp, R.V., 1967, San Jacinto fault zone in the Peninsular Ranges of Southern California: Geological Society of America Bulletin, 78:705-729.

Sharp, R.V., 1972, Map showing recently active breaks along the San Jacinto fault zone between the San Bernardino area and Borrego Valley, California: U. S. Geological Survey Miscellaneous Geologic Investigations Map 1-675, scale 1:24,000, 3 sheets.

Sharp, R.V., 1975, En echelon fault patterns of the San Jacinto Fault zone. In: Crowell, J.C. (ed.) San Andreas Fault in southern California; a guide to San Andreas Fault from Mexico to Carrizo Plain: Special Report - California Division of Mines and Geology, n. 118, p. 147-152.

Sharp, R.V., 1979, Some characteristics of the eastern Peninsular Ranges mylonite zone: Open-File Report - U. S. Geological Survey, Report: OF 79-1239, pp.258-267.

Sharp, R.V., 1981, Variable rates of late Quaternary strike slip on the San Jacinto fault zone, Southern California: Journal of Geophysical Research, v. 86, p. 1754-1762.

Shearer, P., Hauksson, E. and Lin, G., 2005, Southern California hypocenter relocation with waveform cross-correlation; Part 2, Results using source-specific station terms and cluster analysis: Bulletin of the Seismological Society of America, 95, 904-915.

Steely, A.N., 2006, The evolution from late Miocene west Salton detachment faulting to cross-cutting oblique strike-slip faults in the southwest Salton Trough, California [M.S thesis]: Utah State University, 253 p. 3 plates. Scale 1:24,000.

Steely, A.N., Janecke, S.U., Dorsey, R.J., and Axen, G.J. (in press) Early Pleistocene initiation of the San Felipe fault zone, SW Salton Trough, during reorganization of the San Andreas fault system: Geological Society of America Bulletin, 2009.

Weldon, R.J., Meisling, K.E., and Alexander, J., 1993, A Speculative history of the San Andreas fault in the central Transverse Ranges, in, Powell, R.E., Weldon, R.J., and Matti, J. eds., The San Andreas fault system; displacement, palinspastic reconstruction, and geologic evolution: Geological Society of America Memoir 178, p. 161-178.

Winker, C.D., and Kidwell, S.M., 1996, Stratigraphy of a marine rift basin: Neogene of the western Salton Trough, California. In Abbott, P.L., and Cooper, J.D., (eds.), Field conference guidebook and volume for the annual convention, San Diego, California, May, 1996, Bakersfield, California, Pacific Section: American Association of Petroleum Geologist, p. 295-336.

11

Table 1. Summary of slip rates across the San Jacinto fault zone (From Janecke et al., in prep.)

Author (in chronological order)	Method	Rate for SJFZ	Rate for SAF	Time scale	Comments
Coolidge and Whitten, 1956 As cited in Sharp, 1967	geodetic network Very long baseline	24 mm/yr¥	ND	Short	
Sharp, 1967	Geologic	25 mm/yr	ND	~1 Ma	
Savage and Prescott, 1976	geodetic network	25 mm/yr¥	ND	6 yrs	
Savage et al., 1979	Long baseline	17±9 mm/yr¥	25±8 mm/yr	4 yrs	
Sharp, 1981	paleoseismology	10±2 mm/yr 8-12 mm/yr	ND	since 0.73 Ma	Lowest rate from paleoseismic or neotectonic study
King and Savage, 1983	Long baseline	(SJFZ=88% of SAF) 21.9 mm/yr#	(SJFZ=88% of SAF) 25 mm/yr#	8 yrs	
Rockwell et al., 1990	Paleoseismology /neotectonic	10±2 mm/yr 8-12 mm/yr is preferred, 5-23 mm/yr is the total range of results	ND	50 kyr	
Morton and Matti, 1993	Geologic	25-30 km/1.5m.y. 17.4-20 mm/yr		1.4 Ma	
Matti and Morton, 1993	Geologic	25-30 km/1.2 m.y. 20.1 to 25 mm/yr		1.2 Ma	
Bennett et al., 1996	GPS	9±2 mm/yr	23±2 mm/yr	15 yrs	Lowest rate from GPS analysis
Kendrick et al., 2002	neotectonics	> 20 mm/yr			
Anderson et al., 2003	GPS	SJFZ>=SAF ≥19.5 mm/yr#	SJFZ>=SAF ≤ 19.5 mm/yr#	15 yrs	Highest rate from GPS analysis
McCaffrey, 2005	GPS	13.5 mm/yr	25.3 mm/yr	15 yrs	
Meade and Hager, 2005	GPS block model	11.9±1.2 mm/yr	23.3 ± 0.5	15 years	
Fay and Humphreys, 2005	GPS	14.5 ±0.8 mm/yr	22.3±0.7 mm/yr	15 yrs	
Becker et al., 2005	GPS plus stress inversion	15.3±11 14.5±9	23±8 mm/yr 22.9±8 mm/yr	15 yrs	
Rockwell et al., 2006*	paleoseismology	>16 mm/yr	ND	4 kyr	Highest rate from paleoseismic or neotectonic study, but this rate could be in error (T. Rockwell, per comm., 2007)
Fialko, 2006	InSAR plus GPS	20±1 mm/yr	25± 3 mm/yr	8 yrs-InSAR, 20 yrs GPS	
This study	Lifetime geologic slip rate	17.8 +2.6 -2.3 mm/yr	ND	0.8 to 1.3 Ma	

¥Linear slip rate was calculated from the rotational strain rate reported in this article

*Site crosses just one of several strands that were active in the Quaternary (Janecke, unpublished data) and therefore may capture less than the full slip rate. The earthquakes clustered in time, however, making the rate higher than average (Rockwell, oral comm., 2006).

We calculated a rate of slip by assuming a combined slip rate of 38.9 mm/yr across both the San Jacinto and southern San Andreas fault. This value is the average of all the rates in this table.

12

Table 2A Lifetime slip rates across the San Jacinto fault zone

Fault zone	Fault within fault zone	Structural segment (s) along the fault (see fig. 3b)	Slip estimate (since ~0.5 Ma)	Offset feature	Estimated age of initiation of the fault segment	Lifetime slip rate (interval rate)	Source of data used to calculate the slip rate
San Jacinto	Clark (folding in the damage zone was not included)	Santa Rosa and Arroyo Salada	14.4 km* no error was given in Sharp (1967)	Succession of tonalite, marble, migmatite, mylonite	1.0 to 1.1 Ma	13.7 +0.7 -0.6 mm/yr	Sharp, 1967; Lutz et al., 2006
San - Jacinto	Coyote Creek (folding in damage zone was not included)	Coyote Ridge	3.5±1.3 km *	Tonalite, marble, migmatite, mylonite	0.9 to 0.8 Ma	4.1 +1.9 -1.7 mm/yr	This study, updated from data in Sharp, 1967; Dorsey 2002
Total slip rate across the San Jacinto fault zone in its lifetime					**SUM**	**17.8 +2.6 -2.3 mm/yr**	**This study**

Table 2B. ~0.5 Ma slip rates across the San Jacinto fault zone

Fault zone	Fault within fault zone	Structural segment (s) along the fault (see fig. 3b)	Slip estimate (since ~0.5 Ma)	Offset feature	Estimated age of initiation of the fault segment	Lifetime slip rate (interval rate)	Source of data used to calculate the slip rate
San Jacinto	Clark	San Felipe Hills	(5.6 ±0.4 km)†	Calculated from amount of N-S shortening in Pliocene-Pleistocene sedimentary rocks	<~0.55±0.2 Ma,	≥10.2 + 6.9 -3.3 mm/yr	Kirby, 2005; Janecke et al., 2005; this study
San Jacinto	Coyote Creek	Borrego Mountain and Borrego Badlands	1-2 km†	North-dipping marker bed near contact between Olla and Diablo formations	< 0.6 Ma	2.5 ± 0.8 mm/yr	Steely, 2006, this study
Minimum slip rate across the San Jacinto fault zone since ~0.5 to 0.6 Ma					**SUM**	**(≥12.7 + 7.7 -4.1 mm/yr)**	**This study**

Table 2C Lifetime slip rate across parts of the San Felipe fault zone

Fault zone	Fault within fault zone	Structural segment (s) along the fault (see fig. 3b)	Slip estimate (since ~ 0.5 Ma)	Offset feature	Estimated age of initiation of the fault segment	Lifetime slip rate (interval rate)	Source of data used to calculate the slip rate
San Felipe	Sunset	Sunset	<2.5 km	Provenance link between displaced Ocotillo formation and its possible source area in the La Posta pluton	1.3 to 1.1 Ma	<2.1 ± 0.2 mm/yr	Steely, 2006
San Felipe	San Felipe	Pinyon Mountain and Mescal Bajada	4 to 13.5 km* 6.5 km preferred‡	West Salton detachment fault and base of the Eastern Peninsular Ranges mylonite zone	~1.3 to 1.1 Ma	~5.4 +6.9 -2.3 mm/yr ()	Steely, 2006, and this study

* displacement of crystalline markers or preexisting structural feature

† displacement is based on deformed or offset Pliocene-Pleistocene sedimentary rocks

‡Three separate methods were used to estimate the right slip and ~6.5 km is the overlap between methods. From Janecke et al., in prep.

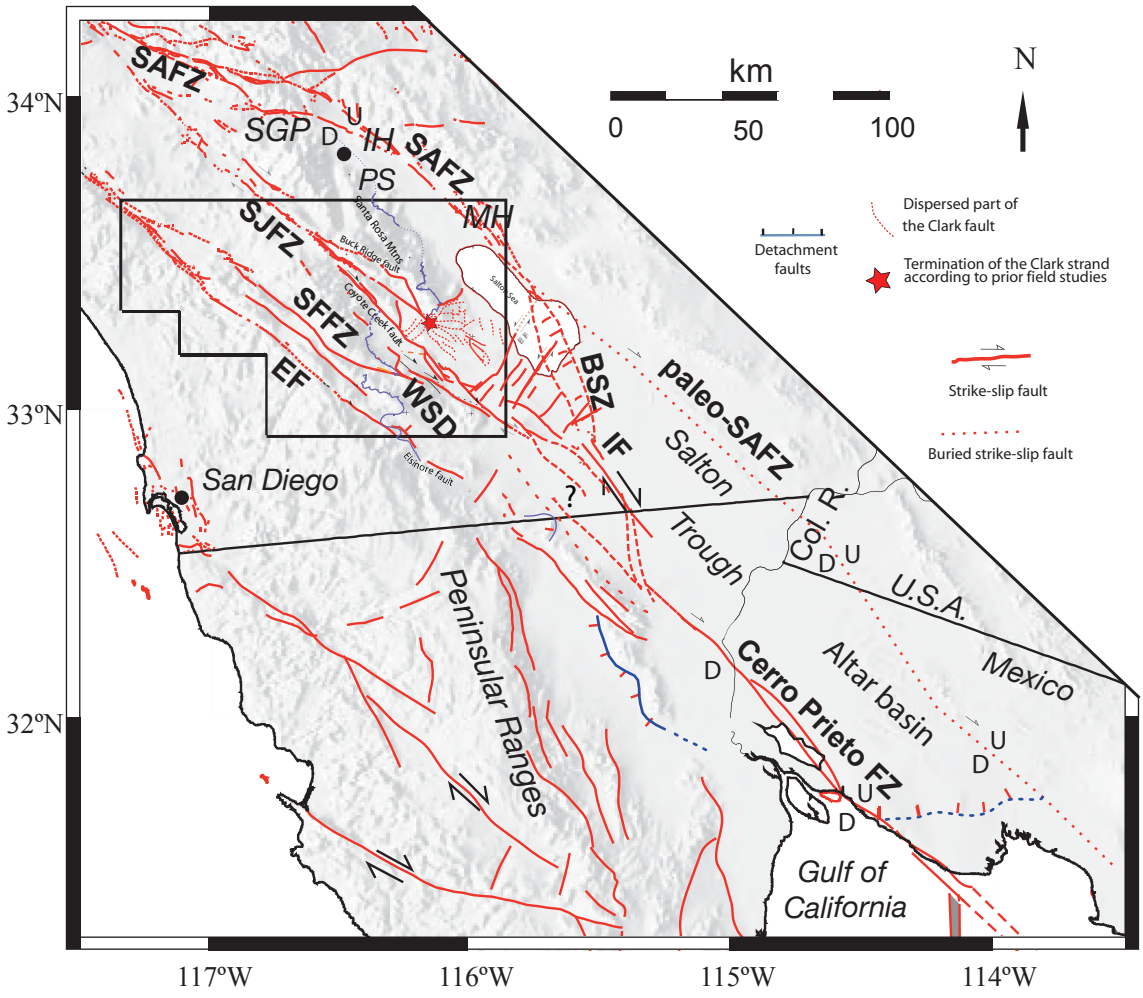

Figure 1. Regional fault map showing how the San Jacinto fault and San Felipe fault link with the southernmost San Andreas fault, Brawley seismic zone, and Imperial faults farther to the southeast. Notice that the Cretaceous mylonite (green) is offset about 15km across the Clark fault yet the fault was thought to terminate at the star by most prior workers. Spatial distributions of microseismicity are also xx (Magistrale, 2002; Shearer et al. 2005). Modified from many sources including Jennings, 1977, 1994; Janecke et al., 2004; Kirby, 2005; Hudnut et al., 1989. Axen and Fletcher, 1998, Steely, 2006, Lutz, 2005, Kirby 2005; Janecke, unpublished mapping. Need regional map that shows left step in SAF, San Timoteo badlands Tectonic overview of southern California and northwestern Mexico. San Felipe fault zone (SFFZ) is in red, other strike-slip faults are in black; SAFZ-San Andreas fault zone; SJFZ-San Jacinto fault zone; EF-Elsinore fault; BSZ-Brawley Seismic Zone; IF-Imperial fault; SJFZ-San Jacinto fault zone. SGP, San Gorgonio Pass; PS, Palm Springs . Oblique-slip detachment faults are in blue including the WSD-West Salton detachment fault. Fault locations are from Jennings (1977) and Axen and Fletcher (1998). From Janecke et al., in prep.

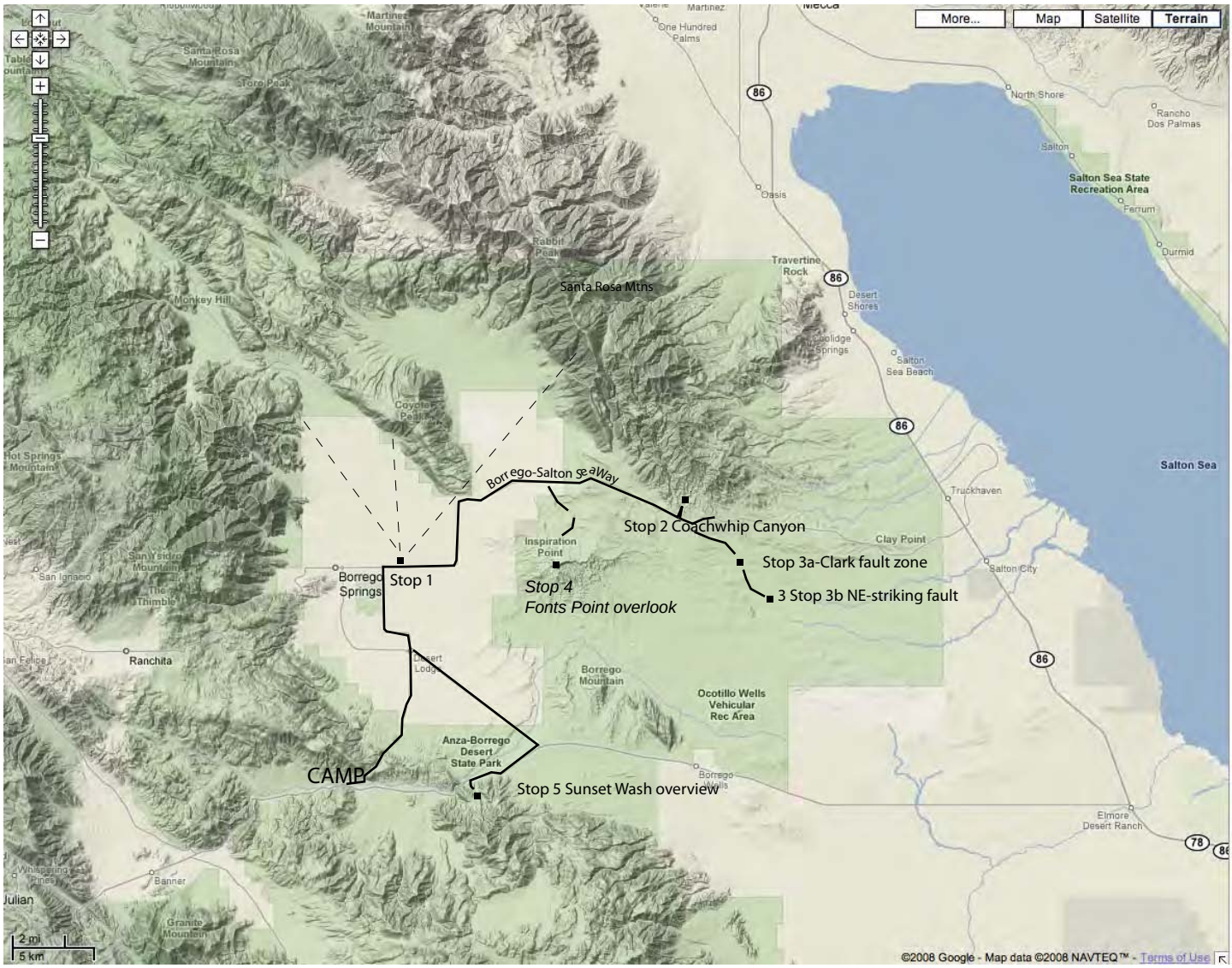

Figure 2. Map showing the locations of the stop on Day 2. Stop 4 and 5 are best visited late in the day shortly before sunset.

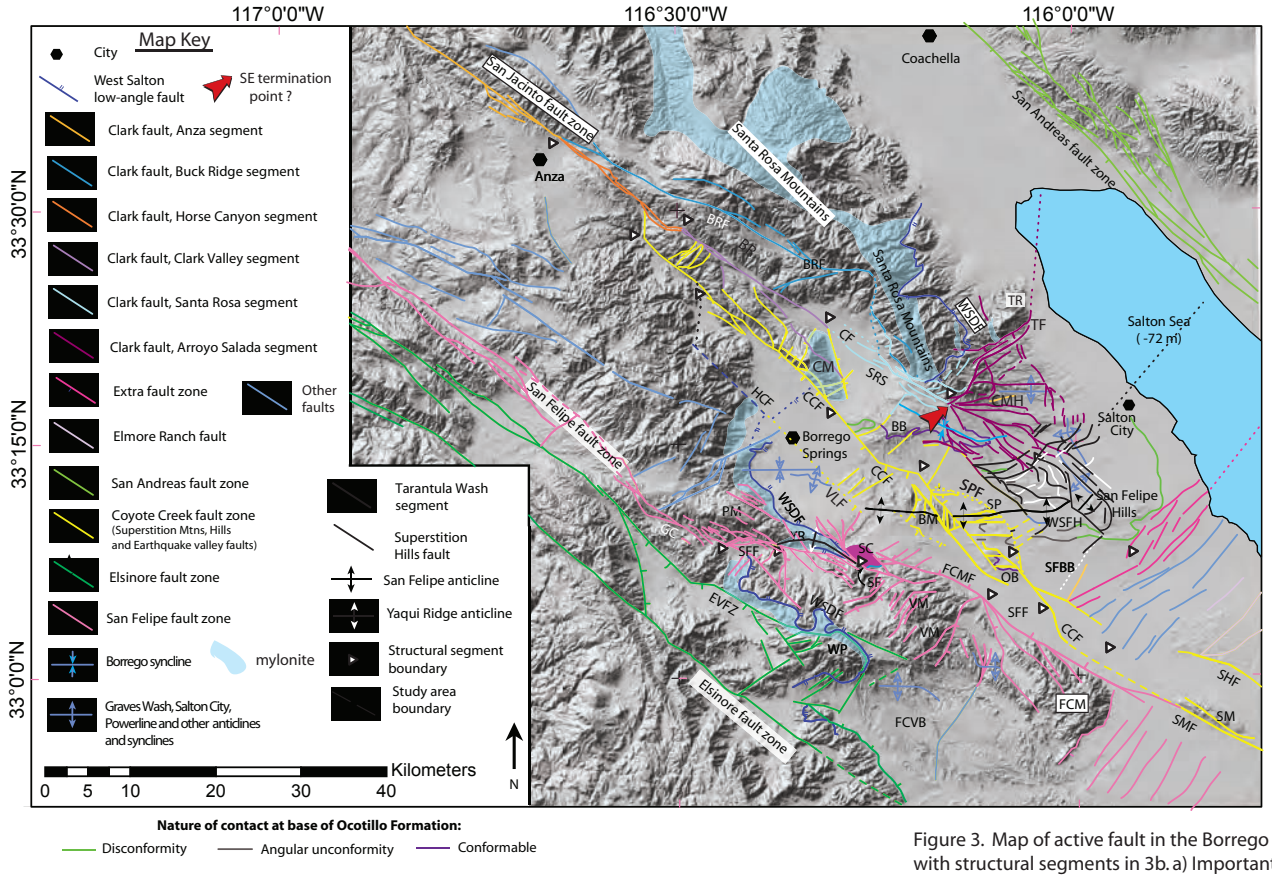

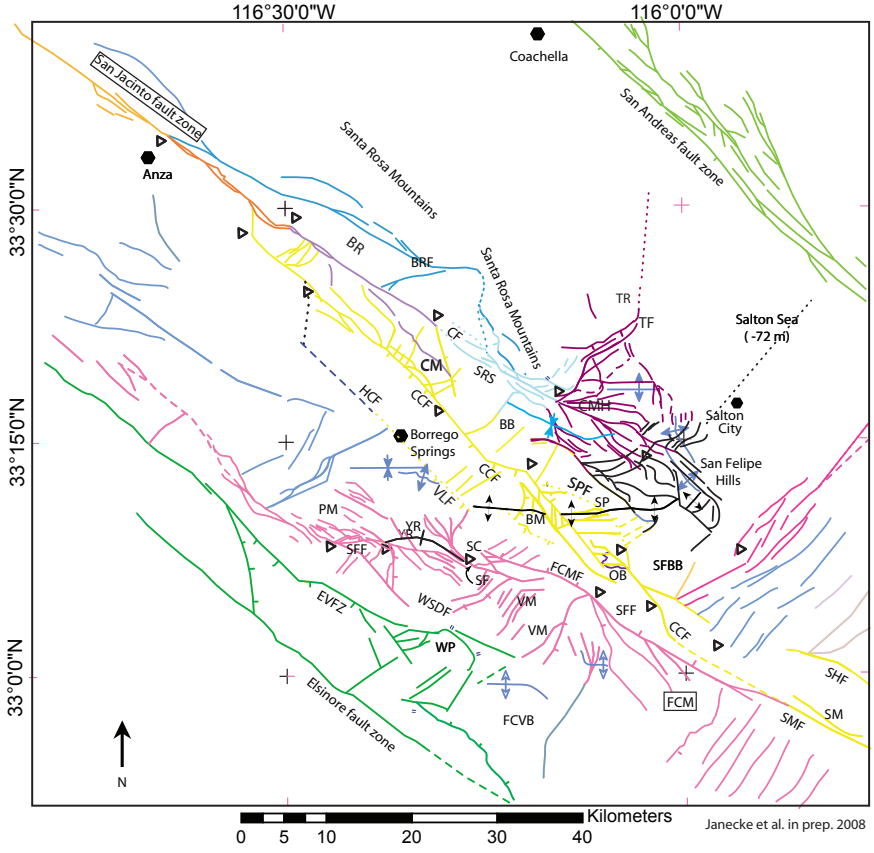

Figure 3. Map of active fault in the Borrego Springs area with structural segments in 3b. a) Important structural features of Borrego Springs area and the nature of the basal contact of the Ocotillo Formation in the SW Salton Trough. Note that the West Salton low-angle fault is folded and cut by dextral strike-slip fault zones. 3b. Names of structural segments and positions of boundaries between them are modified from Sanders (1989), Kirby (2005), Steely (2006) and this study and are placed at major bends, steps and changes in structural style. BRF-Buck Ridge fault; NW-FCMF-NW Fish Creek Mountain fault; Segments of Clark fault: AS-Arroyo Salada segment; CVS-Clark Valley segment; HCS-Horse Canyon segment; TWS-Tarantula Wash segment; CVS-Clark Valley segment; SRS-Santa Rosa segment; Segments of Coyote Creek fault: BBS-Borrego Badlands segment; BMS-Borrego Mountain segment; CRS-Coyote Ridge segment; CS-central segment; SS-Superstitions segment; SHS-Superstition Hills segment; SMS=Superstition Mountains segment. Segments of San Felipe fault zone: GC-Grapevine Canyon segment; MBS-Mescal Bajada segment; PR-Pinyon Ridge segment NF; NW-FCMF-NW Fish Creek Mountain fault; SE-FCMF-SE Fish Creek Mountain fault. Other names: BB-Borrego Badlands; BM-Borrego Mountain; BSF-Borrego Sink fold belt; Borrego syncline-BS; BRF-Buck Ridge fault; CCF-Coyote Creek fault; CF-Clark fault; DF-Dump Fault; ER-Elmore Ranch fault; EVFZ-Earthquake Valley fault zone; FCM-Fish Creek Mountains; FCMF-Fish Creek Mountains fault; FCVB-Fish Creek-Vallecito basin; GC-Grapevine Canyon; H-Henderson Canyon fault; HC-Hell Canyon fault; KF-Kane Springs fault; OB-Ocotillo Badlands; PR-Pinyon Ridge; SFH- San Felipe Hills; SM-Split Mtn anticline; SC-Sunset conglomerate of the Ocotillo Formation (xx pink); SF-Sunset fault; SFBB=San Felipe-Borrego basin; SFF-San Felipe fault; SR-Santa Rosa fault; SM-Superstition Mountain; SPF-Squaw Peak fault; SH-Superstition Hills; TB-Tierra Blanca Mountains; VLF-Veggie line fault; VM-Vallecito Mountains; VFCB= Vallecito-Fish Creek basin; WSDF-West Salton detachment fault; WP-Whale Peak; YR-Yaqui Ridge. Faults are compiled and modified from Rogers, 1965; Jennings, 1977; Kennedy and Morton, 1993; Morton, 1999; Kirby, 2005; Lutz, 2005; Kennedy, 2000; 2003; Kennedy and Morton, 2003; Morton and Kennedy, 2003; and this study. Mylonite was modified from Sharp (1979), Kairouz (2005) and Steely (2006). Modified from Janecke et al. (in prep.).

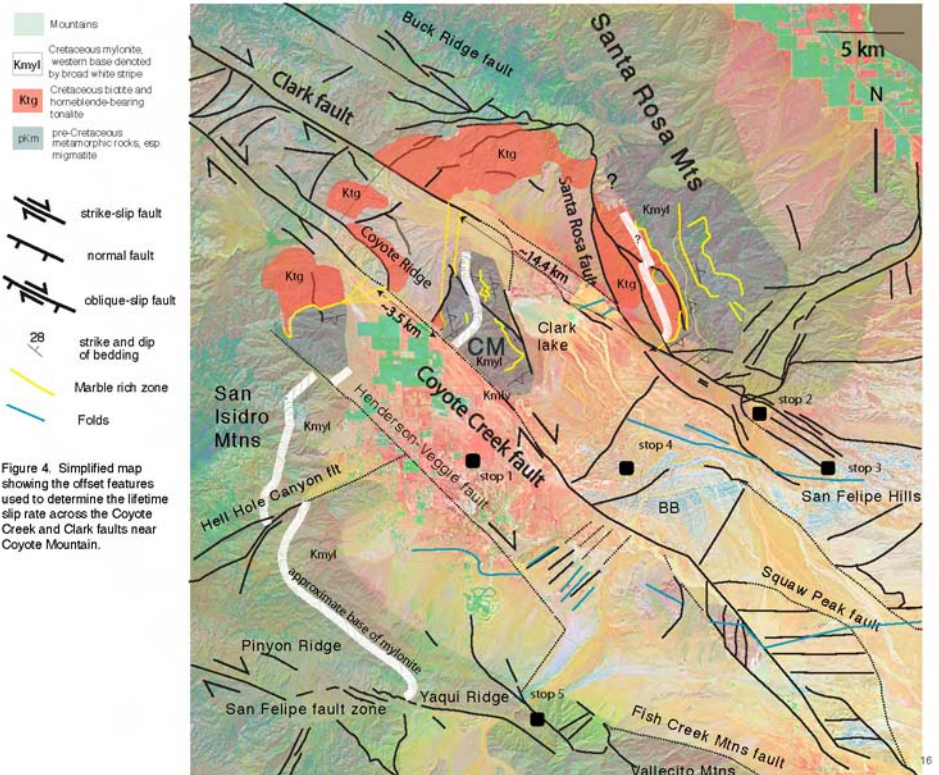

Figure 4. Simplified map showing the offset features used to determine the lifetime slip rate across the Coyote Creek and Clark faults near Coyote Mountain.

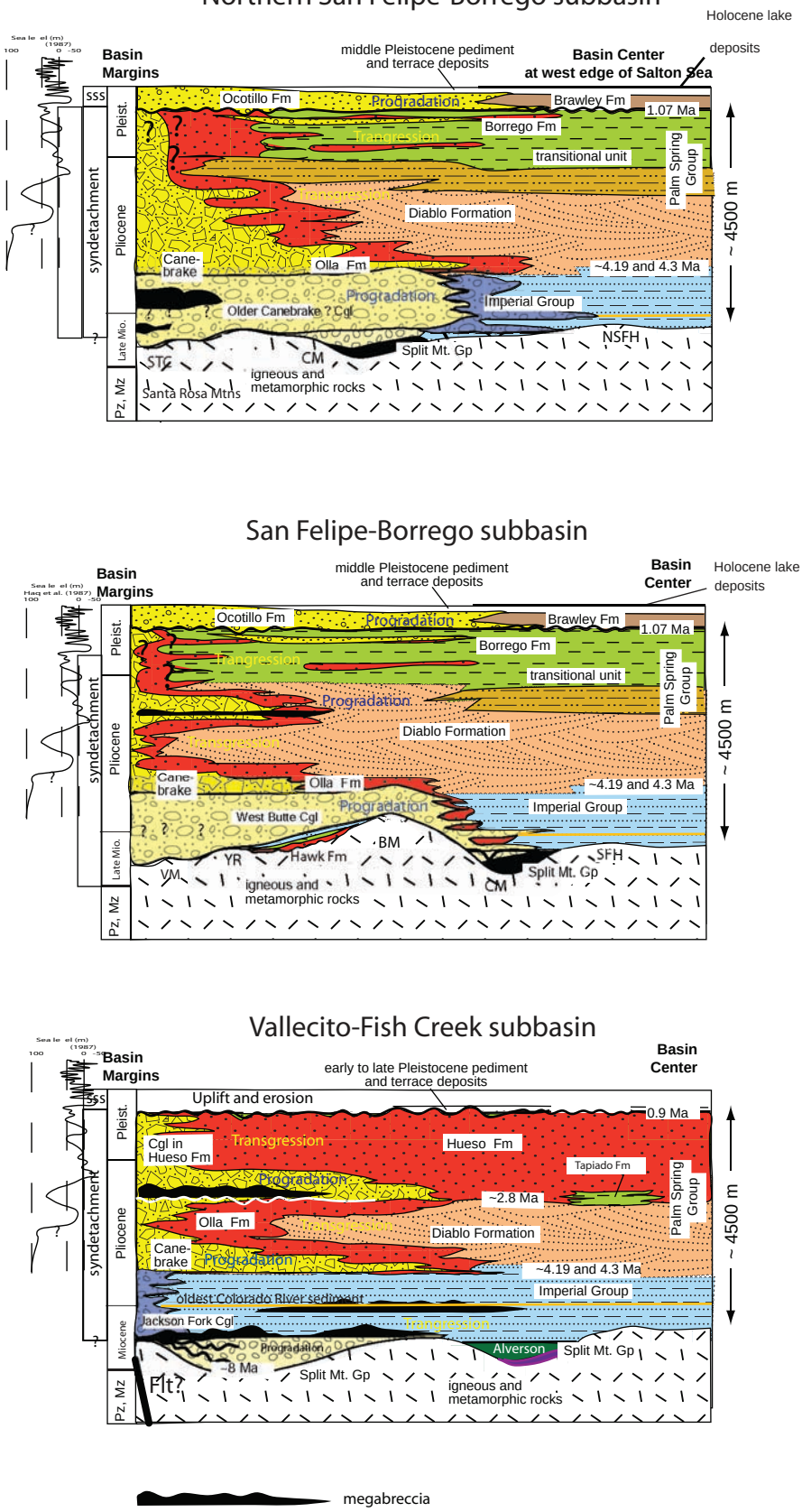

Figure 5. Simplified geologic column of the San Felipe-Borrego basin and Fish Creek-Vallecito subbasin showing lateral changes from the basin-bounding structures to the distal interior of the basin (Janecke et al., in prep.). Data from Dibblee, 1954, 1984, 1996; Winker and Kidwell, 1996; Dorsey, 2006; Dorsey et al., 2007; Kirby, 2005; Belgarde, 2007; Steely, 2006, and Janecke, unpublished mapping.

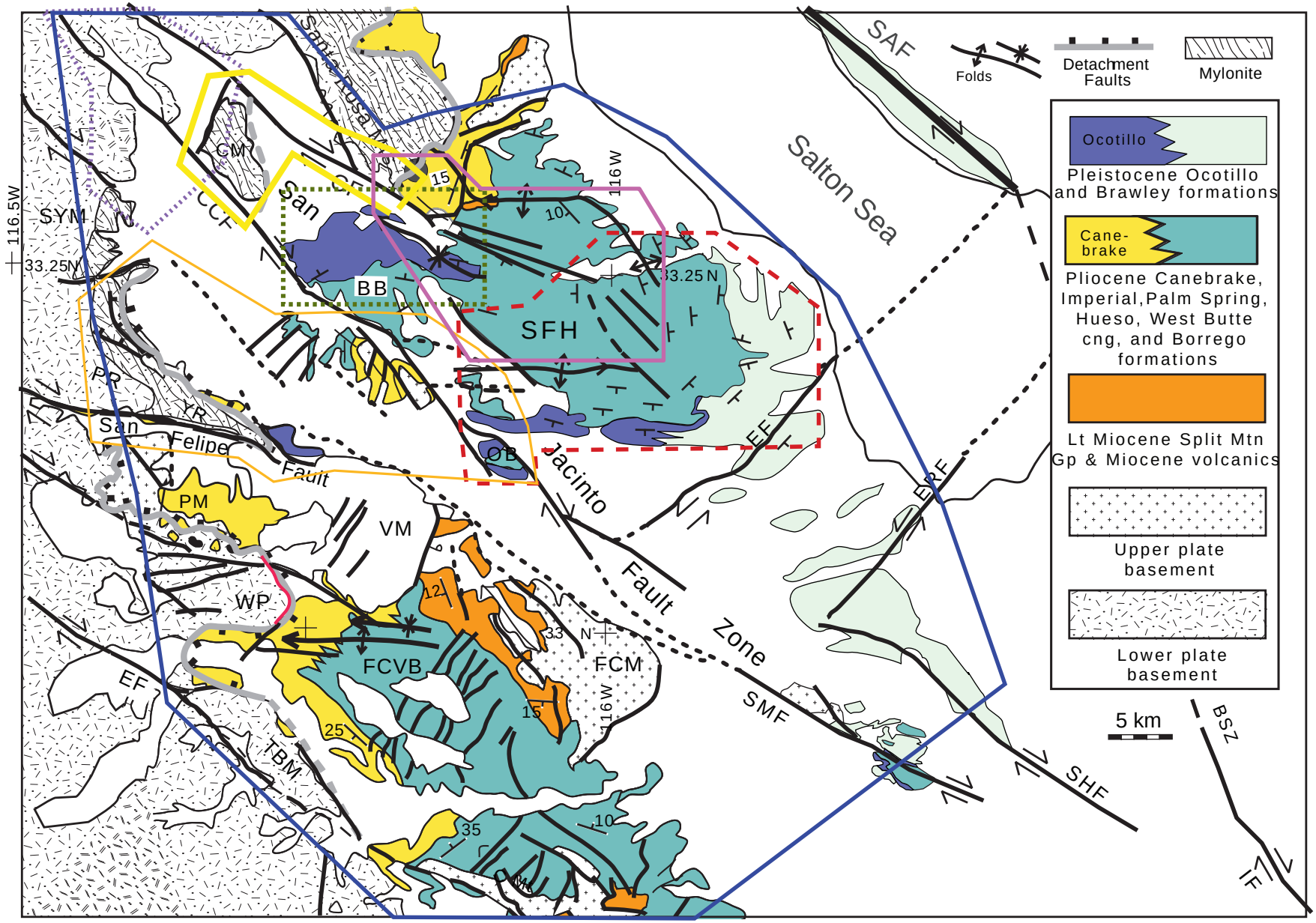

Figure 6. Regional and simplified geologic map showing the locations of recent field studies in San Jacinto and San Felipe fault zones. Kirby (2005, red outline), Lutz (2005, lime green outline), Steely (2006, orange outline), Belgarde (pink outline) and Forand (in prep., yellow), Janecke and Dorsey (unpublished, blue).

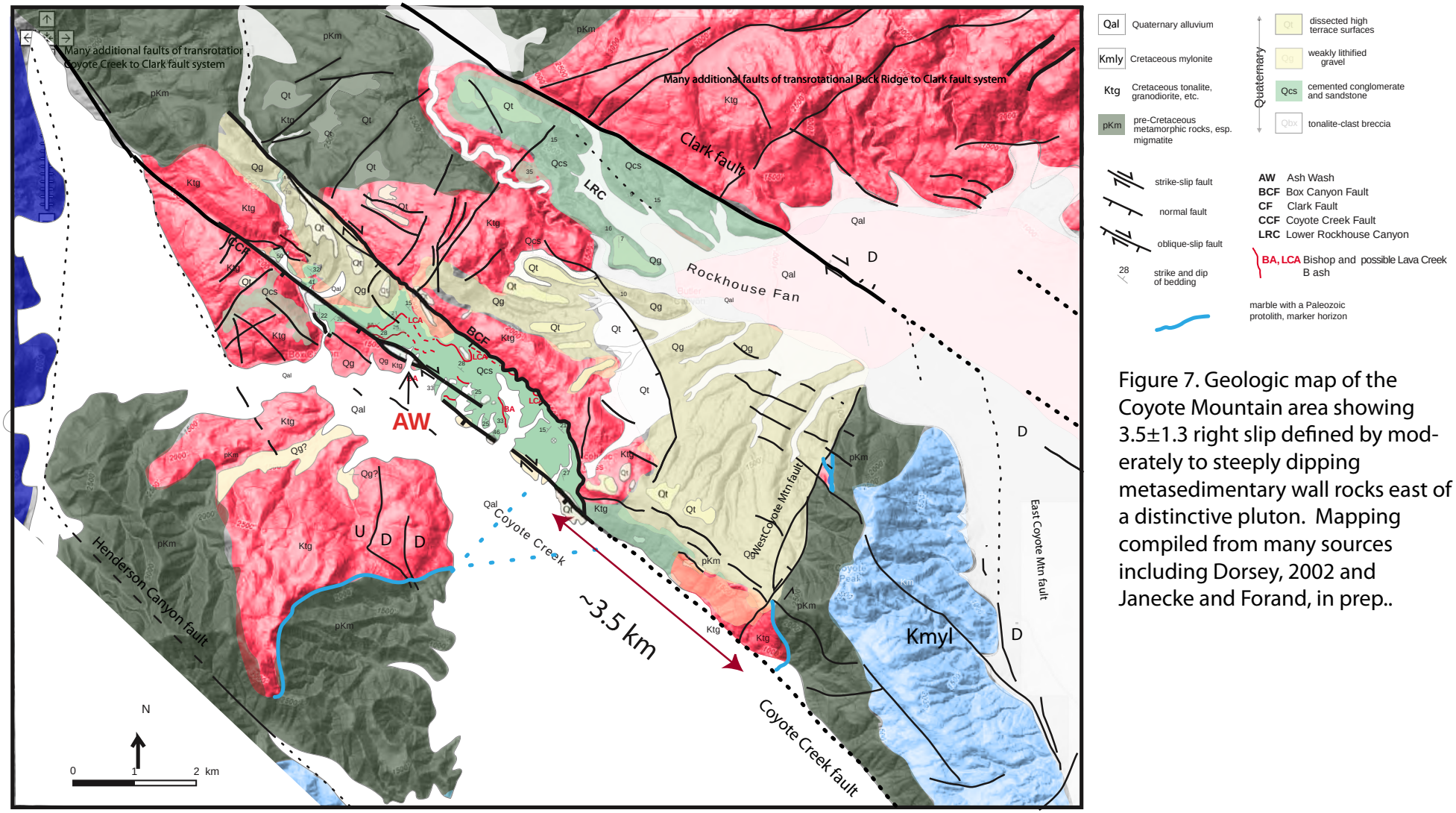

Figure 7. Geologic map of the Coyote Mountain area showing 3.5±1.3 right slip defined by moderately to steeply dipping metasedimentary wall rocks east of a distinctive pluton. Mapping compiled from many sources including Dorsey, 2002 and Janecke and Forand, in prep..

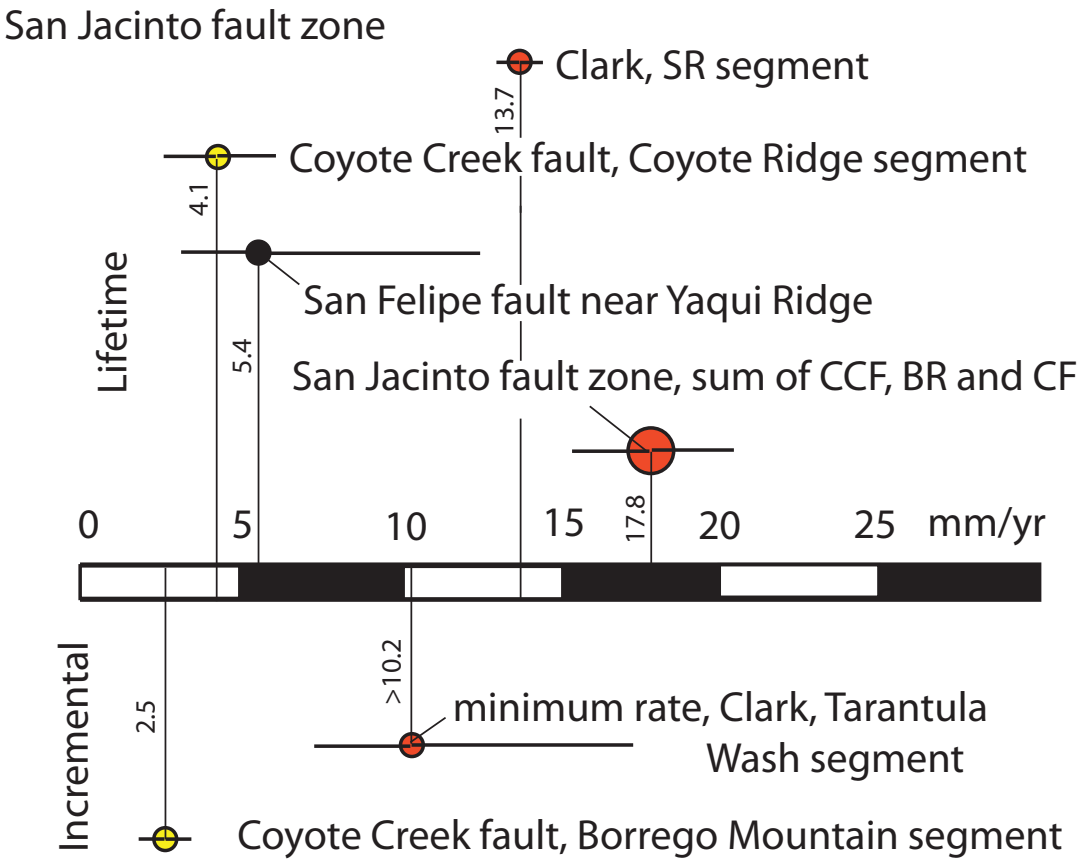

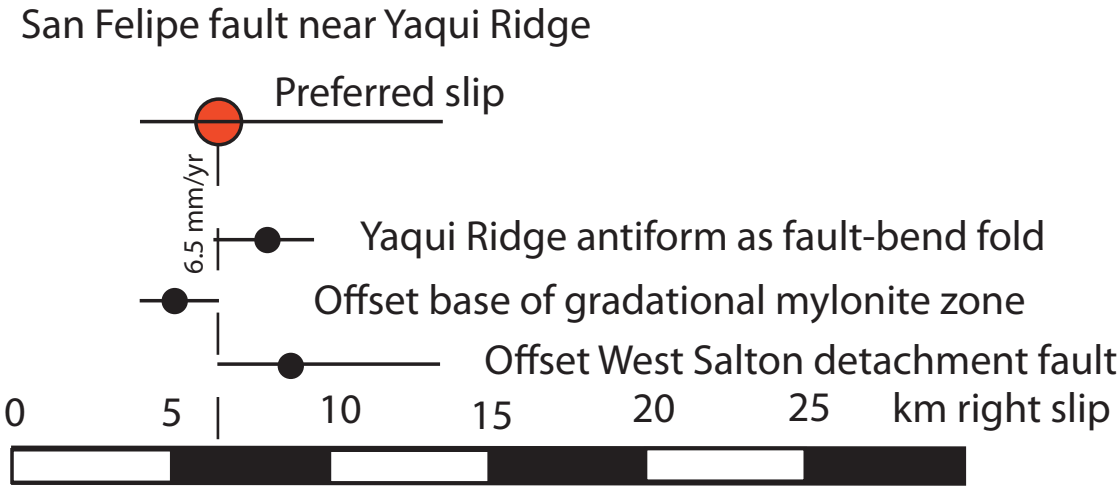

Figure 8. (a) Graph of slip rates across the San Jacinto fault zone and San Felipe fault zone. Lifetime slip rates are above the x axis and 0.5 Ma slip rates are below the x axis. CCF=Coyote Creek fault, BR=Buck Ridge fault. CF=Clark fault, SR=Santa Rosa segment.

(b) Displacement across the San Felipe fault zone near Yaqui Ridge.

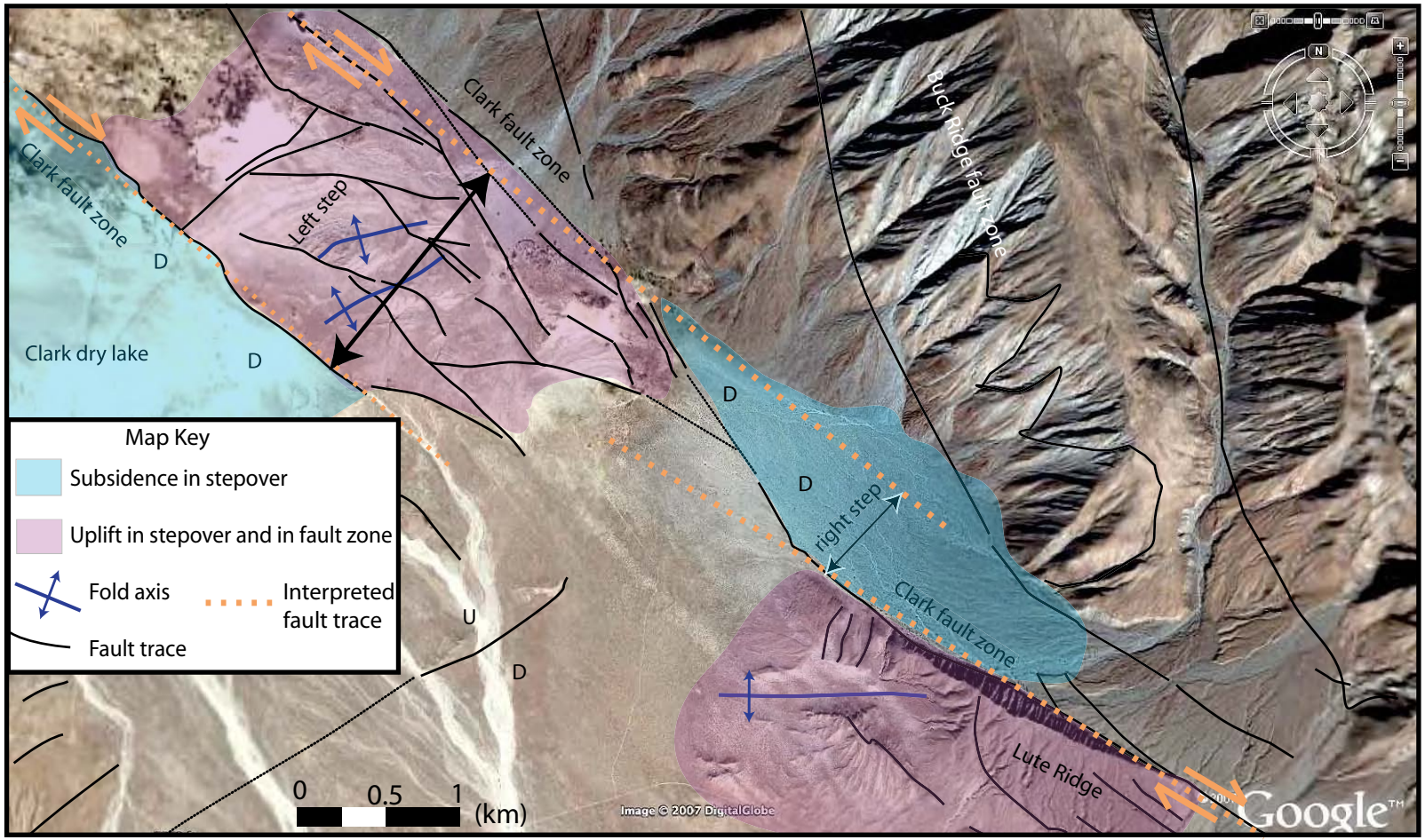

Fig. 9 Google Earth image and geology of the southeast part of the Santa Rosa Segment. Geological interpretation by S. Janecke. Notice the stepovers between the fault traces. From Belgarde (2007).

Figure 10. Geologic map of the Santa Rosa, Arroyo Salada and part of the Tarantula Wash segments of the Clark fault (Plate 1 of Belgarde and Janecke, in Belgarde 2007).

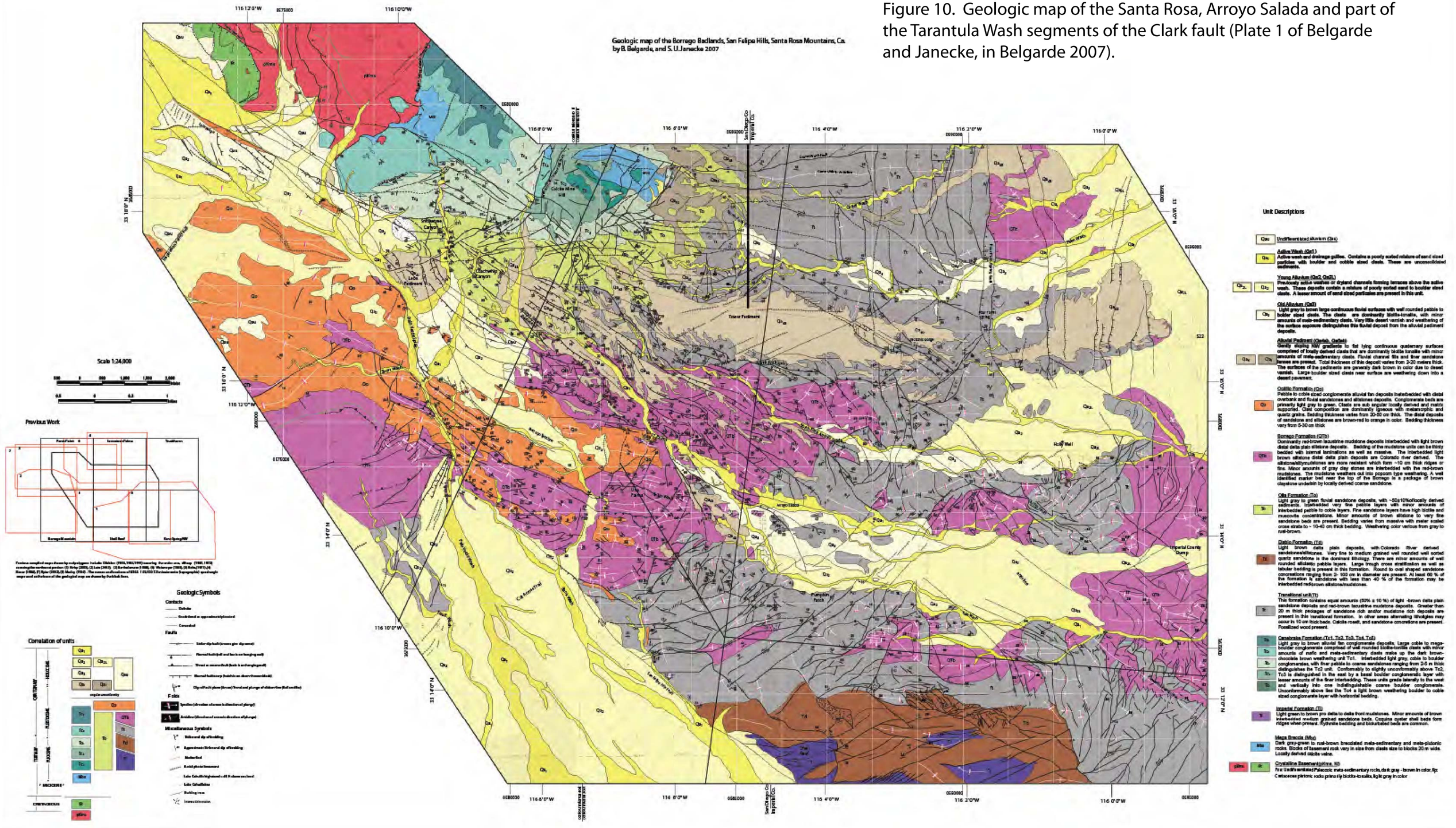

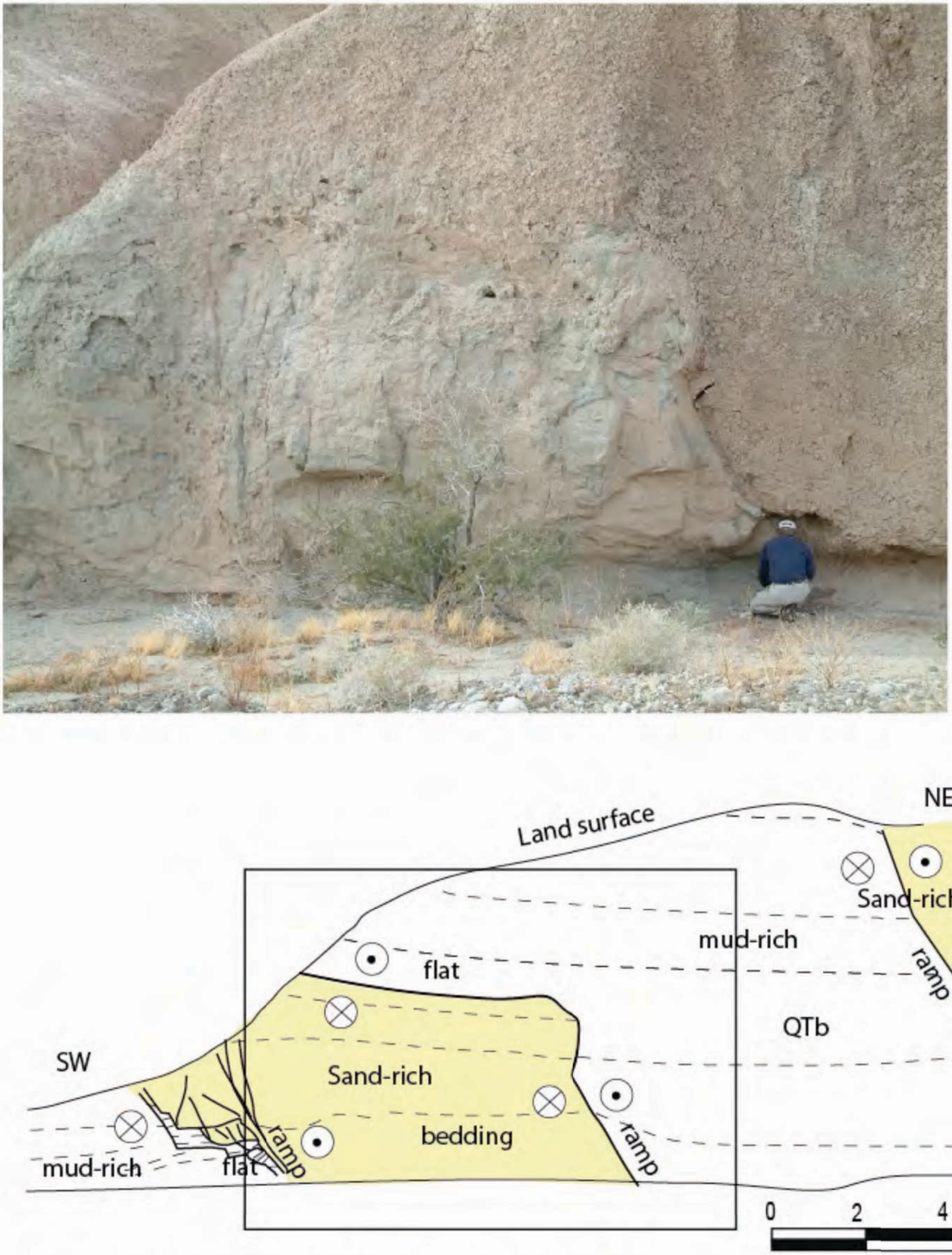

Figure 14 (a) Photograph looking NW at a strand of the Clark fault NE of Arroyo Salada. b) Sketch of ramp and flats in a dextral strike-slip fault zone with mud-rich (white) and sand-rich (yellow) sedimentary rocks. Refer to (a) for the photograph of part of this sketch. Modifield from Belgarde (2007).

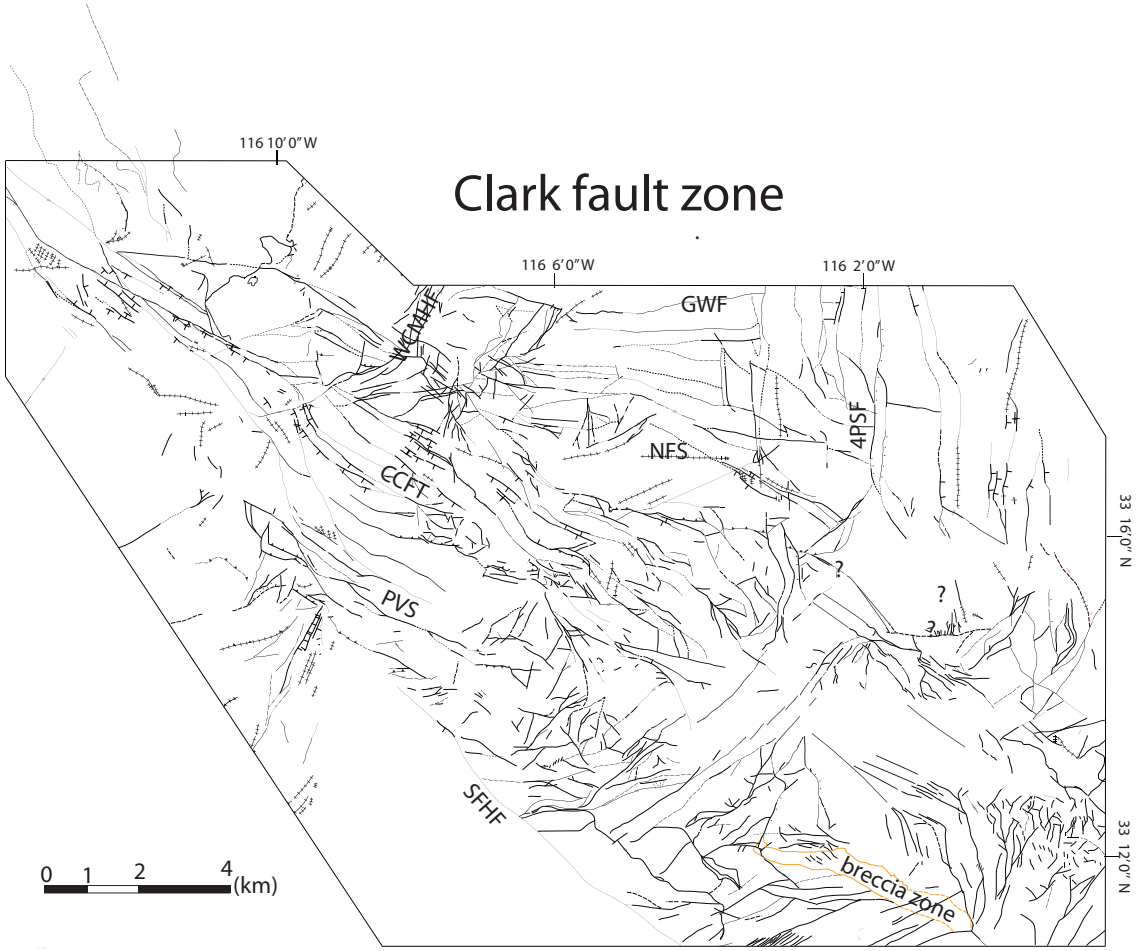

Figure 11. Simplified fault map showing the main elements of the fault zone in figure 10, including the three structural segments of the fault (Belgarde and Janecke, in Belgarde 2007). Refer to Figure 10 for legend. Modified from Belgarde (2007)

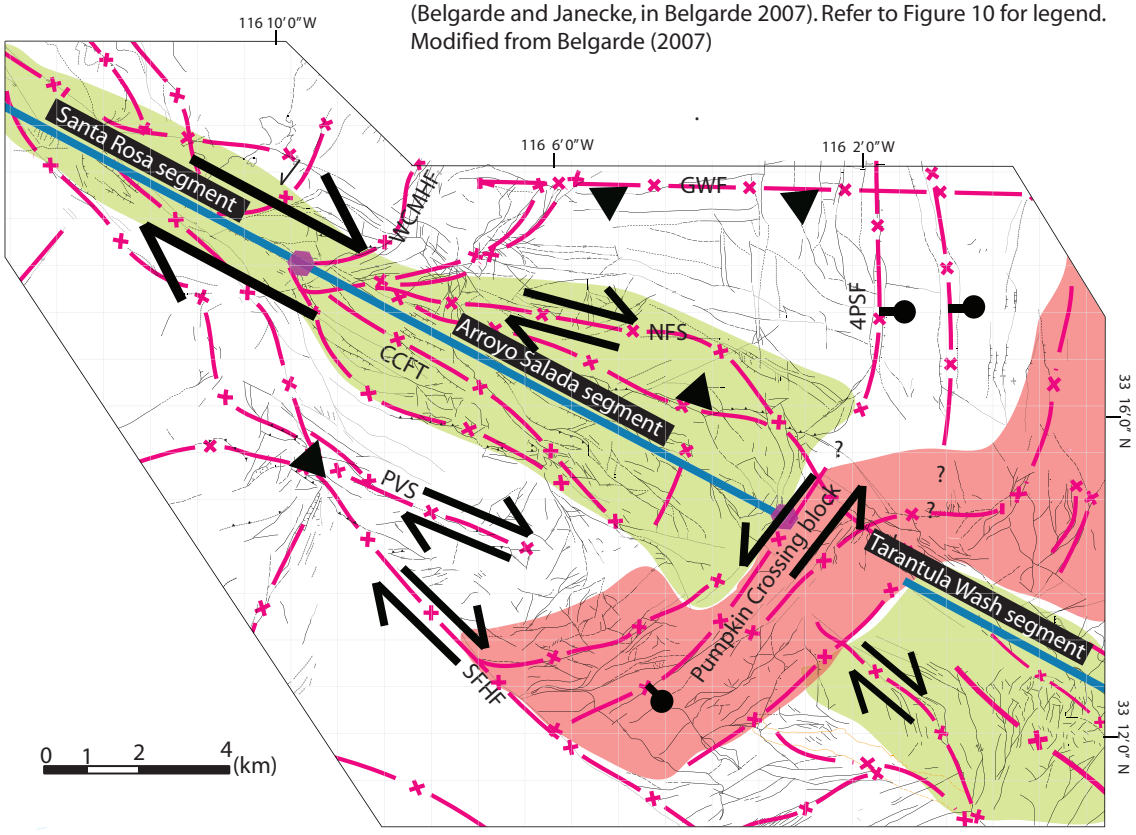

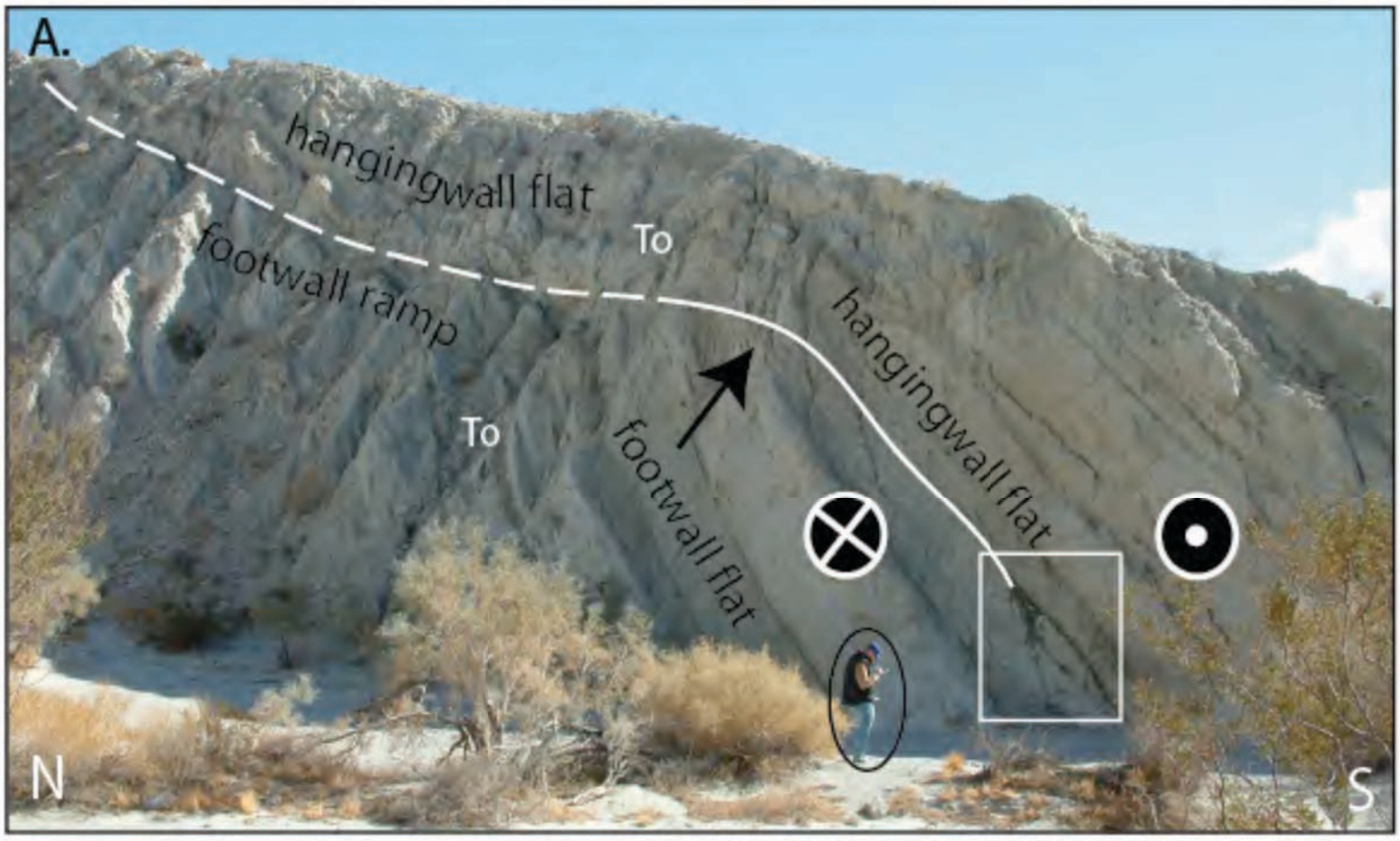

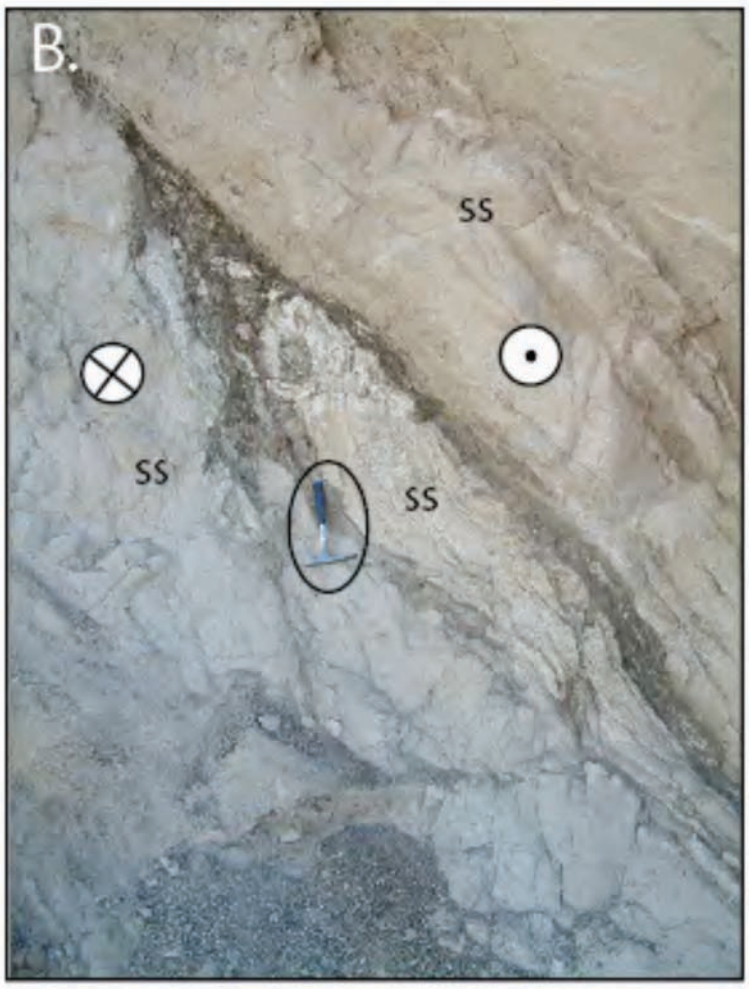

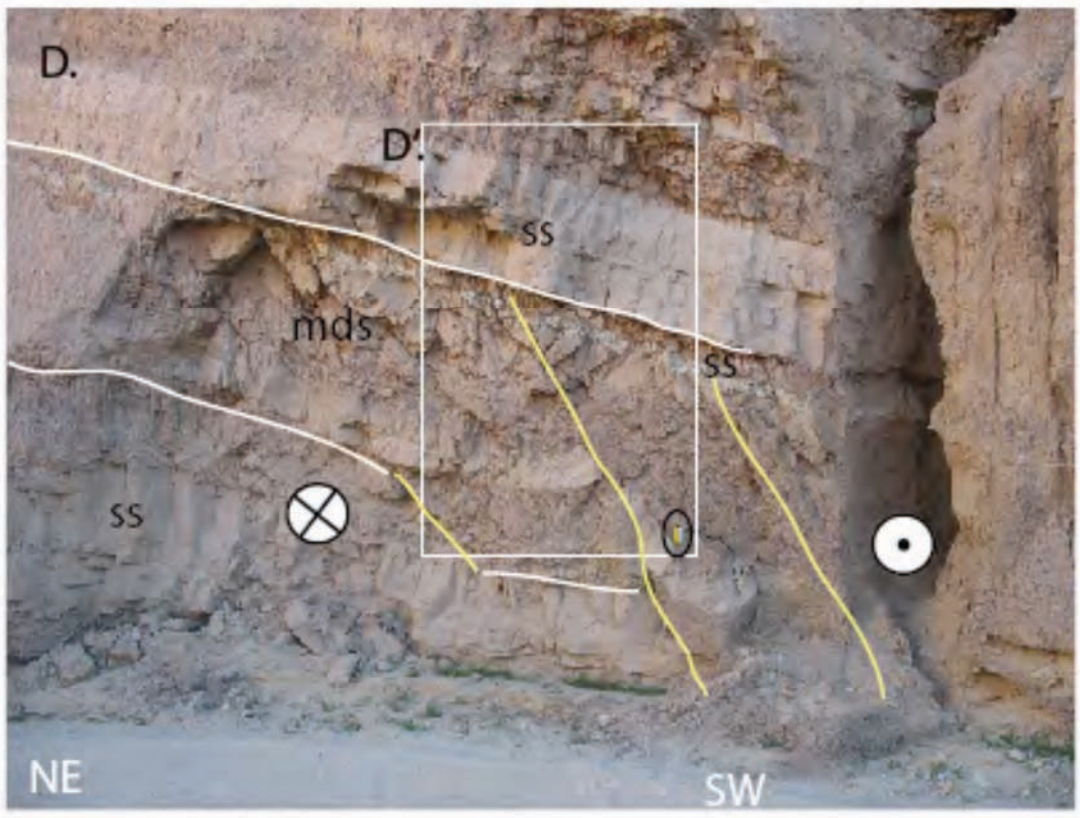

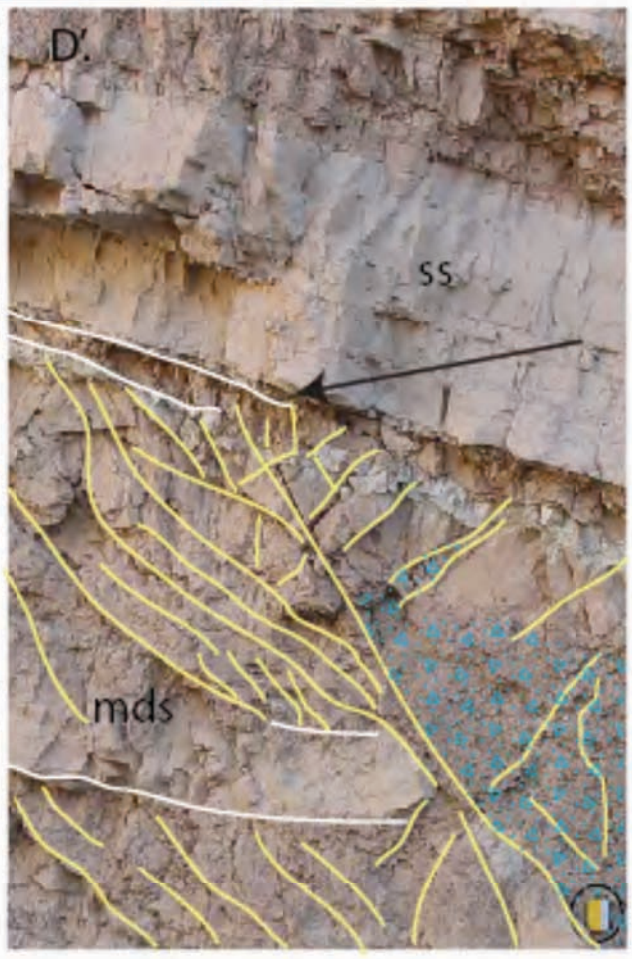

Figure 12. Stop 2. a-c Photographs looking SE along a major strand of the Clark fault with a ramp and flat geometry in Coachwhip Canyon. Clay gouge is brown and forms pods localized along a fraction of the fault zone. Elsewhere the fault is only a mm thick and difficult to identify. From Belgarde (2007). D and D' Another example of a strike slip fault with ramps and flats.

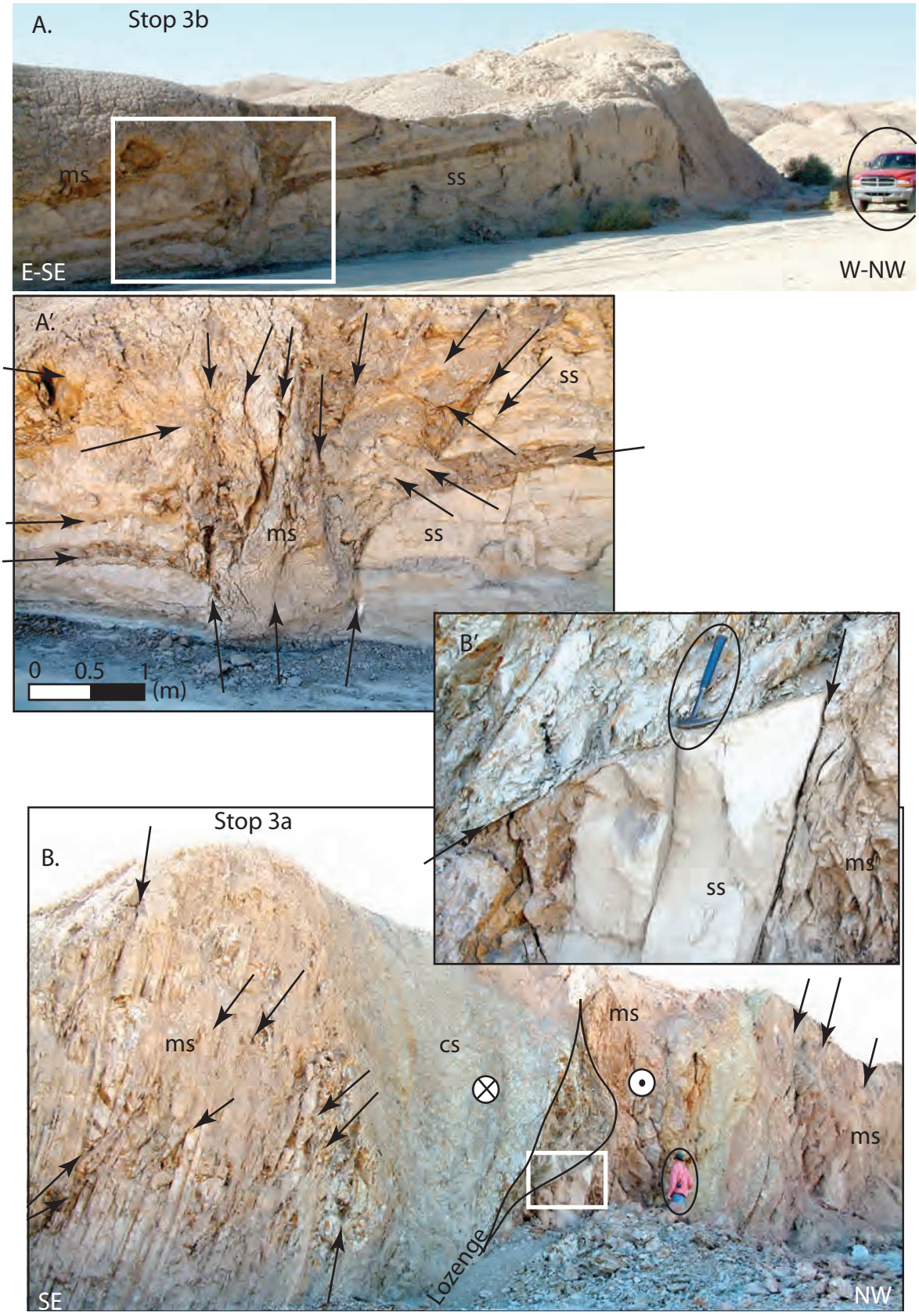

Fig. 13. (A, A′) Photograph looking at a fault zone in the transitional formation along the south side of Tule Wash (UTM, 0584259, 3677873). The fault trace has a trend of ~175° and dies out ~ 300 meters south of this outcrop. Deformation associated to the fault preferentially splays into mud-rich beds. (A) 2 m tall truck for scale (A′) Close up of the fault zone, faults are indicated by the black arrows. (B, B′) Photograph of an outcrop of a large fault along the south edge of Arroyo Salada Wash near the 17 Palms (UTM, 0583048, 3679832). 6 ft tall person for scale. Fault zone is ~ 20 meters wide and contains multiple steep fault surfaces (black arrows) and fault blocks. The general trend of this fault trace is east-west to the east of the out crop and the western extent is unclear due to the wash. The strike and dip of a major fault surface within this deformation zone is 65,65° SE and the rake of slickenlines are ~ 18° E NE. (B′) The 3 meter tall lozenge shaped structure in the gray claystone truncates a block of undeformed sandstone, 30 cm long hammer for scale. From Belgarde (2007).

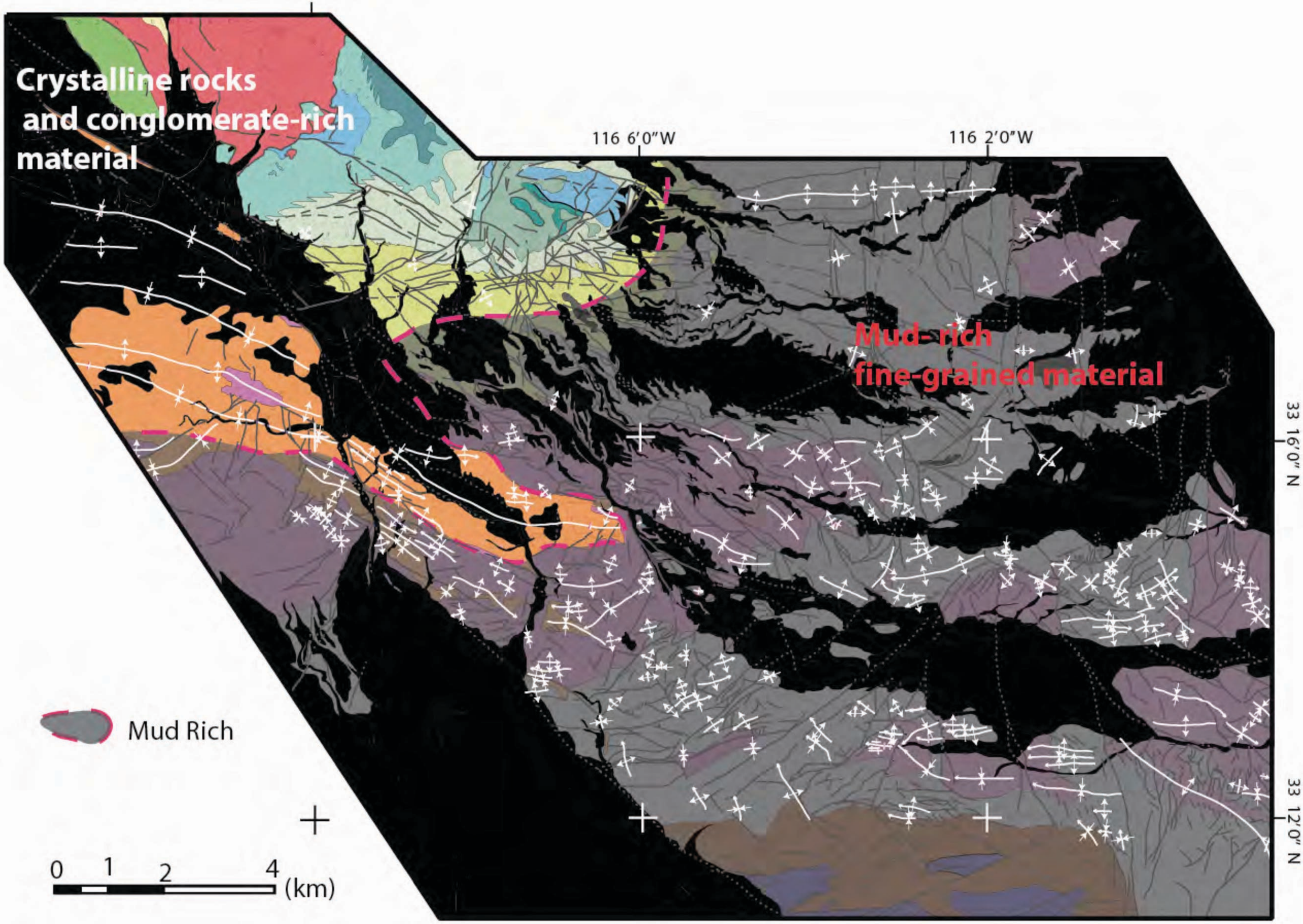

Figure 14. Geologic map illustrating the intense folding strains in the mud-rich units within the Clark fault zone (Belgarde and Janecke, in Belgarde 2007). Dark colors represent mud-rich latest Miocene to Quaternary units. Refer to Figure 10 for legend.

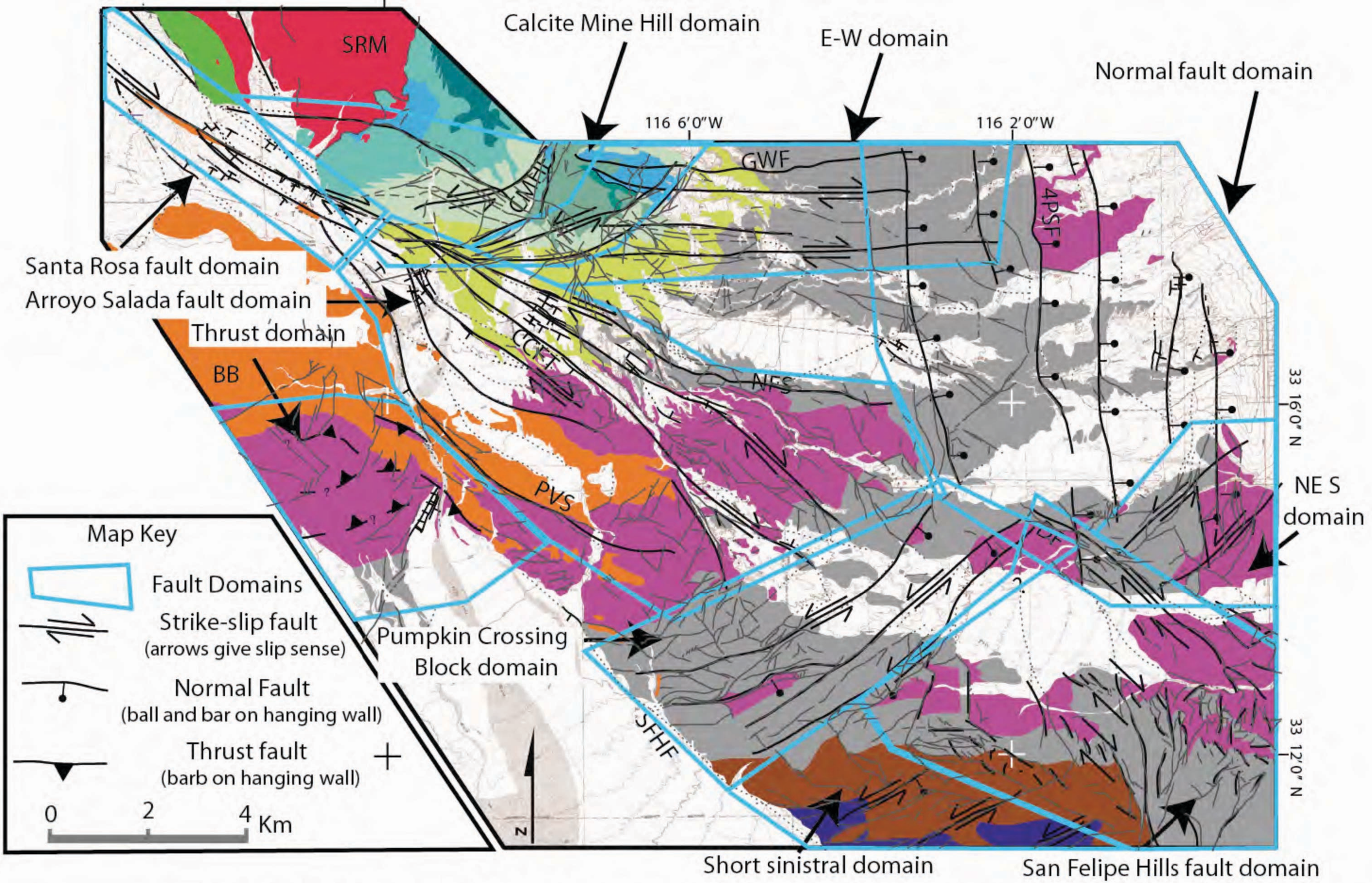

Figure 16 Fault domains of the Clark fault zone. Refer to plate 1 for the key to the geological map in the background. Major structures that characterize each domain are indicated in black. Note that most fault domains overlap. SFHF- San Felipe Hills fault; NE S- NE sinistral domain; PVS- Palo Verde Splay; NFS- North Fork Splay; CCFT- Central Clark fault trace, BB- Borrego Badlands; SRM- Santa Rosa Mountains; GWF- Graves Wash fault; 4PSF- Four Palms Spring fault; DF- Dump fault; CMHF- Calcite Mine Hill fault. Modified from Belgarde (2007).

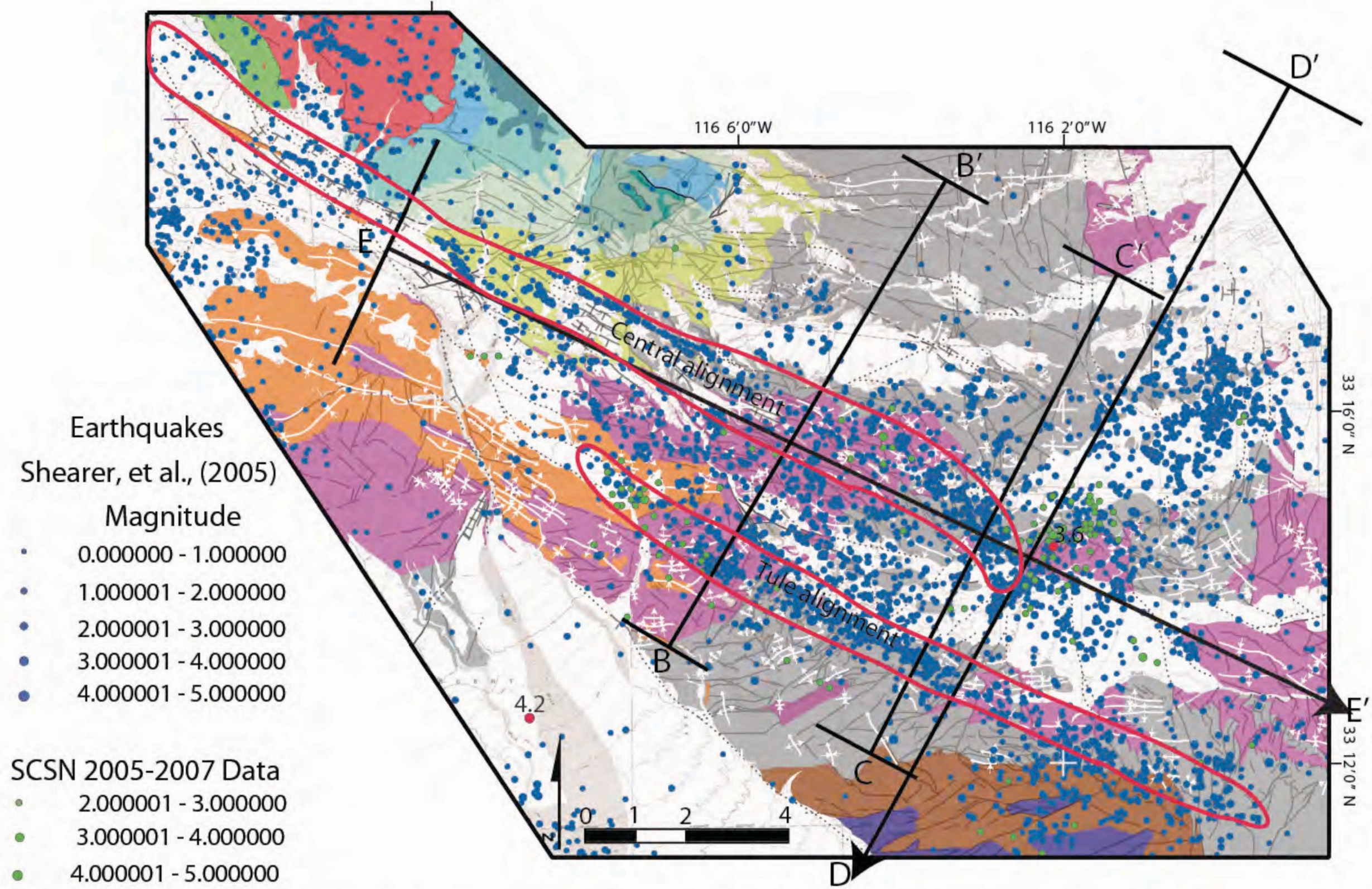

Figure 17. Correlation between microseismicity and geology of the Clark fault zone. Refer to Plate 1 for the key to the geological map. Quaternary alluvium is white. Blue epicenters are from Shearer et al's (1982-2002) catalog and green epicenters (2002-2005) are from the SCSN catalog. The most recent ML 4.2, and 3.6 earthquake epicenters are labeled and highlighted in red. Cross sections, B-B′, C-C′ and D-D′ from figure 3-16 are shown. Refer to figure 3-15 for the location of A-A′. End bars on cross sections represent width of selection zone. Note the excellent correlation between faults and earthquakes along the Central alignment abut the clear mismatch between the Tule Wash alignment and mapped structures above it. Modified from Belgarde (2007).

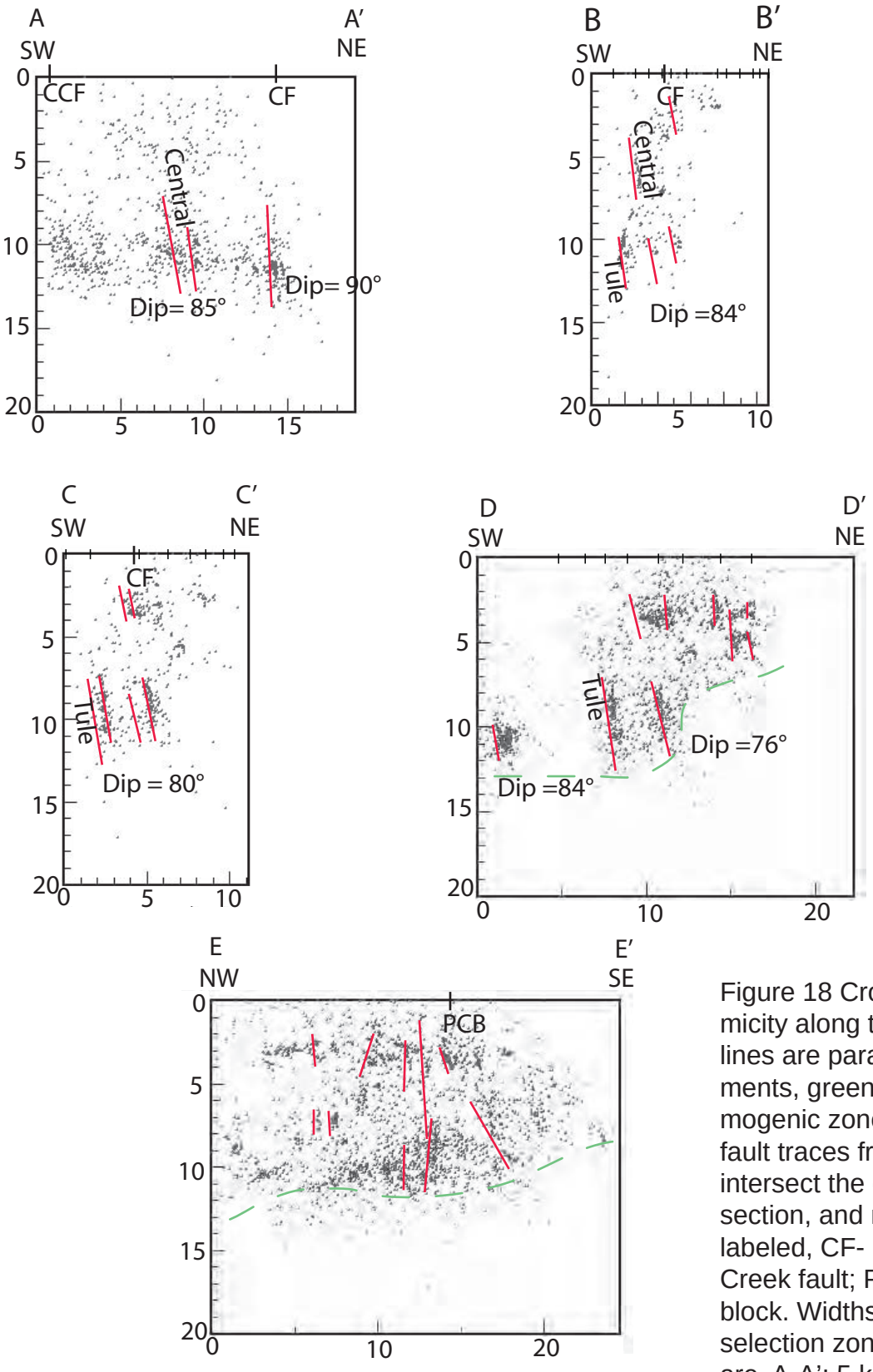

Figure 18 Cross sections of microseismicity along the Clark fault zone. Red lines are parallel to earthquake alignments, green denotes the base of seismogenic zone, Black indicates where fault traces from the geological map intersect the central trace of each cross section, and major fault traces are labeled, CF- Clark fault; CCF- Coyote Creek fault; PCB - Pumpkin Crossing block. Widths of the selection zones for each cross section are, A-A': 5 km, B-B': 2 km, C-C': 2 km, D-D': 3.5 km, E-E' 5.5 km. Modified from Belgarde (2007). Data from Shearer et al. (2005)

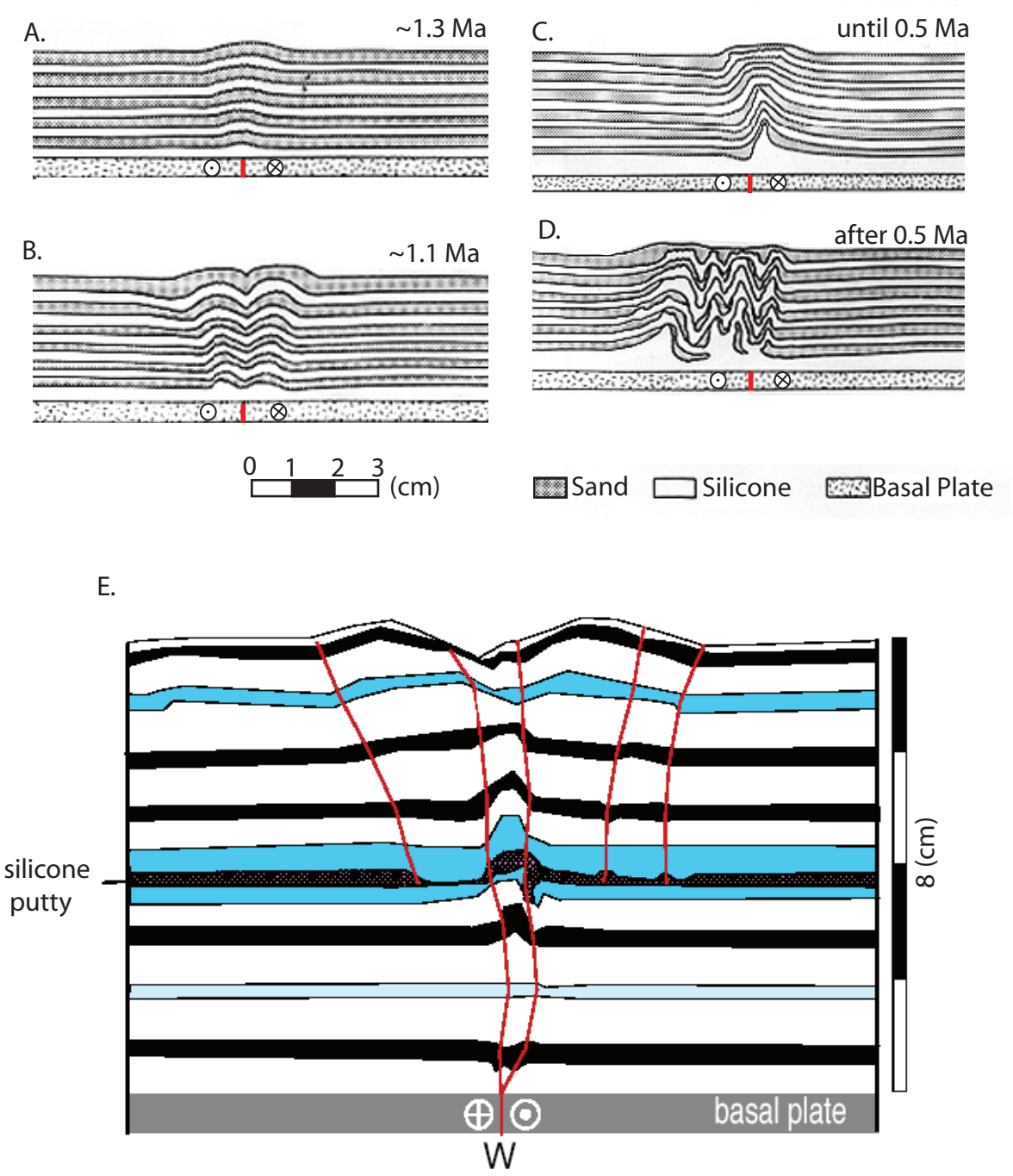

Fig. 19 Cross sectional views of laboratory experiments of strike-slip faults in sedimentary rocks. A-D from Richard et al. (1995), Cross section of models. The section lines are perpendicular to the strike-slip fault. Estimated dates of the Clark fault zone from Kirby et al. (2007). Experiments (A), (B), and (C) are shown after 8 cm of left lateral displacement; experiment (D) after 20 cm of left-lateral offset. (E) Model from Le Guerroué and Cobbold unpublished data included with permission. Cross section of a block model containing a detachment horizon made of silicone putty. Folding and related faulting due to strike slip motion of the basal plate is depicted in this cartoon of the original sandbox model. A "pitch-fork" shaped fault zone formed. From Belgarde (2007).

Early Pleistocene initiation of the San Felipe fault zone, SW Salton Trough, during reorganization of the San Andreas fault system

Alexander N. Steely*
Susanne U. Janecke†
Department of Geology, Utah State University, Logan, Utah 84322-4505

Rebecca J. Dorsey
Department of Geological Sciences, University of Oregon, Eugene, Oregon 97405, USA

Gary J. Axen
Department of Earth and Environmental Science, New Mexico Institute of Mining and Technology, Socorro, New Mexico 87801, USA

ABSTRACT

Structural and stratigraphic analyses along the western margin of the Salton Trough show that the San Andreas fault system was reorganized in early Pleistocene time from a system dominated by two fault zones (the San Andreas fault and the West Salton detachment fault) to a network of dextral faults that include the San Andreas and at least four dextral faults to the southwest. The San Felipe fault zone, one of these dextral faults, has ~5.8 ± 2.8 km of right separation and consists of three principal faults in the Peninsular Ranges. These are the San Felipe fault in the WNW, Sunset fault in the middle, and Fish Creek Mountains fault in the ESE. They form a left-stepping array and bound domains in which the Sunset Conglomerate, the older West Salton detachment fault, and Cretaceous mylonitic rocks below the detachment are folded about WNW-trending folds. A complex flower structure within the left-stepovers probably produced this fault-parallel folding. Because all the rocks within stepovers of the San Felipe fault zone, from Cretaceous to Pleistocene, are deformed about WNW-trending folds and record broadly similar shortening strains, we infer a Quaternary age of deformation. Parts of the San Felipe fault zone cut latest Pleistocene to Holocene surficial deposits, and the fault zone is likely active.

Evidence for early Pleistocene initiation of the San Felipe fault zone is preserved in conglomerate NE of the Sunset fault. Poorly sorted angular boulder conglomerate and pebbly sandstone of the Sunset Conglomerate are ~600 m thick and lie in angular unconformity on the Pliocene Palm Spring Group. The conglomerate coarsens upward and toward the fault, and is dominated by plutonic clasts derived from SW of it. Conglomerate beds contain up to 10% sandstone clasts recycled from older basin fill and accumulated in proximal to medial alluvial fans that were shed to the NE from uplifted rocks along the then-active Sunset fault.

Based on lithologic, stratigraphic, structural, and compositional similarities, we correlate the Sunset Conglomerate to the Pleistocene Ocotillo Formation. Clasts of recycled sandstone record erosion of detachment-related basin fill that predates the San Felipe fault and once covered the Vallecito and Fish Creek mountains. These crystalline-cored mountain ranges first emerged from beneath basin fill during early slip above the nascent San Felipe fault ca. 1.1–1.3 Ma. Later, the San Felipe fault zone cut upward, folded, cut across, and deactivated the West Salton detachment fault within a ~9-km-wide contractional bend and pair of left-steps. Areas that accumulated sediment within this stepover zone between ca. 1.1 and ca. 0.6 Ma are currently being inverted and folded.

Initiation of the San Felipe fault in early Pleistocene time was a significant event in the reorganization of the southern San Andreas fault system. The Quaternary dextral faults broadened the plate boundary zone southwestward from roughly 25 km (during coeval slip on the San Andreas fault and West Salton detachment fault) to 50–70 km, and mark a change in the dominant structural style from transtension to distributed dextral faulting south of the Big Bend.

Keywords: strike-slip fault, Ocotillo Formation, contractional step, reorganization, detachment fault.

INTRODUCTION

Rocks and structures in the Salton Trough contain a record of complex late Cenozoic deformation and sedimentation related to the evolution of the Pacific–North America plate boundary in southern California and northern Mexico (Fig. 1) (Dibblee, 1954; Atwater, 1970; Sharp, 1972; Crowell, 1981; Winker, 1987; Winker and Kidwell, 1986, 1996; Axen and Fletcher, 1998; Dorsey, 2006; Steely, 2006). During late Miocene (?) and Pliocene time the West Salton detachment fault was a major structure that produced the Salton supradetachment basin in its hanging wall (Axen and Fletcher, 1998; Dorsey, 2006). The detachment probably continued to slip into the early Pleistocene based on the presence of lower Pleistocene conglomerate and megabreccia shed from its footwall (Axen, and Fletcher, 1998; Winker and Kidwell, 2002; Dorsey and Janecke, 2002; Dorsey et al., 2006; Kairouz, 2005). Plate boundary strain during this time was divided between the master southern San Andreas fault and the secondary West Salton detachment fault (Axen and Fletcher, 1998). Beginning sometime in Pleistocene time, the relatively simple two-fault zone system was replaced by a more complex system in which roughly half of the strain was distributed unevenly across new dextral-oblique faults south of the Big Bend in the San Andreas fault (Morton and Matti, 1993). This incompletely

†E-mail: susanne.janecke@usu.edu
*E-mail: asteely@gmail.com

doi: 10.1130/B26239.1; 15 figures; 1 table.

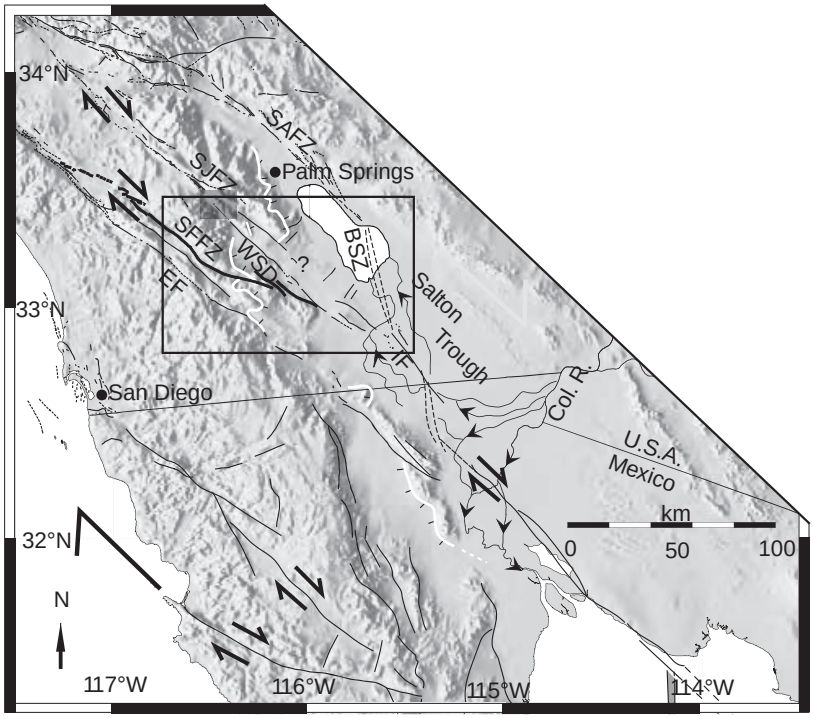

Figure 1. Tectonic overview of southern California and northern Mexico. San Felipe fault zone (SFFZ) is in bold black; other strike-slip faults are in black; SAFZ—San Andreas fault zone; SJFZ—San Jacinto fault zone; IF—Imperial fault; SJFZ—San Jacinto fault zone; EF—Elsinore fault; BSZ—Brawley Seismic Zone. Oblique-slip detachment faults are in white including the WSDF—West Salton detachment fault. Fault locations are from Jennings (1977) and Axen and Fletcher (1998). Modified from Kirby et al. (2007). Box is approximate location of Figure 2.

understood event disrupted and deactivated most of the West Salton detachment fault, reorganized the San Andreas fault system, and after some additional modifications, resulted in the current fault system of southern California. The San Andreas, the San Jacinto, Elsinore, Earthquake Valley, and San Felipe fault zones are the principal Quaternary faults in this region (Figs. 1 and 2). Our focus is on the San Felipe fault zone in the center of the system of new faults.

This study seeks to answer several important questions: When did the San Felipe fault zone initiate SW of the San Andreas fault? Was there a temporal overlap between the nascent San Felipe fault zone and the older West Salton detachment fault? If so, what was the duration of coeval slip? Did the new dextral faults initiate simultaneously or diachronously? How did the San Felipe fault zone develop through time, what was its structural style, and did it accumulate enough slip to be classified as a moderate-sized dextral fault within the San Andreas fault system? Did initiation of the San Felipe fault zone reorganize the supradetachment basin that had formed in the Pliocene above the West Salton detachment fault, as Lutz et al. (2006) and Kirby et al. (2007) proposed? What was the basinal response to the growing San Felipe fault zone? Is the San Felipe fault zone currently inactive, as some have suggested? Answering these questions will lead to a better understanding of the major kinematic and structural change that occurred within the San Andreas fault system during the Pleistocene.

In this paper we integrate new data sets with previous magnetostratigraphic studies and basin and structural analysis in the western Salton Trough to document an oblique strike-slip fault zone that cut, folded, and deactivated the West Salton detachment fault during deposition of the syntectonic Ocotillo Formation along the SW margin of the newly formed San Felipe–Borrego subbasin (Housen et al., 2005; Lutz et al., 2006; Kirby et al., 2007). We first describe the regional setting, stratigraphic relationships, and the age of the San Felipe fault zone. We then examine and interpret structural geometries in the central contractional part of the fault zone, and integrate these interpretations into a broader regional context.

To better understand the timing and structural style of this major tectonic reorganization along the plate boundary, we characterize and date the transition from slip on the West Salton detachment fault to slip on the San Felipe fault zone in the western Salton Trough (Figs. 1 and 2). We examined exposures near Yaqui Ridge at the SW margin of the San Felipe–Borrego subbasin to constrain the stratigraphic and structural evolution of these structures (Fig. 3). Geologic mapping over an area of ~2.5 U.S. Geological Survey (USGS) 7.5 quadrangles was carried out at scales of 1:12,000 and 1:24,000 in the Borrego Mountain, Borrego Sink, Harper Canyon, Whale Peak, and Squaw Peak 7.5 USGS quadrangles (Steely, 2006). Stratigraphic, sedimentologic and structural analyses reported here are condensed from Steely (2006).

Regional Geology

The San Felipe fault zone strikes WNW, and is oriented ~10°–20° counterclockwise from the adjacent San Jacinto and Elsinore fault zones. It is a major dextral strike-slip fault that approaches the Elsinore fault zone in the WNW and projects toward the Superstition Mountain segment of the San Jacinto fault zone to the ESE (Dibblee, 1954; Rogers, 1965; Figs. 1 and 2). The San Felipe and Elsinore fault zones were previously inferred to have initiated by or before ca. 2 Ma in the Peninsular Ranges, with little significant slip since ca. 0.9 Ma (Lamar and Rockwell, 1986; Hull and Nicholson, 1992; Magistrale and Rockwell, 1996). However, recent work in the adjacent San Felipe Hills (Kirby, 2005; Kirby et al., 2007) and Borrego Badlands (Lutz, 2005; Lutz et al., 2006) documents a major stratigraphic and structural reorganization at ca. 1.1 Ma that is interpreted as initiation of the San Felipe fault in the early Pleistocene, not its demise. Because these studies examined basin fill in a distal position relative to the San Felipe fault zone, the ca. 1.1 Ma stratigraphic changes were linked to the basin-bounding San Felipe fault zone using indirect methods (Lutz et al., 2006; Kirby et al., 2007). This study examines deposits within and proximal to the San Felipe fault zone in order to assess its age of initiation and activity, and to determine if it is partially coeval with the West Salton detachment fault at Yaqui Ridge.

The adjacent San Jacinto fault zone strikes NW, is almost 300 km long, and merges with the Imperial fault in the SE and the San Andreas fault in the NW (Figs. 1 and 2) (Sharp, 1967; Sanders, 1989). Many previous studies of the San Jacinto fault zone show that it is an early Pleistocene-Recent fault with high slip rates that allow some plate motion to bypass the eastern

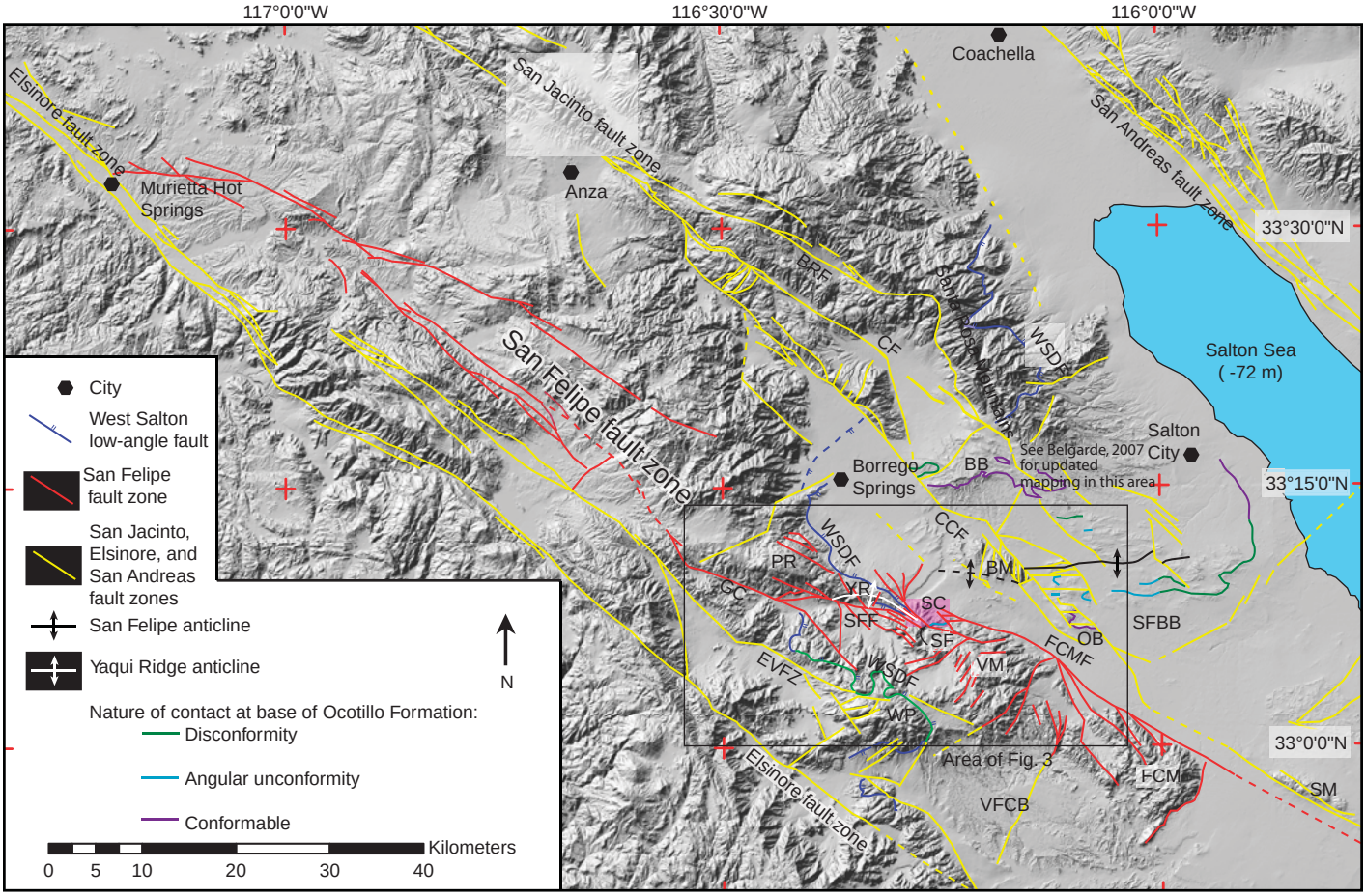

Figure 2. Important structural features of southern California and the nature of the basal contact of the Ocotillo Formation in the western Salton Trough. Faults of the San Felipe fault zone (SFFZ) are red. Note that the West Salton low-angle fault is folded and cut by dextral strike-slip fault zones at Yaqui Ridge. Green denotes a part of the West Salton detachment fault that is still active within the dextral fault system to the south. Faults are compiled and modified from Rogers (1965); Jennings (1977); Kennedy and Morton (1993); Kirby (2005); Lutz (2005); Kennedy (2000, 2003, and this study). BB—Borrego Badlands; BM—Borrego Mountain; BRF—Buck Ridge fault; CCF—Coyote Creek fault; CF—Clark fault; EVFZ—Earthquake Valley fault zone; FCM—Fish Creek Mountains; FCMF—Fish Creek Mountains fault; GC—Grapevine Canyon; OB—Ocotillo Badlands; PR—Pinyon Ridge; SC—Sunset Conglomerate of the Ocotillo Formation (pink); SF—Sunset fault; SFF—San Felipe fault; SFBB—San Felipe-Borrego subbasin; SM—Superstition Mountain; VFCB—Vallecito–Fish Creek subbasin; VM—Vallecito Mountains; WP—Whale Peak; WSDF—West Salton detachment fault; WSFH—western San Felipe Hills; YR—Yaqui Ridge.

half of the Big Bend in the San Andreas fault (e.g., Sharp, 1967; Bartholomew, 1968; Rockwell et al., 1990; Matti and Morton, 1993; Morton and Matti, 1993; Bennett et al., 1996; Dorsey, 2002; Kendrick et al., 2005; Janecke et al., 2005b; Fialko, 2006; Lutz et al., 2006; Kirby et al., 2007). The San Jacinto, San Felipe, Earthquake Valley, and Elsinore dextral strike-slip fault zones cut obliquely across the western Salton Trough, are currently active, and deform late Pleistocene and/or Holocene deposits (Rockwell et al., 1990; Hull and Nicholson, 1992; Morton and Matti, 1993; Dorsey, 2002; Kirby, 2005; Lutz et al., 2006; Belgarde, 2007; this study).

Most of the West Salton detachment fault zone has been or is being uplifted and exhumed between and adjacent to younger dextral faults (Axen and Fletcher, 1998; Kairouz, 2005; Matti et al., 2006; Steely, 2006; Belgarde, 2007). Only one or two short segments of the detachment fault continue to slip in an area north of Whale Peak, where younger crosscutting dextral strike-slip faults may be activating patches of the preexisting detachment fault (Figs. 2 and 3) (Kairouz, 2005; Steely, 2006). The West Salton detachment fault partly reactivated the Eastern Peninsular Ranges mylonite zone. This mid- to late-Cretaceous, west-directed, reverse- to thrust-sense shear zone underlies all but the southernmost part of the West Salton detachment fault (Schultejann, 1984; Lough, 1993; Axen and Fletcher, 1998; Steely, 2006). The West Salton detachment fault and mylonite generally strike NNW and dip ENE, but both vary in their strike and locally even in their dip direction (Axen and Fletcher, 1998; Kairouz, 2005; Steely, 2006). We use the regional ENE dip-direction of the >125-km-long detachment fault and mylonite zone as reference directions for structural analysis.

Some original variation in the strike of the mylonite and detachment fault is possible in the study area at Yaqui Ridge and elsewhere along the detachment fault (Steely, 2006). Adjacent to the San Felipe–Borrego subbasin there are many changes in strike, and locally even the dip direction due to deformation adjacent to and within younger dextral faults zones. This pattern is most obvious near the Clark, Hell Hole Canyon, and San Felipe fault zones (Steely, 2006; Belgarde, 2007). The antiformal West Salton

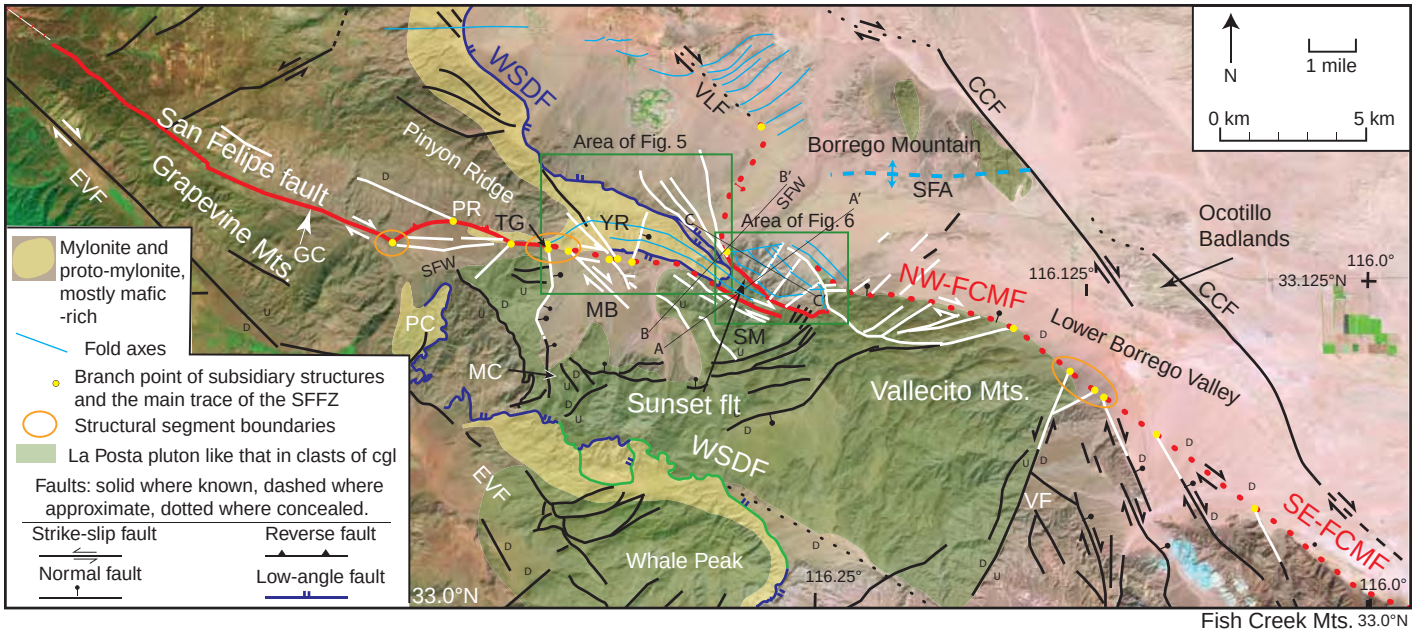

Figure 3. The central portion of the San Felipe fault zone near Yaqui Ridge in red and white. Red denotes the major traces, and white denotes smaller splays and connector faults. Note the overall contractional left bend in the fault zone from the SE Fish Creek Mountain fault to the San Felipe fault. Faults of the West Salton detachment fault (WSDF) are blue. Active parts of the WSDF are green. Mescal Bajada structural segment is east of Tamarisk Grove (TG) and Pinyon Ridge structural segment is west of it. CCF—Coyote Creek fault; EVF—Earthquake Valley fault; GC—Grapevine Canyon; MB—Mescal Bajada; PC—Plum Canyon; NW-FCMF—Northwest Fish Creek Mountain fault; PBF—Perpendicular Bluff fault; PC—Plum Canyon; SE-FCMF—Southeast Fish Creek Mountain fault; SFA—San Felipe Anticline; SFW—San Felipe Wash; SM—Sunset Mountain; TG—Tamarisk Grove; VF—Vallecito fault; VLF—Veggie Line fault; WSDF—West Salton detachment fault; YR—Yaqui Ridge. Uncolored basement west of the WSDF consists of biotite schist, fine-grained tonalite, and mafic-rich tonalite unlike clasts in the Sunset Conglomerate. Structures were compiled from Dibblee (1984), Kairouz (2005), Steely (2006), and this study.

detachment fault at Whale Peak may be the only documented original corrugation to display a reversal in dip directions. Preliminary paleomagnetic data there are consistent with ~30° of postdetachment tightening of the originally more open antiformal corrugation (B. Housen and G. Axen, 2006, written commun.). The structural geometries of the West Salton detachment fault are complex, mostly beyond the scope of this paper, and the subject of ongoing research.

Stratigraphy

Overview

Sedimentary rocks in the San Felipe–Borrego subbasin of the Salton Trough have an aggregate thickness of roughly 5 km and include the Late Miocene (?) to Pliocene Imperial Group, the Pliocene to Pleistocene Palm Spring Group, and the Pleistocene Ocotillo and Brawley Formations (Fig. 4) (Dibblee, 1954, 1984, 1996; Morley, 1963; Reitz, 1977; Lutz, 2005; Kirby, 2005; Dorsey, 2006; Steely, 2006; Belgarde, 2007). Sediments of the Imperial and Palm Spring groups accumulated in a large supradetachment basin during generally E- to ESE-directed slip across the West Salton detachment fault (Kairouz, 2005; Steely, 2006). These deposits record complex interactions among different geologic structures, the Colorado River delta system, fluvial systems flowing off the Peninsular Ranges, and the Gulf of California seaway (Winker and Kidwell, 1986, 1996, 2002; Axen and Fletcher, 1998; King et al., 2002; Dorsey, 2006; Steely, 2006; Dorsey et al., 2007).

Postdetachment deposits of the early to middle Pleistocene Ocotillo Formation and its finer grained lateral equivalent, the Brawley Formation, overlie the older basin-fill deposits along a contact that changes laterally from conformable to an angular unconformity (Figs. 2 and 4) (Dibblee, 1984; Lutz, et al., 2006; Kirby et al., 2007). Below we provide a brief summary of the Pliocene Palm Spring Group, and then focus on postdetachment Pleistocene deposits that accumulated at the SW margin of the San Felipe–Borrego subbasin (Fig. 2).

Syndetachment Stratigraphy

Palm Spring Group

Diablo Formation, Olla Formation, and Canebrake Conglomerate. The Plio-Pleistocene Palm Spring Group conformably overlies the Imperial Group and includes the laterally equivalent Diablo and Olla formations and Canebrake Conglomerate, and the overlying Borrego and Hueso formations (Fig. 4) (Dibblee, 1984, 1996; Winker and Kidwell, 1996). The Diablo Formation accumulated in the subaerial fluvial-deltaic part of the Colorado River system in the Salton Trough. Its sandstone is typically tan to yellow-orange and contains distinctive, rounded hematite-coated quartz grains derived from the Colorado Plateau (Winker, 1987; Winker and Kidwell, 1996; Steely, 2006; Dorsey et al., 2007). The Olla Formation is also fluvial but it contains >20%–50% locally derived sand derived from the Peninsular Ranges plutons (Winker, 1987; Winker and Kidwell, 1996; Kairouz, 2005; Kirby, 2005; Steely, 2006; Belgarde, 2007). The Diablo and Olla Formations pass laterally W and SW into locally derived Canebrake Conglomerate near Yaqui Ridge (Fig. 5). There the Canebrake Conglomerate is faulted against Cretaceous mylonitic rocks along the West Salton detachment fault.

Borrego Formation. The lacustrine Borrego Formation overlies the Diablo Formation along a complexly interbedded and gradational contact in the San Felipe–Borrego subbasin

(Fig. 4) (Dibblee, 1954, 1984; Dorsey et al., 2005; Kirby, 2005; Belgarde, 2007). The Borrego Formation may be up to ~1.6–1.8 km thick in the San Felipe Hills and Borrego Badlands and consists of claystone, mudstone, and lesser sandstone and marlstone (Tarbet and Holman, 1944; Bartholomew, 1968; Dibblee, 1984; Kirby, 2005). The Borrego Formation accumulated in a perennial freshwater to brackish lake that experienced few lake-level lowstands in the San Felipe Hills (Kirby et al., 2007). The sill of the Borrego lake depocenter is traditionally interpreted as the delta of the Colorado River (Dibblee, 1954), but may have been a now-buried structural barrier that blocked incursion of marine waters from the Gulf of California early during its deposition (Dorsey et al., 2005). Coarse pebbly sandstone is typically rare, in the Borrego Formation but becomes common (up to ~50%) in the southwestern Borrego Badlands. There, we have found rare but distinctive clasts of well-cemented sandstone reworked from the underlying Diablo, Olla, or lower Borrego Formations in one conglomerate bed ~95 m below the top of the Borrego Formation.

Hueso Formation. In the Fish Creek–Vallecito basin, south of our study area (Fig. 2), the Borrego Formation is absent and the sandy to pebbly Hueso Formation is the chronostratigraphic equivalent (Winker, 1987; Winker and Kidwell, 1996; Dorsey, 2006). The Hueso Formation is ~0.9–1.3 km thick, 2.8–0.9 Ma, overlies the Diablo and Olla Formations, and is laterally equivalent to the upper part of the Canebrake Conglomerate (Johnson et al., 1983; Winker, 1987; Winker and Kidwell, 1996; Kairouz, 2005; Dorsey et al., 2006). It is coarser than the Borrego Formation, is locally derived, and contains no sediment from the Colorado River. Near Whale Peak, Canebrake Conglomerate that is laterally continuous with the upper part of the Hueso Formation is cut by the West Salton detachment fault (Kairouz, 2005). This relationship provides direct evidence that this part of the detachment fault continued to slip into the latest Pliocene and early Pleistocene.

The character and significance of the transition from the muddy Borrego Formation in the north to the sandy Hueso Formation in the south is poorly understood because the uplifted Vallecito and Fish Creek mountains now separate exposures of these two dissimilar but once-contiguous units (e.g., Dorsey et al., 2005; Kirby et al., 2007). Our study area east of Yaqui Ridge is one of the few locations that preserves sedimentary rocks in the area between exposures of the Hueso and Borrego Formations, and therefore should expose rocks of this age. However, the Borrego and Hueso Formations are absent along an angular unconformity between the Diablo

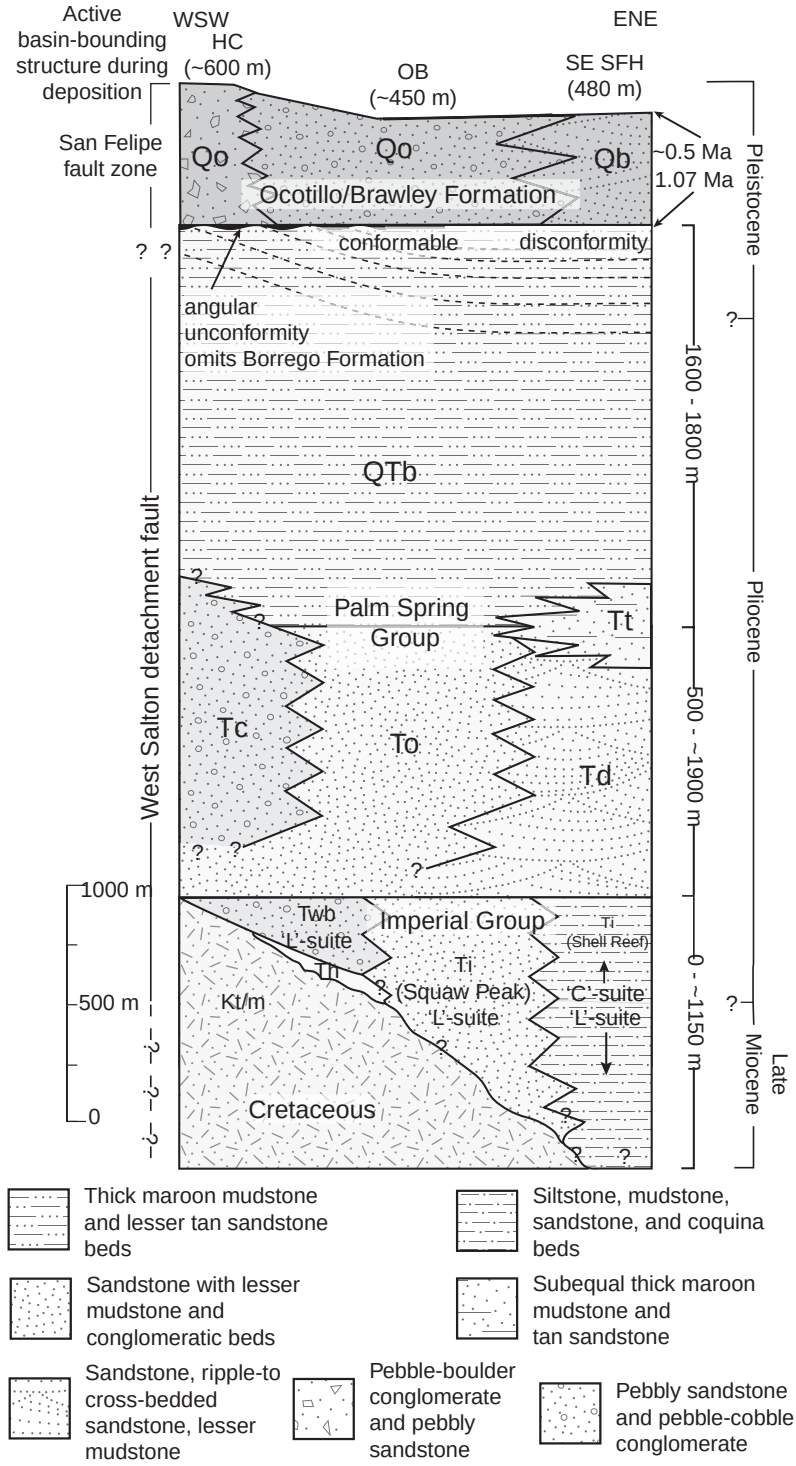

Figure 4. Generalized stratigraphic column for the SW Salton Trough showing laterally equivalent units, approximate thickness patterns, and active structures. Thicknesses of the Ocotillo and/or Brawley Formation are from this study at Harper Canyon (HC), and Kirby et al. (2007) at Ocotillo Badlands (OB) and SE San Felipe Hills (SE SFH). Other thicknesses are shown as the average of reported thicknesses (Morley, 1963; Reitz, 1977; Dibblee, 1984; Dorsey et al., 2006; Kirby, 2005; Lutz, 2005). Tc—Canebrake Conglomerate; To—Olla Formation; Td—Diablo Formation; Tt—Palm Spring–Borrego transitional unit; Ti—Imperial Formation; Th—Hawk Canyon Formation; Twb—West Butte Conglomerate; Kt/m—Cretaceous plutonic rocks and local metaplutonic and metasedimentary rocks; QTb—Borrego Formation; Qo—Ocotillo Formation; Qb—Brawley Formation.

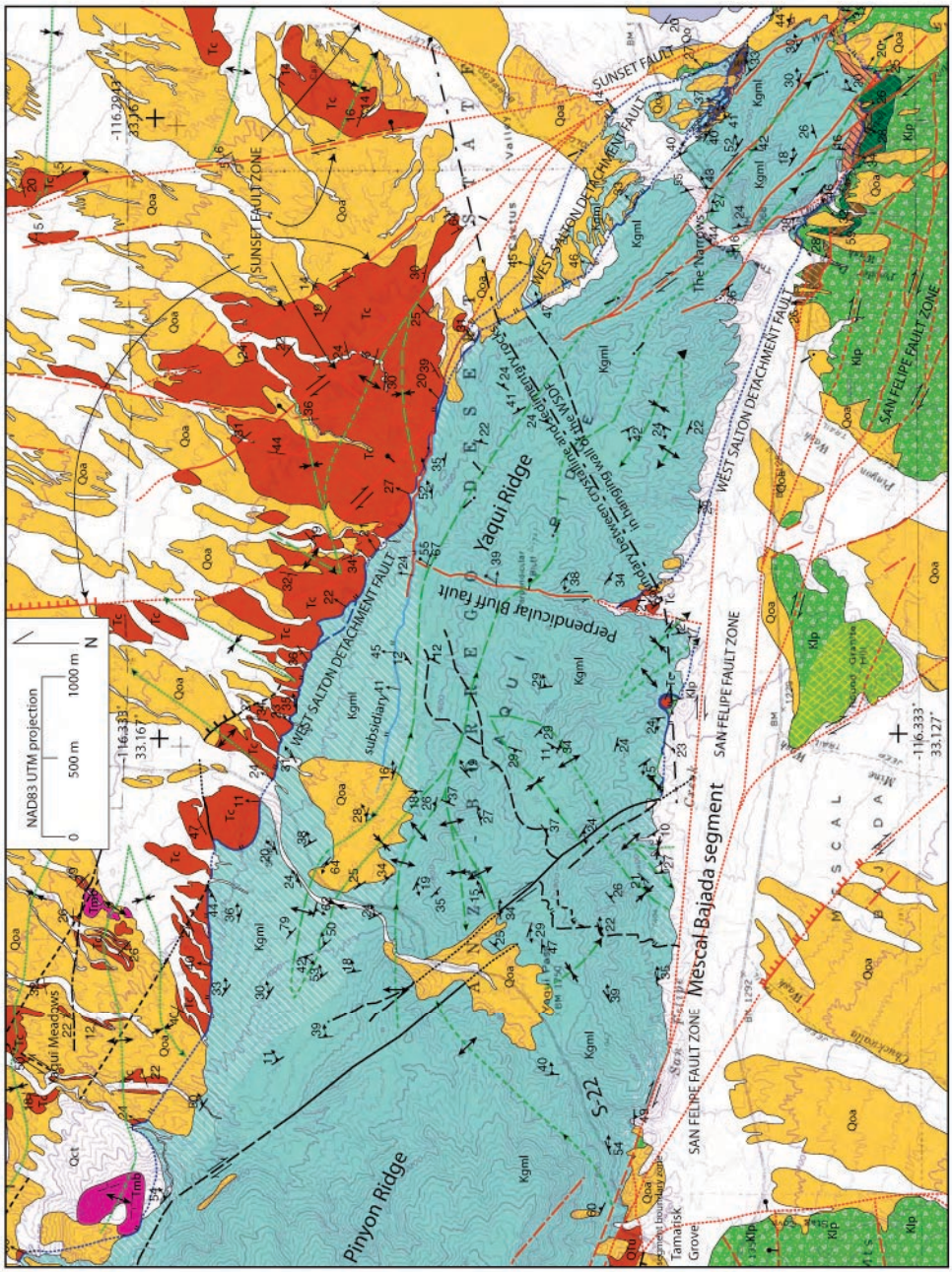

Figure 5. Simplified geological map of the Yaqui Ridge area. Modified from Steely (2006). Key and color scheme is the same as Figure 6. YRA—Yaqui Ridge antiform. Representative strike and dip data are shown for clarity. Additional data constrain positions of structures and interpretations in Figure 13. Faults are coded by color: West Salton detachment fault—blue, Faults of the San Felipe fault zone—red, other strike slip faults—black. UTM—Universal Transverse Mercator.

Formation and younger Sunset Conglomerate of the Ocotillo Formation. The absence of Borrego-age deposits in this area is due to erosion and/or nondeposition, as discussed below.

Postdetachment Stratigraphy

Ocotillo and Brawley Formations

The Ocotillo Formation is a widespread unit of coarse-grained alluvial sandstone, conglomerate, and interbedded finer grained lithologies (Fig. 4) (Dibblee, 1954; Bartholomew, 1968; Dibblee, 1984; Lutz et al., 2006; Kirby et al., 2007). The Brawley Formation is the finer grained, fluvial-deltaic lateral equivalent of the Ocotillo Formation (Kirby et al., 2007). The age of the Ocotillo and Brawley Formations is ca. 1.1–0.5 Ma based on magnetostratigraphy in the Borrego Badlands (Lutz, 2005; Lutz et al., 2006), Ocotillo Badlands (Brown et al., 1991), and San Felipe Hills (Kirby, 2005; Kirby et al., 2007). In the Borrego Badlands, the base of the Ocotillo Formation is ca. 1.05 Ma and the top is ca. 0.6 Ma (Lutz et al., 2006). In the San Felipe Hills, 18 km SE of the Borrego Badlands, the disconformable base of the laterally equivalent Brawley Formation is also ca. 1.1 Ma, and the erosional top of the formation is 0.5–0.6 Ma (Kirby et al., 2007).

The nearly synchronous progradation of pebble- to sand-dominated alluvial to fluvial deposits of the Ocotillo and Brawley Formations over the clay-rich lacustrine Borrego Formation has been interpreted to record major basin reorganization during initiation of the San Felipe and San Jacinto dextral strike-slip fault zones (Kirby et al., 2007; Lutz et al., 2006). The widespread and abrupt end of deposition of the Ocotillo and Brawley Formations at ca. 0.5–0.6 Ma in the San Felipe–Borrego subbasin probably reflects a second, less significant structural reorganization related to changes in the geometry and kinematics of the San Jacinto and San Felipe fault zones (Kirby, 2005; Lutz et al., 2006).

In this paper, we examine and describe a belt of conglomerate exposed along the northern flank of the Vallecito Mountains that was previously correlated to the Pliocene Canebrake Conglomerate (Dibblee, 1984; Winker and Kidwell, 1996). We show that it is instead a proximal facies of the Pleistocene Ocotillo Formation. Because this belt is not contiguous with other outcrops of the Ocotillo Formation, we informally name this unit the Sunset Conglomerate of the Ocotillo Formation. We then use this coarse basin-margin facies to locate and infer the age of the active basin-bounding fault system and to further refine and test the hypotheses of Lutz et al. (2006) and Kirby et al. (2007) regarding the age and evolution of the San Felipe fault zone.

Sunset Conglomerate

Description. The Sunset Conglomerate is exposed NE of the Sunset fault (a short strand of the San Felipe fault zone) and SW of the Fish Creek Mountains fault. The unit covers an area ~5.7 km long and up to 2.6 km wide (Fig. 6). The NW-striking dextral-oblique Sunset fault places Sunset Conglomerate and locally exposed underlying Pliocene Palm Spring Group against Cretaceous tonalite SW of the fault. The Sunset Conglomerate lies along a slight angular (10º–15º) unconformity on the Canebrake, Olla, and Diablo Formations of the Palm Spring Group, and the intervening Borrego Formation is absent across this contact (Fig. 6). The Sunset Conglomerate is at least 600 m thick based on geological cross sections and map-based estimates (Figs. 6 and 7). Lateral equivalents of the Sunset Conglomerate are inferred to exist in the subsurface E and ENE of the Fish Creek Mountains fault.

The Sunset Conglomerate consists of light-gray to gray-tan, moderately to weakly cemented, poorly sorted coarse to pebbly sandstone, pebble to cobble conglomerate, and angular to subrounded cobble to boulder conglomerate. Overall this unit coarsens upsection from pebbly sandstone near the base to boulder conglomerate with angular to rounded clasts near the top. It also coarsens laterally from coarse sandstone ~2 km NE of the fault to angular cobble to boulder conglomerate near the fault in the SW. Bedding in proximal deposits near the Sunset fault is typically characterized by 0.5- to 2-m-thick interbedded coarser and finer conglomerate beds that locally contain outsized clasts of small to large boulders up to 4 m in diameter (Fig. 8). Proximal deposits contain <20%–30% sand and distal deposits typically contain >50% sand. Distal exposures of the Sunset Conglomerate are characterized by weakly to moderately bedded, poorly sorted, planar to low-angle, trough cross-stratified, coarse to pebbly sandstone and lesser pebble to cobble conglomerate (Fig. 8). Beds average 1–50 cm thick and tonalite clasts range from angular to subrounded. Overall, distal exposures are tanner in color than exposures proximal to the Sunset fault and, although not extensively studied, contain a significant population of pink hematite-coated rounded quartz sand grains.

Imbricated clasts (n = 58 sites, 3–10 clasts per site) and trough axes (n = 3 sites, 3–5 axes per site) show overall paleotransport toward N57ºE ± 12º when corrected for bedding tilt, with a spread of 120º about the average direction (Fig. 9). This ENE-directed paleoflow is approximately perpendicular to the N25ºW–N55ºW strike of the Sunset fault (Figs. 6 and 9).

Biotite-bearing tonalite (La Posta–type, see key of Fig. 6) and associated plutonic rocks (85%) dominate clasts in the Sunset Conglomerate, with lesser metamorphic rocks (8%) and deformed and chloritically altered plutonic rocks (3%) (Figs. 8A–E and 10). A small but significant population of clasts (average = 4%) are composed of distinctive light tan to tan-pink sandstone (Figs. 8 and 10). These sandstone clasts contain pink rounded and hematite-coated quartz grains derived from the Colorado River, are locally present throughout the Sunset Conglomerate, and account for up to 10% of clasts at some locations.

Depositional processes and environment. We interpret the poorly sorted, matrix-supported, pebble to angular boulder conglomerate with outsized clasts near the Sunset fault as debris-flow deposits that accumulated on a steep arid alluvial fan. Northeastward lateral fining into poorly sorted sandstone and sandy pebble conglomerate reflect a down-fan transition into sandy and gravelly sheet-flood deposits with minor shallow stream channels. The lateral continuity of these facies and the paleoflow indicators suggest deposition in the upper and middle part of an alluvial fan that was bounded on its SW margin by the Sunset fault.

Provenance and recycling. Biotite-bearing La Posta–type tonalite clasts, which dominate the Sunset Conglomerate (64%), are identical to plutonic rocks on the SW side of the Sunset fault (Figs. 5, 6, and 10). La Posta–type plutonic rocks are widely exposed south of a poorly understood, approximately west-trending boundary with Canebrake Conglomerate in the hanging wall of the West Salton detachment fault at Yaqui Ridge (Fig. 5). More mafic Granite Mountain–type tonalite and mylonitic rocks, which are widespread in the immediate footwall of the West Salton detachment fault, are exposed along Yaqui Ridge less than 500 m west of the westernmost exposure of the Sunset Conglomerate on the N-NW side of this boundary, and are not present as clasts in the Sunset Conglomerate (Figs. 3, 5, 6, and 10).

Distinctive well-cemented, tan-pink sandstone clasts, like those in the Sunset Conglomerate, are present in the Ocotillo Formation throughout the western Salton Trough (Fig. 8). This clast type was also found in one conglomerate bed in the upper Borrego Formation of the southwestern Borrego Badlands. Hematite-coated, well-rounded quartz grains are diagnostic of sand derived from the Colorado River (Merriam and Bandy, 1965) and are especially abundant in fluvial-deltaic sandstone of the Diablo Formation of the Palm Spring Group, a unit that contains many large well-cemented concretions (Winker, 1987; Winker and Kidwell, 1996). The upper Imperial Group and Borrego Formation contain less of this distinctive sandstone, have few

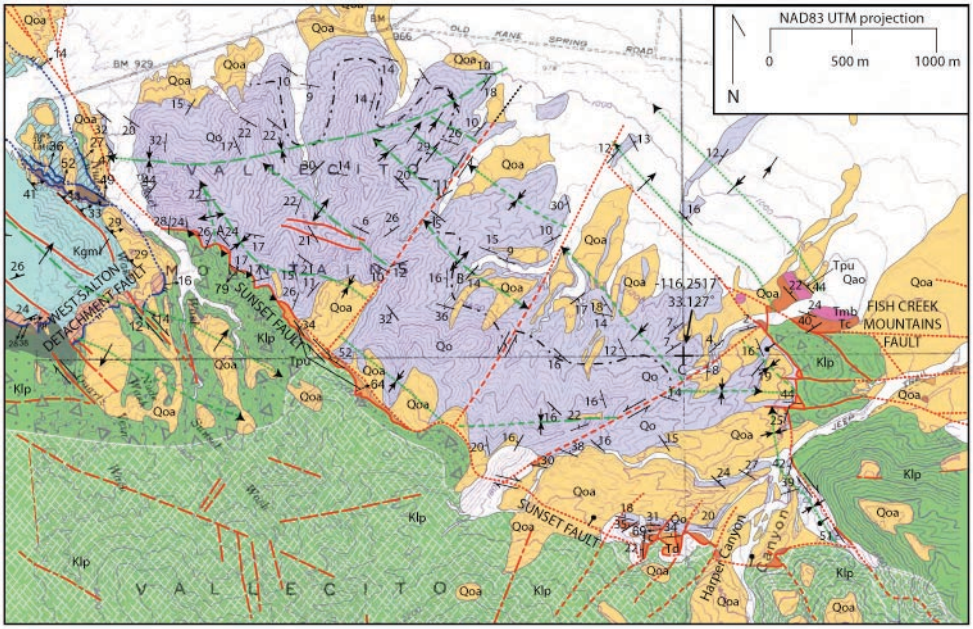

Q — Quaternary deposits: includes Recent and older alluvium, colluvium, and talus

Qoa — Quaternary old alluvium deposits

Qo — Quaternary Ocotillo Formation (Sunset conglomerate)

QTu — undivided Quaternary-late Tertiary deposits in San Felipe Wash

Palm Spring Group:

Tpu — Pliocene Olla and Diablo formations

Tmb — Pliocene megabreccia deposit

Tc — Pliocene Canebrake Conglomerate

Klp — Cretaceous 'La Posta-type' tonalite

Kgml — Cretaceous mixed 'Granite Mountain-' and 'La Posta-type' diorite and tonalite (contains much mylonite and proto-mylonite)

cg — cohesive fault gouge/microbreccia

Ksm — Cretaceous biotite/psammitic schist and other metasedimentary rocks

cx — brittle and lesser ductile chloritic fault rocks

WSDF alteration/damage zone

heavily to moderately fractured rock

brecciated rock

Strike and dip of bedding

Solid-state mylonitic foliation with lineation direction (Eastern Peninsular Ranges Mylonite Zone)

Fault dip and dip direction

Faults: solid where known, long dash where approximate, short dash where inferred, dotted where concealed.

Normal fault: ball and bar on down-thrown side

Strike-slip fault: arrows indicate sense of separation

Thrust fault: barb on up-thrown side

Low-angle fault: ticks on hanging wall

Fault scarp: ticks on down-thrown side

Lineament from aerial photographs

Fold axes: solid where known, long dash where approximate, short dash where inferred, dotted where concealed.

Approximate boundary between coarse- (above) and fine-grained (below) Ocotillo Formation

plunging anticline

plunging syncline

plunging monocline

Figure 6. Simplified geologic map of the folded Sunset Conglomerate and bounding structures. Figure 5 slightly overlaps the western edge of this map. Faults of the San Felipe fault zone (SFFZ) are red and faults of the West Salton detachment fault (WSDF) are blue. Modified from Steely (2006). Note the changing dip-direction along the strike of the Sunset fault, consistent with its being mostly a strike-slip fault.

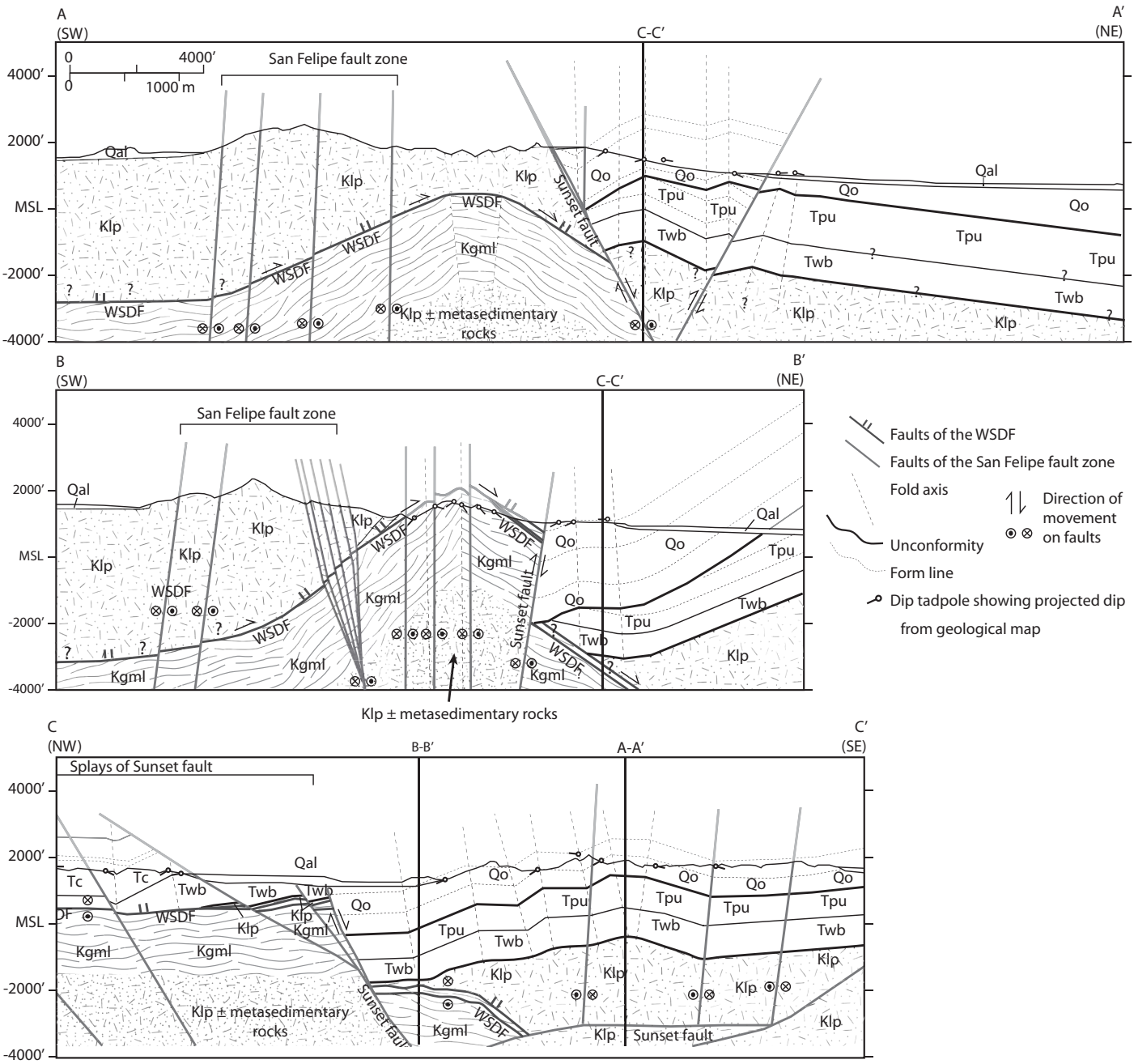

Figure 7. Geological cross section across Yaqui Ridge and one section constructed parallel to Yaqui Ridge. See Figure 3 for the locations of cross-section lines. Kgml—Cretaceous Granite Mountain–type diorite and granodiorite; Klp—Cretaceous La Posta–type tonalite; Qal—Quaternary alluvium; Qo—Quaternary Ocotillo Formation (Sunset Conglomerate) ~~, 2~~); QTu—undifferentiated Quaternary-Tertiary deposits; Tc—Pliocene Canebrake Formation; Td—Pliocene Diablo Formation; Tmb—Pliocene Yaqui Ridge megabreccia; To—Pliocene Olla Formation; Tpu—Pliocene Palm Spring Group undifferentiated; Twb—Pliocene West Butte Conglomerate; WSDF—West Salton detachment fault.

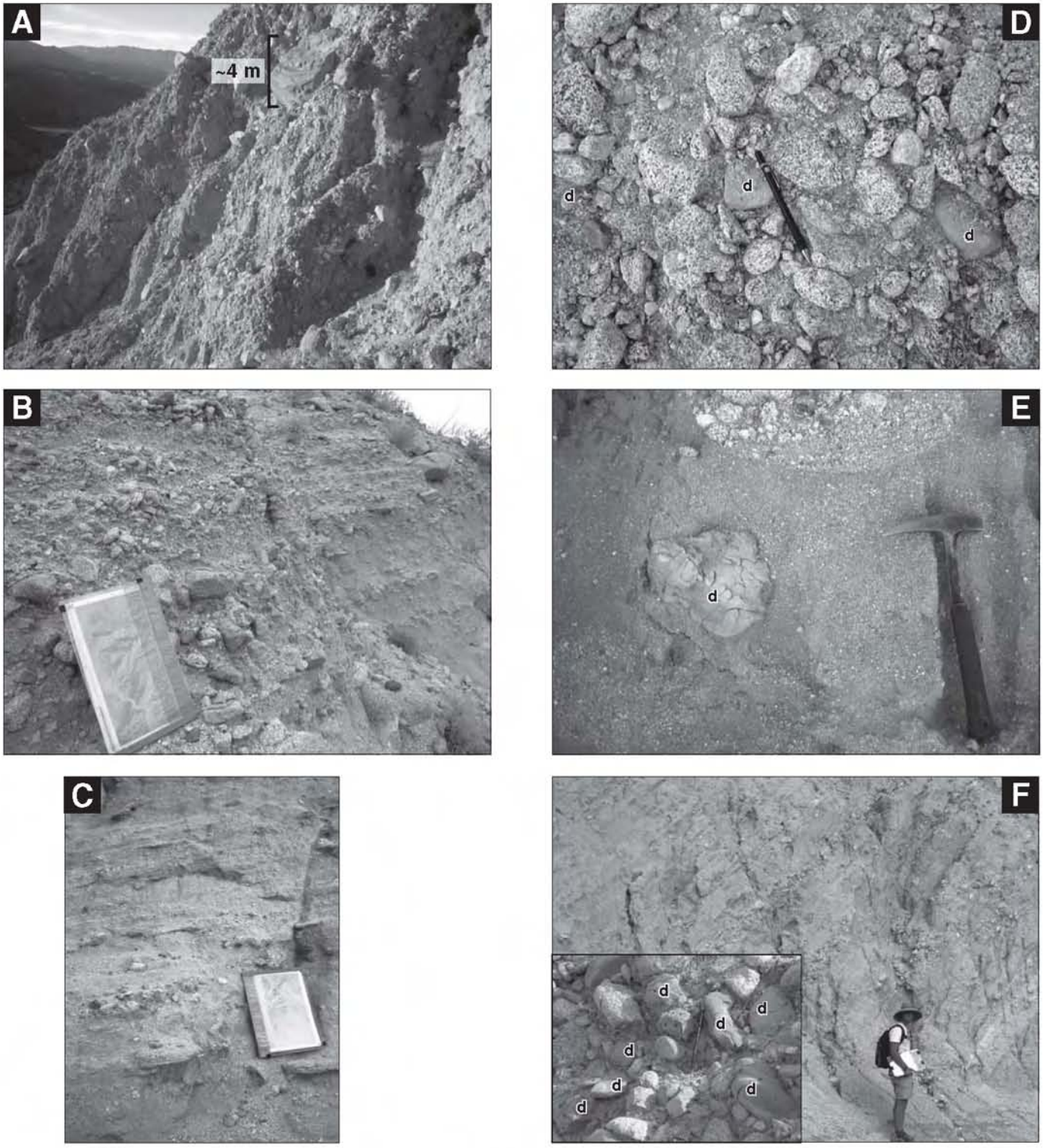

Figure 8. Photographs of the Sunset Conglomerate. (A) Sunset Conglomerate <30 m from the Sunset fault, large boulder is ~4 m in diameter. (B) Sunset Conglomerate ~1 km NE of Sunset fault, map board is 28 × 44 cm. (C) Sunset Conglomerate ~2 km NE of the Sunset fault. (D) Sunset Conglomerate dominated by La Posta–type tonalite with several prominent tan recycled sandstone clasts derived from the Diablo Formation (D). (E) Base of conglomerate-filled channel and outsized cobble of Diablo Formation in the Sunset Conglomerate. (F) Tilted pebbly sandstone beds of the Ocotillo Formation in the Ocotillo Badlands. Inset of Ocotillo Formation dominated by recycled clasts derived from the Diablo Formation.

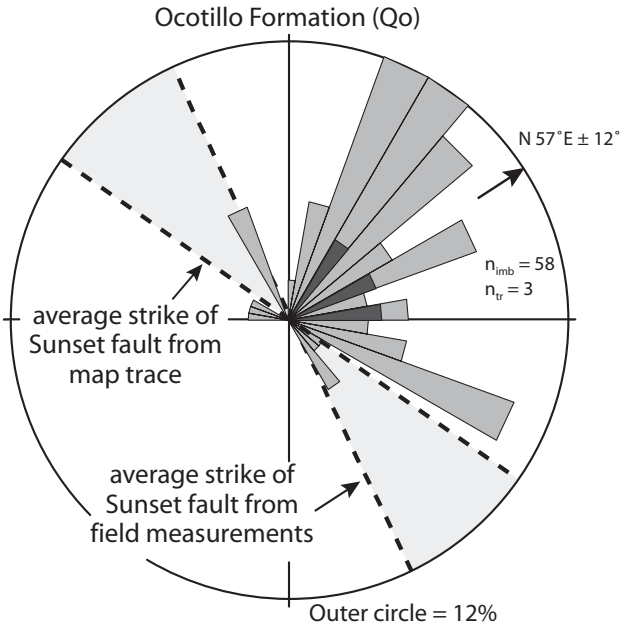

Figure 9. Rose diagram of paleocurrents from the Ocotillo Formation (Sunset Conglomerate). Light-gray petals are measurements from tilt-corrected poles to clast imbrications; dark-gray petals are measurements from tilt-corrected trough axes. Bidirectional trough axes are plotted in the same quadrant as the unidirectional imbrications. Nimb—number of imbrications; ntr— number of trough axes.

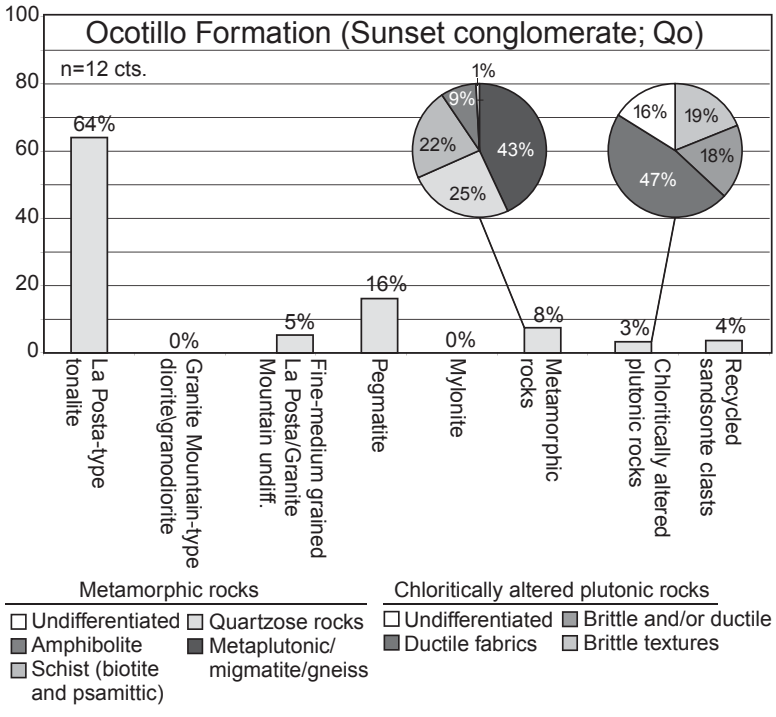

Figure 10. Clast count for the Ocotillo Formation (Sunset Conglomerate). Pie charts represent the percentage of different chloritic or metamorphic rocks within the binned populations. Each clast count represents 50 clasts at a single location. Clast populations are labeled with percentages (18%).

concretions, weather to other colors and/or have weak cementation (Reitz, 1977; Dibblee, 1984; Kirby, 2005). No shells from the Imperial Group or mudstone clasts from the Borrego Formation were observed in the Sunset Conglomerate.

The presence of distinctive sandstone clasts in the Sunset Conglomerate records recycling of older Pliocene basin-fill sedimentary rocks from the source area of the younger Sunset Conglomerate. We interpret the hematite-coated quartz grains in sandy matrix of the distal Sunset Conglomerate to be Colorado River–derived sand grains recycled from the same older basin fill. For the reasons listed above, the Diablo Formation is the most likely source of the tan recycled sandstone clasts and sand grains.

Metamorphic and chloritically altered clasts comprise ~10% of the clasts in the Sunset Conglomerate (Fig. 10). These lithologies cannot be derived from the large body of La Posta–type plutonic rocks SW of the Sunset fault and also do not match mylonites from the immediate footwall of the West Salton detachment fault near the Sunset Conglomerate. The damage zone in the hanging wall of the West Salton detachment fault and the Pliocene Canebrake Conglomerate contain these rock types (~34% of the clasts in the Canebrake Conglomerate have this composition; Steely, 2006). The Canebrake Conglomerate underlies the Sunset Conglomerate and occurs in the hanging wall of the West Salton detachment fault near the Sunset Conglomerate. The proximity of the underlying Canebrake Conglomerate and the erosion implied by the angular unconformity between the Sunset Conglomerate and the Canebrake Conglomerate suggest that the small population of metamorphic and chloritically altered clasts (~10%) is most likely reworked from the older Canebrake Conglomerate nearby. More distant source areas may also have contributed.

Correlation and age. Based on the similar stratigraphic position, thickness, basal contact, grain size, depositional environments, paleoflow, composition, and sandstone clasts recycled from the Palm Spring Group, we interpret the Sunset Conglomerate to be a proximal facies of the Ocotillo Formation (Fig. 4). Because the Sunset Conglomerate overlies the Palm Spring Group along an angular unconformity, it must be younger than the Palm Spring Group and thus cannot correlate to the Canebrake Conglomerate or West Butte conglomerate (Fig. 4). The Ocotillo Formation and much older West Butte conglomerate are the only units in the San Felipe–Borrego basin that have angular unconformities at their base like the Sunset Conglomerate (Dibblee, 1984; Brown et al., 1991; Lutz et al., 2006; Steely, 2006; Kirby et al., 2007). The ~600 m thickness of the Sunset Conglomer-

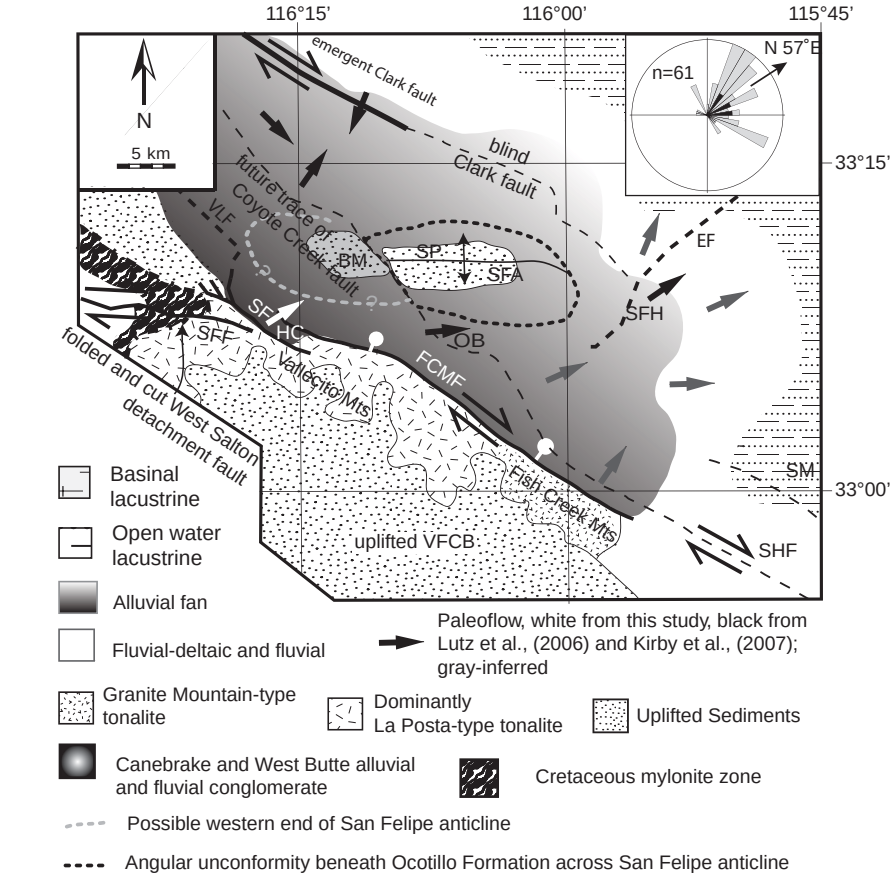

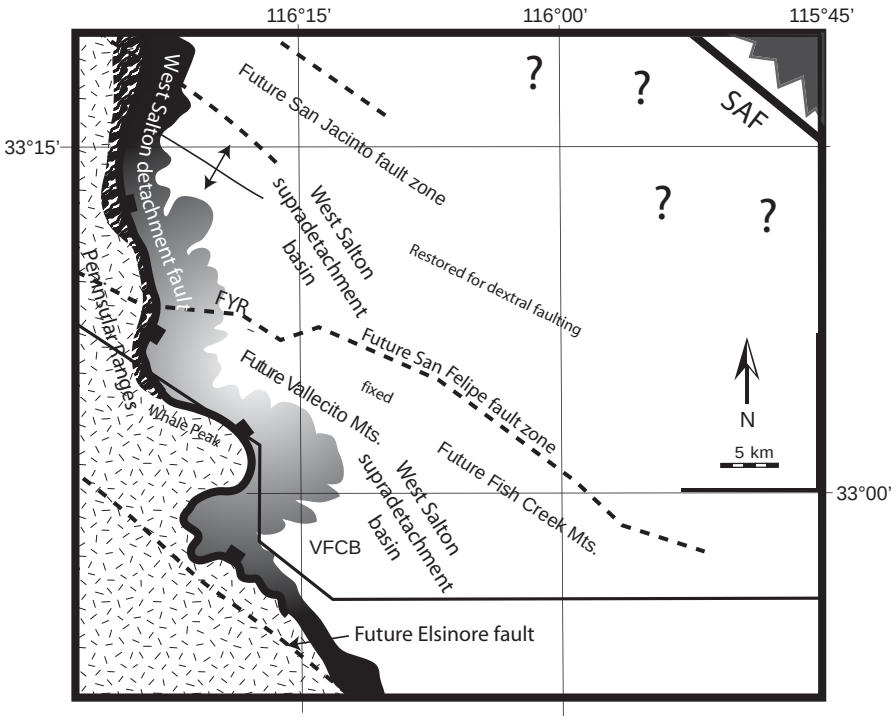

Figure 11. (A) Paleogeography during deposition of the Ocotillo and Brawley Formations just after 1 Ma. BM—Borrego Mountain; EF—Extra fault; FCMF—Fish Creek Mountains fault; VFCB—Fish Creek–Vallecito basin; HC—Harper Canyon; SFA—San Felipe anticline; OB—Ocotillo Badlands; SFH—San Felipe Hills; SFF—San Felipe fault; SF—Sunset fault; SHF—Superstition Hills fault; SM—Superstition Mountains; SRM—Southern Santa Rosa Mountains; VLF—Veggie line fault. Rose diagram shows paleoflow from the Sunset Conglomerate unit of the Ocotillo Formation near Harper Canyon. Lighter shades represent finer grain size. Modified from Kirby et al. (2007). (B) Paleogeography ca. 3–4 Ma during simultaneous slip across the West Salton detachment fault and the San Andreas fault (SAF). Younger dextral offsets were restored NE of the San Felipe fault zone. Note outline of area that matches Figure A.

ate is similar to, but somewhat thicker than the maximum thickness of the Ocotillo Formation in the Borrego Badlands (~500 m; Lutz et al., 2006), Ocotillo Badlands (450 m), and the correlative Brawley Formation in the eastern San Felipe Hills (480 m) (Kirby et al., 2007). This is consistent with our correlation.

Regionally, the Ocotillo Formation is dominated by sandy conglomerate and sandstone, and records sheet-flood deposition in medial to distal alluvial fan, bajada, and fluvial environments (Lutz et al., 2006). The laterally equivalent Brawley Formation records deposition in distal fluvial, fluvial-deltaic, and lacustrine environments (Kirby et al., 2007). The Sunset Conglomerate was deposited in proximal to medial alluvial fan environments upslope of these medial to distal fan deposits. Its thickness and grain size patterns show that it is syntectonic to slip on the dextral-oblique Sunset fault. The Ocotillo and Brawley Formations are also interpreted as syntectonic deposits related to initiation and slip on the dextral San Felipe fault zone SW of the San Felipe–Borrego subbasin (Lutz et al., 2006; Kirby et al., 2007). Our study strongly supports their interpretation.

Paleocurrents in the Ocotillo Formation are spatially variable in the SW Salton Trough and are generally directed E to ENE in the central and eastern part of the subbasin (Fig. 11; Lutz et al., 2006; Kirby et al., 2007). The Ocotillo Formation in the Borrego Badlands thickens northeastward toward the Clark fault of the San Jacinto fault zone (Lutz et al., 2006), and Kirby et al. (2007) document southwestward coars-

ening toward the San Felipe fault zone. The thinnest sections are in the middle of the basin across the crest of the San Felipe anticline (Lutz et al., 2006; Kirby et al., 2007). The Sunset Conglomerate also has NE-directed paleotransport and coarsens SW toward the dextral-oblique Sunset strand of the San Felipe fault zone. The somewhat greater thickness of the Sunset Conglomerate compared to that of the Ocotillo and Brawley Formations in the San Felipe Hills and Ocotillo Badlands is consistent with overall SW thickening toward the main basin-bounding faults of the San Felipe–Borrego basin (Fig. 11). Clast lithologies in the Ocotillo Formation and Sunset Conglomerate are nearly identical. Both units contain plutonic and metamorphic rocks derived from local highlands, and sandstone clasts and sand grains recycled from older basin fill of the Palm Spring Group (Figs. 8 and 11) (Bartholomew, 1968; Dibblee, 1984; Lutz et al., 2006; Kirby et al., 2007).

These data indicate that the Sunset Conglomerate is the proximal lateral equivalent of the Ocotillo and Brawley Formations, which are well dated elsewhere at ca. 1.1–0.6 Ma (Figs. 4 and 11; Lutz et al., 2006; Kirby et al., 2007). Thus the age of the Sunset Conglomerate is also inferred to be ca. 1.1–0.6 Ma, although the angular unconformity and absence of Borrego Formation beneath the Sunset Conglomerate introduce some uncertainty into this age assignment. Because the entire Ocotillo Formation accumulated in only ~0.5 m.y., the basal Sunset Conglomerate is probably no more than ~0.2 Ma m.y. younger or older than other parts of the Ocotillo Formation. We therefore estimate the age of the basal Sunset Conglomerate to be ca. 1.1 ± 0.2 Ma, which means that the oldest synkinematic deposits are likely to be slightly younger or older than basal deposits of the Pleistocene Ocotillo Formation, where it has been precisely dated.

STRUCTURAL GEOLOGY

In this section we examine the geometry and kinematics of the San Felipe fault zone to establish the structural setting of the postdetachment deposits, to characterize segments and structural features along the San Felipe fault zone, and to assess the relationship between the San Felipe fault zone and the West Salton detachment fault.

San Felipe Fault Zone

Overview

The San Felipe fault zone is a major structure that is almost as long as the better known faults of the San Jacinto and Elsinore fault zones. About 150 km long, it is a dextral to dextral-oblique fault that strikes NW to WNW and consists of anastomosing and branching fault strands (Figs. 2 and 3). Strands of the fault zone were first described by Dibblee (1954, 1984) and Rogers (1965) in the SW Salton Trough as a set of strike-slip faults that bound the south side of Yaqui Ridge and the N side of the Vallecito and Fish Creek Mountains, connecting west-northwestward to the Agua Caliente, Aguanga, and Murrieta Hot Springs faults (Kennedy and Morton, 2003). Based on prior nomenclature and studies (e.g., Dibblee, 1984, 1996), we use the name San Felipe fault zone to refer to the entire collection of fault strands from Murrieta Hot Springs in the NW to the front of the Fish Creek Mountains in the SE. We restrict the name San Felipe fault to the portion of the fault zone that is south of Yaqui and Pinyon ridges and extends NW into Grapevine Canyon (Rogers, 1965; Wagner, 1996). We introduce a new name, the Fish Creek Mountains fault, for the eastern continuation of the San Felipe fault zone on the NE margin of the Vallecito and Fish Creek mountains (e.g., Dibblee, 1954, 1984, 1996; Kirby, 2005). Dibblee (1954, 1984, 1996) incorrectly mapped the Fish Creek Mountains fault as continuous with the San Felipe fault. In this study we identify and analyze three structural segments along the central ~15 km of the San Felipe fault zone—the Pinyon Ridge, Mescal Bajada, and Northwest Fish Creek Mountain segments (Fig. 3)—and describe the newly identified Sunset fault between the latter two segments.

The central San Felipe fault zone has an overall sigmoidal map pattern, with N55°W–striking faults along Grapevine Canyon and the NE side of the Fish Creek and Vallecito Mountains (Fig. 3). These segments are connected by a ~15-km-long zone of transpressive E-W–striking faults and folds south of Pinyon and Yaqui ridges. This part of the fault zone consists of the Pinyon Ridge and Mescal Bajada structural segments (Fig. 3). Boundaries of the segments coincide with the tips of major folds, bends in the fault, left and right steps, branch points in the fault zone, and major changes in structural style within the fault zone (Fig. 3; Steely, 2006). The Pinyon Ridge and Mescal Bajada structural segments are only 6.75 and 9 km long, respectively, and despite their distinct characteristics might instead be subsegments of a single, longer segment (Fig. 3).

North of the Mescal Bajada segment, the West Salton detachment fault dips ~20° SW in its westernmost exposure on the south side of Yaqui Ridge (Fig. 5). The detachment fault is also exposed south of the San Felipe fault near Plum Canyon 5.8 ± 2.8 km farther west (Fig. 3), although the cutoff of the detachment fault is buried by alluvium along San Felipe Wash. Slickenlines measured on the main subvertical fault strand within the Pinyon-Mescal segment boundary are dominantly subhorizontal and suggest that horizontal displacements exceed vertical displacements along this part of the fault zone. The distributions of rock units on either side of the Mescal Bajada segment also indicate horizontal displacements in excess of vertical displacements (Steely, 2006). Taken together, these data suggest that the 5.8 ± 2.8 km right separation measured from the displaced detachment fault is mostly the result of dextral slip across the fault zone. Fault strands within the Pinyon Ridge and Mescal Bajada segments displace and fold late Pleistocene deposits.

The structural geology of the fault zone is complex along the Pinyon Ridge and Mescal Bajada segments, and there are several subsidiary faults and folds that diverge from the central fault zone. One moderately to steeply ENE-dipping fault that crosses Yaqui Ridge (Perpendicular Bluff fault) is 1.8 km long (Fig. 5), and has slickenlines that rake from 25° to 90°N (n = 3). A prominent E-facing topographic scarp along this fault suggests that there is a normal component of displacement. In the south this fault displaces the West Salton detachment fault in a sinistral-normal sense and produces ~500 m of left-separation. To the N the fault does not cross a 1- to 2-km-long subsidiary footwall strand of the West Salton detachment fault with moderate N dips (Fig. 5). The Perpendicular Bluff fault may be cut by the detachment strand, it may lose displacement northward, as indicated by northward thinning of the prominent alteration zone, or it may transfer some slip onto a part of the subsidiary detachment fault.

Three left-stepping, en echelon fault strands comprise a major structural boundary at the E end of the Mescal Bajada segment of the San Felipe fault zone (Fig. 3). From NW to SE these are the San Felipe fault, the Sunset fault, and the Fish Creek Mountains fault (Figs. 3, 5, and 6). These three faults bound two distinct contractional stepovers that we collectively name the Narrows stepover. The Sunset Conglomerate is folded in the stepover between the Sunset and Fish Creek Mountains faults. The older Eastern Peninsular Ranges mylonite zone and West Salton detachment fault either have an older fold-like geometry or are folded in the stepover between the San Felipe and Sunset fault. Both the mylonite and detachment fault are cut by subsidiary small-offset dextral faults between the Sunset and San Felipe faults (Figs. 5 and 6). The folded mylonite and detachment fault define the Yaqui Ridge antiform (Schultejann, 1984). The antiform has a limited lateral extent

and ends or bends southwestward at the saddle (and possible wind gap) that defines the boundary between Yaqui and Pinyon Ridges. The antiform does not appear to persist westward (Fig. 5).

Sunset Fault

The NW-striking Sunset fault is located between the San Felipe fault to the west and the Fish Creek Mountains fault to the east and parallels the San Felipe fault for ~7.5 km (Figs. 3, 5, and 6). The boundary between the Sunset fault and the Fish Creek Mountains fault is a faulted transpressional left stepover in which the two faults are parallel for ~2.5 km and bound complexly folded and faulted Pleistocene Sunset Conglomerate (Figs. 3 and 6). Along most of its length the Sunset fault places the Sunset Conglomerate and units of the underlying Palm Spring Group against plutonic Cretaceous tonalite (Fig. 6). Locally, thin belts of moderately to steeply dipping fault-bound slivers of Palm Spring Group are upturned along the fault.

The Sunset fault zone persists for ~10.8 km from near Harper Canyon WNW to the N side of Yaqui Ridge. It changes west-northwestward from a single fault to a 4-km-wide by 5-km-long horsetail splay of small faults that vary up to ~90° in strike (Figs. 3, 5, and 6). Immediately WNW of San Felipe Wash the main strand of the Sunset fault becomes an E- to ESE-dipping normal fault that is buried by the alluvium of San Felipe Wash. This normal fault has ~1 km of dip-slip separation based on stratigraphic and structural relationships and analyses of cross sections (Fig. 7C; Steely, 2006). Other subsidiary strands strike NNW to WNW, have small offsets, and cut and uplift older alluvium and Canebrake Conglomerate (Fig. 5). Degraded fault scarps are present along portions of the horsetail splay in older alluvium.

Plutonic rocks SW of the single-stranded part of the Sunset fault are brecciated in a 0.5- to 5-m-wide zone. They are locally bleached white and have a chalky texture (Fig. 6). Fracturing is well developed up to several hundred meters from the fault surface (Fig. 6). The tonalite in the hanging wall of the West Salton detachment fault is also brecciated for hundreds of meters above the detachment, and this damage zone has a folded form coincident with the Yaqui Ridge antiform. The damage zone SW of the Sunset fault overlaps with the older damage zone above the detachment fault.

Southeast of the horsetail splay, the Sunset fault strikes N55ºW ± 10°, and three-point analyses shows that it is usually steep and changes both its dip and dip-direction along strike (Fig. 5). Near San Felipe Wash the fault dips steeply SW, near Harper Canyon the fault dips moderately to steeply ENE, and in between it is vertical (Figs. 6 and 7). Measurements from primary fault surfaces (n = 12) further document the waviness and variable dip direction of the fault (Fig. 12A).

The Sunset fault zone preserves complex slickenline patterns consistent with both strike-slip and dip-slip movements (Fig. 12A). These data and the map relationships suggest that the Sunset fault has complex slip patterns with dominant dextral strike-slip deformation and less NE-down slip. Although no shear-sense indicators were observed along the fault, its variable dip direction, overall NW strike, steep to moderate dip, and proximity to other similarly oriented faults with demonstrable dextral offset indicate that the Sunset fault is a dextral fault with smaller reverse and normal components of slip (Fig. 7).

The absence of displaced steeply dipping markers prevents a precise measurement of offset across the Sunset fault. A maximum slip estimate can be made from the provenance, grain size, and paleocurrents of the Sunset Conglomerate. Provenance studies show that ~64% of clasts in the conglomerate were derived from La Posta–type plutonic rocks (and 85% from all La Posta–related rock types) that are widespread in the hanging wall of the West Salton detachment fault. There are no clasts of mylonite or Granite Mountain–type tonalite derived from the footwall of the detachment, despite the footwall being in close proximity to the conglomerate. The tonalite clasts include angular boulders up to 4-m diameter near the Sunset fault (Fig. 8). This relationship requires that the Sunset Conglomerate was close to a La Posta–type tonalite source area during deposition. La Posta–type tonalitic rocks have a unique spatial distribution in this area and are only exposed E and S of Yaqui and Pinyon Ridges. This rock type is easy to identify because the mafic minerals are mostly biotite and are not abundant (green shading in Fig. 3) (Steely, 2006). Exposures of La Posta–type tonalite in the Whale Peak and Pinyon Ridge areas cannot be the source because they lie structurally beneath a thick carapace of mylonite and protomylonite border phases of the La Posta pluton (Granite Mountain type) that are notably more mafic in composition and are not present in clasts of the Sunset Conglomerate (Fig. 3; Kairouz, 2005; Steely, 2006). Based on the very coarse clast size of some proximal Sunset Conglomerate (Fig. 3) and fault-perpendicular paleocurrents, we infer that the Sunset Conglomerate must have been located directly NE of La Posta–type tonalite during deposition.

If we use the westernmost outcrop of La Posta–type tonalite above the West Salton detachment fault as our most distant sediment dispersal point, then slip on the Sunset fault is limited to less than 5 km of dextral separation. However, restoration greater than 1–2 km reconstructs a large area of mylonite with a more mafic Granite Mountain–type protolith in the source area of the Sunset Conglomerate (Fig. 3). Therefore our preferred estimate of ~1–2 km right-lateral strike-slip displacement across the Sunset fault is at the lower end of the plausible range. Greater dextral slip should have produced a mylonite-clast and Granite Mountain–clast- bearing conglomerate unlike the Sunset Conglomerate. This ~1–2 km right-slip estimate for the 10.8-km-long Sunset fault is less than that for the much longer San Felipe fault (5.8 ± 2.8 km) and is consistent with the Sunset fault being a short strand in a double stepover of the San Felipe fault zone.

Folds in and near the San Felipe Fault Zone

Folds deform all of the Cenozoic sedimentary rocks and some of the crystalline rocks in the study area (Fig. 3). We identified and analyzed this deformation in discrete structural domains and found that the directions and magnitudes of shortening vary across the area. There are five domains: (1) the folded Cretaceous mylonite at Yaqui Ridge, (2) the folded Late Cenozoic West Salton detachment fault, (3) folded Pleistocene Sunset Conglomerate, and (4 and 5) two domains of folded Pliocene sedimentary rocks near Yaqui Meadows (Fig. 13). We use structural analyses, map patterns, and shortening estimates from cross sections augmented by strain estimated from average interlimb angles to describe and compare folding trends, spacing, style, and strains in the three domains within the 9-km-wide Narrows stepover. We then compare folding patterns in the stepover with those in the remaining two domains of folded sedimentary rocks farther to the WNW in order to compare deformation related to the San Felipe fault zone with other folding strains.

We calculate horizontal shortening from cross sections and augment that data set by also calculating strain from the modal interlimb angles of folds (Table 1; Fig. 14). The interlimb method was used and tested by Kirby (2005) and Steely (2006). Shortened lengths were calculated from modal interlimb angle in two domains after approximating the folds there as one larger kink fold with one interlimb angle (Fig. 14). Folds may have a kink-fold geometry or a cylindrical geometry as long as fold limbs have fairly uniform orientations. Field data (Figs. 5, 6, and 13) indicate regular fold spacing and geometries in this area, and permit this simplification if two-fold limbs are clear in the stereogram, as they are at Yaqui Ridge (Fig. 12). In places where we

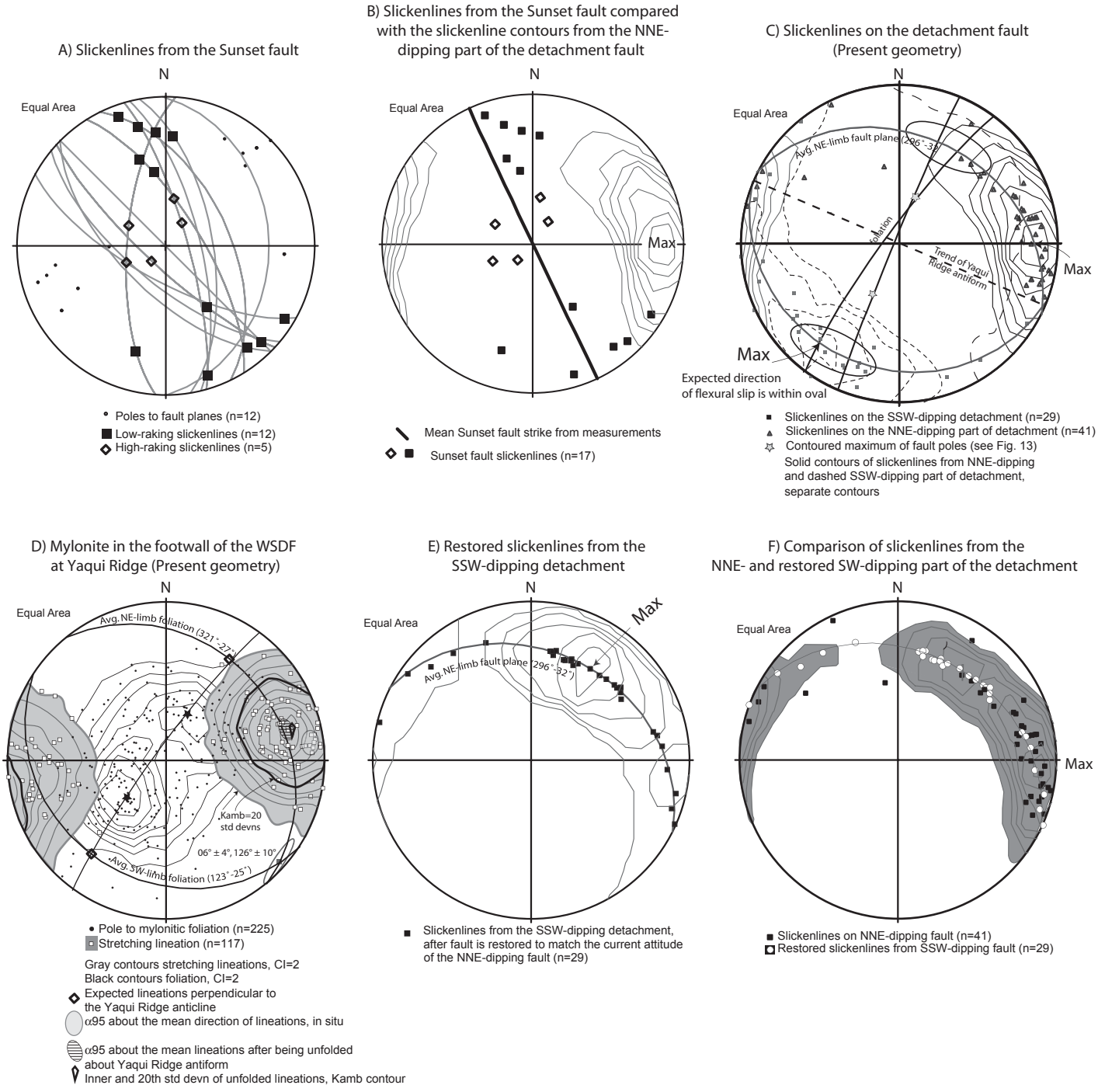

Figure 12. Geometry and kinematics of the Sunset and West Salton detachment faults (WSDF). (A) Slickenlines on the Sunset fault display significant scatter with more strike-slip and oblique vectors than dip-slip vectors. Note the variable dip direction of the Sunset fault. (B) Present-day geometry of the West Salton detachment fault, associated slickenlines, and fold axis. (C) Notice that strike-slip vectors on the Sunset fault do not have corresponding slickenline populations on the WSDF. This suggests that the Sunset fault was not kinematically linked to the WSDF and reactivation of the WSDF was limited or did not occur. (D) Scatter and contour plot of Cretaceous mylonitic foliations and stretching lineations in the footwall of the West Salton detachment fault. See text for discussion of unfolded data set. (E) Slickenlines from the SW-dipping part of the West Salton detachment after rotation to match the attitude of the detachment on the NNE-dipping part of the fault. The original attitude of the fault plane is not known. We restored the fault to a planar geometry in order to facilitate comparison of slickenline directions. Note the maximum Kamb contour in the NE quadrant. (F) Comparison of slickenlines directions on the NNE- and SW-dipping parts of the detachment fault. Note that slip in the 20° to 60° direction is far more common on the SW-dipping fault plane than on the NNE-dipping one. Slickenlines scattered around 90° are present on both parts of the detachment fault. Contour lines apply to slickenlines on the NNE-dipping part of the fault.

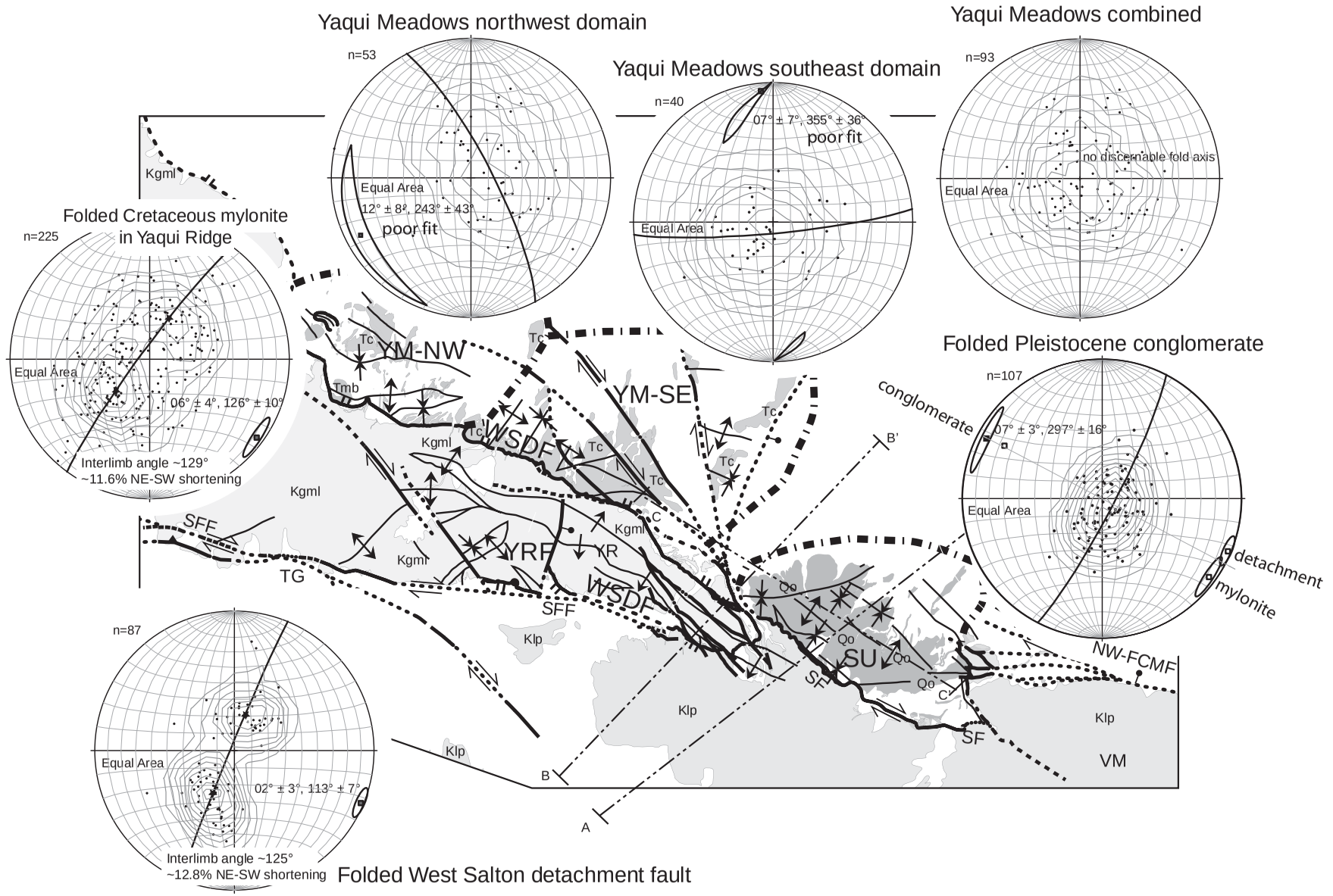

Figure 13. Simplified geologic map of the Yaqui Ridge area showing fold domains (dotted-dashed outlines) and their relationship to mapped fold traces and bounding faults of the San Felipe fault zone. Inset stereograms show individual fold domains and their interlimb angles where they can be determined. For each of three domains in the Narrows stepover, we compiled a best-fit cylindrical fold axis with its error oval in the SE quadrant of the stereonet depicting the folded Quaternary sedimentary rocks in the Sunset domain. Note that all the rocks within the Narrows stepover zone of the San Felipe fault zone, from Cretaceous to Middle Pleistocene, are deformed about identically trending upright folds, within uncertainties. This trend is different from that in folds outside of the stepover and strongly suggests that the shortening in the stepover of the San Felipe fault zone is Quaternary. Data in Sunset and Yaqui Meadows domains are poles to bedding. NW-FCMF—Northwest Fish Creek Mountains fault; SF—Sunset fault; SFF—San Felipe fault; SM—Sunset Mountain; VM—Vallecito Mountains; WSDF—West Salton detachment fault; YM-NW—Yaqui Meadows northwest domain; YM-SE—Yaqui Meadows SE domain; YR—Yaqui Ridge; YRF—Yaqui Ridge fault; SU—Sunset fold domain.

TABLE 1. STRUCTURAL ANALYSIS OF FOLDED ROCKS IN FIVE DOMAINS

Domain	Age of folded feature(s)	Fold-axis trend and plunge	Interlimb angle	NE-SW shortening from interlimb angle	NE-SW shortening from cross-section analysis
Yaqui Ridge footwall mylonite	Cretaceous	126° ± 10° 06° ± 4°	~129°	~11.5%	N/A
West Salton low-angle fault	Late Cenozoic	113° ± 7° 02° ± 3°	~125°	~13%	~11%–14%
Sunset Domain (Sunset Conglomerate)	Pleistocene	307° ± 12° 01° ± 2°	N/A	N/A	~7%–8% (~11%–12%)
Yaqui Meadows NE	Pliocene	243° ± 43° 12° ± 8°	N/A	N/A	N/A
Yaqui Meadows SW	Pliocene	355° ± 36° 07° ± 7°	N/A	N/A	N/A
Yaqui Meadows combined	Pliocene	No fold axis	N/A	N/A	N/A

Notes: Parentheses reflect addition of strain in angular unconformity. IL—Interlimb angle.

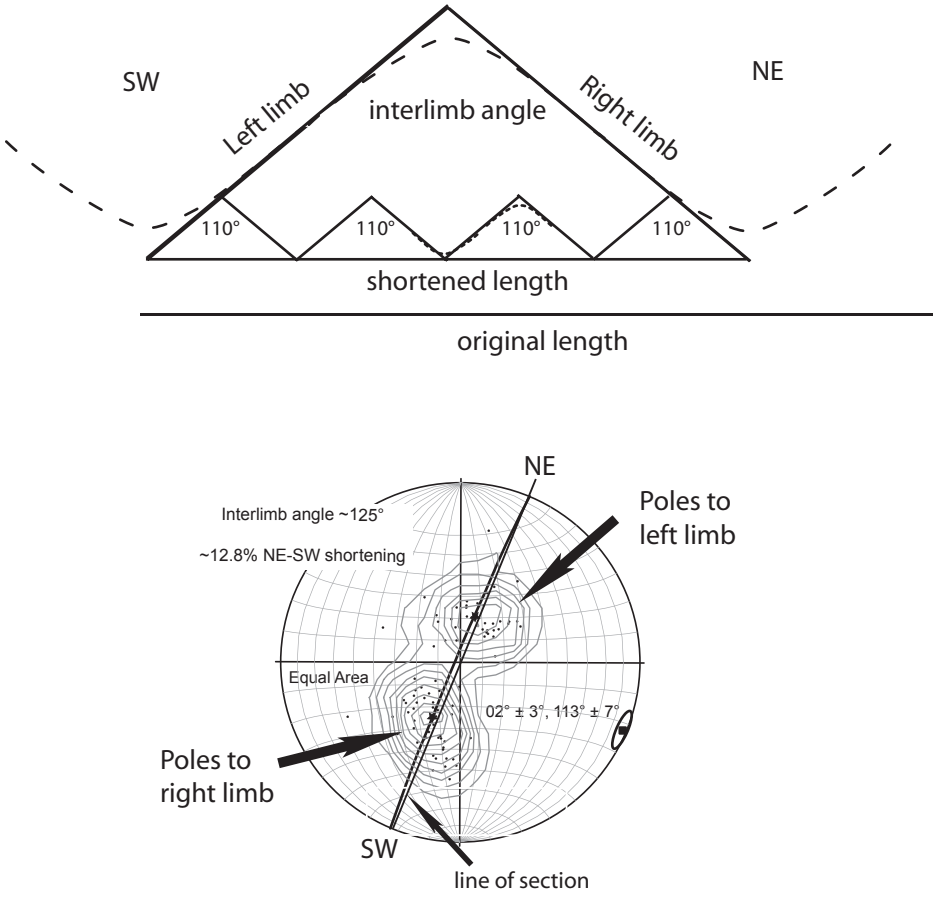

Figure 14. Technique to determine shortening strains from stereograms of folded bedding, faults and foliation to augment cross-sectional analysis. Diagram shows that treating a group of small folds as a single larger fold is robust. Shortened length is calculated from modal interlimb angle in each domain. Folds may have a kink-fold geometry or a cylindrical geometry as long as fold limbs have fairly uniform orientations. Shortening calculated using modal dips of fold limbs and interlimb angles. Field data (Figs. 5, 6, and 13) indicate regular fold spacing and geometries in this area, and permit this simplification. Modified from Kirby (2005). Shortening calculated using a kink geometry is comparable to that calculated using a concentric geometry. Both types of folds are present.

can estimate horizontal shortening using both methods, there is good agreement between these two methods (Table 1; see below).

We also analyze mylonitic stretching lineations from the Cretaceous mylonite and slickenlines from the West Salton detachment fault to help constrain the timing, geometry, and mechanism of folding at Yaqui Ridge. Lineations on the NNE-dipping side of the antiform plunge ENE, whereas lineations on the opposite limb plunge W to WSW.

Folded Mylonite at Yaqui Ridge: Description and First-Order Analysis

This domain encompasses all the rocks in the footwall of the West Salton detachment fault along Yaqui Ridge. There, foliated to mylonitic plutonic rocks of the Eastern Peninsular Ranges mylonite zone and local lozenges of metasedimentary rocks define NW, NE, and E-W–trending folds (Figs. 5 and 13). Map analysis shows that WNW-trending folds are dominant with fewer short E-W–trending and ENE-trending folds (Fig. 5). Along most of Yaqui Ridge, two monoclines define an antiformal box fold with hinges 300–600 m apart. These monoclines generally parallel the West Salton detachment fault on the N flank of Yaqui Ridge, define the crest of the antiform in the footwall, and are ~0.25 km SSW of the detachment fault (Fig. 5). The San Felipe fault zone also parallels the monoclines.

The monoclines change northwestward into anticlines in an area where several smaller synclines merge with and link the major anticlines. One of the dominant NW-trending anticlines dies out to the NW, whereas the other NW-trending anticline changes orientation and may be continuous with the NE-trending anticline that intersects the San Felipe fault zone at the boundary between the Pinyon Ridge and Mescal Bajada structural segments (Figs. 5, 6, and 13).

Our mapping of fold axes and structural analysis of 225 foliation measurements shows that ESE-plunging folds dominate Yaqui Ridge (Figs. 5, 7, 12, and 13). The best-fit cylindrical fold plunges 06º ± 4º and trends 126º ± 10º. The dominant ESE plunge of the folds is probably due to the original easterly dip of the Cretaceous thrust-related fabrics. The NE- and E-trending folds are not evident in the stereonet in part because fewer attitudes were collected where these folds dominate. Cross folds may contribute to some of the dispersion in the data set but do not obscure the dominant pattern.

The lack of a distinct marker unit in the mylonite precludes a rigorous cross-sectional analysis of shortening. Although data are scattered, an interlimb angle of ~129º is measured from the contoured center of poles to each fold limb (Figs. 13 and 14). The interlimb angle in this

domain yields ~11.5% NE-SW shortening of the mylonite across Yaqui Ridge (Table 1). An original NNE- to ENE-dipping mylonite zone is likely, given regional relationships, but this dip direction is not required for the strain calculation (see below).

Stretching lineations in the mylonite show a strong ENE-trending population on the NE-dipping limb, and a WSW-trending population on the opposite limb (Fig. 12D). The lineations are neither parallel nor perpendicular to the Yaqui Ridge antiform.

Folded West Salton Detachment Fault: Description and First-Order Analysis

We analyzed the antiformal geometry of the West Salton detachment fault along the NE and S sides of Yaqui Ridge (Figs. 5, 6, 7, and 13). At the SE tip of Yaqui Ridge, E of the Narrows, NE-dipping, SE-dipping, and SW-dipping parts of the West Salton detachment fault define an ESE-plunging box-shaped antiform (Figs. 5 and 6). This box fold is coincident with the box fold defined by the foliations in the underlying footwall at map scale and indicates that either the mylonite and detachment fault were folded during the same event, or the detachment fault reactivated a preexisting box-shaped antiform in the Cretaceous mylonite zone. The ESE plunge of the fold in the detachment fault is likely inherited from the original ENE dip of the West Salton detachment fault, based on its consistent easterly dip along its ~150 km trace length (Todd et al., 1988; Axen and Fletcher, 1998).

Stereonet analysis of 87 fault-plane measurements show two limbs that define a 02º ± 3º–plunging, 113º ± 7º–trending fold axis (Figs. 13 and 14). Measurement of horizontal NE-SW shortening calculated from two cross sections shows that the West Salton detachment fault was shortened by ~11.5%–14.0% across Yaqui Ridge (Fig. 7; Table 1). An interlimb angle of 125º is measured from the contoured poles to the detachment on the north and south side of Yaqui Ridge. We calculate ~13% NE-SW shortening of the detachment fault across Yaqui Ridge, and by assuming that the detachment fault was nearly planar and dipping before folding. Unfolding was done about the axis of the Yaqui Ridge antiform. This second method of strain analysis does not require that we know the original orientation of the fault near Yaqui Ridge, merely that it was nearly planar before folding. Within errors, the shortening of the detachment fault measured from the cross section and calculated using the interlimb method is identical. Both methods produce the same direction and magnitude of shortening as that recorded in the folded Cretaceous mylonite (Fig. 13; Table 1).

Slickenlines from the NNE-dipping detachment fault preserve scattered slickenlines concentrated around a top-east direction, whereas the SW-dipping detachment fault has greater dispersion with a SW-trending maximum and scattered slickenlines elsewhere (Fig. 12C). The many SW-plunging slickenlines on the SW-dipping part of the fault require transport of the hanging wall up and over Yaqui Ridge and are geologically implausible slip directions for the detachment fault in its current geometry. When the SW-dipping detachment fault and its slickenlines are restored about the Yaqui Ridge antiform (Fig. 12E), many scattered slickenlines rotate to congruence with the E-trending maximum on the NNE-dipping part of the detachment fault (Figs. 12C, 12E, and 12F) as predicted, if the detachment fault was folded after these E-plunging slickenlines formed. We interpret these data as evidence for folding of the detachment fault and the underlying mylonite after the top-to-the-E detachment slip. The E-trending maximum defines the dominant slip direction across the detachment fault, and is evidence for highly oblique dextral-normal slip across the West Salton detachment fault at Yaqui Ridge (Steely, et al., 2004; Steely, 2006).

When slickenlines from the two limbs are compared (Figs. 12C and 12F), it is clear that the two limbs preserve different slip histories, in addition to sharing a population of E-plunging slickenlines that range from ENE to ESE. Over 80% of the slickenlines on the NNE-dipping part of the fault are in the E-plunging population, as are a third of the slickenlines from the SW-dipping parts of the detachment fault (Fig. 12F). The remaining slickenlines are located in the middle of the NE or SW quadrants. This population is far more abundant on the SW-dipping limb in either its restored geometry (Figs. 12E and 12F) or its current geometry (Fig. 12C). We interpret the populations of slickenlines as evidence that both parts of the fault experienced top-to-the-E displacement, whereas NE-directed slip was limited largely to the SW-dipping part of the fault.

Folded Quaternary Sedimentary Rocks: Description and First-Order Analysis

The Sunset domain exposes NW-striking Pliocene to Quaternary sedimentary rocks between the Sunset fault and the Fish Creek Mountains fault (Figs. 6 and 13). Map analysis shows that folds in the Sunset Conglomerate have two orientations. There is a dominant set of WNW-plunging folds in the central part of the domain, and a subordinate pair of E- and W-plunging monoclines at the N and south ends of the domain (Fig. 6). Overall, there are four to five NW-plunging folds parallel to and within ~1.5 km of the Sunset fault. The central anticline in this domain is offset in a left-stepping sense by NE-striking left-lateral faults (Fig. 6). Together the folds transform a 1.7-km-wide, SW-dipping homocline in the WNW into a 1.25-km-wide, NE-dipping homocline in the ESE.

When the attitude of bedding of Pleistocene beds in the Sunset domain are analyzed (n = 107), stereonet analysis shows an overall 07º ± 3º–plunging, 297º ± 16º–trending, cylindrical fold axis. This direction is parallel to the nine fold hinges that we mapped (Fig. 6) and parallel to both the Sunset fault and the Fish Creek Mountains fault (Fig. 13). There is somewhat more scatter in this data set than in some of the other domains due to the greater measurement error associated with the bedded conglomerate and pebbly sandstone. Cross-section analysis of the Sunset domain shows a minimum of ~7%–8% NE-SW horizontal shortening (Fig. 7; Table 1). The 10°–15° NE-dipping angular unconformity at the base of the Sunset Conglomerate may represent an additional ~3.5%–4% NE-SW shortening that occurred before deposition of the Sunset Conglomerate for a total NE-SW shortening of ~11% to ~12% (Table 1).

Folded Sedimentary Rocks outside the San Felipe Fault Zone at Yaqui Meadows: Description and Analysis

There are two areas of folded Canebrake Conglomerate of the Pliocene Palm Spring Group in the hanging wall of the West Salton detachment fault along the NNE side of Yaqui and Pinyon Ridges that we named the NW and SE Yaqui Meadows domains (Fig. 13). These rocks are located west of the Narrows stepover in the San Felipe fault zone and are cut by the distal ends of the Sunset fault zone. Mapping of the NW Yaqui Meadows domain revealed mostly W-plunging folds (Fig. 5). The SE Yaqui Meadows domain also preserves E-W–trending folds and at least three NNE-plunging folds at a high angle to the West Salton detachment fault (Figs. 5 and 13). The detachment fault is not folded about these NNE-plunging axes and probably acted as a décollement surface during the folding.

The NW Yaqui Meadows domain shows significant scatter of bedding attitudes on a stereogram with no meaningful fold axis evident on the stereonet despite the presence of several clear mapped folds (n = 53) (Fig. 13). The SE Yaqui Meadows domain also shows a significant scatter of bedding attitudes (n = 40) (Fig. 13).

When the attitudes from the NW and SE Yaqui Meadows area are combined, bedding attitudes display significant scatter with no dominant fold axis on the stereogram (Fig. 13). This is likely due to interference between the multiple trends of folds at high angles to one another. E-W–

trending folds near Yaqui Meadows probably reflect wrench deformation. We have not identified a mechanism to produce the handful of NE-plunging folds in the area. It is noteworthy that there is no evidence for NW-trending folds in either the map pattern or the stereogram around Yaqui Meadows. NW-trending folds are localized between en echelon faults of the San Felipe fault zone.

INTERPRETATION AND DISCUSSION

Timing of Initial Uplift along the San Felipe Fault Zone

The northeastward tilt of older sedimentary rocks beneath the angular unconformity at the base of the Sunset Conglomerate and the lack of Borrego or Hueso Formations across this contact indicate a period of uplift and tilting prior to deposition of the basal Sunset Conglomerate. Because our study area is astride a poorly understood paleogeographic boundary between the thicker Borrego-filled subbasin to the north (up to 1.8 km thick) and the thinner Hueso-filled subbasin to the south (~1.3 km thick), it is impossible to know the thickness of Hueso- or Borrego-age sediment missing across the angular unconformity. Using reasonable exhumation rates of 2–10 mm/yr and complete erosion of the maximum possible thickness of Hueso or Borrego Formation, ~0.1–0.9 m.y. would be required to erode these units before deposition of the Sunset Conglomerate began. Alternatively, if the Borrego or Hueso Formations were thin or absent in this area, then the unconformity could have formed over ~~less than~~ a period of <0.1 m.y. This analysis does little to constrain the age of initial deformation because we cannot estimate the thickness of the Borrego or Hueso Formations near Yaqui Ridge.

Therefore, we examined basin fill for evidence of the earliest uplift along the SW margin of the San Felipe–Borrego subbasin. Rare recycled sandstone clasts in conglomerate of the upper Borrego Formation (95 m below the base of the Ocotillo Formation) in the southwestern Borrego Badlands provide the earliest record of basin inversion and uplift along the SW basin margin. Although the rate of sediment accumulation in the upper Borrego Formation is not well known, it is likely less than the high rates in the lower Ocotillo Formation (1.4–3.9 mm/yr) (Lutz et al., 2006; Kirby et al., 2007). Using a reasonable range of sediment-accumulation rates (0.5–2 mm/yr), the ~100 m thickness of upper Borrego Formation with recycled clasts, and the ca. 1.1 Ma age of the basal Ocotillo Formation in the Borrego Badlands where the basal contact is conformable (Lutz et al., 2006), the oldest recycled clasts were probably deposited ca. 1.1–1.3 Ma. These recycled clasts record erosion of quartz-rich sandstone from either the Diablo or the lower Borrego Formations and provide the earliest evidence of uplift and erosion within the future San Felipe fault zone. Aside from this one conglomerate bed in the Borrego Formation, there is currently no other sedimentary evidence for uplift along the SW margin of the San Felipe–Borrego subbasin prior to 1.1–1.3 Ma.

We interpret these data as evidence that there was little or no uplift in the San Felipe fault zone prior to deposition of the uppermost Borrego or lower Ocotillo Formation. We further infer that the lag time between initiation of the San Felipe fault (which inverted and destroyed some of the older supradetachment basin) and earliest deposition of reworked sandstone clasts in the new basin was probably <0.2 m.y. The close spatial association between the uplifted areas in the Vallecito and Fish Creek Mountains and the San Felipe fault zone provides evidence that the San Felipe fault zone produced the uplift. Altogether these relationships show that the San Felipe fault zone initiated no earlier than ca. 1.1–1.3 Ma and breached the surface shortly afterward.

Geometry of Initial Uplift along the San Felipe Fault Zone

Northeastward tilt of rocks beneath the Sunset Conglomerate prior to deposition of the Sunset Conglomerate, and the location of the uplifted area adjacent to the San Felipe fault zone, are consistent with growth of a NE-facing fault-propagation monocline above the nascent, upward-growing tip of the Sunset and Fish Creek Mountains faults. A fault-propagation fold above a dextral-oblique fault will produce uplift during early stages of development, similar to a fault-propagation fold above a growing reverse or normal fault (Gawthorpe et al., 1997; Sharp et al., 2000). Once the fault tip reaches the surface, accommodation space is quickly created on the downthrown side of the fault (in this case the NE side), and deposition begins (Gawthorpe et al., 1997). Although the San Felipe fault zone is predominantly a strike-slip fault, it has a significant NE-side–down component of slip in the Narrows stepover and along the Fish Creek Mountains fault and a smaller component of SW-down slip on the Pinyon Ridge structural segment (Dibblee, 1996; Steely, 2006). A fault-propagation fold above the Sunset fault can explain uplift and erosion of Plio-Pleistocene basin fill (Diablo, Borrego, and/or Hueso Formations) shortly prior to deposition of the basal Sunset Conglomerate. This model also explains the original NE dip of older basin-fill deposits beneath the angular unconformity below the Sunset Conglomerate. A second, SW-facing monocline associated with the E end of the San Felipe fault at Yaqui Ridge may have formed in a similar manner, but sedimentary evidence for such an evolution is not preserved there.

The Sunset fault may cut the West Salton detachment fault at depth or merge laterally and at depth with it. We prefer the first interpretation because other faults of the fault zone, ~~like~~ such as the San Felipe fault, cut and offset the detachment along San Felipe Wash by many kilometers, and because small-offset dextral strike-slip faults between the San Felipe and Sunset fault cut the West Salton detachment fault near the tip of Yaqui Ridge. Both relationships show that dextral faults cut the detachment fault instead of reactivating it (Figs. 3 and 5). Second, there is no Ocotillo Formation in the hanging wall of the detachment fault north of Yaqui Ridge as would be expected if it was active during the first half of the San Felipe fault zone's history. Finally, the two faults have dissimilar dominant slip directions and the faults are nearly orthogonal where they are closest to each other (Fig. 7C). The slip vectors measured on the Sunset fault, although few in number, are distinctly different from major slickenline population on the West Salton detachment fault (Figs. 12B and 12C). Sunset fault slickenlines overlap in trend with less than 6%–7% of slickenlines on all parts of the detachment fault, and overlap even less with slickenlines on the nearest part of the detachment on the north side of Yaqui Ridge (Fig. 12B).

These relationships conflict with an alternate possibility, that there was some folding and uplift of basin fill during late stages of slip on the West Salton detachment fault, before the San Felipe fault was fully formed. We do not favor this alternate model because the San Felipe fault zone clearly cuts the detachment fault and was active long enough to accumulate significant right slip. Syndetachment tilting should have been toward the detachment fault (to the SW) rather than the observed dip direction beneath the angular unconformity (to the NE). In addition, the detachment fault was active during all of Pliocene time yet did not produce a Pliocene uplift within the future San Felipe fault zone.

Age of the Sunset Fault and Paleogeography of the Sunset Conglomerate

Our data show that the Sunset and Fish Creek Mountains faults controlled deposition of the Sunset Conglomerate along the SW margin of the newly formed San Felipe–Borrego subbasin of the Salton Trough (Fig. 11). Based on correlation to more distal, well-dated parts of the Ocotillo Formation (Lutz et al., 2006; Kirby et

al., 2007), the oldest Sunset Conglomerate is estimated to be ca. 1.1 ± 0.2 Ma. We infer that the Sunset fault had ruptured to the surface by that time, was creating accommodation space, and had cut the detachment fault. Our data also show that the Sunset Conglomerate accumulated in a syntectonic alluvial fan with sedimentary transport to the NE away from the bounding San Felipe fault zone.

Emergence of the San Felipe fault zone records a major, structurally controlled change in the paleogeography of the San Felipe–Borrego region from one controlled largely by oblique low-angle extension across the West Salton detachment fault to one dominated by strike-slip faults (Figs. 11A and 11B). The presence of clasts recycled from the Palm Spring Group requires uplift and erosion of older basin-fill deposits SW of the Sunset fault and erosion of the Palm Spring Group from newly uplifted highlands in the proto-Vallecito Mountains and proto-Fish Creek Mountains. The absence of the Borrego and Hueso Formations, coupled with the angular unconformity beneath the Sunset Conglomerate, suggests that NE tilting or folding accompanied this uplift event. The deposits of the Palm Spring Group that once covered the plutonic mountain core have been stripped by erosion since the early Pleistocene. Initiation of the San Felipe fault zone inverted and eroded parts of the basins of the western Salton Trough and caused crystalline-cored fault blocks (the Vallecito and Fish Creek Mountains) to emerge from beneath the sedimentary floor of the basin. Our work supports the original hypothesizes of Kirby (005), Lutz et al. (2006), and Kirby et al. (2007) (Fig. 11).

Origin of the Yaqui Ridge Antiform

Several hypotheses (in end member or in combination) can plausibly explain the folded form of the Cretaceous mylonite and detachment fault at Yaqui Ridge (Figs. 6, 7, and 13): (1) the original folded form of the mylonite could date back to Cretaceous thrusting and be an original corrugation that was reactivated by the West Salton detachment fault; (2) folding may be entirely or partially syndetachment faulting; and/or (3) the fold could result entirely from deformation within the San Felipe fault zone. For clarity we restrict our discussion of the antiform's origin to the process that generated opposing dips, and we do not address whether departures from regional strike of the detachment fault and/or its underlying mylonite zone are original or secondary. Comparison of the NE-dipping mylonite at Yaqui Ridge with regional trends (Sharp, 1967) suggests that its strike is slightly counterclockwise of the mylonite farther north. This is due to some original waviness in the mylonite zone and/or anticlockwise rotation.

Hypothesis 1: Folding during Cretaceous Thrusting

If the antiformal shape of the mylonite at Yaqui Ridge is a primary feature that formed during Cretaceous thrusting, then it must be possible for the slickenlines on the West Salton detachment fault (which effectively reactivated the Cretaceous mylonite) to have formed and been active in their current orientation. In addition, stretching lineations in the Cretaceous mylonite on both antiformal limbs should record a feasible thrust-related direction of slip in present-day coordinates, and so are most likely to align either down the nose of the Yaqui Ridge antiform or be perpendicular to it. Other orientations of the mylonitic lineation are less likely because high strains of sheath folds and triclinic folds are not evident, and the antiform is in the wrong orientation to be a thrust ramp (see below). In an original Cretaceous corrugation, a tighter clustering of mylonitic stretching lineations is expected in present coordinates than if we structurally "unfold" the antiform. If unfolding the foliation about the Yaqui Ridge antiform improves the clustering of the lineations, then folding of the mylonitic fabric probably occurred after the lineations formed in the Cretaceous.

The above tests show that creation of the Yaqui Ridge antiform in the Cretaceous during thrusting is very unlikely. Most importantly, the slickenlines on the West Salton detachment fault could not have formed on a detachment with an original antiformal shape. Improbable reverse-sense slip is required on the detachment by this interpretation during the time when the top-to-the-E– and top-to-the-NE–trending slickenlines were produced on the SW-dipping part of the detachment fault. Second, transport in the mylonite, as recorded in the top-to-the-WSW–stretching lineations, is neither perpendicular to the Yaqui Ridge antiform, nor parallel to the antiform (Fig. 13). The oblique angle between the antiform and the lineations requires a complex, triclinic origin such as sheath folding or formation of an oblique thrust-related ramp that dips in the transport direction, if the observed geometries are original and Cretaceous. A thrust ramp with such a dip direction is improbable. Third, the stretching lineations define a good cluster in their current orientations (Fig. 13) but restore to a significantly tighter congruent cluster after unfolding of the mylonitic fabric about the Yaqui Ridge antiform. Currently the 20-sigma Kamb contour of the lineations spans ~130° of the net's 180° width, and the modal direction of the Kamb contour does not overlap the mean vector at the α_{95} level. Unfolding the stretching directions about the Yaqui Ridge antiform produces a population that is more clustered. The 20-sigma Kamb contour of the unfolded lineation spans ~85° of the net, and there is an excellent overlap of the modal Kamb direction and the mean vector (α_{95} = 4.4°). The geometry of the mylonitic lineations is more consistent with folding of the mylonite after Cretaceous time, but the lineations alone do not require it. Fourth, preliminary paleomagnetic studies show post-mylonitic tilting and folding in the Yaqui Ridge antiform, and are inconsistent with the antiform being an original corrugation (Bernard Housen, 2002, 2007, written commun.). All in all, the simplest interpretation is to fold all the structural elements after Cretaceous time during a single period of folding and faulting.

Hypotheses 2 and 3: Syndetachment versus Postdetachment Folding

Our mapping shows that folds in the mylonite at Yaqui Ridge and the folded detachment fault in the left stepover between the San Felipe fault and the Sunset fault have geometries nearly identical to those of folds in the Pleistocene Sunset Conglomerate in the adjacent stepover between the Sunset and Fish Creek Mountains faults (Figs. 5, 6, and 12). Fold axes reflect identical NE-SW–shortening directions, and fold hinge lines have similar spacing. Cross folds, at an angle to the dominant trend, are present but subordinate in both stepovers. Folds within the stepovers of the San Felipe fault zone have a much more consistent shortening direction (NE-SW) than folds that formed outside the Narrows stepover near Yaqui Meadows (weak N-S) (Fig. 13). Folds within the San Felipe fault zone consistently trend WNW to NW, and represent roughly 10 ± 3% NE-SW horizontal shortening.

Despite some scatter in the stereonets of bedding attitudes, it is clear from the map patterns and fold analyses that the trend of the dominant folds that deform the Pleistocene Sunset Conglomerate is identical to the trend of the Yaqui Ridge antiform (Figs. 3 and 13). Plunge directions differ, however. We infer that the WNW plunge of the folds in the Sunset Conglomerate is due to northwestward tilting of the Sunset Conglomerate toward a SE-dipping normal fault buried along San Felipe Wash (Figs. 7C and 13). The ESE plunge of the folded Cretaceous mylonite and the detachment fault is inherited from the original easterly dip of these features, as noted above.

The total amount of NE-SW horizontal shortening is about a third greater in the Yaqui Ridge antiform than in the Pleistocene Sunset

Conglomerate (Table 1). The difference in strain could reflect spatial or temporal differences in strain, or both. There might be more accumulated strain in the stepover between the San Felipe fault and the Sunset fault than in the second stepover between the Sunset fault and the Fish Creek Mountain fault. Variations in the fault geometry could produce modest differences in folding strains in adjacent stepovers of a single fault zone. Alternatively, the "extra" strain in the crystalline rocks could have been created by: (1) initial deformation in the San Felipe fault zone before or during deposition of the Sunset Conglomerate; (2) a small-magnitude antiform inherited from the Cretaceous mylonite zone; and/or (3) a small-magnitude antiform created during slip on the West Salton detachment fault.

If we add the ~3.5%–4% NE-SW shortening reflected in the NE-tilted angular unconformity beneath the Sunset Conglomerate to the shortening from the cross section of the Sunset Conglomerate, there is no significant discrepancy in the amount of shortening between the two adjacent stepovers (Table 1). The additional strain is late Pliocene to Pleistocene and strongly suggests that initial deformation in the San Felipe fault zone started before deposition of the oldest Sunset Conglomerate ca. 1.1 ± 0.2 Ma, and that little or none of the folding dates back to Cretaceous thrusting.

Because most of the shortening is preserved as folds in the Pleistocene Sunset Conglomerate, roughly two-thirds of folding occurred after the end of conglomerate deposition, that is, after ca. 0.6 Ma. The angular relationships across the unconformity (Figs. 5 and 6), however, are consistent with a continuum of NE-SW shortening and transpression beginning before deposition of the oldest preserved Sunset Conglomerate. Thus folding of the Sunset Conglomerate is likely the result of persistent NE-SW shortening. NE-SW contraction started before deposition of the basal Sunset Conglomerate, was ongoing during deposition of the conglomerate, persists to the present, and is currently exhuming the conglomerate. We did not directly observe growth strata in the Sunset Conglomerate, in part due to discontinuous exposures, but we infer that that they are present.

Based on the above summary, we favor an interpretation in which the Sunset Conglomerate, the Cretaceous mylonite on Yaqui Ridge, and the West Salton detachment fault experienced a single episode of shortening in the double left stepover of the San Felipe fault zone, rather than representing multiple deformational events. Our data and analyses do not preclude some SW tilting of the south limb of the Yaqui Ridge antiform during the latest stages of detachment faulting, but we emphasize that it must be a small portion of the overall tilt. Folds in the stepover were produced by transpressional strain transfer across the 9-km-wide contractional left-step in the San Felipe fault zone. These two contractional stepovers provide a soft link between the Mescal Bajada segment of the San Felipe fault, the Sunset fault, and the WNW end of the Fish Creek Mountains fault. We infer that the San Felipe fault zone may be a continuous structure in the subsurface, however, and that the double left step and WNW-trending folds at the present level of exposure are all part of a complex flower structure that developed structurally above a continuous or nearly continuous fault zone. A flower structure explains the strong parallelism between fold axes in the stepover zones and the strike of the en echelon dextral faults, a parallelism that is difficult to explain with wrench fault models. Fault-bend folding in a three-dimensional flower structure is more likely to explain the parallelism of the folds and faults than strain partitioning because the available slickenline data on the San Felipe fault zone are inconsistent with strain partitioning between faults.

Other models for the origin of folds at Yaqui Ridge and in the Sunset Conglomerate are not favored because they do not predict the observed fold geometries; they are inconsistent with the strong spatial association of the WNW- to NW-trending folds with the more contractional segments and stepovers in the San Felipe fault zone. Extensional folding processes are very unlikely to explain these NW-trending folds, because extensional processes rarely produce the observed trains of folds or such complex, locally interfering three-dimensional fold patterns (e.g., Janecke et al., 1998; 2005a). The presence of four to five closely spaced folds in a fold train parallel to the Sunset fault, within a large left-stepping contractional stepover in a major regional strike-slip fault zone, is difficult to explain with extensional fold models. We also reject wrench folding as a viable mechanisms because it predicts that most fold axes would trend E-W, oblique to the bounding faults rather than parallel to them. Folding and faulting in the Sunset Conglomerate and at Yaqui Ridge is the result of contraction and fault-bend folding within two left steps in the right-lateral San Felipe fault zone, and of contraction north of the E-striking segments of the San Felipe fault.

In summary, our data suggest that the majority of folding across the Yaqui Ridge antiform and in the Sunset Conglomerate domain occurred as a result of oblique transpression within a major double left step and restraining bend in the San Felipe fault zone. Folding probably started just prior to deposition of the Pleistocene Sunset Conglomerate, with the bulk of shortening occurring during and after deposition of the youngest preserved beds. Although a low-amplitude original corrugation and/or slight folding during detachment faulting are permitted by the data, a single folding event in the Quaternary provides a simpler explanation.

Evidence for Flexural Slip Folding in the Yaqui Ridge Antiform

Slickenline data from the West Salton detachment fault are complex and show a large dispersion around a modal top-to-the-east slip direction (Fig. 12C). This top-to-the-east population is present on both limbs of the Yaqui Ridge antiform. The current antiformal shape of the detachment is not geologically plausible during slip across it, however. It would require the impossible—that the hanging wall of the detachment fault had reverse-sense slip across the SSW-dipping part of the detachment fault when both the E- and NE-trending slickenlines were forming. Such slip can develop easily, if there is a breakup fault or secondary breakaway to back tilted part of the detachment fault. However, our multi-university research group has identified no such fault near Yaqui Ridge in the seven years of detailed mapping. Large expanses of the hanging wall demonstrably do not have such a structure (Steely, 2006; Janecke unpublished mapping). Altogether the lineation and slickenline data show that the Yaqui Ridge antiform (the detachment fault and the underlying mylonite) cannot be an original corrugation or fold that predates slip across the detachment fault. The mylonite was likely much more planar but dipping prior to folding.

During folding of an originally NE- (?) to ENE-dipping mylonite and West Salton detachment fault to its current symmetric antiformal geometry, there must have been greater reorientation and tilting of the SW-dipping limb than of the NE- or N-dipping limb. A symmetric antiform would result from monoclinal folding of originally dipping features. In effect, the Yaqui Ridge antiform has one tilted limb, like a monocline, not two tilted limbs, like an anticline. Significant northeastward tilting of the NE-dipping part of the detachment fault is unlikely because the fault has such a low dip (Figs. 2, 7, and 13).

It is striking that the incongruent dip-slip slickenlines that are so numerous on the SW-dipping part of the West Salton detachment fault (Figs. 12C, 12E, and 12F) are distributed in a plane perpendicular to the axis of the Yaqui Ridge antiform (113° ± 7° and 126° ± 10°). We suggest that these dip-slip slickenlines on the SW-dipping part of the detachment fault formed during flexural slip across the fault plane within

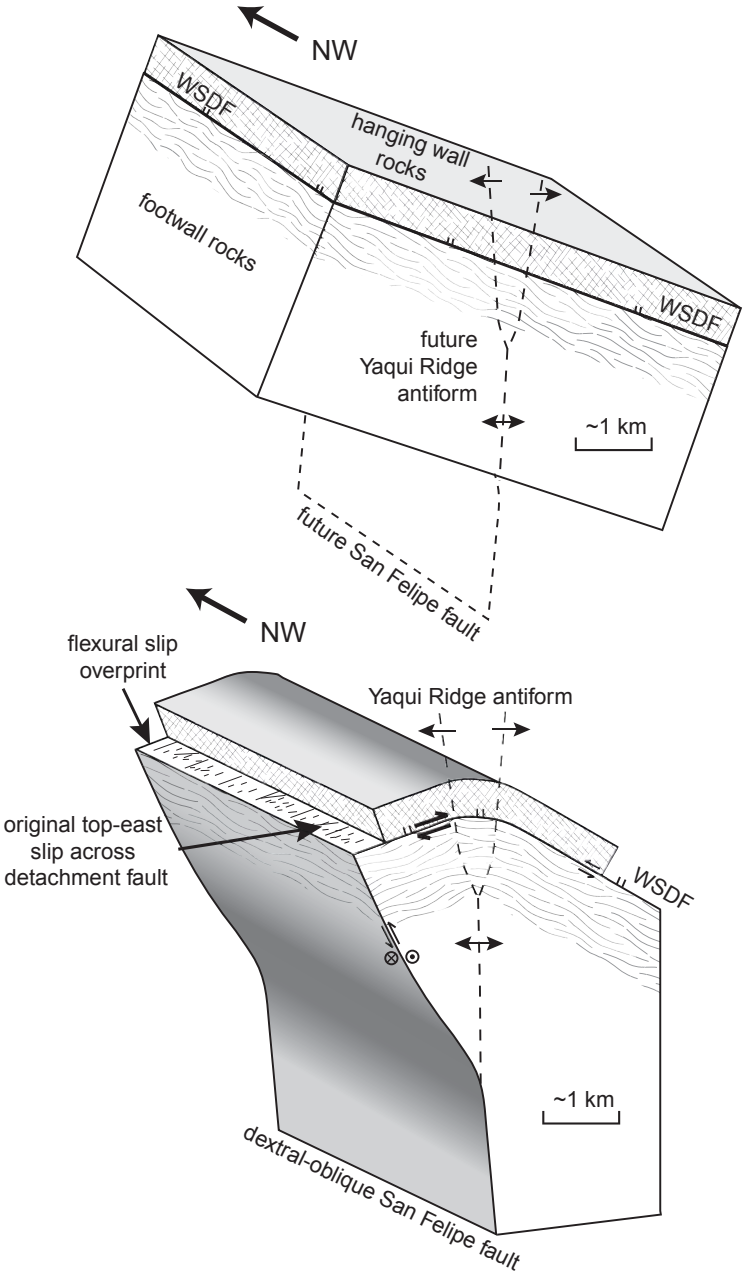

Figure 15. Schematic diagram showing the formation of slickenlines due to flexural slip between the hanging wall and footwall of the West Salton detachment fault (WSDF) during younger monoclinal folding. Note that formation of the Yaqui Ridge antiform is the result of a SW-dipping monocline that deformed an originally NNE- to ENE-dipping mylonite and detachment fault.

a growing, SW-facing monocline (Fig. 15), in a manner originally suggested by Axen and Fletcher (1998) to explain disparate slip indicators reported by Stinson and Gastil (1996) farther south along the detachment fault. The east-northeastward regional dip direction of the detachment fault and this monocline model predict that there was less reorientation and flexural slip across the NE-dipping part of the detachment fault, and therefore many fewer NE-plunging dip-slip slickenlines are expected there. This prediction agrees with the data (Fig. 12). Seventeen percent of the slickenlines on the NE-dipping part of the detachment lie near the center of the NE quadrant, whereas 80% of the slickenlines on the SW-dipping limb have this dip-slip trend and are perpendicular to the antiform (Figs. 12 and 15) (Steely, 2006). The 90° angular difference between the WNW trend of the Yaqui Ridge antiform and the SW-plunging slickenlines SW of the antiform is the difference predicted by the monoclinal flexural-slip model (Fig. 12C). Crosscutting relationships between NE- and E-trending slickenlines are not preserved within the fault zone, so it was not possible to further test our hypothesis by assessing whether NE-trending slickenlines are younger than the E-trending ones.

In summary, our data show that the footwall mylonite and West Salton detachment fault at Yaqui Ridge have an antiformal shape that cannot be attributed to an original corrugation of the Cretaceous mylonite, folding of the mylonite before detachment slip, or folding of the detachment fault and mylonite during slip on the detachment fault. Regional relationships and our structural analysis suggest that the mylonite and detachment fault were originally NNE- to ENE-dipping and much more planar before the early Pleistocene, although their predeformational strike may have departed somewhat from regional trends. A SW-facing monocline explains the antiformal shape of an originally ENE- to NNE-dipping mylonite and detachment fault at Yaqui Ridge. Flexural slip along the detachment fault during folding in the Narrows stepover can produce the anomalous dip-slip population of slickenlines (NE- and SW-plunging) that are more abundant on the SW-dipping part of the detachment fault than on the NNE-dipping part of the fault. We therefore document two monoclines along the San Felipe fault zone: a short NE-facing monocline that probably formed above the upward propagating NE-side down Sunset fault and a longer SW-facing monocline near the San Felipe fault.

Deactivation of the West Salton detachment fault and the duration of temporal overlap with the San Felipe fault zone

We initiated this study in part to determine if the initiation of dextral faults SW of the southern San Andreas fault quickly deactivated the older West Salton detachment fault (abrupt episodic behavior) or if there was a large demonstrable overlap in activity on the two fault systems (more complex evolving behavior). The answer to this question would indicate when the West Salton detachment fault was last active as a single, ~125-km-long structure that was continuous from Palm Springs in the north to the Vallecito–Fish Creek basin in the south. The distinction between slip on a coherent detachment fault and continuing slip on much smaller parts of the detachment is important because

the tectonic and basinal implications of these two contrasting modes are very different. In the former case (coherent detachment fault), the entire western Salton basin would continue to subside, whereas the second mode would allow continued slip on parts of the detachment coeval with new, younger structures. This should produce localized uplifts and basins as the original supradetachment basin was partly dismembered by dextral faults.

The West Salton detachment fault was a coherent structure from the late Miocene (?) or Pliocene into the early Pleistocene based on stratigraphic relationships (Axen and Fletcher, 1998; Winker and Kidwell, 2002; Dorsey and Janecke, 2002; Kairouz, 2005; Dorsey, 2006; Dorsey et al., 2006; Lutz et al., 2006; Matti et al., 2006). A period of overlapping activity between the San Felipe fault zone and the West Salton detachment fault may be indicated by relationships along the Perpendicular Bluff fault, the N-striking splay of the San Felipe fault system described above. This sinistral-oblique fault offsets the main trace of the West Salton detachment in the south but does not cut a short, subsidiary strand of the detachment in the N that is localized within the footwall of the main detachment fault (Fig. 5). This relationship has been used as evidence for continued slip on the N-dipping part of the detachment fault after the S-dipping part was tilted southward and therefore deactivated, while the remainder of the detachment continued to slip. This geometry was interpreted as evidence for clockwise rotation of slip vectors on the West Salton detachment fault through time as the strain field evolved from transtension to dextral faulting (Axen et al., 2004). This "overlapping slip" model implies continued slip across the detachment N of Yaqui Ridge while the San Felipe fault was beginning to cut across it and deactivation of the SW-dipping part of the fault. The continued detachment slip on the NE side of Yaqui Ridge was then transferred eastward to another structure—presumably to the Sunset fault—for a period of time. The Sunset and Fish Creek Mountains faults are the only mapped structures available to accommodate slip from any still-active part of the detachment fault after deactivation in the south (Steely, 2006).

Both structural and stratigraphic lines of evidence make this overlapping slip model unattractive, though none completely rule it out: (1) The abrupt stratigraphic change from regional detachment-related subsidence (during deposition of the Borrego Formation) to localized basin subsidence and block uplift (during deposition of the Ocotillo Formation and erosion of the uplifted fault blocks along the San Felipe fault zone) occurred rapidly throughout the western Salton Trough at ca. 1.1 Ma (Lutz et al., 2006; Kirby et al., 2007). This result is not predicted if the detachment fault were still an active structure creating accommodation space on a regional scale. A gradual stratigraphic change from open lacustrine mud-dominated facies to basin-margin sand to gravel-dominated facies is expected in the San Felipe–Borrego basin, if there was coeval slip on the two structures. Instead the change is sharp and abrupt. (2) Strands of the San Felipe fault zone near Yaqui Ridge cut and offset the detachment fault 5.8 ± 2.8 km and show that this dextral fault zone is a younger crosscutting structure. Once the San Felipe fault cut the detachment on the south side of Yaqui Ridge, we infer that the detachment stopped slipping on both sides of the crossing fault. (3) The steep, SW-dipping reverse-dextral geometry of the Sunset fault nearest the gently NE-dipping West Salton detachment fault does not favor a transfer of strain between the two oppositely dipping faults. Furthermore, there is no overlap of slip directions between the detachment fault and the Sunset fault (Fig. 12), and we know of no evidence for strain partitioning because there is no suitable fault for partitioning nearby (Steely, 2006). (4) Initial top-to-the-NE slip across the West Salton detachment fault (Axen et al., 2004) is inconsistent with evidence for a large original corrugation in the West Salton detachment fault at Whale Peak. A corrugation there is required by the lack of an ESE-plunging fold in the hanging wall of the detachment that aligns with the corrugation and has the same strain as the fold-like form of the detachment fault (Kairouz, 2005). This major ESE-plunging antiformal corrugation is positioned in such a way as to preclude top-to-the-NE slip across the West Salton detachment fault at Whale Peak and Yaqui Ridge when it existed. (5) The overlapping slip model predicts that the detachment was active longer north of Yaqui Ridge than south of it, yet the opposite is true (Kairouz, 2005; Dorsey, 2008, written commun.). (6) Early Pleistocene deactivation of the West Salton detachment fault is also implied by the basinal studies of Johnson et al. (1983), Dorsey (2006), Lutz et al. (2006), and Kirby et al. (2007). (7) Finally, the relationship between the Perpendicular Bluff fault and the subsidiary detachment fault at Yaqui Ridge might be the result of the San Felipe fault zone reutilizing a short piece of a preexisting subsidiary detachment fault as it transforms the soft link in the Narrows stepover of the San Felipe fault zone into a hard link. Figure 5 shows this latter interpretation using color-coded faults.

The transition from Pliocene-age slip on the West Salton detachment fault to slip on new dextral-oblique faults was structurally complex and occurred at ca. 1.1 ± 0.2 Ma at Yaqui Ridge. Our data strongly suggest an abrupt change between the two fault systems, but may permit a more gradual change with at most a few hundred thousand years of overlapping activity. In any case, we infer that the West Salton detachment fault stopped being a major, regional structure in early Pleistocene time, by or before ca. 1.1 ± 0.2 Ma when the San Felipe fault zone initiated and cut across it. The West Salton detachment fault was certainly inactive by ca. 0.6 Ma.

Role of the San Felipe Fault in the San Andreas Fault System

The San Felipe fault zone is one of four dextral faults in southern California that together have accommodated roughly half of the motion across the San Andreas fault system since early Pleistocene time. The other half is taken up by the southern San Andreas fault itself (e.g., Fialko, 2006). The estimated 5.8 ± 2.8 km of right separation across the San Felipe fault zone near Yaqui Ridge on the San Felipe fault is greater than the right separation across the better known southern Elsinore fault (~2.5 km; Todd, 2004) and the Coyote Creek fault of the San Jacinto fault zone (~1–4 km; Janecke et al., 2005b; Steely, 2006). Because the San Felipe fault strikes toward the western Elsinore fault zone it may divert some of the slip from the NW third of the Elsinore fault zone onto other faults. This could help explain the apparent along-strike displacement gradient of the Elsinore fault zone (Magistrale and Rockwell, 1996). The San Jacinto fault zone dwarfs the San Felipe fault zone in its total right separation (19–29 km; Sharp, 1967; Hill, 1984) but the basinal effects of the San Felipe fault zone greatly exceeded those of the San Jacinto fault zone, perhaps because the San Felipe fault zone produced more vertical deformation (Fig. 11). All the data indicate nearly simultaneous initiation of the San Jacinto and San Felipe fault zones near the western margin of the Salton Trough in the early Pleistocene (Lutz et al., 2006; Steely, 2006; Kirby et al., 2007; this study). This reorganization represents a major transition from transtension localized on two major faults to distributed dextral faulting in a wide complex zone comprised of at least four dextral fault zones. Other data sets show that the transition also results in widespread transpression south of the Big Bend (Janecke and Belgarde, 2007).

CONCLUSIONS

The San Felipe fault zone initiated in Pleistocene time and is part of a relatively new geometry of the larger San Andreas fault system.

We date its inception to the early Pleistocene, when it cut, folded, and deactivated the West Salton detachment fault in a restraining bend and contractional stepover near Yaqui Ridge. The San Felipe fault zone propagated to the surface at ca. 1.1 ± 0.2 Ma, may have initiated in the subsurface slightly before then, and is therefore coeval with the adjacent San Jacinto and Elsinore faults. It is not an older dextral fault as some previous workers suggested. The San Felipe fault zone accumulated up to 5.8 ± 2.8 km of right slip, and continues to be active in late Pleistocene to Holocene time. Near Yaqui Ridge the fault zone consists of the left-stepping, en echelon, San Felipe, Sunset, and Fish Creek Mountains faults at the E end of an ~15-km-long, E-W–striking restraining bend. Overall the fault steps ~9 km to the left by bending and stepping near Yaqui Ridge. The dextral-oblique Sunset fault is in the middle of this complex left stepover and bend, and controlled deposition of the Pleistocene Sunset Conglomerate of the Ocotillo Formation. Deactivation of the West Salton detachment fault near Yaqui Ridge probably occurred rapidly as the southernmost San Andreas fault system changed from a partially transtensional mode to a wrench and dextral mode of deformation.

The Sunset Conglomerate consists of angular boulder conglomerate to conglomeratic coarse sandstone, was deposited in alluvial fans with NE transport, coarsens up and toward the basin-bounding Sunset fault, and contains recycled sandstone clasts from exhumed Pliocene basin fill. The appearance of recycled clasts in the Ocotillo Formation throughout the SW Salton Trough records uplift and stripping of older basin fill from the paleo-Vallecito and Fish Creek Mountains. Initiation of the San Felipe fault zone had a major impact on the supradetachment basin above the older West Salton detachment fault, and separated it into the Vallecito–Fish Creek subbasin in the south and the San Felipe–Borrego subbasin in the north. The San Jacinto fault zone produced more subtle basinal changes at roughly the same time (Lutz et al., 2006; Kirby et al., 2007).

The San Felipe fault zone is little more than 1 m.y. old near Yaqui Ridge, yet it has already experienced major topographic inversions and kinematic and geometric changes. We currently identify three stages of fault growth and deformation. An initial, broad, fault-propagation monocline faced NE during the blind upward growth of the tip of the Sunset and Fish Creek Mountains faults ca. 1.1–1.3 Ma. A SW-facing monocline probably initiated at about the same time NE of the San Felipe fault and ultimately produced the Yaqui Ridge antiform. The first phase of deformation began to disrupt slip across the West Salton detachment fault, eroded some of the Borrego or Hueso Formation that may have been present in the Vallecito Mountains, and tilted Pliocene sedimentary rocks ~10°–15° to the NE. The second phase began at ca. 1.1 ± 0.2 Ma when three left-stepping faults of the San Felipe fault zone breached the surface. This initiated deposition of the Sunset Conglomerate of the Ocotillo Formation NE of the Sunset dextral-oblique fault, and resulted in rapid progradation of conglomerate and pebbly sandstone throughout the newly subdivided San Felipe–Borrego basin. A NE-down component of slip on the Sunset and Fish Creek Mountains faults produced >600 m of accommodation space for the Sunset Conglomerate of the Ocotillo Formation. During the third and current phase of deformation, which started roughly 0.5–0.6 Ma, NE-SW shortening continues, and former areas of subsidence and sediment accumulation are being inverted and exhumed within the fault zone.

ACKNOWLEDGMENTS

Thanks to R. Crippen, R. Blom, and T. Rockwell for merged Landsat and SPOT data of the area. This research was supported by grants from the National Science Foundation (to S.U. Janecke, R.J. Dorsey, and G.J. Axen) and Petroleum Research Fund of the American Chemical Society (S.U. Janecke). G. Jefferson and the staff of the Anza-Borrego Desert State Park kindly housed our field crews and provided logistical support. Rick Allmendinger's stereonet program was essential for analysis and plotting. This research benefited from insightful discussions with J. Evans, B. Housen, G. Jefferson, S. Kirby, A. Lutz, B. Belgarde, T. Rockwell, and R. Weldon. Thorough reviews by Victoria Langenheim, Jonathon Nourse, Walter Sullivan, and two anonymous reviewers improved the final version of the article.

REFERENCES CITED

Atwater, T., 1970, Implications of plate tectonics for the Cenozoic evolution of western North America: Geological Society of America Bulletin, v. 81, p. 3513–3536, doi: 10.1130/0016-7606(1970)81[3513:IOPTFT]2.0.CO;2.

Axen, G.J., and Fletcher, J.M., 1998, Late Miocene-Pleistocene extensional faulting, Northern Gulf of California, Mexico and Salton Trough, California: International Geology Review, v. 40, p. 217–244.

Axen, G., Kairouz, M., Steely, A.N., Janecke, S.U., and Dorsey, D.J., 2004, Structural expressions of low-angle faults developed in wrench settings: An example from the West Salton detachment fault system: Geological Society of America Abstracts with Programs, v. 36, p. 548.

Bartholomew, M.J., 1968, Geology of the northern portion of Seventeen Palms and Font's Point quadrangles, Imperial and San Diego Counties, California, [M.S. thesis]: Los Angeles, University of Southern California, 60 p.

Belgarde, B.E., 2007, Structural characterization of the three SE segments of the Clark fault, Salton Trough, California [M.S. thesis]: Utah State University, 4 plates, map scale 1:24,000, 216 p.

Bennett, R.A., Rodi, W., and Reilinger, R.E., 1996, GPS constraints on fault slip rates in southern California and northern Baja, Mexico: Journal of Geophysical Research, v. 101, no. B10, p. 21,943–21,960, doi: 10.1029/96JB02488.

Brown, N., Fuller, M.D., and Sibson, R.H., 1991, Paleomagnetism of the Ocotillo Badlands, southern California, and implications for slip transfer through an antidilational fault jog: Earth and Planetary Science Letters, v. 102, p. 277–288, doi: 10.1016/0012-821X(91)90023-B.

Crowell, J.C., 1981, An outline of the tectonic history of southeastern California, *in* Ernst, W.G., ed., The geotectonic development of California: Englewood Cliffs, New Jersey, Rubey Volume I, Prentice-Hall, p. 583–600.

Dibblee, T.W., Jr., 1954, Geology of the Imperial Valley Region, California: Geology of southern California: California Division of Mines Bulletin, v. 170, p. 21–28.

Dibblee, T.W., Jr., 1984, Stratigraphy and tectonics of the San Felipe Hills, Borrego Badlands, Superstition Hills, and vicinity, *in* Rigsby, C.A., ed., 1984, The Imperial Basin-tectonics, sedimentation, and thermal aspects: Society for Sedimentary Geology (SEPM), Pacific Section, p. 31–44.

Dibblee, T.W., Jr., 1996, Stratigraphy and tectonics of the Vallecito-Fish Creek Mountains, Vallecito Badlands, Coyote Mountain, and Yuha Desert, southwestern Imperial basin, *in* Abbott, P.L. and Seymour, D.C., eds., 1996, Sturtzstroms and detachment faults, Anza-Borrego Desert State Park, California. South Coast Geological Society Annual Field Trip Guide Book, no. 24, p. 59–79.

Dorsey, R.J., 2002, Stratigraphic record of Pleistocene initiation and slip on the Coyote Creek fault, lower Coyote Creek, Southern California, *in* Barth, A., ed., Contributions to crustal evolution of the southwest United States: Boulder, Colorado, Geological Society of America Special Paper 365, p. 251–269.

Dorsey, R.J., 2006, Stratigraphy, tectonics, and basin evolution in the Anza-Borrego Desert region, *in* Jefferson, G.T., and Lindsay, L.E. eds., Fossil treasures of Anza-Borrego Desert: San Diego, California, Sunbelt Publications, p. 89–104.

Dorsey, R.J., and Janecke, S.U., 2002, Late Miocene to Pleistocene West Salton detachment fault system and basin evolution, southern California: New insights: Geological Society of America Abstracts with Programs, v. 34, no. 6, p. 248.

Dorsey, R.J., Janecke, S.U., Kirby, S.M., McDougall, K.A., and Steely, A.N., 2005, Pliocene evolution of the lower Colorado River in the Salton Trough: Tectonic controls on regional paleogeography and the regional Borrego Lake, *in* Reheis, M.C., ed., Geologic and biotic perspectives on late Cenozoic drainage history of the southwestern Great Basin and lower Colorado River region: Conference Abstracts: U.S. Geological Survey Open-File Report 2005-1404, p. 13.

Dorsey, R. J., Fluette, A., McDougall. K. A., Housen, B. A., Janecke, S. U., Axen, G. A., and Shirvell, C. R., 2007, Chronology of Miocene-Pliocene deposits at Split Mountain Gorge, southern California: A record of regional tectonics and Colorado River evolution: Geology, v. 35, p. 57–60.

Dorsey, R. J., Fluette, A. L., Housen, B. A., McDougall, K. A., Janecke, S. U., Axen, G. J., Shirvell, C., 2006, Chronology of Late Miocene to Early Pliocene Sedimentation at Split Mt. Gorge, Western Salton Trough: Implications for Development of the Pacific-North America Plate: Abstracts for NSF MARGINS program, Workshop on Rupturing of Continental Lithosphere: Ensenada Mexico, January 9-13, p. 23–24: http://rclcortez.wustl.edu/Workshop_Abstracts.pdf.

Fialko, Y., 2006, Interseismic strain accumulation and the earthquake potential on the southern San Andreas fault system: Nature, v. 441, p. 968–971, doi: 10.1038/nature04797.

Gawthorpe, R.L., Sharp, I., Underhill, J., and Gupta, S., 1997, Linked sequence stratigraphic and structural evolution of propagating normal faults: Geology, v. 25, p. 795–798, doi: 10.1130/0091-7613(1997)025<0795:LSSAE>2.3.CO;2.

Hill, R.I., 1984, Petrology and petrogenesis of batholithic rocks, San Jacinto Mountains, southern California, [Ph.D. thesis]: Pasadena, California Institute of Technology, 800 p.

Housen, B.A., Dorsey, R.J., Janecke, S.U., and Axen, G.J., 2005, Rotation of Plio-Pleistocene sedimentary rocks in the Fish Creek Vallecito Basin, western Salton Trough, California: Eos (Transactions, American Geophysical Union), v. 86, #GP13A–0039.

Hull, A.G., and Nicholson, C., 1992, Seismotectonics of the northern Elsinore fault zone, Southern California: Bulletin of the Seismological Society of America, v. 82, no. 2, p. 800–818.

Janecke, S.U., and Belgarde, B.E., 2007, The width of dextral fault zones and shallow décollements of the San Jacinto fault zone, southern California: Palm Springs, California, Annual Meeting of the Southern California Earthquake Center, v. 17. http://www.scec.org/meetings/2007am/index.html

Janecke, S.U., Vandenburg, C.J., and Blankenau, J.J., 1998, Geometry, mechanisms and significance of extensional folds from examples in the Rocky Mountain Basin and Range Province, U.S.A: Journal of Structural Geology, v. 20, p. 841–856, doi: 10.1016/S0191-8141(98)00016-9.

Janecke, S.U., Dorsey, R.J., Kickham, J.C., Matoush, J.P., and McIntosh, W., 2005a, Geologic map of the Bachelor Mountain Quadrangle, southwest Montana: Montana Bureau of Mines Open-File Report 525, scale 1:24,000, 28 p.

Janecke, S.U., Kirby, S.M., Langenheim, V., Steely, A.N., Dorsey, R., Housen, B., and Lutz, A., 2005b, High geologic slip rates on the San Jacinto fault zone in the SW Salton Trough, and possible near-surface slip deficit in sedimentary basins: Geological Society of America Abstracts with Programs, v. 37, no. 7, p. 275.

Jennings, C.W., 1977, Geologic map of California: Sacramento, California, California Division of Mines and Geology, scale 1:750,000.

Johnson, M., Officer, C.B., Opdyke, D., Woodard, G.D., Zeitler, P.K., and Lindsay, E.H., 1983, Rates of late Cenozoic tectonism in the Vallecito-Fish Creek basin, western Imperial Valley, California: Geology, v. 11, p. 664–667, doi: 10.1130/0091-7613(1983)11<664:ROLCTI>2.0.CO;2.

Kairouz, M.E., 2005, Geology of the Whale Peak Region of the Vallecito Mountains: Emphasis on the kinematics and timing of the West Salton detachment fault, southern California, [M.S. thesis]: Los Angeles, University of California, 56 p.

Kendrick, K.J., Morton, D.M., Wells, S.G., and Simpson, R.W., 2002, Spatial and temporal deformation along the northern San Jacinto Fault, southern California: Implications for slip rates (*in* Paleoseismology of the San Andreas fault system): Bulletin of the Seismological Society of America, v. 92, no. 7, p. 2782–2802.

Kennedy, M.P., and Morton, D.M., 2003, Preliminary geologic map of the Murrieta 7.5 quadrangle, Riverside County, California: U.S. Geological Survey Open-File Report 03-189.

King, T., Cox, B.F., Matti, J.C., Powell, C.L., II, Osterman, L.E., and Bybell, L.M., 2002, Previously unreported outcrops of Neogene Imperial Formation in southern Santa Rosa Mountains, California, and implications for tectonic uplift: Geological Society of America Abstracts with Programs, v. 34, p. 124.

Kirby, S.M., 2005, The Quaternary tectonic and structural evolution of the San Felipe Hills, California [M.S. thesis]: Logan, Utah State University, 182 p.

Kirby, S.M., Janecke, S.U., Dorsey, R.J., Housen, B.A., McDougall, K., Langenheim, V., and Steely, A., 2007, Pleistocene Brawley and Ocotillo Formations: Evidence for initial strike-slip deformation along the San Felipe and San Jacinto fault zones, California: The Journal of Geology, v. 115, no. 1, p. 43–62, doi: 10.1086/509248.

Lamar, D.L., and Rockwell, T.K., 1986, An overview of the tectonics of the Elsinore fault zone, *in* Ehlig, P., ed., Guidebook and volume on neotectonics and faulting in southern California, Cordilleran Section: Geological Society of America, p. 149–158.

Lough, C.F., 1993, Structural evolution of the Vallecito Mountains, Colorado Desert and Salton Trough Geology: San Diego, California, San Diego Association of Geologists, p. 91–109.

Lutz, A.T., 2005, Tectonic controls on Pleistocene basin evolution in the central San Jacinto fault zone, southern California, [M.S. thesis]: Eugene, University of Oregon, 136 p.

Lutz, A.T., Dorsey, R.J., Housen, B.A., and Janecke, S.U., 2006, Stratigraphic record of Pleistocene faulting and basin evolution in the Borrego Badlands, San Jacinto fault zone, Southern California: Geological Society of America Bulletin, v. 118, no. 11, p. 1377–1397, doi: 10.1130/B25946.1

Magistrale, H., and Rockwell, T., 1996, The central and southern Elsinore fault zone, southern California: Bulletin of the Seismological Society of America, v. 861, p. 791–803.

Matti, J.C., and Morton, D.M., 1993, Paleogeographic evolution of the San Andreas fault in southern California: A reconstruction based on a new cross fault correlation, in Powell, R.E., et al., eds., The San Andreas fault system: Displacement, palinspastic reconstruction, and geologic evolution: Geological Society of America Memoir 178, p. 107–159.

Matti, J.C., Morton, D.M., Cox, B.F., Landis, G.P., Langenheim, V.E., Premo, W.R., Kistler, R., and Budahn, J.R., 2006, Fault bounded late Neogene sedimentary deposits in the Santa Rosa Mountains, southern California: Constraints on the evolution of the San Jacinto fault: Eos (Transactions, American Geophysical Union), v. 87, no. 52, T21B-0407.

Merriam, R., and Bandy, O.L., 1965, Source of upper Cenozoic sediments in the Colorado delta region: Journal of Sedimentary Petrology, v. 35, p. 911–916.

Morley, E.R., 1963, Geology of the Borrego Mountain quadrangle and the western portion of the Shell Reef quadrangle, San Diego County, California [M.S. thesis]: Los Angeles, University of Southern California, 138 p.

Morton, D.M., and Matti, J.C., 1993, Extension and contraction in an evolving divergent strike-slip fault complex: The San Andreas and San Jacinto fault zones at their convergence in Southern California, *in* Powell, R.E., Weldon, R.J., and Matti, J.C., eds., The San Andreas fault system: Displacement, palinspastic reconstruction, and geologic evolution: Geological Society of America Memoir, v. 178, p. 217–230.

Reitz, D.T., 1977, Geology of the western and central San Felipe Hills, northwestern Imperial County, California [M.S. thesis]: Los Angeles, University of Southern California, 155 p.

Rockwell, T., Loughman, C., and Merifield, P., 1990, Late Quaternary rate of slip along the San Jacinto fault zone near Anza, Southern California: Journal of Geophysical Research, v. 95, p. 8593–8605, doi: 10.1029/JB095iB06p08593.

Rogers, T.H., 1965, Santa Ana sheet: California Division of Mines and Geology Geologic Map of California, scale, 1:250,000.

Sanders, C.O., 1989. Fault segmentation and earthquake occurrence in the strike-slip San Jacinto fault zone, California, *in* Schwartz, D.P., and Sibson, R.H., eds., Proceedings of Conference XLV: A workshop on fault segmentation and controls of rupture initiation and termination: U.S. Geological Survey Open-File Report OF 89-0315, p. 324–349.

Schultejann, P.A., 1984, The Yaqui Ridge antiform and detachment fault: Mid-Cenozoic extensional terrane west of the San Andreas fault: Tectonics, v. 3, no. 6, p. 677–691, doi: 10.1029/TC003i006p00677.

Sharp, I., Gawthorpe, R.L., Underhill, J., and Gupta, S., 2000, Fault propagation folding in extensional settings: Examples of structural style and synrift sedimentary response from the Suez Rift, Sinai, Egypt: Geological Society of America Bulletin, v. 112, no. 12, p. 1877–1899, doi: 10.1130/0016-7606(2000)112<1877:FPFIES>2.0.CO;2.

Sharp, R.V., 1967, San Jacinto fault zone in the Peninsular Ranges of southern California: Geological Society of America Bulletin, v. 78, p. 705–730, doi: 10.1130/0016-7606(1967)78[705:SJFZIT]2.0.CO;2.

Sharp, R.V., 1972, Tectonic setting of the Salton Trough, *in* Sharp, R.V., ed., The Borrego Mountain earthquake of April 9, 1968: U.S. Geological Survey Professional Paper, p. 15.

Steely, A.N., Janecke, S.U., Dorsey, R.J., and Axen, G.J., 2004, Evidence for Late Miocene-Quaternary low-angle oblique strike-slip faulting on the West Salton detachment fault, southern California: Geological Society of America Abstracts with Program, v. 36, no. 4, p. 37.

Steely, A.N., 2006, The evolution from late Miocene West Salton detachment faulting to cross-cutting oblique strike-slip faults in the SW Salton Trough, California [M.S. thesis]: Utah State University, 253 p., 3 plates, scale 1:24,000.

Stinson, A.L., and Gastil, R.G., 1996, Mid- to Late-Tertiary detachment faulting in the Pinyon Mountains, San Diego County, California: A setting for long run-out landslides in the Split Mountain Gorge area, *in* Abbott, P.L., and Seymour, D.C., eds., Sturtzstroms and detachment faults, Anza-Borrego Desert State Park, California: Santa Ana, California, South Coast Geological Society, p. 221–244.

Tarbet, L.A., and Holman, W.H., 1944, Stratigraphy and micropaleontology of the west side of the Imperial Valley, California: American Association of Petroleum Geologists Abstracts, v. 28, p. 1781–1782.

Todd, V.R., 2004, Preliminary geologic map of the El Cajon 30′ × 60′ quadrangle, southern California: U.S. Geological Survey Open-File Report 2004-1361, scale 1:100,000, 30 p.

Todd, V.R., Erskine, B.E., and Morton, D.M., 1988, Metamorphic and tectonic evolution of the northern Peninsular Ranges batholith, southern California, *in* Ernst, W.G., ed., Metamorphism and crustal evolution of the western United States (Rubey Volume VII): Englewood Cliffs, New Jersey, Prentice-Hall, p. 894–937.

Wagner, D.L., 1996, Geologic map of the Tubb Canyon 7.5. quadrangle, San Diego County, California: California Division of Mines and Geology Open-File Report 96-06.

Winker, C.D., 1987. Neogene stratigraphy of the Fish Creek-Vallecito section, southern California: Implications for early history of the northern Gulf of California and Colorado delta [Ph.D. thesis]: Tucson, University of Arizona, 494 p.

Winker, C.D., and Kidwell, S.M., 1986, Paleocurrent evidence for lateral displacement of the Colorado River delta by the San Andreas fault system, southeastern California: Geology, v. 14, p. 788–791, doi: 10.1130/0091-7613(1986)14<788:PEFLDO>2.0.CO;2.

Winker, C.D., and Kidwell, S.M., 1996, Stratigraphy of a marine rift basin: Neogene of the western Salton Trough, California, *in* Abbott, P.L., and Cooper, J.D., eds., Field conference guidebook and volume for the annual convention: San Diego, California, American Association of Petroleum Geologists, Pacific Section, p. 295–336.

Winker, C.D., and Kidwell, S.M., 2002, Stratigraphic evidence for ages of different extensional styles in the Salton Trough, southern California: Geological Society of America Abstracts with Programs, v. 34, no. 6, p. 884.

Manuscript Received 2 April 2007
Revised Manuscript Received 7 May 2008
Manuscript Accepted 27 May 2008

Printed in the USA

EARLY PLEISTOCENE INITIATION AND STRUCTURAL COMPLEXITIES OF THE SAN JACINTO AND SAN FELIPE FAULT ZONES, WESTERN SALTON TROUGH: PART II

Susanne Janecke[1], Becky Dorsey[2], and Benjamin Belgarde[1]
[1]Utah State University and [2]University of Oregon

Contributors:

D. Forand, B. Housen, S. Kirby, V. Langenheim, A. Lutz, T. Rittenhour, and A. Steely

FIELD GUIDE AND ROAD LOG

Stop 1: Borrego Springs Airport (33° 15.447' N, 116° 19.532' W). Overview and introduction. (NOTE: we may drive a short north on a dirt road located about 0.4 mi. west of the airport, in order to get a better view). From here we can see the SW edge of Coyote Mountain and the SW side of the Santa Rosa Mountains (see photos in the appendix). Figure 2 shows the points of interest on the north edge of San Isidro Mountains (likely not in view), SW edge of Coyote Mountain (CM) and the SW part of the Santa Rosa Mountains. Look for the white marble-rich intervals between the biotite and hornblende-bearing tonalite to the west and the dark weathering biotite-rich migmatite to the east. These units correlate across the fault zones. Table 2 shows the displacement estimates from this analysis as well as the lifetime slip rates. See Figures 1 to 10. Appendix figure 1, 2

Drive NE from stop 1 along the Borrego-Salton Seaway highway toward Salton City. About 8.5 miles from the airport is Lute Ridge to the north. This prominent hill has an escarpment on its far, NE side that coincides with the main trace of the Clark fault. Numerous smaller scarps displacement the pediment that lies in angular unconformity on folded older Quaternary conglomerate. Figure 10 shows a new interpretation of the uplift in Lute Ridge and the folding in low hills a few kilometers to the NW. We interpret this area as preserving extensional and contractional steps between subparallel strands of the dextral Clark fault zone. See Belgarde (2007) for details.

Continue driving east to the turn-off into Coachwhip Canyon on the left/north side of the road. The turn off is not all that well marked. Drive about 0.5 miles to stop 2.

STOP 2: Coachwhip Canyon (33° 17.428' N, 116° 8.949' W). Figure A3, A4 and A5. Figure 9, 10, 12, 13. Park and examine the multiple strands of the Clark fault that parallel bedding in pebbly sandstone of the fine Canebrake and coarse Olla formations. The beds dip south and the faults do too. Microseismicity shows that at least one strand of the Clark fault about 0.5 km farther up the canyon dips steeply to the SE at depth (Fig. 17)(Belgarde, 2007). This requires a bend in the fault plane and reversal of the dip direction. Notice the well-developed clay gouge in excellent exposures of the fault. Other parts of the fault have almost no gouge and could be mistaken for intact bedding planes, particularly in areas of typical exposure. This exposure of the fault is along strike of a scarp in late Pleistocene pediment deposits. Refer to figures 5, 6, 11,

12 and 13. OSL ages range from 21.72 ± 1.19 to 62.26 ± 4.05 ka in these pediment deposits (Rittenhour, Janecke and Belgarde, unpublished).

Coachwhip Canyon illustrates the character of the Clark fault zone in moderately well-lithified units like the Canebrake Formation. Faults dominate in these settings. Where mud becomes a major constituent, folding becomes much more common in the fault zone and the Clark fault broadens (Fig. 15). The Clark fault zone is up to 18 km wide in map view in the Arroyo Salada and Tarantula Wash segments (Belgarde, 2007) (Fig. 13).

Exit Coachwhip Canyon. Drive east on the paved highway to the turn-around and pull-out at 33° 17.044'N 116° 7.788'W. This is about 1.5 miles to the east. The scarp that coincides with the fault exposed at stop 2 is located about 2/3 of the way from Coachwhip Canyon to the turn around. On the way to the turn-around notice the numerous SW-facing fault scarps on the pediment surface. Each of these scarps is along strike of a bedding parallel fault strand of the Clark fault zone in Coachwhip Canyon. We dated this pediment deposit in an exposure about 1 km SSE of the turn around. From the turn-around it is about 1 km SSE to the location of a dated portion of this pediment surface. A fine-grained sand-bearing bed near the base of the pediment deposit produced a late Pleistocene OSL age of 30.71 ±2.34 ka OSL age (Rittenhour, Belgarde, and Janecke, unpublished data).

Turn around and drive back to Arroyo Salada. Turn south opposite Coachwhip Canyon and drive ESE down Arroyo Salada, past the primitive campground, for about 3.5 miles. Two wheel drive is adequate unless it has rained.

Stop 3a: Clark fault zone in Arroyo Salada (33° 15.363' N, 116° 6.559' W). A wide steep fault zone is exposed in the west wall of Arroyo Salada (Belgarde, 2007). This is one of the main strands of the Clark fault zone in the Arroyo Salada segment. Note how the main fault planes parallel bedding planes and are very thin. Prior to a fortuitous rock fall, this fault zone looked like it was intact stratigraphic section. Slickenlines range in direction and include an important population of strike-slip slickenlines. If stop 3a is poorly exposed due to weathering, continue SE to stop 3b. This stop further illustrates the hidden faulting in the sedimentary units. This fault was mapped as a minor thrust fault by Jarg Pettinga but the horizontal slickenlines show that it is instead a major central strand of the Clark fault zone. At least half a dozen similar strands parallel this one, and there is significant deformation dispersed across a region ~18 km wide perpendicular to the fault zone at this spot (Figs. 10, 11, 12, 14,16).

Stop 3b: alternate to stop 3a (33° 14.305' N, 116° 5.804' W). If stop 3a has been covered over by gully wash or we are running ahead of time, continue to stop 3b another 1.7 to 2 miles to the SSE. Drive SE past the turn-off to 17 Palms and turn right into a narrow track leading to Tule Wash. Whenever the road splits turn left or follow any signs to Tule Wash, and drive to the fault exposed at stop 3b. This smaller fault has a NE strike and is a left-oblique strike-slip fault. It is exciting because it is one of a large population of NE– to E-striking left-oblique faults that dominate the SW 40% of the Clark fault's damage zone in the Arroyo Salada and Tarantula Wash fault segment (Fig. 12). The deep structure beneath these left-oblique faults is completely different, however, and consists of a 6-13 km deep planar fault, which is called the Tule Wash fault (Belgarde, 2007)(Fig. 17 and 18). The Tule Wash fault dips steeply NE and passes beneath the shallow and subvertical NE-striking faults exposed at the surface. A decollement surface must separate the incompatible structures at the shallow and deep levels. We envision a left-

oblique fault array on an “overpass” and a steeply NE-dipping dextral fault on an “underpass” (Janecke and Belgarde, 2007, 2008)(Figs. 12, 17, 18). Decollements and pitchfork fault structures, like those modeled by Le Guerroué and Cobbold in Figure 19 E, may facilitate this behavior.

Crossing strike-slip faults also interfere with one another at the same structural level in other parts of the field area (Fig. 11). Mutual interference and mutual bending developed in these situations.

Turn around and return to pavement. Drive west on the Borrego-Salton Seaway Highway for about 5.5 miles. Turn SW (left) into Fonts Wash and follow the signs and track up to Fonts Point in the south.

Stop 4: Fonts Point (33° 15.454' N, 116° 13.958' W). The view looking south from Fonts Point provides a breath-taking vista of the Borrego and Ocotillo formations exposed in the southern Borrego Badlands, as well as other features including Borrego Mountain which is cut by strands of the Coyote Creek fault, the complexly faulted eastern of the Peninsular Ranges, and low-lying sedimentary rocks of the western Salton Trough. Here we are standing at the top of a precipitous erosional escarpment that is currently retreating to the north as a result of ongoing uplift and erosion in the Borrego Badlands. Figure A11.

The Ocotillo Formation is exposed beneath and east of Fonts Point in the erosional escarpment. Using magnetostratigraphy calibrated with the 0.76-Ma Bishop Ash, the sharp base of the Ocotillo Formation was dated at 1.05 ± 0.03 Ma (Lutz, 2005; Lutz et al., 2006). This contact records abrupt expansion of alluvial-fan and fluvial systems that prograded rapidly into and across the former Borrego lake depocenter at this time. Paleocurrent data show that coarse sediment entered the basin from multiple newly emergent sources located south and SW (Vallecito Mts.), west and NW (San Ysidro Mts.), north (Coyote Mt.), and NE (southern Santa Rosa Mts.) of the Borrego Badlands depocenter (Lutz et al., 2006). A systematic up-section increase in C-suite sandstone clasts recycled from the Arroyo Diablo Formation provides evidence for uplift and exhumation of the former hangingwall basin of the WSDF (ibid). Isopach and facies patterns record syn-basinal titling to the NE in response to growth of the San Felipe anticline and oblique slip on the Clark fault (ibid). Based on this and companion studies by Kirby et al. (2007) and Steely et al. (in press), we conclude that rapid progradation of the Ocotillo and Brawley formations across the western Salton Trough was driven by a dramatic increase in sediment flux from the eastern Peninsular Ranges at ~1.1 Ma. This marks a major, tectonically controlled basin reorganization that resulted from initiation of the San Jacinto and San Felipe fault zones and related onset of uplift and erosion in the former hangingwall of the Late Cenozoic West Salton detachment fault.

The Fonts Point Sandstone (FPS) is a thin, well-cemented, widespread sandstone characterized by a stripped calcic paleosol with deep calcite-filled fissures, which in this area rests on the Ocotillo Formation. Lutz et al. (2006) inferred that deposition of the FPS began at ~0.60 ± .02 Ma based on: (1) presence of the 740-ka Thermal Canyon ash in the upper Ocotillo Formation, 49 m below the contact with the FPS; (2) a likely range of sediment-accumulation rates based on correlation to the nearby, well dated Beckman Wash section; and (3) detailed mapping and visual inspection of the contact which indicate that the Ocotillo-FPS contact in this area (from Fonts Point to Inspiration Point) is concordant and conformable. Subsequent mapping by Dorsey

around Inspiration Point supports this interpretation. Farther to the north and south, the base of the FPS is clearly an angular unconformity that truncates early folds and faults in the western Borrego Badlands. Our preferred age for the FPS is not 100% confident and deserves to be further tested. Recent dating of nearby Quaternary terraces and pediment deposits using cosmogenic isotopes (Le et al, this volume) and OSL (T. Rittenour, Janecke and Belgarde) reveals that many terrace deposits that superficially resemble the mesa-capping FPS have much younger ages ranging from about 20 to 60 Ka. Although the deep, stripped nature of calcic paleosols in the FPS suggests that it probably is much older than most of the Late Quaternary pediment deposits, we cannot be certain there was no break between deposition of the uppermost Ocotillo Formation and the basal FPS, even where the contact is concordant and appears conformable. New data are needed to resolve existing uncertainty in the age of the FPS and the depositional - deformational events that it brackets.

Return to pavement and drive past Borrego Springs to the Yaqui Narrows area. Turn east into Nude Wash north of the Narrows. Park where the wash is no longer drivable and hike SW along the wash for about 0.3 miles. Admire the exceptional exposures of pseudotachylyte and fault rocks (Kairouz, 2005, Steely, 2006; Janecke et al. (2008)) on the way to an overlook at Stop 5.

Stop 5: Overview of San Felipe fault zone (33° 7.962' N, 116° 17.264' W). This stop (which is based on Steely, 2006 and Steely et al., in press) illustrates the typical relationship between Pleistocene to Recent strike slip faults and Ocotillo Formation. We are located within a double contractional stepover of the San Felipe fault zone. This relatively unknown dextral strike slip fault reaches from the NW Elsinore fault to the SE part of the San Jacinto fault zone. It is about 60 km long from end to end. In the Yaqui Ridge area there is a cross-cutting relationships between the San Felipe fault zone and the older West Salton detachment fault, as well as syntectonic deposits shed from the nascent San Felipe fault zone. Structurally, the San Felipe fault zone steps left from the large fault on the N side of the Fish Creek Mountains and Vallecito Mountains (the Fish Creek Mountains fault) to the San Felipe fault. The San Felipe fault is south of here under San Felipe Wash and at the base of Yaqui Ridge. A small fault called the Sunset fault is parallel to these two larger structures and lies a couple hundred meters NE of our stop. Slip steps from the Fish Creek Mountains fault to the Sunset fault and then SW to the San Felipe fault. A thick section of folded and faulted conglomerate is north of the Sunset fault, whereas the folded West Salton detachment, mylonite and other crystalline rocks lie south of the Sunset fault. See Steely et al. (in press) for an overly long structural discussion of this stepover.

Our purpose today is to illustrate the stratigraphic and sedimentary record of initial slip in the San Felipe fault zone. The conglomerates that we can see from here, on the NE side of Sunset Wash, were correlated to the Pliocene Canebrake Conglomerate by Dibblee (1954). Detailed mapping and analysis by Steely et al. (in press) shows that this conglomerate correlates instead to the early to middle Pleistocene Ocotillo Formation. The Canebrake is derived from the footwall of the West Salton detachment fault (Axen and Fletcher, 1998; Kairouz, 2005; Steely, 2006). The conglomerate along Sunset Wash does not contain a single clast of mylonite derived from the footwall of the detachment fault, despite being located as little a 300 m NE of the detachment fault. Its provenance was exclusively in the hanging wall of the detachment fault and most of the sediment was shed from displaced and uplifted plutonic rocks immediately SW of the Sunset fault (See figures in Steely et al., in press). Paleocurrents show dispersal to the NE, grain size decreases in that direction, and the composition and grain size are perfectly concordant with

those in the Ocotillo formation nearby. Boulders up to 4 m across near the Sunset fault attest to active tectonism within the San Felipe fault zone and across the Sunset fault during deposition of the conglomerate. An angular unconformity, missing units beneath the Ocotillo Formation about a km SE of here, and the presence of recycled sandstone clasts derived from the Pliocene Arroyo Diablo Formation further support our interpretation.

Very similar relationships exist adjacent to the San Jacinto fault zone, and show that the Ocotillo formation, and its finer lateral equivalent, the Brawley Formation, were deposited in a new sedimentary basin ringed by brand new dextral oblique strike slip faults. The Ocotillo formation thickens by a factor of ~2 NE toward the Clark fault from a condensed section near Font's Point (Stop 4)(Lutz et al., 2007). The Ocotillo Formation coarsens in that direction and contains distinctive clasts shed from the NE side of the Clark fault. Paleocurrents indicate southward flow. Westward thickening and coarsening, and eastward paleocurrent show that the East Coyote Mountain fault was an active structure within the San Jacinto fault zone starting about 1.05 Ma (Lutz et al., 2006). A disconformity and angular unconformity separate the Ocotillo and Brawley formation from the underlying basin fill, and mark the change from syndetachment to syn-strike slip deposition.

Concluding remarks: Many lines of evidence now show that the San Felipe and San Jacinto fault zone are early Pleistocene dextral faults with high lifetime slip rates. Refined and new displacement estimates, combined with magnetostratigraphic dating of the Borrego/Ocotillo contact are the main constraint on this. In addition, the San Jacinto fault zone is far more complex and broad than generally thought. This is especially true where the fault deforms mud-rich sedimentary rocks but dispersed faults are also developed in the crystalline damage zone adjacent to the central part of the fault zone. We believe that this dispersed deformation partly explains the lower slip rates determined in neotectonic studies (e.g. Le et al., this volume) when compared to slip rates inverted from GPS data and calculated using offset bedrock features (Fig. 8, tables 1 and 2)(Janecke et al., in prep.).

Refer to the Field guide for references and figures.

Appendix: Additional photos of field trip stops.

Stop 1 (Day 3). Fish Creek-Vallecito Basin

Climate or tectonic control on progradation of the Hueso Fm? Integration of stratigraphy, paleomagnetism, and ^{10}Be paleo-erosion rates

Kim Le[1], Becky Dorsey[2], Mike Oskin[1], Bernie Housen[3], Tom Peryam[2]

(1) University of California, Davis; (2) University of Oregon; (3) Western Washington University

ABSTRACT:

We present preliminary results of an integrated stratigraphic and geochemical study designed to discern the role of climate- versus tectonic-forcing of landscape evolution and basin sedimentation. This ongoing study focuses on the Fish Creek-Vallecito basin (FCVB) that formed in the hanging wall of the West Salton Detachment fault. The uppermost strata of this basin, the Hueso formation, record an abrupt progradation of locally derived sediments into the Salton Trough at ~2.9 Ma. After 0.9 Ma sedimentation ceased and the basin underwent rapid uplift and erosion in response to mid- to late Quaternary transpression. High concentrations of ^{10}Be (~10^5 atoms/g) in sediments deposited in the basin records slow erosion rates from upland sediment sources in the adjacent eastern Peninsular Range. New high-resolution magnetostratigraphy provides the necessary age control to correct for radioactive decay of ^{10}Be and invert these concentrations for upland catchment-average erosion rates. The corrected concentrations of ^{10}Be indicate an approximately 40% decline in erosion rate from 3 Ma to present. Three samples collected from sediments ~2.9 Ma, ~1.7 ma, and ~1.2 Ma imply erosion rates decreased from 55 ± 12 m/Myr, 47 ± 9 m/Myr, to 34 ± 6 m/Myr. A ^{10}Be-derived erosion rate from modern sediments of 31 ± 4 m/Myr is also consistent with this overall trend. Tectonic forcing of erosion rates through growth of footwall relief across the West Salton Detachment should yield an increase in basin-average erosion rate with time – a predication opposite of the observed trend. Thus we hypothesize that the ^{10}Be data set may record the progressive decay of erosion rate in the source following an initial, as-yet undocumented increase due to climate forcing. Such an increase could have been forced by enhanced climate variability following the onset of northern hemisphere glaciation at ~2.5-3 Ma. Alternatively, erosion rates may have slowed as a result of gradual uplift and increasing aridity in the rain shadow of the Peninsular Ranges, and progradation of the Hueso formation into the Salton Trough may have been driven by slowing basin subsidence rate. Additional ^{10}Be data, combined with information from stratigraphic and paleosol analyses, is needed to further test hypotheses for climatic and tectonic controls on Plio-Pleistocene erosion and basin filling in the FCVB.

Preliminary Plio-Pleistocene stable-isotope and paleosol data from the Fish Creek-Vallecito basin, southern California: Insights into paleoclimate from pedogenic carbonate

Peryam, Dorsey, Bindeman, Housen, Palandri For AGU mtg, fall 2008

In this study we use detailed measurements and isotopic analyses of paleosols in the Fish Creek-Vallecito basin (FCVB), southern California, to interpret changes in Pliocene-Pleistocene paleoclimate in the area. The FCVB currently lies in a hyperarid rain shadow (MAP = 15-17 cm) formed by the Peninsular Ranges. The timing of Peninsular Range uplift is not known, although recent work suggests it could have begun as recently as early Pleistocene (Mueller et al., 2006). Previous paleoclimate studies used isotopic data from ostracodes (Cosma, 2002) and horse teeth (Brogenski, 2001); there has been no prior comprehensive study of paleosols in the basin.

In the FCVB, abundant paleosols are exposed in a thick, tilted stratigraphic section that accumulated in the hanging wall of the West Salton detachment fault. New high-resolution magnetostratigraphic dating allows us to determine the age of paleosol horizons to within 0.01-0.3 m.y. Pedogenic carbonate nodules from 23 horizons ranging in age from 3.7 to 1.0 Ma, spanning a thickness of 2.5 km, were analyzed for oxygen and carbon isotopic compositions on a Gasbench and Finnegan MAT 253 mass spectrometer. The data reveal an increase in carbonate d18O values from -10.5 +/- 0.1 ‰ to -9.2‰ +/- 0.2 ‰ (VPDB) at about 2.5-3.0 Ma. Carbon isotope values in pedogenic carbonate fluctuate between -10.4‰ and -3.8‰ (VPDB) with no apparent trend. A total of forty-nine paleosols were described in the study interval. Most paleosols have shallow carbonate (Bk) horizons and thin, poorly-developed A horizons.

Our finding of an increase in d18O corresponds broadly to a previous study of fossil horse teeth (Brogenski, 2001), which recorded a 2‰ increase in d18O in meteoric water at ~2 Ma. Preliminary recalculation of Brogenski's fossil site ages suggests that the change in d18O occurred earlier than previously reported, around 2.4 Ma. The increase in d18O at ~2.5-3.0 Ma coincides with a global climate change caused by the onset of northern hemisphere glaciation, and may reflect (1) a change in isotopic composition of the atmospheric water-vapor source, (2) an increase in enriched Pacific Ocean-derived storms and decrease in the concentration of isotopically depleted monsoonal sources, or (3) an increase in soil water evaporation driven by an increase in local temperature or of summer precipitation. The observed increase in d18O is opposite of the change that would be produced by the onset of a rain shadow in the FCVB. This suggests that uplift of the Peninsular Ranges occurred before 3.7 Ma or after 1 Ma, or perhaps took place in two stages (before 3.7 Ma *and* after 1 Ma).

We interpret the majority of paleosols as Aridisols that formed under arid to semi-arid conditions. Measurements of depth to the soil carbonate (Bk) horizon show an average decompacted depth to Bk of 19.7 +/- 1 cm, which corresponds to a mean annual precipitation of ~25 cm (Retallack, 2005). This is similar to modern annual rainfall in coastal San Diego and is 8-10 cm more than in the present-day FCVB. While there is considerable scatter in depth-to-Bk measurements, clear trends are not apparent, suggesting that aridity was the dominant climate condition in the basin between 3.7 and 1.0 Ma. Other indicators of climate change in the area, including rise and fall of lake levels and inferences from floral and faunal assemblages, may reflect external factors (i.e. fluvial inflow) rather than local climate conditions.

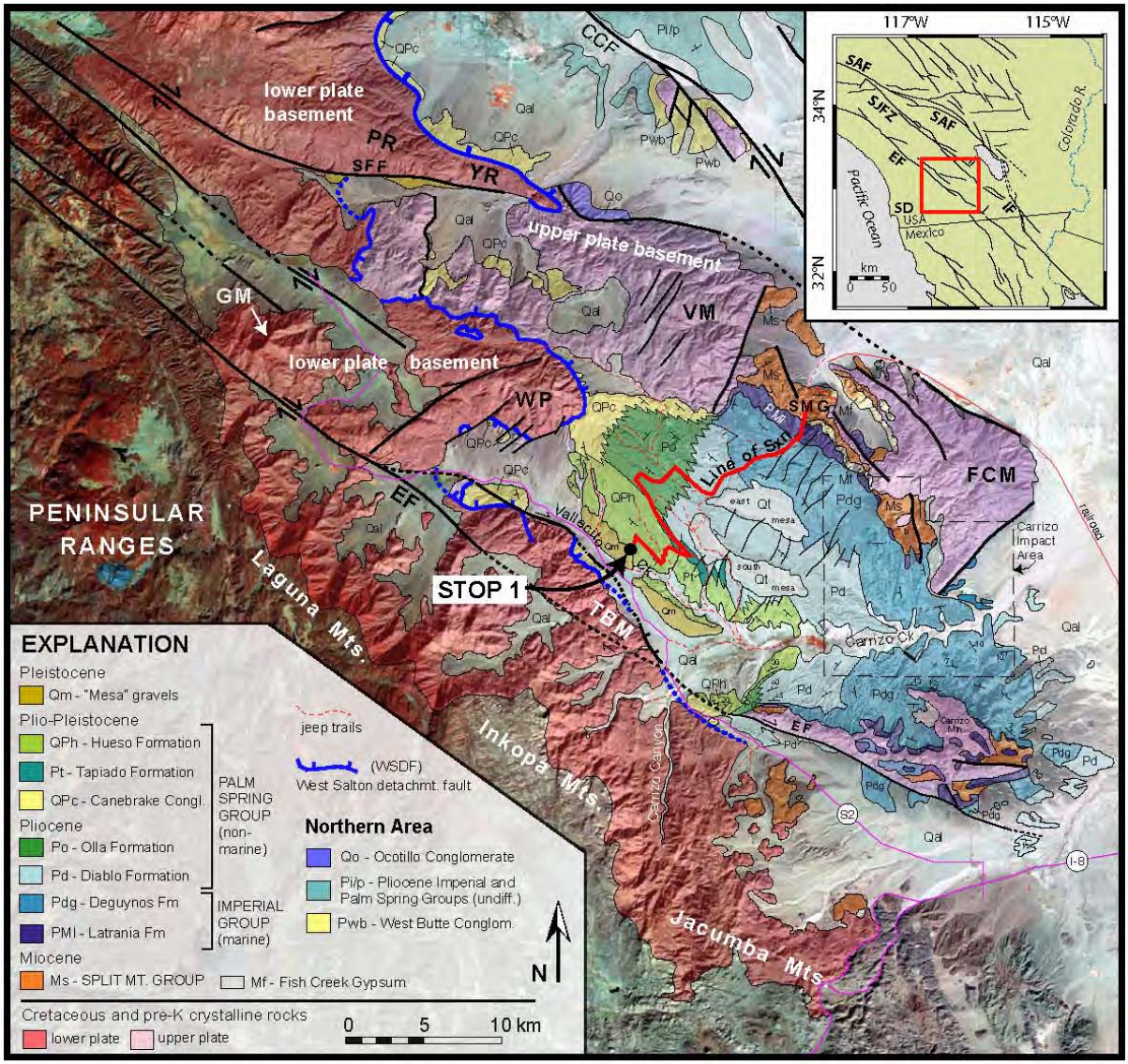

Figure 1. Geologic map of the Fish Creek – Vallecito basin and surrounding area, modified from Winker (1987), Winker and Kidwell (1996), Dibblee (1996), Axen and Fletcher (1998), Kairouz (2005), Steely (2006), Axen (unpubl.), and Dorsey (unpubl.). CCF, Coyote Creek fault; FCM, Fish Creek Mountains; GM, Granite Moutnain; PR, Pinyon Ridge; SFF, San Felipe fault; SMG, Split Mountain Gorge; TBM, Tierra Blanca Mountains; VM, Vallecito Mountains; YR, Yaqui Ridge; WP, Whale Peak.

Introduction:

Testing the role of climate versus tectonic forcing of sediment production (e.g. Zhang et al., 2001) can be accomplished through documenting changes in erosion rates over time and relating these changes to basin architecture and tectonic history. ^{10}Be archived in sedimentary basins may be a sensitive recorder of paleo-erosion rates, so long as other components of ^{10}Be ingrowth are quantified. The accumulation of cosmogenic ^{10}Be in quartz measures the lifetime of sediment within 1 to 2 m of the surface. This lifetime includes five components: (1) erosion of bedrock, (2) hillslope transport, (3) fluvial transport, (4) burial in a depocenter, and (5) exhumation of the buried

sediment (Balco and Stone, 2005). The FCVB (Fig. 1) provides an ideal setting to use ^{10}Be in buried sediments to extract paleo-erosion rates because the sediment source area can be well constrained and the basin underwent rapid rates of sediment burial and exhumation (0.6 mm/yr and >2 mm/yr). These rapid rates minimize the ingrowth of ^{10}Be during burial and exhumation of the sediment (components 4 and 5), thus we can isolate the part of the system that reflects erosion and sediment transport in upland catchments (components 1-3). In this study we integrate stratigraphy, paleomagnetic data, and detrital ^{10}Be concentrations to extract a record of paleo-erosion rates from ~3.0 Ma to 0.9 Ma, and compare these to ^{10}Be-derived erosion rates from modern streams. Geologic mapping and stratigraphic analysis constrains the basin history and sediment source areas. New high-resolution magnetostratigraphy provides precise timing of sediment deposition necessary for defining burial rates and correcting ^{10}Be concentrations for radioactive decay ($t_{1/2}$ = 1.36 Myr). ^{10}Be concentrations in the basin are one to two orders of magnitude greater than corrections for sediment burial and exhumation, and thus these concentrations faithfully record process rates (predominantly erosion rate) in the geomorphic system during the Pliocene and early Quaternary.

Geologic Setting and Stratigraphy:

The FCVB was originally part of a large, Late Cenozoic sedimentary basin that formed in the hanging wall of the West Salton detachment fault (WSDF) and was bounded on the northeast side of the Salton Trough by the San Andreas fault (Dibblee, 1954, 1984; Axen and Fletcher, 1998; Dorsey, 2006). Regional extension, transtension, and crustal subsidence led to late Miocene deposition of coarse alluvial deposits and overlying marine turbidites, followed by Pliocene to early Pleistocene subsidence and filling of the Salton Trough with a thick section of marine and nonmarine deposits (Dibblee, 1954, 1984; Woodard, 1963, 1974; Kerr, 1982; Winker, 1987; Kerr and Kidwell, 1991; Dibblee, 1996;

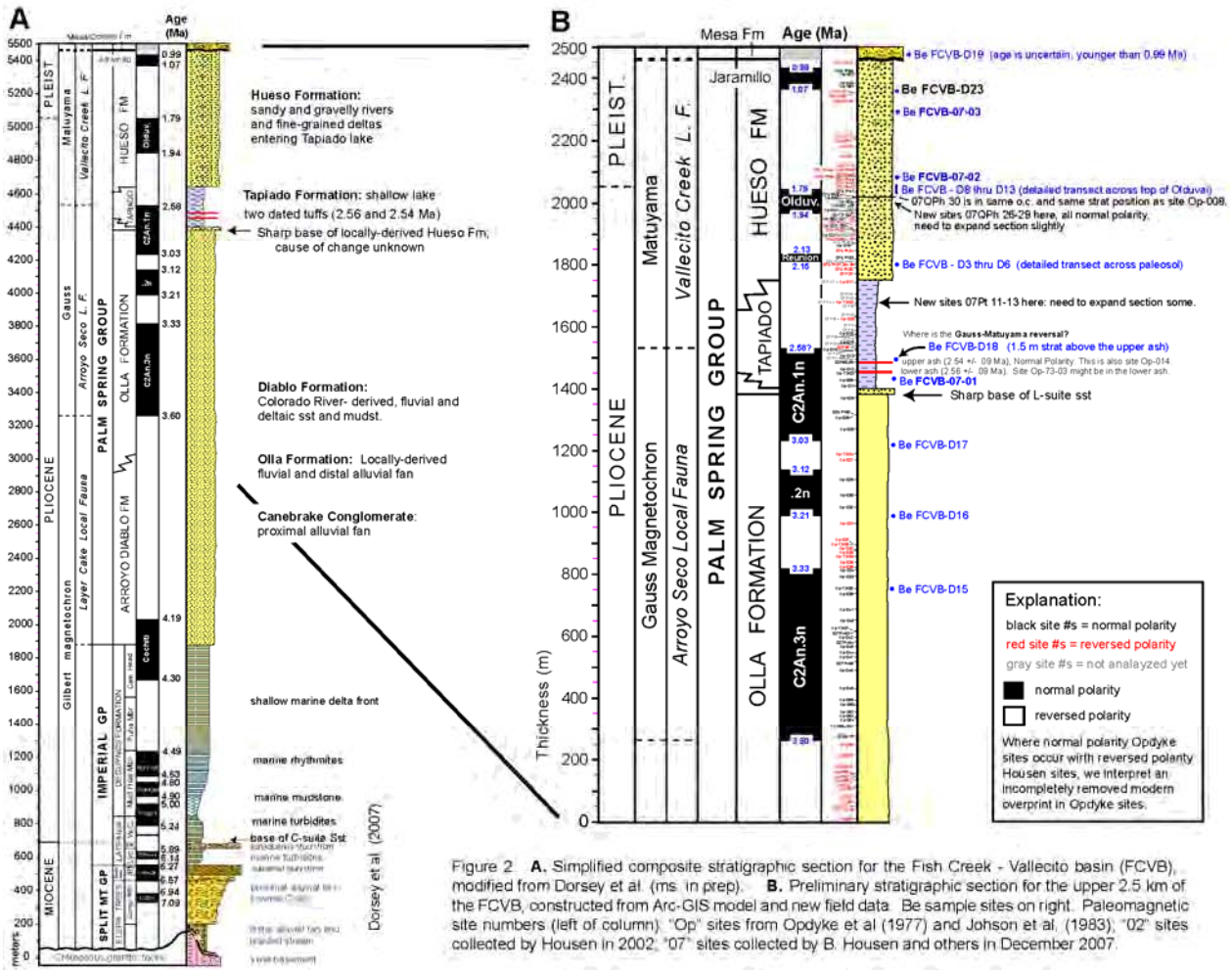

Figure 2. **A.** Simplified composite stratigraphic section for the Fish Creek - Vallecito basin (FCVB), modified from Dorsey et al. (ms. in prep). **B.** Preliminary stratigraphic section for the upper 2.5 km of the FCVB, constructed from Arc-GIS model and new field data. Be sample sites on right. Paleomagnetic site numbers (left of column): "Op" sites from Opdyke et al (1977) and Johson et al. (1983); "02" sites collected by Housen in 2002; "07" sites collected by B. Housen and others in December 2007.

Winker and Kidwell, 1996; Axen and Fletcher, 1998; Dorsey et al., 2007). The Colorado River constructed a large fluvial-deltaic system, recorded in the widespread Arroyo Diablo Formation, that prograded into and filled the basin at the north end of the Gulf of California during Pliocene time (Winker and Kidwell, 1986). Sediment derived from local basement uplifts, including the footwall of the WSDF, produced coarse Plio-Pleistocene conglomerate and sandstone that interfinger laterally with Colorado River sediment and make up a narrow belt of coarse alluvial facies that flank the margins of the basin (e.g., Winker and Kidwell, 1996; Kairouz, 2005).

The base of the Hueso Formation is a sharp but conformable contact that records the abrupt last appearance of Colorado River derived sand in the FCVB (Figs. 1 and 2; Winker, 1987). Where the Hueso overlies the Arroyo Diablo Formation, the contact is marked by an abrupt change from Colorado River- to locally-derived sand. In this study, we are especially focused on understanding underlying control(s) on this reorganization of sediment dispersal in the basin. The Tapiado Fm is a fine-grained unit of interbedded lacustrine mudstone, siltstone and sandstone that passes laterally to the NW and SE into the lower Hueso Fm. The Hueso Formation contains a wide range of lithofacies including locally-derived fluvial sandstone, conglomerate interbedded with sandstone, and thin-bedded sandstone with mudstone transitional to the Tapiado Formation. At the top of the section, the Hueso Formation is overlain by a thin Quaternary gravel unit that was named the Mesa Formation by Woodard (1963) (Fig. 3). The transition from the Hueso Formation to overlying gravels is a complex progressive unconformity that contains subtle fanning dips, calcic paleosols, reworked sandstone clasts, and thin lacustrine carbonates.

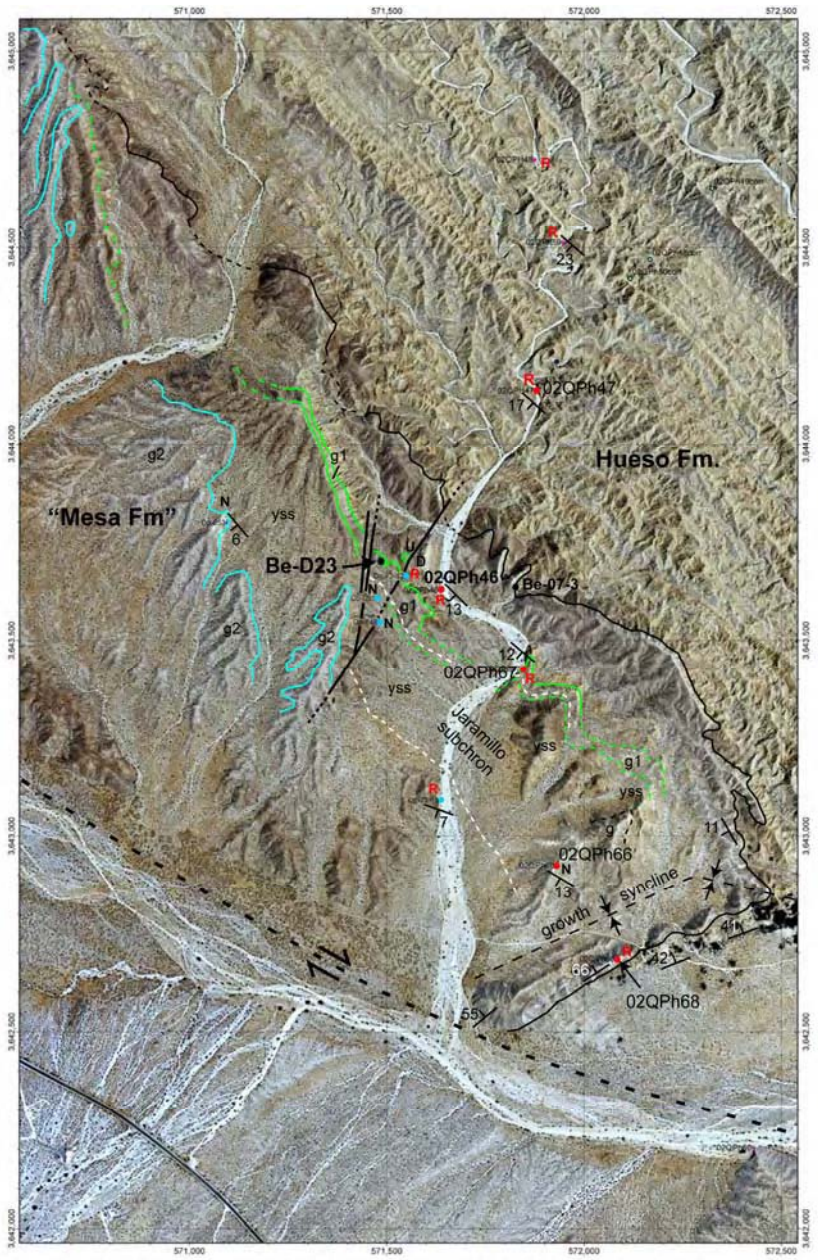

Figure 3. Preliminary geologic map of lower View of the Badlands Wash. Includes paleomag sites (B. Housen, red dots; Johnson et al., 1983, blue dots) and two Be sampling sites. Contact between Hueso and Mesa formations is a progressive unconformity. Unpubl. mapping by B. Dorsey (2008).

The end of deposition and onset of uplift in the FCVB was part of tectonic reorganization and was linked to initiation of the southern Elsinore fault at about 1 Ma (Johnson et al., 1983). Strands of the WSDF at Whale Peak and the NE Tierra Blanca Mountains continued to slip during early slip on the modern Elsinore fault zone in this area, as indicated by recent mapping which shows that the WSDF cuts post-1 Ma deposits of the "Mesa Formation" (c.f. Woodard, 1963) (G. Axen and R. Dorsey, unpubl. map data). Strands of the Elsinore fault on the NE margin of the Tierra Blanca Mountains appear to closely follow and cross-cut older low-angle normal (or oblique-slip) faults of the low-angle WSDF (Fig. 1), suggesting possible reactivation and interaction of the two fault systems during Early Pleistocene time. Strands of the WSDF in this area appear to now be inactive, and active faulting (+/- related folding) is dominated by high-angle strike-slip and oblique-slip faults of the Elsinore fault zone (Fig. 1).

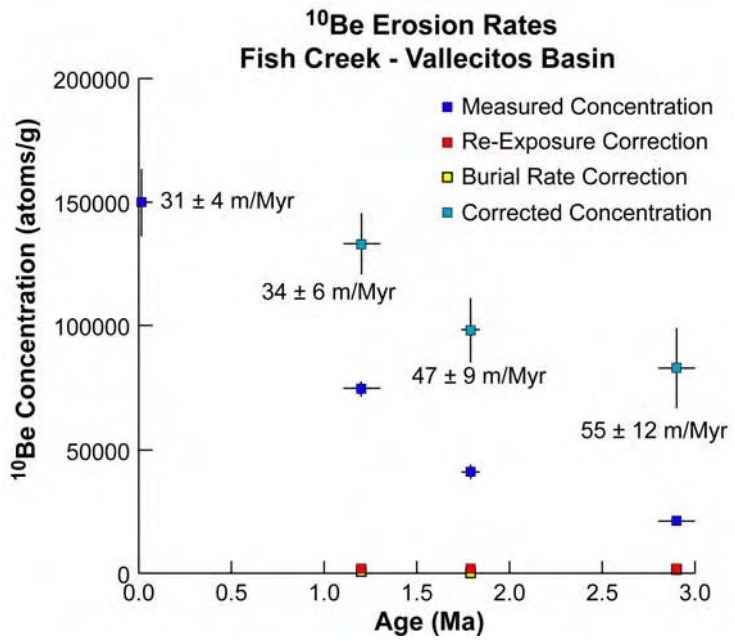

Figure 4. Plot of paleo-erosion rates for the Fish Creek-Vallecito basin derived from ^{10}Be concentrations from samples of the Hueso formation. These data show that upland erosion rates declined from 55 ± 12 m/Myr to 34 ± 6 m/Myr during deposition of the Hueso formation. A sample from Vallecito creek, plotted at 0 Ma for comparison, shows a similar concentration to the corrected value from the uppermost Hueso formation. ^{10}Be concentrations in basin sediments ranged from $2x10^4$ to $8x10^4$ atoms/g. Corrections for burial and re-exposure of the sediments are an order of magnitude lower than this. Error bars for these corrections are smaller than the size of plotted points. Decay of ^{10}Be accounts for the largest component of correction to the concentrations, and the age error accounts for most of the uncertainty in the erosion rates. Both spallation and muon production pathways for ^{10}Be are modeled (Brown et al., 1995). Errors are 95% confidence.

^{10}Be Paleo-Erosion Rates:

A suite of 20 ^{10}Be samples were collected from the Hueso formation and surrounding source streams. At present we only have results for four of these samples: three from the Hueso formation and one from the Vallecito creek upstream of the badlands. For each ^{10}Be sample from the basin sediments we used detailed stratigraphic analysis to characterize its depositional setting. We chose samples from the base of thick channel-fill sandstones deposits that we interpret were buried quickly. Because ^{10}Be decays with a half-life of 1.36 Myr, the time between burial and exhumation of the sediment must to be taken into account in order to invert ^{10}Be concentrations for paleo-erosion rate. To make this correction we use a new, high-resolution magnetostratigraphic chronology of depositional ages from the FCVB (Fig.3). In addition to the zero-age sample from Vallecito creek, three ^{10}Be samples were collected from the bases of thick channel-fill sandstones with estimated ages of ~2.9 Ma, 1.7 Ma, and 1.2 Ma.

The results from our four detrital ^{10}Be samples show that the FCVB yields a robust paleo-erosion rate record. Samples from the FCVB yielded high concentrations of cosmogenic ^{10}Be, ranging from $2x10^4$ to $8x10^4$ atoms/g in sediments dating from 2.9 Ma to 1.2 Ma (Fig. 4). Decay of ^{10}Be accounts for the largest correction to these concentrations, and for the largest component of uncertainty in the paleo-erosion rates. Burial and exhumation corrections are more than an order of magnitude lower (~10^3 atoms/g). Erosion rates calculated from the corrected ^{10}Be concentrations decrease over time, from 55 ± 12 m/Myr to 34 ± 6 m/Myr (Fig. 4). The corrected concentrations compare favorably to the concentration of ^{10}Be in modern stream sediments, $15x10^4$ atoms/g, which yield an erosion rate of 31 ± 4 m/Myr. The overall decline in paleo-erosion rate recorded in ^{10}Be concentrations from about 2.9 Ma to the present is consistent with adjustment of a landscape to an increase in erosion rate driven by climate change. However, we need ^{10}Be measurements from locally derived sediments from below the Hueso formation

to test this hypothesis. Samples from these strata await analysis at PRIME lab. At this time we cannot completely rule out that a change in relief production on the escarpment may have influenced sediment production. It is also possible that a decrease in tectonically driven subsidence rate was the primary driver of progradation.

Field Trip Stop 1, Day 3:
^{10}Be Sample site Be-D23 / Paleomagnetic sample site 02QPH46

This stop is located in the upper part of the Plio-Pleistocene Hueso Formation, very close to the top of a 5.5-km thick SW-dipping section that fills the FCVB (Figs. 1, 2). We are close to the fault-bounded southwestern margin of the basin, at the eastern margin of the Peninsular Ranges. The upper Hueso Formation in the lower part of View of the Badlands Wash contains abundant yellow sandstone with thin calcic paleosols interbedded with sandy pebble to pebble-cobble conglomerate. These deposits record deposition in a high-energy stream system with broad shallow gravel-rich channels flanked by sandy flood plains. Look on the west side of the wash and try to find paleomagnetic sampling site 02QPh46 (Fig. 3). This sample was collected by Bernie Housen in 2002 from a thin pedogenic carbonate, and analyzed by him at Western Washington University. We have combined paleomagnetic data from many sites like this with results of previous magnetostratigraphic studies (Opdyke et al., 1977; Johnson et al., 1983), to establish a high-precision chronostratigraphy for the entire FCVB section (Dorsey et al., in prep; Figs. 1, 2). This site has a reversed magnetic polarity and is located a short distance east of (below) the base of the Jaramillo subchron (1.07 Ma). Southeast of here along strike, the map pattern reveals an interesting growth syncline that records folding during deposition of this part of the section (Fig. 3). Syndepositional folding was accompanied by tilting that produced the fanning dips and progressive unconformity in the transition from the Hueso to Mesa Formation.

We will walk up a short side wash to view the location where we collected coarse sands from the upper Hueso Formation for ^{10}Be analysis (FCVB-D23 on Fig. 3). The sample was collected from the lower 10 cm of a 4.0 m thick sandstone interbed in a thick gravel unit designated informally as “g1” (Fig. 3). We collected sample FCVB-D23 to the best of our knowledge near the base of the Jaramillo subchron (1.07 Ma) in between paleomagnetic sampling sites 02QH46(R) and OP-51 to correct for radioactive decay of ^{10}Be in the sample.

Analysis of FCVB-D23 is in progress. We expect its concentration to be similar to nearby sample FCVB-07-D2, with concentration 7.5 $\pm$ 0.5 x 10^4 atoms/g. Three corrections are applied before inverting this concentration for a paleo-erosion rate. Exhumation of the sample at a rate of 2.0 $\pm$ 0.5 mm/yr accounts for less than 4000 atoms/g of ^{10}Be. Radioactive decay, and the accompanying uncertainty of sample age, contributes the largest correction of 6.1 $\pm$ 0.7 x 10^5 atoms/g. Because we sampled the base of a 2-m thick paleo-channel, burial of the sample accounts for the smallest correction, less than 1000 atoms/g. After correction we estimate that the sediment coming into the FCVB at ~1.2 Ma had a ^{10}Be concentration of 1.33 $\pm$ 0.12 x 10^5 atoms/g, indicating an erosion rate of 34 $\pm$ 6 m/Myr.

REFERENCES

Axen, G. J., and Fletcher, J. M., 1998, Late Miocene-Pleistocene extensional faulting, northern Gulf of California, Mexico and Salton Trough, California. International Geology Review, v. 40, p. 217-244.

Balco G., Stone J.O. Measuring middle Pleistocene erosion rates with cosmogenic nuclides in buried alluvial sediment, Fisher Valley, southeastern Utah. Earth Surface Processes and Landforms 30, 1051-1067 (2005)

Brown, E.T., Bourles, D.L., Colin, F., Raisbeck, G.M., Yiou, F., and Desgarceaux, S., 1995, Evidence of muon-induced production of 10Be in near-surface rocks from the congo: Geophysical Research Letters, v. 22, p. 703-706.

Dibblee, T. W., Jr., 1954, Geology of the Imperial Valley region, California, Geology of Southern California, California Division of Mines Bulletin 170, p. 21-28.

Dibblee, T.W., 1984, Stratigraphy and tectonics of the San Felipe Hills, Borrego Badlands, Superstition Hills, and vicinity. In: Rigsby, C. A. (ed.) The Imperial Basin - Tectonics, Sedimentation, and Thermal Aspects. Los Angeles, California, Pacific Section S.E.P.M., p. 31-44.

Dibblee, T. W., Jr., 1996, Stratigraphy and tectonics of the Vallecito-Fish Creek Mountains, Vallecito Badlands, Coyote Mountains, and Yuha Desert, southwestern Imperial Basin. In Sturzstroms and Detachment Faults Anza-Borrego Desert State Park California, edited by P.L. Abbott and D.C. Seymour, South Coast Geological Society Annual Field Trip Guide Book Number 24, p. 59-80.

Dorsey, R.J., 2006, Stratigraphy, tectonics, and basin evolution in the Anza-Borrego Desert region. In: Jefferson, G.T. and Lindsay, L.E. (eds.) Fossil Treasures of Anza-Borrego Desert. Sunbelt Publications, San Diego, CA, p. 89-104.

Dorsey, R.J., Fluette, A., McDougall, K.A., Housen, B.A., Janecke, S.U., Axen, G.J., and Shirvell, C.R., 2007, Chronology of Miocene-Pliocene deposits at Split Mountain Gorge, southern California: A record of regional tectonics and Colorado River evolution. *Geology*, vol. 35, p. 57-60.

Dorsey, R.J., Housen, B.A., Janecke, S.U., and Fanning, M., in prep, Stratigraphic record of crustal subsidence within a transform plate-boundary zone: Late Miocene to Pleistocene Fish Creek-Vallecito Basin, southern California. To be submitted to Basin Research.

Johnson, N.M., Officer, C.B., Opdyke, N.D., Woodard, G.D., Zeitler, P.K., and Lindsay, E.H., 1983, Rates of late Cenozoic tectonism in the Vallecito-Fish Creek basin, western Imperial Valley, California. Geology, v. 11, p. 664-667.

Kairouz, M.E.*, 2005, Geology of the Whale Peak region of the Vallecito Mountains: Emphasis on the kinematics and timing of the West Salton detachment fault, southern California [M.S. thesis], University of California, Los Angeles, 156 pp.

Kerr, D. R., 1982, Early Neogene continental sedimentation, western Salton Trough, California [M.S. thesis]. San Diego State University, San Diego, California, 138 p.

Kerr, D. R., and Kidwell, S. M., 1991, Late Cenozoic sedimentation and tectonics, western Salton Trough, California. In: Walawender, M. J., and Hanan, B. B., eds., Geological Excursions in Southern California and Mexico. San Diego, California, Department of Geological Sciences, San Diego State University, p. 397-416.

Kirby, S. M., 2005, The Quaternary structural and tectonic evolution of the San Felipe Hills, CA. [M.S. thesis], Utah State University, 3 plates, 181 p.

Kirby, S.M., Janecke, S.U., Dorsey, R.J., Housen, B.A., Langenheim, V., McDougall, K., and Steely, A.N., 2007, Pleistocene Brawley and Ocotillo formations: Evidence for initial strike-slip deformation along the San Felipe and San Jacinto fault zones, southern California. *Journal of Geology*, vol. 115, p. 43-62.

Lutz, A.T., 2005, Tectonic controls on Pleistocene basin evolution in the central San Jacinto fault zone, southern California [M.S. thesis]. University of Oregon, 136 p.

Lutz, A.T., Dorsey, R.J., Housen, B.A., and Janecke, S.U. (2006) Stratigraphic record of Pleistocene faulting and basin evolution in the Borrego Badlands, San Jacinto fault zone, southern California. Geological Society of America Bulletin, p. 1377-1397.

Opdyke, N. D., Lindsay, E. H., Johnson, N. M., and Downs, T., 1977, The paleomagnetism and magnetic polarity stratigraphy of the mammal-bearing section of Anza Borrego State Park, California. Quaternary Research, v. 7, p. 316-329.

Steely, A.N., 2006, The evolution from late Miocene west Salton detachment faulting to cross-cutting oblique strike-slip faults in the southwest Salton Trough, California [M.S thesis]: Utah State University, 253 p. 3 plates. Scale 1:24,000.

Steely, A.N., Janecke, S.U., Dorsey, R.J., and Axen, G.J. (in press) Early Pleistocene initiation of the San Felipe fault zone, SW Salton Trough, during reorganization of the San Andreas fault system: Geological Society of America Bulletin, 2009.

Winker, C.D., 1987, Neogene stratigraphy of the Fish Creek-Vallecito section, southern California: implications for early history of the northern Gulf of California and the Colorado Delta [Ph.D. thesis]: University of Arizona, 494 p.

Winker, C.D., and Kidwell, S.M., 1986, Paleocurrent evidence for lateral displacement of the Pliocene Colorado River delta by the San Andreas Fault system, southeastern California. Geology, v. 14, p. 788-791.

Winker, C.D., and Kidwell, S.M., 1996, Stratigraphy of a marine rift basin: Neogene of the western Salton Trough, California, in Abbott, P. L., and Cooper, J. D., eds., Field conference guidebook and volume for the American Association of Petroleum Geologists annual convention, p. 295-336.

Woodard, G.D., 1963, The Cenozoic succession of the West Colorado Desert, San Diego and Imperial Counties, southern California [Ph.D. thesis]: University of California, Berkeley, 494 p.

Woodard, G.D., 1974, Redefinition of Cenozoic stratigraphic column in Split Mountain Gorge, Imperial Valley, California. American Association of Petroleum Geologists Bulletin, v. 58, p. 521-539.

Elsinore Fault: Day 3 (Stop 2)

Slip rates of the Elsinore fault in the southern Coyote Mountains determined by ^{230}Th/U dating of pedogenic carbonate in offset landforms

Kate E. Fletcher
Department of Earth and Planetary Science, University of California- Berkeley, 307 McCone Hall, Berkeley, California, 94720-4767, USA
Tom K. Rockwell
Department of Geological Sciences, San Diego State University, 5500 Campanile Drive, San Diego, CA 92182-1020, USA
Warren D. Sharp
Berkeley Geochronology Center, 2455 Ridge Road, Berkeley, California, 94709, USA
Kim Le
Department of Geology, University of California- Davis, 1 Shields Avenue, Davis, California, 95616-8605, USA

ABSTRACT

On the western slopes of the Coyote Mountains, southwest Imperial Valley, a series of alluvial fans are progressively offset by the Elsinore fault. These fans can be correlated to their source drainages because of their distinctive clast assemblages, thereby defining measurable offsets on the fault. Using U-series on pedogenic carbonate, we have dated three fan remnants that are offset by 59 ± 21 m, 83 ± 31 m and 580 ± 110 m. In CM gravels 10's ka and older, carbonate forms continuous, dense, yellow coatings up to 3 mm thick on the undersides of clasts. Porous white carbonate may completely engulf clasts, but is not dateable. Carefully selected samples of dense, innermost carbonate lamina weighing ~10 to 100 milligrams analyzed by TIMS contain 0.4- 3.8 ppm U, have median ^{238}U/^{232}Th ratios (the ratio of U to "common Th") ~ 40, and therefore are geochemically suitable for precise U-series dating. Carbonate coatings generally yield reproducible U-series ages for sub-samples from the same microstratigraphic horizon, consistent with U-Th systems that have remained closed. Reproducible ages among coatings from the same soil indicate that inherited coatings, though observed in outcrop, have been avoided during sample selection. Because accumulation of datable thicknesses of carbonate likely requires hundreds to a few thousand's of years, U-series on pedogenic carbonate provide minimum ages for deposition of host alluvium. However, recent comparisons of ages obtained for late Pleistocene alluvium in southern California using U-series on pedogenic carbonate and ^{10}Be surface exposure techniques indicate that this "time-lag" for U-series ages may be small relative to other errors inherent to the two techniques.

The three progressively offset alluvial fan remnants we have studied in the Alverson Canyon area afford the opportunity to examine the constancy of slip rate on the southern Elsinore fault. To date, our results indicate that the Elsinore fault in the southern Coyote Mountains has slipped at a maximum mean rate of ~1.9 mm/yr over the past ~40 ka, and perhaps at the much higher rate of ~5.3 mm/yr between 40 and >135 ka. In recent ruptures, slip on the Elsinore increased to the northwest from Alverson Canyon, and if this pattern persisted in the past, our slip rates may underestimate slip rates in the central part of the range. Accordingly, if our dates closely approximate deposition of the offset fans, the Elsinore fault may have carried ~10-20% of the total slip between the Pacific and North American plates before slowing at $\geq$ 40 ka.

INTRODUCTION

The Elsinore-Laguna Salada fault (ELSF) is one of the principal strands of the San Andreas fault system in southern California (Fig. 1), however its seismic potential is often de-emphasized due to previous estimates of a low slip rate. Nevertheless, the fault zone has produced two historic earthquakes over M6, with the 1892 event estimated at >M7 and resulting in ~5 m of slip (Mueller and Rockwell, 1995); thus further investigation of the long-term slip rate on the ELSF is warranted.

Several studies have focused on the northern section of the fault zone, and have yielded rates of about 5 mm/yr for the late Quaternary (Millman and Rockwell, 1986; Vaughan and Rockwell, 1986; Rockwell, 1990; Magistrale and Rockwell, 1996). These studies, whilst thorough, relied on soil development to estimate the age of offset landforms, resulting in relatively low precision slip rate estimates. Our new study examines the southern section of the Elsinore fault and employs U-series dating of pedogenic carbonate, and in one case ^{10}Be surface exposure dating, to obtain dates for offset landforms and buried soils.

The Coyote Mountains Field Site

The Coyote Mountains, located in the southwestern Imperial Valley region of southern California (Fig. 1), were uplifted by transpressive slip on the southern Elsinore fault. Incision and denudation has resulted in the generation at the range front of a series of alluvial fans that cross the Elsinore fault and are progressively displaced from their sources by slip on the fault. Uplift has also resulted in exposure of the early Miocene Alverson Andesite, an andesitic basalt that is present only in certain canyons within the range. Displaced fans that emanated from canyons where the Alverson Andesite is exposed therefore contain a distinctive assemblage of gravel clasts and may be confidently related to their canyon of origin using quantitative determinations of framework clast composition.

In the southern Coyote Mountains range, in the area surrounding Alverson Canyon, two fan surfaces and one buried soil are displaced across the fault within ~700 m (Fig. 2). These surfaces and buried soil have been correlated to their source drainages using clast counting and dated by U-series on pedogenic carbonate to estimate slip rates on the southern Elsinore fault averaged over multiple time scales.

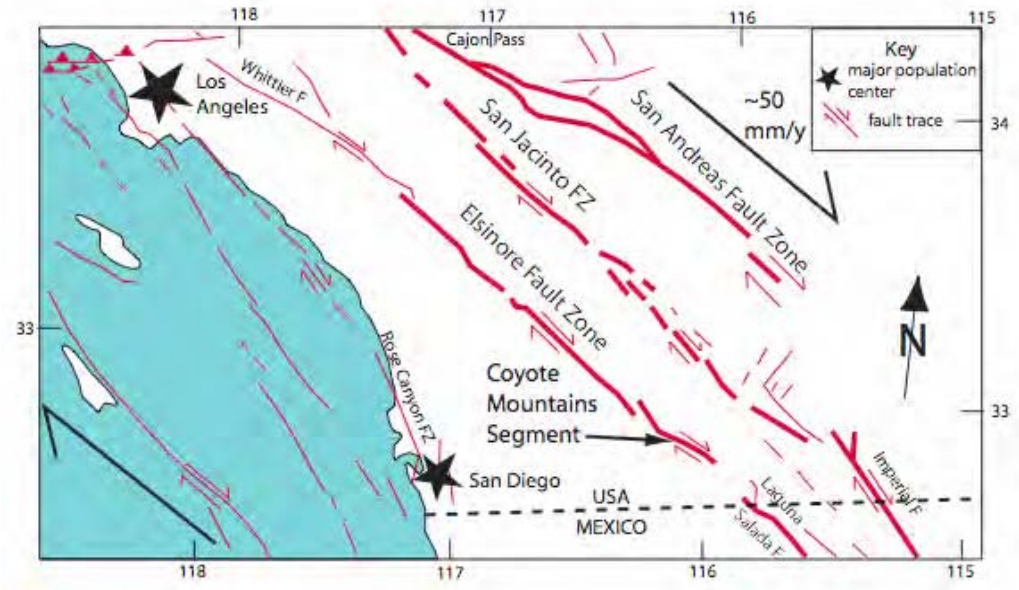

Figure 1: Map of southern California showing major faults and study area on the Coyote Mountains segment of the Elsinore Fault. Most of the Pacific-North American relative plate velocity of ~50 mm/yr is accommodated in the area shown.

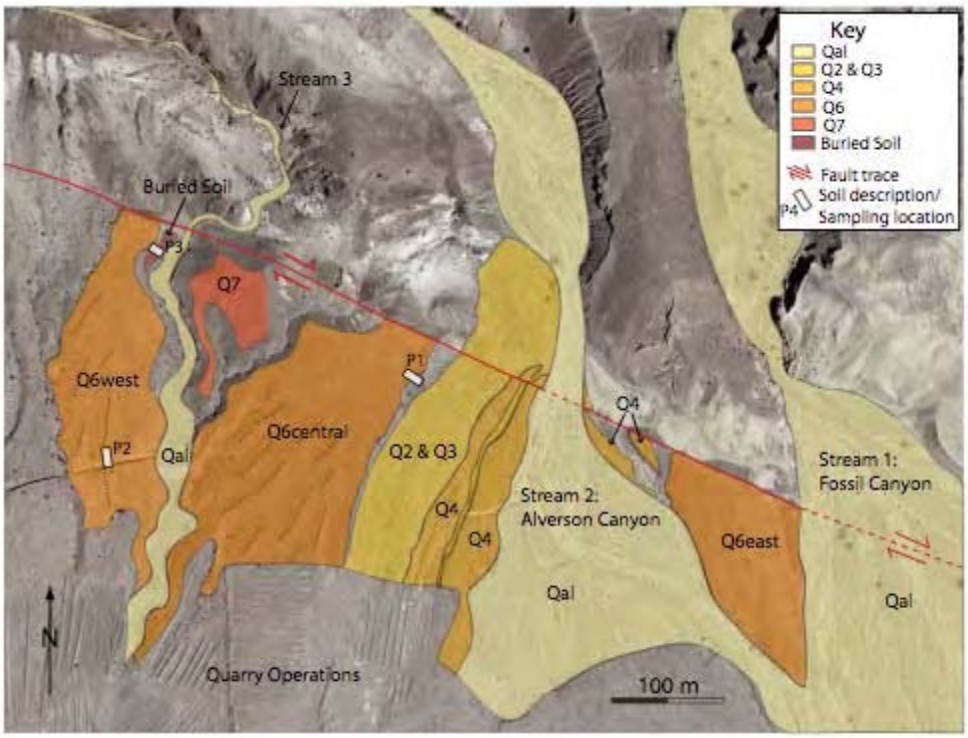

Figure 2: Google Earth image of the southwestern flank of the Coyote Mountains near Alverson Canyon showing the Elsinore fault (heavy red line), selected displaced fan surfaces, active streams with extent of modern alluvium, and locations of soil pits sampled for U-series dating.

OFFSET DETERMINATIONS

Offsets were estimated by determining the provenance of surfaces and buried soils, and measuring their displacement from their source streams. The provenance of two offset fans and a buried soil were determined by point counting clast lithologies in active streams and fan surfaces/buried soils and comparing their

The point counting technique, while good to a first order approximation, is subject to several confounding issues:

1. The variable preservation of different clast types may cause a shift in statistics for older surfaces towards more stable lithologies.

2. Secular changes in the geology of the source stream may result in clast population variations between the modern stream and older deposits that exceed the margin of error.

statistics (Fig. 3). Clast proportions were determined by counting clast-types at 10 cm grid-points on a 1 m square grid of fencing wire. In order to collect a representative sample from each surface 3 to 8 grid locations were randomly selected. Total counts tallied on each surface exceeded 300 in all cases.

3. Inequant clasts may result in higher or lower counts depending on whether counts are taken in map or profile view. For example, foliated metamorphic rocks tend to be deposited broad-side up, resulting in higher counts in map view than in profile view.

Regardless of these caveats, populations of 300-600 grid points yielded definitive matches between displaced alluvial fans and their sources, indicating that this is a useful method for distinguishing among plausible sources with lithologically distinct clast populations (Fig. 3).

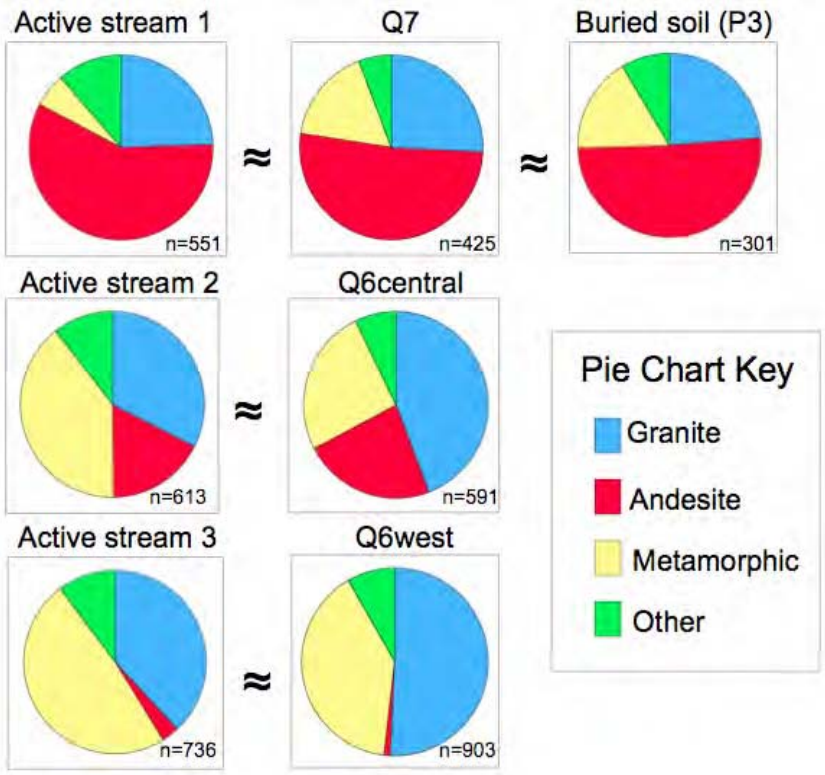

Figure 3: Point counting results from active streams (left column, see Figure 2 for locations), and displaced fans and buried soil (center, right).

The smallest offset we have studied is on the fan surface Q6west, which is correlated to active stream 3. Deposition of this fan was bounded on its eastern side by the Q7 surface. It is possible that deposition of the fan occurred before there was an inflection of the stream just above the fault (i.e. before Q7 moved in front of the stream). The offset in this case would be determined by realigning the western margin of the fan with the western edge of the canyon above the stream inflection, resulting in a maximum offset of 80 m. If the inflection was not formed by Q7 moving in front of the stream, the Q6west surface may have been deposited with the stream in its current position. If this is the case the offset can be measured by realigning the western margin of the fan with the western margin of the current stream as it crosses the fault, resulting in a minimum offset of 38 m. The maximum and minimum offsets combined result in an estimated offset of 59 ± 21 m.

The fan surface Q6central is offset by 83 ± 31 m from its source, active stream 2. We measured from the western edge of the offset fan to the western edge of the Q2 & Q3 fan where it crosses the fault for a minimum offset of 52 m, and from the eastern edge of the fan to the eastern edge of the active stream for a maximum offset of 114 m. The minimum and maximum measurements were averaged to estimate probable amount of offset, and the error is ± half of the difference between the minimum and maximum offsets. We do not differentiate between the active stream and the young fan that is composed of Q2, Q3 and Q4 deposits in our offset estimate, because the young fan is not appreciably offset across the fault.

The buried soil of the Q7 fan is correlated to active stream 1 and is offset by the largest amount, 580 ± 110 m. This offset estimate is determined by measuring from the buried soil back to the middle of active stream 1, and the uncertainty is ± half the width of the active stream.

SOIL CHARACTERISTICS

The soils at the Coyote Mountains field site display characteristics typical of arid to semi-arid climates, with carbonate morphology, fines and observed by freshening natural exposures (P1

and P3) and in a previously cut excavation (P2). The soils developed on surfaces Q6central (observed at Pedon 1; P1 on map) and Q6west (P2) both have stage I+ to II carbonate morphology, with carbonate coatings forming mostly on the bottoms of clasts (Fig 4A), but with some clasts having more extensive coverage. The buried soil (P3) has more mature carbonate morphology with carbonate coatings frequently engulfing the clasts and in some places carbonate forms laminar sills. Interestingly, in our experience, dense dateable carbonate only occurs on the bottoms of clasts, even in the much older P3 soil.

^{230}Th/U DATING OF PEDOGENIC CARBONATE

Background

Pedogenic carbonate coatings (also called cutans, pendants or rinds) accumulate as thin lamina on gravels in soils under arid to semi-humid conditions (Pustovoytov, 2002). Accumulation of pedogenic carbonate on the soil profile scale follows a well documented progression, with development of carbonate coatings on the bottoms of gravel clasts occurring at the outset (Gile et al., 1966; Machette, 1985; Mayer et al., 1988). During pedogenisis, Ca^{+2} ions derived from aeolian dust, rainwater and Ca bearing minerals in the soil profile (Machette, 1985; Capo and Chadwick, 1999) are leached from the upper soil horizons, along with U and other soluble elements. Carbon dioxide from the atmosphere and respired from plant roots dissolves in soil pore waters forming bicarbonate ion ($HCO3^-$). Carbonate precipitation, typically at depths of about 50 to 200 cm, may be caused by increasing ion strength resulting from evaporation, transpiration or freezing, degassing of CO2 from the soil water, or changing the solubility of $CaCO_3$ as solutions move along temperature gradients in soils (Birkeland, 1984). Dust flux appears to have the greatest influence on carbonate accumulation rate (Machette, 1985), however other factors such as precipitation and evaporation also have an effect (McFadden, 1982). The depth to carbonate precipitation is controlled by climate, with wetter climates resulting in deeper carbonate-rich horizons (Arkley, 1963; Retallack, 2005).

The incorporation of uranium into pedogenic carbonate at the time of precipitation enables the use of ^{238}U-^{234}U-^{230}Th (U-series) to date carbonate laminae. Typical oxygen-rich soil-pore waters have U concentrations in the µg/L range (Paces et al., 2002), because of the high solubility of hexavalent uranium in oxidizing conditions. Thorium has low solubility at typical soil water eH and pH, and therefore exists in very low concentrations in soil water (tens to hundreds of pg/L range- Reynolds et al., 2003; Hubert et al., 2006). The activity ratio of ^{238}U/^{234}U in soil water is commonly greater than 1, due to the recoil of ^{234}Th (which decays to ^{234}U) out of mineral grains during ^{238}U decay, crystal lattice damage due to ^{238}U decay and radiation induced oxidation of ^{234}U (Paces et al., 2002, and references therein). Thus pure authigenic pedogenic carbonate typically contains ppm levels of U, will reflect the ^{234}U/^{238}U of the water from which it forms, and will initially have no appreciable thorium. The in-growth of ^{230}Th from the decay of U, is the basis of the ^{230}Th/U dating system (see van Calsteren and Thomas, 2006 for a recent summary).

^{230}Th /U dating of pedogenic carbonate was attempted as early as 1976 (Rosholt et al.) and the technique continues to be utilized and improved upon today. Early studies used large samples (several grams) that were analyzed by alpha spectrometry (e.g. Ku et al., 1979; Szabo, 1981; Szabo and O'Malley, 1985). More recent studies (e.g. Ludwig and Paces, 2002; Sharp et al., 2003; Blisniuk and Sharp, 2003) have utilized thermal ionization mass spectrometry (TIMS) that allows analysis of relatively small (~10-50 mg), carefully chosen samples, while increasing precision. Smaller samples reduce averaging over long depositional intervals and allow for greater selectivity, thereby avoiding visible discontinuities in carbonate deposition, carbonate with secondary porosity that may have not remained closed with respect to U and Th, and carbonate containing visible detritus.

Pedogenic Carbonate: Sample selection, preparation and TIMS analysis

Pedogenic carbonate from the three sites shown in Figure 2 (P1, P2 & P3) has been dated by U-series. Samples were selected from the main carbonate accumulation horizon of each soil, and manifestly inherited coatings were avoided. 'Inherited' refers to clasts with coatings that formed in a more ancient landform, and were eroded and deposited in the current landform with their old carbonate coating int

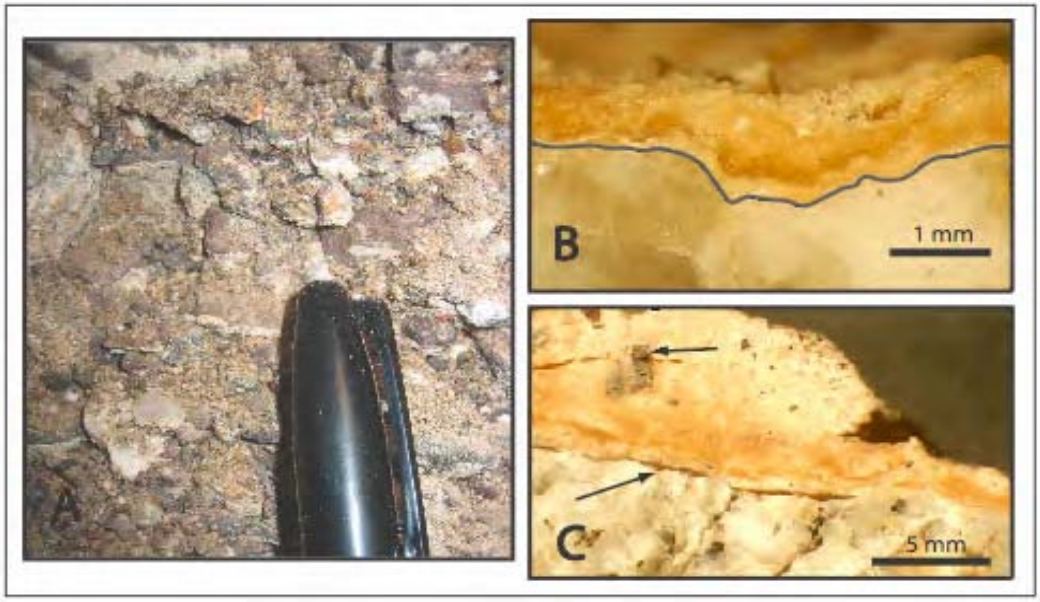

Figure 4: Photographs of pedogenic carbonate from the Q6central surface. A: Field photograph showing stage I carbonate; coatings occur only on the undersides of clasts, indicating inherited coatings are rare or absent. B and C: Cut and polished slabs showing clasts with carbonate coatings (inverted from field position). Coating in B is dense yellow laminated carbonate such as that selected for U-series analyses. Clast-carbonate contact is traced in grey for clarity. Coating in C is unsuitable for U-series due to detachment from the clast (arrow), detrital contamination (arrow) and porosity resulting from partial dissolution.

Table 1: Isotopic data and ages for pedogenic carbonate. Isotopic ratios are reported as activity ratios. All errors are 2σ.

Sample Name[a]	Wt. (mg)	U (ppm)	$^{230}Th/^{232}Th$	Age (10^3 yrs)
Q6central				
CM-SP-01	103.6	1.56	10.1	43.4 ± 4.0
CM-SP-02	102.2	1.45	15.4	41.0 ± 1.3
CM-SP-03	64.24	2.05	22.8	38.9 ± 4.0
CM-SP-09	57.45	1.48	28.9	42.6 ± 2.2
Q6west				
CM-GF-01A	6.74	1.97	4.1	33.3 ± 4.1
CM-GF-01B	17.02	0.97	6.3	33.4 ± 3.6
CM-GF-02Z	25.03	0.39	19.4	35.9 ± 2.5
CM-GF-02A	23.35	1.20	5.6	32.4 ± 3.2
Buried Soil				
CM-S3H-01Z	36.10	1.98	35.8	134.7 ± 4.6
CM-S3H-01A	14.01	3.83	40.0	119.6 ± 11.2
CM-S3H-01B	15.52	2.93	36.4	139.4 ± 12.4
CM-S3H-05	32.02	2.32	32.8	109.0 ± 2.6
CM-S3H-08	35.85	2.23	20.0	115.0 ± 4.0

[a] Samples are designated by clast number, the postscript A, B, etc. denote discrete sub-samples from the same clast coating.

[b] Corrected for detrital U and Th with $^{232}Th/^{238}U$ = 1.21 ± 50%, $^{230}Th/^{238}U$ = 1.0 ± 10%, $^{234}U/^{238}U$ = 1.0 ± 10% (zero error correlations).

[c] Error correlation for $^{230}Th/^{238}U - ^{234}U/^{238}U$.

[d] Back-calculated from the present day, detritus corrected $^{234}U/^{238}U$ and $^{230}Th/U$ age.

Inherited coatings will be emplaced in random orientations throughout the soil profile. Therefore, only clasts with coatings on on their bottom are sampled for dating. In all three soils, laminae of dense yellow carbonate suitable for U-series analysis tend to between about 0.4 to 3.0 mm thick. The buried soil has more powdery white, porous carbonate, but does not have significantly thicker dense yellow carbonate coatings, probably because carbonate accumulation related to pedogenesis ceased after burial of the soil by younger alluvium after perhaps 30 ka or 40 ka.. Burial would cut off accumulation of dense carbonate because accumulation occurs primarily at the evaporation front in a soil, which is commonly between about 0.3 to 2.0 m below the surface in semi arid to arid soils. Carbonate coatings were scrubbed with a nylon brush in the field to remove some of the powdery carbonate in order to assess the thickness and tenacity of the carbonate. Coatings that easily flaked off the clast or crumbled under the force of the brush were discarded. In the laboratory, carbonate coating were scrubbed again with a nylon brush under water, and cleaned ultrasonically in order to remove detrital grains and porous outer layers of carbonate. Clasts were then cut, polished and examined under low power magnification to assess carbonate density, degree of contamination by detrital grains and continuity of carbonate laminations. In many cases individual carbonate laminae can be traced across a coating for up to several centimeters. Dense carbonate with continuous laminations that was relatively free of visible detrital material was selected for analysis. Carbonate was isolated using a combination of chipping with a steel blade and drilling with a diamond-tipped dental bit. The isolated carbonate was cleaned ultrasonically in alcohol, coarsely crushed and further examined under a binocular microscope. Any remaining detrital grains were removed by hand and the sample was cleaned again ultrasonically in alcohol. The crushed and cleaned carbonate was dissolved completely, equilibrated with a ^{236}U-^{233}U-^{229}Th spike, and U and Th were separated using HNO_3-HCl solutions with cation exchange columns. The U and Th were loaded onto separate outgassed Re filaments as a colloidal graphite sandwich (Chen et al., 1986; Edwards et al., 1987) and analyzed by TIMS in single collector, ion-counting mode.

^{230}Th/U Analytical Results

U-series ages are summarized in Table 1. Uranium concentrations range from 0.4 to 3.8 ppm with a median value of 2.0 ppm. Thorium concentrations are between 0.02 to 0.53 ppm with a median value of 0.17 ppm, and $^{230}Th/^{232}Th$ ratios range between 4.1 to 40, with a median value of 20 (all isotope ratios are given as activity ratios). The latter is the ratio of ^{230}Th, which is formed by decay of U, to "common" ^{232}Th, which is derived from detritus included in the carbonate. A useful rule of thumb is that for pedogenic carbonate samples with $^{230}Th/^{232}Th > 10$, correction for initial U and Th isotopes from detritus is minor. Accordingly, most Coyote Mountains pedogenic carbonate is geochemically suitable for precise U-series dating.

Although every effort was made to purify the carbonate dated, some detritus remains, as indicated by small but significant concentrations of ^{232}Th in the analyzed coatings, which would not be expected in pure authigenic carbonate because of the very low solubility of Th in near-surface waters. On the other hand, ^{232}Th occurs at ppm-levels in common crustal silicates along with associated ^{230}Th and U. Accordingly, ages were corrected for U and Th from silicate detritus using ^{232}Th as an index, assuming detritus has typical crustal Th/U ratios and is at secular equilibrium (Ludwig and Paces, 2002; i.e., assumed detritus activity ratios of $^{232}Th/^{238}U = 1.2 \pm 0.6$, $^{230}Th/^{238}U = 1.0 \pm 0.1$, and $^{234}U/^{238}U = 1.0 \pm 0.1$). Uncertainties of ± 50% in the Th/U ratio and ±10% in the $^{230}Th/^{238}U$ and $^{234}U/^{238}U$ ratios of detritus were assigned and propagated through the age calculation.

Carefully selected and purified, dense pedogenic carbonate, analyzed for U andTh isotopes by TIMS, has been shown elsewhere to yield reliable ages for carbonate growth (Ludwig and Paces, 2002; Sharp et al, 2003; Blisniuck and Sharp, 2003; Fletcher et al., in review). Nevertheless, it is prudent to evaluate the possibility of open system behavior and inheritance in our data set to establish the reliability of our ages.

Failure of the assumption of a closed U-Th system would most likely entail U-loss (due to the high solubility of U compared to Th) as a result of leaching or partial dissolution of carbonate and would cause affected ages, if any, to be too old. Leaching and dissolution should result in textural variations that are readily identifiable in polished thick section. Indeed, several clast coatings were rejected during the

early stages of sample preparation due to their lack of preservation of pristine laminar carbonate, abundant visible detritus, or detachment from the host clast (e.g. Fig. 4C). An additional check for open system behavior is the reproducibility of sub-samples from the same carbonate coating. There are three carbonate coatings that have two sub-samples dated in our data set, of which all have ages that agree within 2 sigma uncertainty. The sub-samples of CM-GF-01 have overlapping ages of 33.3 ± 4.1 ka and 33.4 ± 3.6 ka, and GF 02 has ages of 35.9 ± 2.5 and 32.4 ± 3.2 ka. Sub-samples of CM-S3H-01 have ages of 139.4 ± 12.4, 134.7 ± 4.6 ka, and one younger age of 119.6 ± 11.2 ka. The younger age is more likely attributable to sub-sampling of a younger area of the carbonate coating than to an open U-Th system.

Inherited carbonate, if present, could cause calculated ages to be older than the host alluvium. However, carbonate coatings selected from the zone of maximum carbonate accumulation in the dated soil will necessarily include carbonate formed in situ. Since mixtures of inherited and in situ carbonate would not likely occur in consistent proportions, coatings containing such mixtures would be expected to yield sub-sample ages that scatter beyond analytical errors. As discussed above, however, sub-samples from the same coating tend to have good agreement. We therefore conclude that our field and laboratory screening procedures successfully precluded analysis of coatings containing significant amounts of inherited carbonate. Moreover, the active stream beds (Qal) were searched to determine how common inheritance is in the modern system, and it was found that inheritance is not common today, probably because the narrow canyons upstream provide few stable surfaces for carbonate accumulation.

Estimating depositional ages for host alluvium

U-series ages of pedogenic carbonate can provide reliable minimum ages for the deposition of a landform. Innermost carbonate laminae are targeted because they should be the earliest formed, and thus most closely approximate the age of the landform. Even these innermost laminae of carbonate will underestimate the age of a landform because it can take hundreds to perhaps thousands of years to precipitate dateable amounts of carbonate after stabilization of a surface. A survey of young surfaces in the study area, using soil development and recent surface rupture offsets as a guide, indicates that it likely takes several hundred years to accumulate dateable carbonate in this area. In order to collect enough carbonate to produce a precise age we must sample over a finite thickness of the coating, in effect averaging the ages of the individual laminae. For these reasons U-series ages provide a minimum bound for the age of a surface, and the maximum reproducible U-series age is considered the closest approximation of the age of deposition.

Q6west

Two carbonate coatings, each with two sub-samples, were dated from the Q6west surface. These samples have the lowest U concentration and the lowest $^{230}Th/^{232}Th$ activity ratios making them the least favorable for U-series analysis of the samples dated. Nevertheless, Q6west samples show good age reproducibility both with-in coatings and between coatings; 33.3 ± 4.1 ka and 33.4 ± 3.6 ka for GF-01, and 35.9 ± 2.5 ka and 32.4 ± 3.2 ka for GF-02 (Fig. 5), consistent with closed U-Th systems. The weighted mean age, using all four U-series ages, is 34 ± 2 ka, which we interpret to be the minimum age for the Q6west surface.

Q6central

Four carbonate coatings were dated from the Q6central surface, and all U-series ages agree within 2 sigma uncertainties; 43.4 ± 4.0 ka, 41.0 ± 1.3 ka, 38.9 ± 4.0 ka and 42.6 ± 2.2 ka (Fig. 5). The weighted mean age of these samples is 41 ± 2 ka, which is a minimum age for the Q6central surface.

Buried Soil of Q7

Three carbonate coatings were dated from the buried soil, with one of those coatings (CM-S3H-01) having three sub-samples. The samples from the buried soil have the highest U concentration and the highest $^{230}Th/^{232}Th$ activity ratios, making them the most favorable material for U-series dating in the study area. The U-series ages for the buried soil range from about 109 ka to 139 ka. The oldest dates come from the CM-S3H-01 clast, with two of those ages agreeing well within uncertainties; 137.4 ± 4.6 ka and 139.4 ± 12.4 ka (Fig. 5). We take the weighted mean of these two sub-samples, 135 ± 4 ka, to be the minimum age for the buried soil.

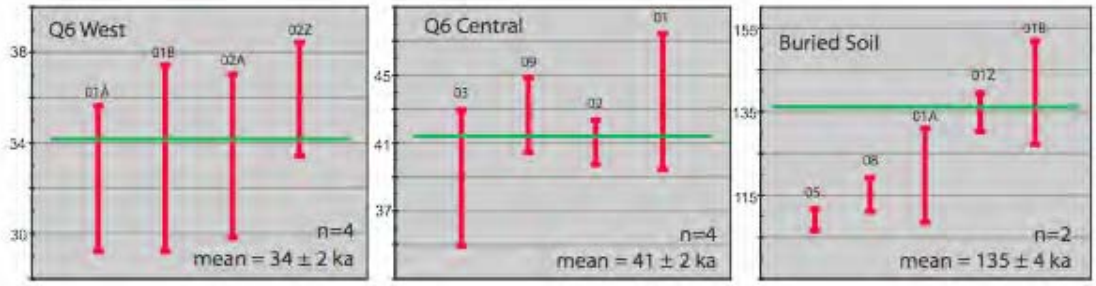

Figure 5: U-series ages of pedogenic carbonate clast-coats. Note that only the two oldest analyses are averaged for the "buried soil". All errors are 2σ.

^{10}Be PROFILE DATING OF Q6central

Samples from a 2-m deep profile through Q6central at P1 were analyzed for ^{10}Be cosmogenic surface exposure dating. Sampling from depth profiles yields estimates of both the age and inheritance of a deposit (Anderson et al., 1996). Six samples were collected: 1 surface sample and 5 buried samples. The surface sample consist of >20 amalgamated chips from the top 1 cm of smooth and rounded quartzite cobbles. All cobbles exhibited moderate varnish development and strong rubification on the underside of the clast, indicating that they have resided at the surface for extended periods. Samples at depth were collected from 5-cm-thick intervals at 10 cm, 45 cm, 70 cm, 115 cm and 170 cm depths.

All samples were processed at the Cosmogenic Nuclide Laboratory at Stanford University. Samples were first crushed and sieved to obtain a grain size fraction between 250-500 µm. This fraction was chemically leached (cleaned) in an ultrasonic bath with a minimum of five acid leaches: (1) a hydrochloric leach for 24 hours; (2) two 2% HF/HNO_3 leaches for ~10 hours each; and (3) one or more 1% HF/HNO_3 leach for ~ 10 hours. A ^{9}Be carrier (^{10}Be/^{9}Be ~ 1 x 10^{-15}) was then added to the clean quartz sample, and approximately 25-50 grams was dissolved in a concentrated 3:1 HF and HNO_3 solution. Once dissolved, the samples were passed through anion and cation exchange columns to remove Fe and Ti and to separate the ^{10}Be fraction. Ammonium hydroxide was added to the ^{10}Be fraction to precipitate beryllium hydroxide. The beryllium hydroxide was oxidized by ignition at 850°C for 30 minutes in boron-free quartz crucibles. The beryllium oxide was then mixed with Nb powder and loaded in steel targets for measurement of ^{10}Be/^{9}Be ratios by accelerator mass spectrometry at Lawrence Livermore National Laboratory. All ^{10}Be ages are calculated using the CRONUS Age Calculator (Balco et al., 2008; http://hess.ess.washington.edu/math/). This uses the scaling factors of Lal (1991) and Stone (2000) and a sea-level, low-latitude production rate of 4.9 ± 0.6 ^{10}Be atoms/gram of quartz/year.

The cosmogenic depth profile yields a model age of 31.5 ± 5.8 ka for Q6central, which takes into consideration the equivalent of 8.9 ± 3.5 ka of inherited ^{10}Be (Fig. 6). However, the ^{10}Be data depart from the expected exponential relationship between ^{10}Be concentration and depth beyond analytic uncertainties (Fig. 6B) suggesting that either: (1) inherited ^{10}Be is not uniform throughout the profile, or (2) the Q6central surface has not been stable since deposition. Moreover, the ^{10}Be model age of 31.5 ± 5.8 is younger than the U-series age of 41 ± 2 ka. Both observations are consistent with lowering of the Q6central surface by a few tens of centimeters, which is our preferred interpretation. Preferential removal of sand and finer-grained materials, for example by deflation or overland flow, would expose cobbles that initially lay at some depth beneath the surface and hence were partially shielded prior to exhumation by surface lowering.

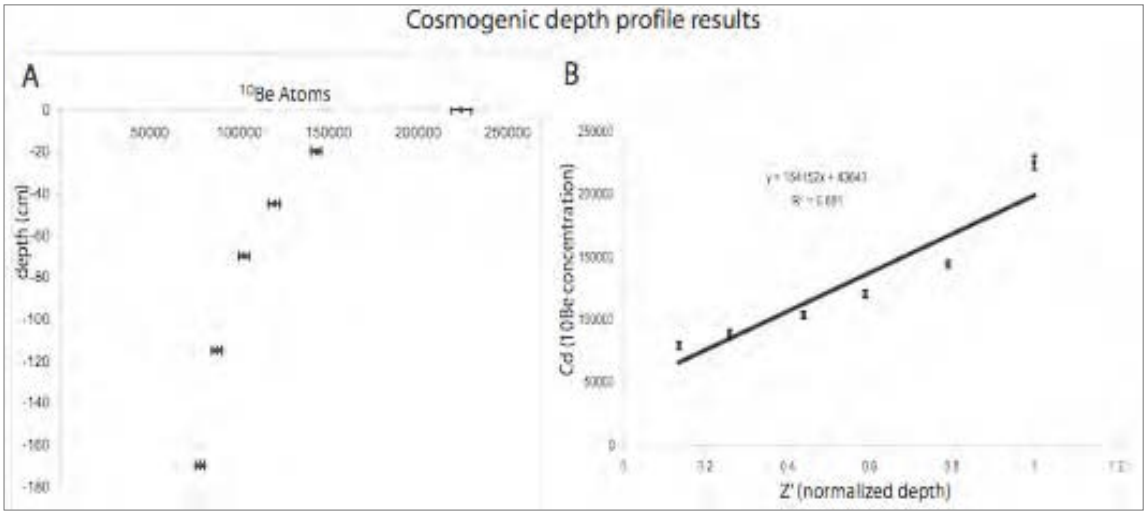

Figure 6: Cosmogenic depth profile results. 5A: plot of total number of ^{10}Be atoms versus depth. 5B: ^{10}Be concentration versus normalized depth, where the slope is proportional to the model age. Note that the surface sample (at right, with highest ^{10}Be concentration) plots off of the trend defined by the buried samples. Fit shown yields an age of 31.5 ± 5.8 ka (1σ).

DISCUSSION

Slip rates for the Elsinore fault

By coupling the offset estimates with the minimum ages provided by U-series dating we can determine maximum slip rates for the southern Elsinore fault averaged over three time intervals; ~34 ka (Q6west), ~41 ka (Q6central) and ~135 ka (Q7buried soil). With an offset of 59 ± 21 m and a minimum age of 34 ± 2 ka, the Q6west surface has a maximum slip rate of 1.7 ± 0.6 mm/yr. The Q6central surface has a minimum age of 41 ± 2 ka and an offset of 83 ± 31 m, which results in an overlapping, but less precise maximum slip rate of 2.0 ± 0.8 mm/yr. The buried soil, with a minimum age of 135 ± 4 ka and an offset of 580 ± 110 m, has a maximum slip rate of 4.3 ± 0.8 mm/yr averaged over ~135 ka.

Figure 7 is a graphical representation of the offset and age information that clearly shows that the ~135 ka buried soil falls off the slip rate trend line of ~1.9 mm/yr defined by Q6west and Q6central. Our new slip rate data suggests that between about 41 ka and 135 ka there was a period of accelerated slip on the southern Elsinore fault, equal to about 5.3 mm/yr. The corresponding rate is likely higher to the northwest where slip is larger in recent ruptures. If slip rate scales with slip in the past several events, then the recent slip rate in the central Coyote Mountains along the Elsinore fault could be as high as 4 mm/yr, consistent with estimates based on short-term slip per event and recurrence information (Rockwell, 1990). Using an average slip per event of 1.4 ± 0.1 mm/yr and assuming a characteristic earthquake model, the recurrence interval for the Elsinore fault in southern Coyote Mountains is 740 ± 200 yrs. If our ~135 ka age for the buried soil is correct, then the slip rate in the central Coyote Mountains prior to 40 ka may have approached 1 cm/yr. If our dates closely approximate deposition of the offset fans, the Elsinore fault may have carried up to 10-20% of the total slip between the Pacific and North American plates, before slowing more recently.

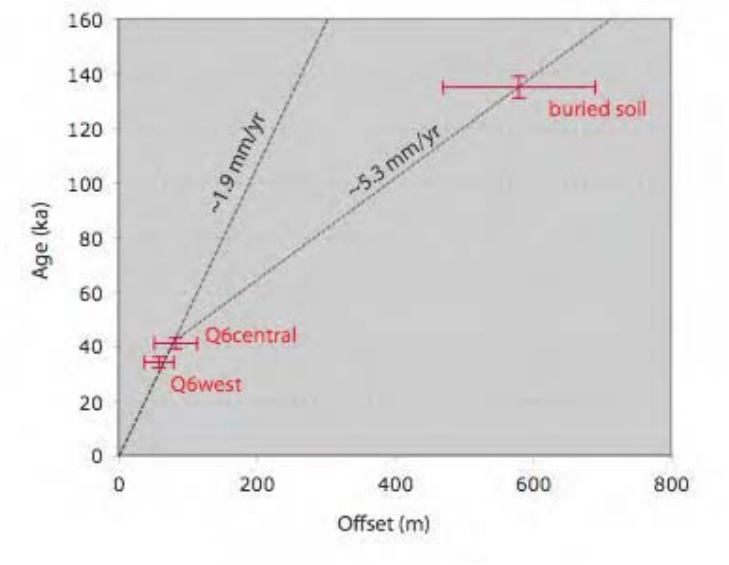

Figure 7: U-series ages vs. offsets for three fans displaced along the southern Elsinore fault. The slopes of the dotted trend lines are proportional to slip rate.

REFERENCES CITED:

Anderson, R.S, J.L. Repka and G.S. Dick. 1996. Explicit treatment of inheritance in dating depositional surfaces using in situ 10Be and 26Al. Geology 24, p.47-51.

Arkley, R. J. 1963. Calculation of carbonate and water movement in soil from climatic data. Soil Science 96, 239-248.

Balco G., J. Stone, N. Lifton, T. Dunai. 2008. A simple, internally consistent, and easily accessible means of calculating surface exposure ages and erosion rates from Be-10 and Al-26 measurements. Quaternary Geochronology 3, 174-195.

Birkeland, P. W. 1984. Soils and geomorphology. United States (USA): Oxford Univ. Press, New York, NY, United States (USA).

Blisniuk, P. M., and W. D. Sharp. 2003. Rates of late quaternary normal faulting in central tibet from U-series dating of pedogenic carbonate in displaced fluvial gravel deposits. Earth and Planetary Science Letters 215, 169-186.

Calsteren, P. van, L. E. Thomas. 2006. Uranium-series dating applications in natural environmental science. Earth Science Reviews, 75, 155-175.

Capo, R. C., and O. A. Chadwick. 1999. Sources of strontium and calcium in desert soil and calcrete. Earth and Planetary Science Letters 170, 61-72.

Chen, J. H., R. L. Edwards, and G. J. Wasserburg. 1986. ^{238}U, ^{234}U and ^{232}Th in seawater. Earth and Planetary Science Letters 80, 241-251

Edwards, R. Lawrence, J. H. Chen, and G. J. Wasserburg. 1987. ^{238}U- ^{234}U- ^{230}Th- ^{232}Th systematics and the precise measurement of time over the past 500,000 years. Earth and Planetary Science Letters 81, 175-192

Fletcher K. E., W. D. Sharp, K. J. Kendrick, W. M. Behr, K. W. Hudnut and T. C. Hanks, $230^{Th}/U$ dating of a late Pleistocene alluvial fan offset along the southern San Andreas fault, in review, GSA Bulletin

Gile, L. H., F. F. Peterson, and R. B. Grossman. 1966. Morphological and genetic sequences of carbonate accumulations in desert soils. Soil Science 101, 347-360

Gosse, J.C., and Phillips, F.M., 2001, Terrestrial in-situ cosmogenic nuclides: Theory and application: Quaternary Science Reviews 20, 1,475-1,560.

Hubert, A., B. Bourdon, E. Pili, and L. Meynadier. 2006. Transport of radionuclides in an unconfined chalk aquifer inferred from U-series disequilibria. Geochimica et Cosmochimica Acta 70, 5437-5454

Kohl, C.P., and K. Nishiizumi, 1992, Chemical isolation of quartz for measurement of insitu-

produced cosmogenic nuclides: Geochimica et Cosmochimica Acta 56, 3,583-3,587.

Ku, T. L., W. B. Bull, S. T. Freeman, and K. G. Knauss. 1979. ^{230}Th -^{234}U dating of pedogenic carbonates in gravelly desert soils of Vidal Valley, southeastern California. Geological Society of America Bulletin 90,1063-1073.

Lal, D., 1991, Cosmic ray labeling of erosion surfaces: in-situ nuclide production rates and erosion models: Earth and Planetary Science Letters, 104, 429-439.

Ludwig, K. R., and J. B. Paces. 2002. Uranium-series dating of pedogenic silica and carbonate, crater flat, Nevada. Geochimica et Cosmochimica Acta 66, 487-506

Machette, M. N. 1985. Calcic soils of the southwestern united states; soils and quaternary geology of the southwestern united states. Special Paper - Geological Society of America 203, 1-21

Magistrale, H. and Rockwell, T. 1996, The central and southern Elsinore fault zone, southern California, Bull. Seism. Soc. Am., 86, 1793-1803.

Mayer, L., L. D. McFadden, and J. W. Harden. 1988. Distribution of calcium carbonate in desert soils; a model. Geology (Boulder) 16, 303-306.

McFadden, L. D. 1988. Climatic influences on rates and processes of soil development in quaternary deposits of southern California; paleosols and weathering through geologic time; principles and applications. Special Paper - Geological Society of America 216, 153-177.

Millman, D.E., and T.K. Rockwell (1986). Neotectonica of the Elsinore fault zone in Temscal Valley, California. *in*, Ehlig, P., ed., *Neotectonics and Faulting in Southern California*, Geol. Soc. Amer., Cordilleran Section, Boulder CO, 159-166.

Paces, J. B., K. R. Ludwig, Z. E. Peterman, and L. A. Neymark. 2002. ^{234}U/ ^{238}U evidence for local recharge and patterns of ground-water flow in the vicinity of Yucca Mountain, Nevada, USA; geochemistry of Yucca Mountain, Nevada; a potential site for a high-level nuclear waste repository. Applied Geochemistry 17, 751-779

Pustovoytov, K. E. 2002. Pedogenic carbonate cutans on clasts in soils as a record of history of grassland ecosystems; reconstruction and modelling of grass-dominated ecosystems. Palaeogeography, Palaeoclimatology, Palaeoecology 177.

Retallack, G. J. 2005. Pedogenic carbonate proxies for amount and seasonality of precipitation in paleosols. Geology (Boulder) 33, 333-336.

Reynolds, B. C., G. J. Wasserburg, and M. Baskaran. 2003. The transport of U- and Th-series nuclides in sandy confined aquifers. Geochimica et Cosmochimica Acta 67, 1955-1972.

Rockwell, T. K., Loughman, C. and Merifield, P., 1990, Late Quaternary rate of slip along the San Jacinto fault zone near Anza, southern California, JGR, 95, 8593.

Rosholt et al. 1976. ^{230}Th/^{234}U dating of travertine and caliche rinds. Geological Society of America, Abstracts with Programs.

Sharp, W. D., K. R. Ludwig, O. A. Chadwick, R. Amundson, and L. L. Glaser. 2003. Dating fluvial terraces by (super 230) Th/U on pedogenic carbonate, wind river basin, wyoming. Quaternary Research (New York) 59.

Stone, J.O., 2000, Air pressure and cosmogenic isotope production: Journal of Geophysical Research, 105, 23,753-23,759.

Szabo, B. J., W. J. Carr, and W. C. Gottschall. 1981. Uranium-thorium dating of quaternary carbonate accumulations in the Nevada test site region, southern Nevada. Open-File Report - U.S.Geological Survey OF 81-0119, 38.

Szabo, B. J., and P. A. O'Malley. 1985. Uranium-series dating of secondary carbonate and silica precipitates relating to fault movements in the Nevada test site region and of caliche and travertine samples from the Amargosa Desert. Open-File Report - U.S.Geological Survey OF 85-0047, 17.

Vaughan, P., and T. Rockwell (1986). Alluvial stratigraphy and neotectonics of the Elsinore fault zone at Agua Tibia Mountain, southern California. *in*, Ehlig, P., ed., *Neotectonics and Faulting in Southern California*, Geol. Soc. Amer., Cordilleran Section, Boulder CO, 177-191.

Optically stimulated luminescence dating littoral sediments in the Imperial Valley, Southern California: the methods, applicability, and problems

Caitlin Kibbe Lippincott, Thomas K. Rockwell
San Diego State University
Lewis A. Owen
University of Cincinnati

Luminescence methods are increasing being used to define ages of Quaternary sediments for paleoseismic, paleoenvironmental and landscape evolution studies. This technique has been successfully applied to dating faulted sediments in the western USA (e.g. Crone et al., 1997; Rockwell et al., 2000; Lee et al., 2001; Kent et al., 2005; Wesnousky et al. 2005) and elsewhere in the world (e.g. Washburn et al., 2001; Rockwell et al., 2008). The methods have the advantage that they can be used to date sediment devoid of organic matter that is required for the standard method of radiocarbon dating. Furthermore, the method allows sediments and landforms to be dated to beyond the standard radiocarbon range of about 30 ka and can be applied to very young sediments (a few decades old). However, like all dating methods there are inherent problems that need to be addressed both in its application, laboratory methods and age calculation.

Luminescence dating is a radiometric method that is based on the time-dependent accumulation of electrons at traps within the crystal lattice of minerals such as quartz and feldspar (Aitken, 1998). Natural ionizing radiation cosmic rays and derived from radioisotopes within the sediment are responsible for the gradual increase in the number of trapped electrons in the crystal lattice of the mineral over time, until a saturation level is reached. The release of the trapped electrons results in a detectable luminescence signal. The intensity of the luminescence is a measure of the amount of radiation-induced electrons, which is dependent upon the rate of ionizing radiation (dose rate) and duration of burial. The electrons within minerals can be stimulated and released with heat or light to create the luminescence. The type of luminescence dating is defined on the basis of the stimulation method, such that stimulation by heat is thermoluminescence (TL), stimulation by visible light is optically stimulated luminescence (OSL) and stimulation by infrared light is infrared stimulated luminescence (IRSL). The most common types are OSL for quartz and IRSL for feldspar. Luminescence signals from feldspar are an order of magnitude greater than for quartz. Quartz, however, is more rapidly bleached than feldspar. Furthermore, quartz does not suffer from the problem of anomalous fading that is common to feldspar that involves the loss of trapped electrons during the sample's burial period. Modern geochronologists who favor OSL and IRSL methods, over TL methods as the former methods more accurately mimic naturally occurring conditions. A range of particle sizes can be used in determination of a luminescence age, but the 4–11 and 90–200 microns particle size are usually used and and are referred to as fine-grain and coarse-grain luminescence dating, respectively. Quartz and feldspar are easily separated for coarse-grain dating. Separating quartz and feldspar for fine-grain work is more complex and commonly polyminerals are used in fine-grain IRSL dating, where only the feldspar is stimulated by infrared. Artificially irradiating subsamples and comparing the luminescence emitted with the natural luminescence can be used to determine the relationship between accumulated radiation energy and luminescence signal. The equivalent dose (De) experienced by the grains during burial can therefore be determined. The ionizing radiation dose rate (Dr), has to be determined to calculate the age. This can be derived from direct measurements or measured concentrations of radioisotopes.

The age is derived using the following equation:

$$\text{Age} = \text{De}/Dr$$

The uncertainty in the age is influenced by the systematic and random errors in the De values and possible temporal changes in the Dr. Temporal changes in the Dr are a consequence of changes in water content and mineral composition within the sediment. This is difficult to determine and hence the dose rate is generally assumed to have remained constant over time.

The age range that can be covered by luminescence dating of sediments is dependent on the unique luminescence properties of the minerals being examined and the environmental dose rate to which those minerals have been subjected. Typically, quartz can be dated back to c. 100–150 ka and feldspar to c.

200–300 ka, with exceptional samples back 1 Ma. Luminescence methods date the last resetting of the trapped electrons; for clastic sediments, this is the last exposure of the mineral grains to sunlight. Sediments generally experience their resetting of the luminescence signal while they are eroded, transported and deposited; thus luminescence methods date the last process of sediment reworking. The prerequisite condition, therefore, for dating sediments with luminescence is that they have experienced sufficient exposure to sunlight to enable a complete resetting (bleaching) of the luminescence signal. Aeolian sediments, for example, are generally very well bleached (their luminescence signal is efficiently reset) because they experience prolonged exposure to sunlight as they are transported by air currents over considerable distances (many kilometers) and for prolonged periods (1 to 10^4 days) being continuously mixed and reworked during their transport cycle. In contrast, other sediments such as fluvial, lacustrine and littoral are commonly deposited very rapidly and may not be fully exposed to daylight (Wallinga, 2002). As such, they may not be completely bleached.

To test the applicability of OSL methods for dating fluvial, lacustrine and littoral sediments, and in particular, the problems associated with partial bleaching, we undertook a study of lake shore berms, fluvial sands and lake shoreline sands to better define the timing of the last Lake Cahuilla highstand. Lake Cahuilla forms when the Colorado River is rerouted from its present course, usually directly into the Gulf of Califronia, to flow north into the Salton Depression. The Colorado delta essentially dams the resultant freshwater lake, maintaining its level to ~13 m above sea level (asl) and measuring up to 5700 km^2 (Fig. 1). Within 12-20 years, Lake Cahuilla can fill to a maximum height of +12 m asl, which at its deepest is 95 m, before flowing along the New River at the south end of the basin back to the Gulf of California (Waters, 1983). Once the Colorado River migrates back to flowing south to the Gulf and a fresh supply of water is no longer flowing into Lake Cahuilla, Waters (1983) calculated it would take 60 years to desiccate the lake at a rate of 1.6 m/yr. Archaeologists have long studied the American Indian populations associated with the lush environments that are created when Lake Cahuilla forms (Waters 1983). Recently, the precise dating of these lakes has become important for paleoseismologists. The most recent southern San Andreas event occurred during the most recent Lake Cahuilla highstand, and the shoreline and lake deposits cover or cross many of the major faults of the southern San Andreas fault system.

Numerous explorers trekked through southern California beginning in the mid 1500's. Diaries and maps were used in this study to further determine when a lake Cahuilla might have been present, mostly notably those of Father Kino in the late 1600 early 1700 and de Anza expeditions in 1774-1776. Radiocarbon dating has been used to determine the timing of this lake highstand, as well as to date paleoseismic events. Using the radiocarbon dates from the last Lake Cahuilla highstand, Gurrola and Rockwell (1996) obtained 1675-1696 or 1724-1777 and 1671-1686 or 1739-1783 from two peat samples, and Sieh and Williams (1990) acquired 1641-1684 or 1725-1807. This creates two age possibilities for the last Lake. However, when historical evidence is brought into the picture, the mid 18^{th} century is unlikely. However, inherent problems with C^{14} dating have limited the usefulness of the technique and their resultant ages for deposits from the last 350 years or so. Therefore the application of OSL methods promises to help refine the chronologies, if partial bleaching is not a problem.

Figure 1. The maximum extent of Lake Cahuilla. The Colorado River normally flows south to the Gulf of California. However, sometimes the Colorado River breaches the delta walls and flows along the Alamo River to the Imperial Valley, filling it until it spills out along the New River. Image from: http://gis.esri.com/ library/userconf/proc00/ professional/papers/ PAP377/p377.htm

Sedimentary deposits were, therefore, examined at three locations: Carrizo Wash, Kane Springs, and Dunaway Road (Fig. 2). Several sediment samples were collected for OSL dating from Berms along Dunaway Road (Fig. 3) and one near Kane Springs. Samples for OSL dating were also taken from lacustrine and fluvial deposits at the Carrizo Wash site (Figs. 2, 4 and 5). Previous works by Ragona (2003) and Verdugo (2008) documented the paleoseismology at a site where the Superstition Mountain Fault intersects the Lake Cahuilla deposits, and these studies have dated charcoal from many stratigraphic units. Unfortunately, the charcoal dates can only be used to resolve maximum age since they were from detrital charcoal, and many layers in the stratigraphic section yielded similar ages suggesting either reworking of the charcoal or a source for charcoal of a common age.

Figure 3. View of the Dunaway Road recessional berms

Figure 2. Locations of the sampling sites

Sediment samples were collected for OSL dating by hammering light-tight tubes into freshly exposed sediments. The tubes remained sealed until processed in the safe light conditions in the Geochronology Laboratory at the University of Cincinnati. Sample preparation follows the methods described in Owen et al. (2007). Approximately 20 g of the dried sub-sample from the sediment sample was ground to a fine powder and sent to the USGS Reactor in Denver for neutron-activation analysis (INAA) to determine the concentration of radioisotopes for dose-rate determination (Rable 1). Variable water content throughout the section may have occurred throughout the history of the section. However, it is not possible to determine the degree of such changes. The dose rate was therefore assumed to have remained constant and a 5±5 % water content value was used to help account for possible changes in water content.

Luminescence measurements were undertaken on quartz for the dominant particle size for each sample using a Riso Automated TL/IRSL/Blue DA-15 C/D

Figure 4. Trench #8 at the Carrizo Wash Site, sampling the various lacustrine and fluvial units.

OSL Dating System. Luminescence from the quartz grains was stimulated using an array of blue light emitting diodes (470 nm, 50 mW/cm2) filtered using a green long-pass GG-420 filter. Detection was through a Hoya U-340 filter. All quartz aliquots were screened for feldspar contamination using infrared stimulation with infrared light emitting diodes (870 nm, 150 mW/cm2). All OSL signals were detected using a 52mm diameter photomultiplier tube

(9235B). Riso Sequence Editor software was used for hardware control.

De measurements were determined on multiple aliquots for each sample using the single aliquot regenerative (SAR) method protocol developed by Murray and Wintle (2000). The De value for every aliquot of each sample was examined using Riso Analysis 3.22b software. Aliquots with poor recuperation (>10%) were not used in the age calculations. Preheat test were undertaken, which show a plateau for De values at ~220°C. Meausrements were therefore measured at 220°C. In fluvial, lacustrine and littoral sediments, a large spread of De values may reflect partial bleaching of sediment (Olley et al., 1999). To assess this problem,

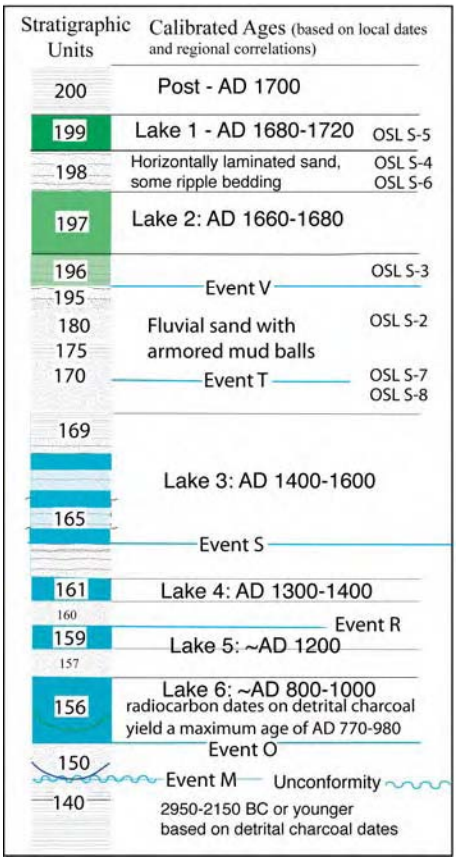

Figure 5. Stratigraphic column showing the OSL sample locations relative to the radiocarbon dates and the interpreted ages from dates at other sites.

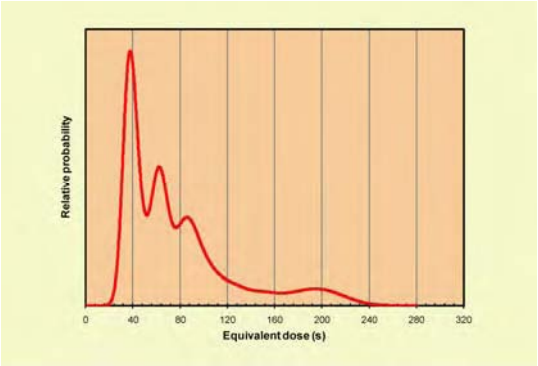

Figure 6. Probability distribution of De values for sample S3. The values are in seconds of irradiation. 1 second is equivalent to 0.129 Gy.

the De values for each sample were plotted using probability distribution plots (Fig. 6). Given the partial bleaching characteristic of the sediments ages were calculated using all the good De data, and the lowest 20%, lowest 10% of the De values, and the lowest De value (Table 1).

The OSL results show that the Dr values are consistent for all the samples ranging between 1.8-2.4 Gy/ka (Table 1). The large spread of De values indicates significant partial bleaching problems (Table 1). The results show that OSL ages on these sediments provide overestimates, even when the lowest De values are used to calculate the ages. However, the problem of partial bleaching becomes less significant with increasing age as the value of the partial bleaching is only a small percentage of the samples age.

Acknowledgements
SCEC for funding this project.

References

Aitken, M.J., 1998. *An introduction to optical dating*. Oxford University Press, Oxford.

Crone, A.J., Machette, M.N., Bradley, L-A. and Mahan, S.A. 1997. Late Quaternary surface faulting on the Cheraw Fault, Southeastern Colorado. *Geologic Investigations Map*, USGS Map I-2591.

Gurrola, L. D. and Rockwell, T. K., 1996. Timing and slip for prehistoric earthquakes on the Superstition Mountain fault, Imperial Valley, southern California. *Journal of Geophysical Research*, 101, B3, 5977-5985.

Kent, G.M., Babcock, J.M., Driscoll, N.W., Harding, A.J., Dingler, J.A., Seitz, G.G., Gardner, J.V., Mayer, L.A., Goldman, C.R., Heyvaert, A.C., Richards, R.C., Karlin, R., Morgan, C.W., Gayes, P.T. and Owen, L.A. 2005. 60 k.y. record of extension across the western boundary of the Basin and Range province: Estimate of slip rates from offset shoreline terraces and a catastrophic slide beneath Lake Tahoe. *Geology*, 33, 365–368.

Lee, J., Spencer, J.Q. and Owen, L.A., 2001. Holocene slip rates along the Owens Valley fault, California: implications for the recent evolution of the Eastern California Shear Zone. *Geology*, 29, 819–822.

Machette, M.N., Personius, S.F. and Nelson, A.R., 1992. The Wasatch Fault Zone, USA. *Annales Tectonicae*, 6, 5-39, 5-39.

Meltzner, A.J., Rockwell, T.K. and Owen, L.A. 2006. Recent and long-term behavior of the Brawley fault Zone, Imperial Valley, California: An escalation in slip rate. *Bulletin of the Seismological Society of America*, 96, 2304-2328.

Murray, A. S., and Wintle, A. G., 2000. Luminescence dating of quartz using an improved single-aliquot regenerative-dose protocol. *Radiation Measurements*, 32, 57-73.

Olley, J.M., Caitcheon, G.G. and Roberts, R.G., 1999. The origin of dose distributions in fluvial sediments, and the prospect of dating single grains from fluvial deposits using optically stimulated luminescence. *Radiation Measurements*, 30, 207-217.

Owen, L.A., Cunningham, W.D., Richards, B., Rhodes, E.J., Windley, B.F., Dornjamjaa, D., Badamgarav, J., 1999. Timing of formation of forebergs in the northeastern Gobi Altai, Mongolia: implications for estimating mountain uplift rates and earthquake recurrence intervals. *Journal of the Geological Society*, 156, 3, 457-464. Erratum: *Journal of the Geological Society*, 156, Contents xii.

Owen, L.A., Bright, J., Finkel, R.C., Jaiswal, M.K., Kaufman, D.S., Mahan, S., Radtke, U., Schneider, J.S., Sharp, W., Singhvi, A.K., Warren, C.N., 2007. Numerical dating of a Late Quaternary spitshoreline complex at the northern end of Silver Lake playa, Mojave Desert, California: a comparison of the applicability of radiocarbon, luminescence, terrestrial cosmogenic nuclide, electron spin resonance, U-series and amino acid racemization methods. *Quaternary International*, 166, 87–110.

Rockwell, T.K., Lindvall, S., Herzberg, M., Murbach, D., Dawsaon, T. and Berger, G., 2000. Paleoseismology of the Johnson Valley, Kicjapoo, and Homestead Valley Faults: clustering of earthquakes in the Eastern California Shear Zone. *Bulletin of the Seismological Society of America*, 90, 5, 1200-1236.

Rockwell, T., Fonseca, J., Madden, C., Dawson, T. Owen, L.A., Vilanova, S. and Figueiredo, P. (2008) Paleoseismology of the Vilariça Segment of the Manteigas-Bragança Fault in Northeastern Portugal. *Special Publication of the Geological Society of London*, in press.

Ragona, D., 2003. A High Resolution Paleoseismic Study in the Southern San Jacinto Fault Zone, Imperial Valley, California. Masters Thesis, 95 pages. San Diego State University.

Verdugo, D., expected Fall 2007. Past Earthquake History and Slip in the Last Five Events on the Southern San Jacinto Fault Zone, Imperial Valley, California. Masters Thesis, in progress. San Diego State University.

Wallinga, J., 2002. Optically stimulated luminescence dating of fluvial deposits: a review. *Boreas*, 31, 303-322.

Washburn, Z., Arrowsmith, J.R., Forman, S.L., Cowgill, E., Wang Xiaofeng, Zhang Yueqiao and Chen Zhengle, 2001. Late Holocene earthquake history of the central Altyn Tagh fault, China. *Geology*, 29, 11, 1051-1054.

Wesnousky S. G., Barron, A. D., Briggs, R. W., Caskey, S. J., Kumar, S. and Owen, L. 2005. Paleoseismic transect across the northern Great Basin. *Journal of Geophysical Research*, 110, B05408, doi:10.1029/2004JB003283.

Waters, M.R., 1983. Late Holocene Lacustrine Chronology and Archaeology of Ancient Lake Cahuilla, California. *Quaternary Research*, 19, 373-387.

Williams, P. L. and Seitz, G. G., 2004. San Andreas fault in the Coachella Valley and Salt Creek: Development of Long-Term earthquake chronology and event offsets. *Abstract for SCEC Annual Meeting.*

Table 1: Summary of OSL data and ages

Sample number	Particle size (µm)	K [a] (%)	Rb [a] (ppm)	Th [a] (ppm)	U [a] (ppm)	Latitude (°N)	Longitude (°W)	Altitude (m asl)	Depth (cm)	Dose rate [b] (Gy/ka)	Equivalent dose (Gy)	Age using all good data (ka)	Age using lowest 20% of aliquots (ka)	Age using lowest 10% of aliquots (ka)	Age using lowest aliquot (ka)	Expected age (ka)
S-2	125-180	1.52	53.1	4.96	1.17	33.002	-115.953	4	165	2.04±0.13	12.96±7.23	11.78±1.87	4.3±1.54	3.6±0.59	3.30±0.58	0.6-0.7
S-3	90-125	1.73	65.2	5.32	1.38	33.002	-115.953	4	120	2.30±0.15	6.82±3.35	4.32±0.38	2.0±0.27	1.92±0.32	1.86±0.32	0.55
S-4	90-125	1.59	62.6	6.61	1.98	33.002	-115.953	4	80	2.41±0.15	4.31±0.55	3.16±0.33	1.79±0.28	1.71±0.36	1.67±0.36	0.35
S-5	90-125	1.6	53.8	4.12	1.2	33.002	-115.953	4	30	2.09±0.14	1.15±0.08	1.24±0.12	0.55±0.08	0.52±0.10	0.55±0.10	0.3
S-6	90-125	1.82	71.5	5.01	1.64	33.002	-115.953	4	106	2.42±0.16	6.02±0.48	4.00±0.33	2.46±0.26	2.24±0.36	2.03±0.27	0.35
S-7	90-125	1.6	55.1	4.55	1.28	33.002	-115.953	4	150	2.11±0.14	21.26±10.87	14.17±1.25	6.11±0.39	4.04±0.78	4.26±0.43	0.5
S-8	90-125	1.77	65.1	4.92	1.51	33.002	-115.953	4	163	2.33±0.15	23.67±8.56	13.08±1.07	7.74±1.54	6.73±0.96	6.07±0.64	0.8
DUN-2	90-125	1.35	42.4	9.45	1.42	32.76	-115.784	2	30.5	2.27±0.13	2.5±0.2	2.96±0.23	1.64±0.63	1.41±3.17	1.25±0.14	0.3
DUN-3	90-125	1.48	44.6	7.25	1.60	32.76	-115.784			2.28±0.14						
		1.52	48.8	3.89	1.24	32.76	-115.784	1	30.5	2.02±0.13	2.61±0.14	2.52±0.32	1.28±0.20	1.26±0.23	1.25±0.23	0.3
		1.42	49.8	5.14	1.42	32.76	-115.784	1	30.5	2.06±0.13						
DUN-3	125-180	1.52	48.8	3.89	1.24	32.76	-115.784	1	30.5	2.02±0.13	1.55±0.39	0.96±0.07	0.73±0.12	0.69±0.17	0.68±0.12	0.3
XDUN3		1.42	49.8	5.14	1.42	32.76	-115.784	1	30.5	2.06±0.13						
KS-4	125-180	1.38	36.3	4.09	0.57	33.1	-115.844	-31	33	1.76±0.12	0.87±0.32	0.34±0.03	0.29±0.06	0.28±0.04	0.28±0.04	0.28

[a] Elemental concentrations from NAA of whole sediment measured at USGS Nuclear Reactor in Denver. Uncertainty taken as ±10%.
[b] Estimated contribution to dose-rate from cosmic rays calculated according to Prescott and Hutton (1994). Uncertainty taken as ±10%. Estimated fractional water content from whole sediment is 5±5%. Total dose-rate from beta, gamma and cosmic components. Beta attenuation factors for U, Th and K compositions incorporating grain size factors from Mejdahl (1979). Beta attenuation factor for Rb arbitrarily taken as 0.75 (cf. Adamiec and Aitken, 1998). Factors utilized to convert elemental concentrations to beta and gamma dose-rates from Adamiec and Aitken (1998) and beta and gamma components attenuated for moisture content.

Road Log

Day 1 November 14th (Friday): Clark fault

Muster at 7:30 am. We will line up along the camp road and head east.

Stop 1. Rockhouse Canyon

Turn **left** (north) on **Yaqui Pass Road** (S3) and proceed for about **6.7** miles to **Borrego Springs Road** - turn **left** (which is to the west at this point) and proceed **5.4** miles (road will bend to the north) to the *circle at Borrego Springs* and turn **right** (to the east) onto **Palm Canyon Drive**. Proceed east past the airport (which is at about 3 miles) and continue for about **7.5** miles to **Rockhouse Trail** (just past the nose of Coyote Ridge). Turn **left** onto **Rockhouse Trail**. From here the road is *unpaved*.

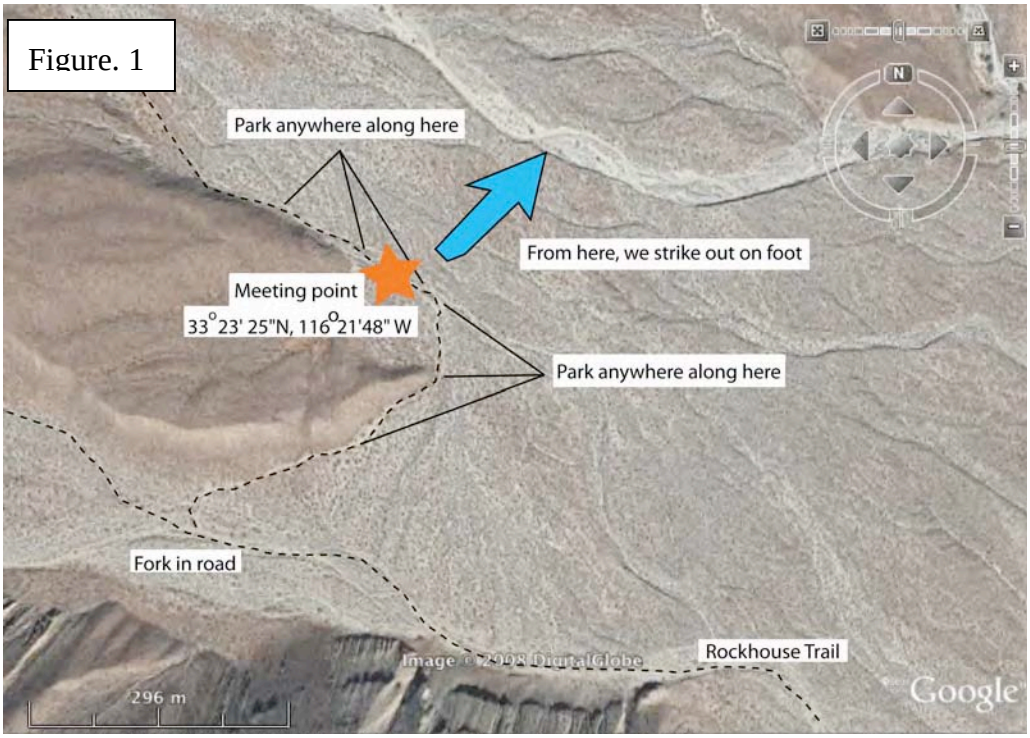

Figure. 1

DO NOT GET STUCK IN THE SAND!

Drive for about **1.5** miles until the road forks and keep left on Rockhouse Trail **(Figure 1).** At another **~2.1** miles, the road bends sharply to the right near the entrance to a small quarry. Continue on Rockhouse Trail (to the right). In another 3.05 miles, the road essentially enters a wash bottom. Continue on Rockhouse Trail for another **~2.7** miles up the wash to a fork in the road near the entrance to a canyon (on your left-straight). You will turn **right** here and go around the nose of the hill about **0.4** miles and park for the long hike. At this point, you are at about 9.75 miles from pavement.

You must park off of the road (i.e., other off-roaders need to have passage). This means that you may end up parking somewhere near the nose of the hill. We will set out on foot from here. See the map detail - the GPS coordinate for the orange star is: **33° 23' 25"N, 116° 21'48" W**. If you have 4WD, take the tougher spots to park - let the 2-wheelers have the hard ground.

The hike is about 4.5 miles overall as the crow flies (see **figure 2**), but there will be elevation change. Plus, there is no trail, so the actual hike will likely be 5-6 miles. We start at ~380 m elevation and will climb to ~650 m elevation (that's ~900 feet of total elevation change, both ways). We will have lunch on the fault, so bring all the food and water you need for the next few hours.

On this trek, we will examine two channels that have been beheaded by the Clark fault. Within the channels are debris flow boulder deposits that we dated with ^{10}Be dating (see Le et al. in prep. guidebook article) to resolve slip rates over two periods of time. We will discuss problems with inheritance of ^{10}Be concentrations, look at fault geomorphology, discuss stream capture models and uncertainties on our estimates of displacement. This is just a spectacular section of the Clark fault!

We will plan to spend as much as 5 hours for this hike, as needed.

Upon returning to the vehicles, turn around and head back to the highway and wait for the lead vehicle. We will proceed east on for about 7.5 miles and park on the side of the highway in a large pull-out area **(Figure**

Figure. 2

3). From here, we will proceed on foot for our second (shorter) hike to the fault - **STOP 2**.

Stop 2. Southern Santa Rosa Mountains
GPS 33° 17' 28.88"N, 116° 10'16.47" W

From the car, we will walk towards the southern Santa Rosa Mountains and across a Holocene alluvial fan surface with well-preserved bar and swale topography. Two sets of Pleistocene alluvial fan deposits are exposed at this location, Qg and Q2b. The oldest deposit, Qg, is an erosional remnant that appears as high rounded mound-like outcrop. These deposits consist of variably weathered pebbles to boulders exposed on a coarse pebbly sand matrix. The Q2b alluvial fan, exposed just northwest of Smoke Tree Canyon, is inset into the Qg deposits. Q2b fans are characterized by relatively smooth to slightly undulating surface morphology. Q2b fan surfaces exhibit strong desert pavement and varnish development, moderate to strong rubification of surface clasts, and very subdued remnant bar and swale microtopograghy.

Starting at the northwestern end of the fault, multiple fault strands horizontally and vertically offset the Q2b surface into a positive flower structure. The Clark fault continues to the south as a single strand. Post Q2b displacement of 51 ± 5 m along the Clark fault is constrained by two deflected channels and at least one beheaded channel. A cosmogenic depth profile was

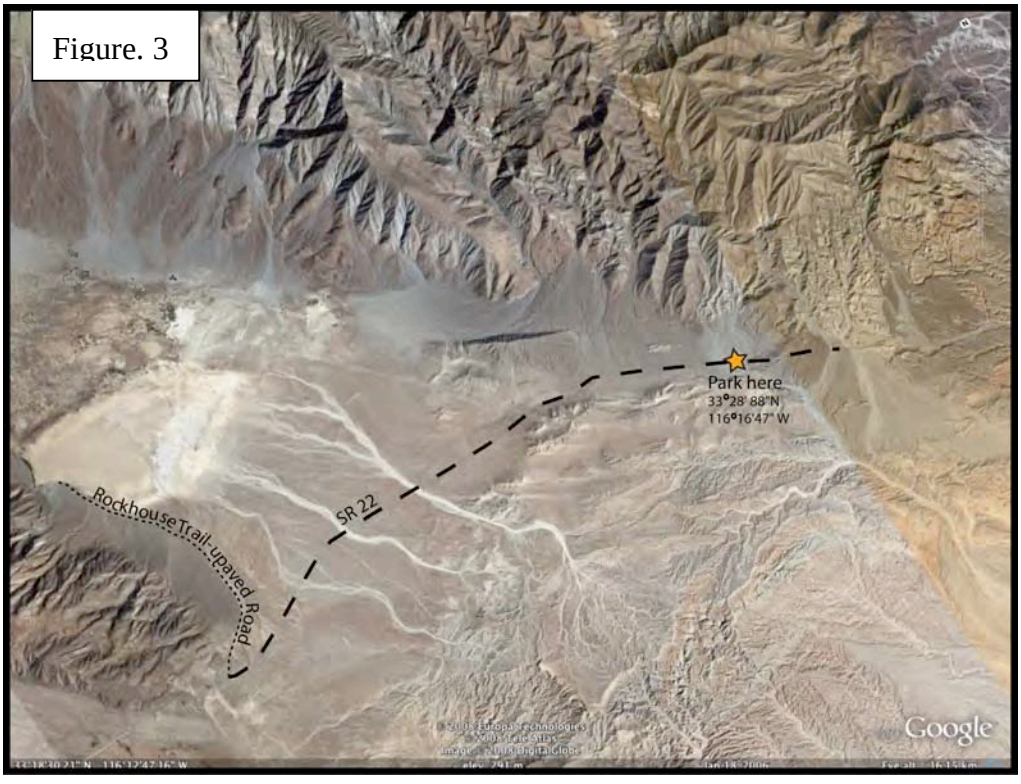

Figure. 3

collected from a natural exposure of the Q2b deposit (see Le et al., in prep). This yielded a surface exposure age of 35 ± 7 ka. If we assume no erosion of the surface, this yields a slip rate of 1.5 ± 0.3 mm/yr. Erosion of the surface would make the age older, resulting in a slower slip rate. Please see Le et al., in prep in the field book for more details.

Day 2 - Saturday, November 15th. Age of the San Jacinto Fault, Basin History, Long-Term Slip. Rate See Fig. 4 for general location of stops.

Stop 1: Borrego Springs Airport (33° 15.447' N, 116° 19.532' W)(see road directions from Day 1). **Overview and introduction**. (NOTE: we may drive a short north on a dirt road located about 0.4 mi. west of the airport, in order to get a better

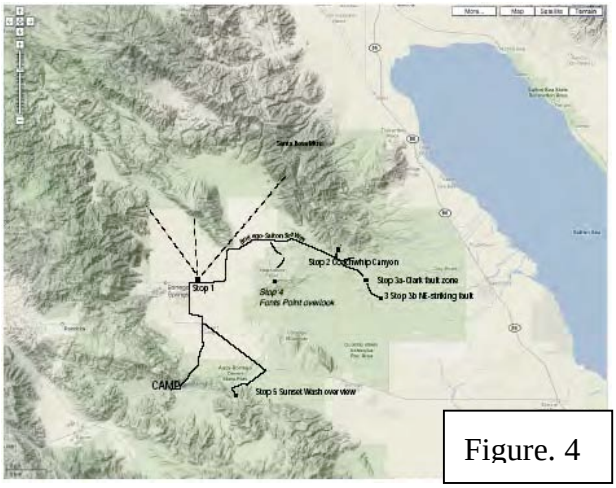

Figure. 4

view). From here we can see the SW edge of Coyote Mountain and the SW side of the Santa Rosa Mountains (see photos in the guidebook). Figure 5 shows the points of interest on the north

Figure. 5

edge of San Isidro Mountains (likely not in view), SW edge of Coyote Mountain (CM) and the SW part of the Santa Rosa Mountains. Look for the white marble-rich intervals between the biotite and hornblende-bearing tonalite to the west and the dark weathering biotite-rich migmatite to the east (figs 5 and 6). These units correlate across the fault zones. Table 2 (in Janecke et al guidebook article) shows the displacement estimates from this analysis as well as the lifetime slip rates. (See Figures 1 to 10 and Appendix figure 1, 2 of the associated guidebook articles.)

Figure. 6

Drive NE from stop 1 along the Borrego-Salton Seaway highway toward Salton City. About 8.5 miles from the airport is Lute Ridge to the north. This prominent hill has an escarpment on its far, NE side that coincides with the main trace of the Clark fault. Numerous smaller scarps displacement the pediment that lies in angular unconformity on folded older Quaternary conglomerate. Figure 10 in the associated guidebook article shows a new interpretation of the uplift in Lute Ridge and the folding in low hills a few kilometers to the NW. We interpret this area as preserving extensional and contractional steps between subparallel strands of the dextral Clark fault zone. See Belgarde (2007) for details.

Continue driving east to the turn-off into Coachwhip Canyon on the left/north side of the road. The turn off is not all that well marked. Drive about 0.5 miles to stop 2.

STOP 2. STOP 2: Coachwhip Canyon (33° 17.428' N, 116° 8.949' W). Figure A3, A4 and A5. Figure 9, 10, 12, 13. Park and examine the multiple strands of the Clark fault that parallel bedding in pebbly sandstone of the fine Canebrake and coarse Olla formations. The beds dip south and the faults do too. Microseismicity shows that at least one strand of the Clark fault about 0.5 km farther up the canyon dips steeply to the SE at depth (Fig. 17)(Belgarde, 2007). This requires a bend in the fault plane and reversal of the dip direction.

Notice the well-developed clay gouge in excellent exposures of the fault. Other parts of the fault have almost no gouge and could be mistaken for intact bedding planes, particularly in areas of typical exposure. This exposure of the fault is along strike of a scarp in late Pleistocene pediment deposits. Refer to figures 5, 6, 11, 12 and 13. OSL ages range from 21.72 ± 1.19 to 62.26 ± 4.05 ka in these pediment deposits (Rittenhour, Janecke and Belgarde, unpublished).

Coachwhip Canyon illustrates the character of the Clark fault zone in moderately well-lithified units like the Canebrake Formation. Faults dominate in these settings. Where mud becomes a major constituent, folding becomes much more common in the fault zone and the Clark fault broadens (Fig. 15). The Clark fault zone is up to 18 km wide in map view in the Arroyo Salada and Tarantula Wash segments (Belgarde, 2007) (Fig. 13).

Exit Coachwhip Canyon. Drive east on the paved highway to the turn-around and pull-out at 33° 17.044'N 116° 7.788'W. This is about 1.5 miles to the east. The scarp that coincides with the fault exposed at stop 2 is located about 2/3 of the way from Coachwhip Canyon to the turn around. On the way to the turn-around notice the numerous SW-facing fault scarps on the pediment surface. Each of these scarps is along strike of a bedding parallel fault strand of the Clark fault zone in Coachwhip Canyon. We dated this pediment deposit in an exposure about 1 km SSE of the turn around. From the turn-around it is about 1 km SSE to the location of a dated portion of this pediment surface. A fine-grained sand-bearing bed near the base of the pediment deposit produced a late Pleistocene OSL age of 30.71 ±2.34 ka OSL age (Rittenhour, Belgarde, and Janecke, unpublished data).

Turn around and drive back to Arroyo Salada. Turn south opposite Coachwhip Canyon and drive ESE down Arroyo Salada, past the primitive campground, for about 3.5 miles. Two wheel drive is adequate unless it has rained.

Stop 3a: Clark fault zone in Arroyo Salada (33° 15.363' N, 116° 6.559' W). A wide steep fault zone is exposed in the west wall of Arroyo Salada (Belgarde, 2007). This is one of the main strands of the Clark fault zone in the Arroyo Salada segment. Note how the main fault planes parallel bedding planes and are very thin. Prior to a fortuitous rock fall, this fault zone looked like it was intact stratigraphic section. Slickenlines range in direction and include an important population of strike-slip slickenlines. If stop 3a is poorly exposed due to weathering, continue SE to stop 3b. This stop further illustrates the hidden faulting in the sedimentary units. This fault was mapped as a minor thrust fault by Jarg Pettinga but the horizontal slickenlines show that it is instead a major central strand of the Clark fault zone. At least half a dozen similar strands parallel this one, and there is significant deformation dispersed across a region ~18 km wide perpendicular to the fault zone at this spot (Figs. 10, 11, 12, 14,16).

Stop 3b: alternate to stop 3a (33° 14.305' N, 116° 5.804' W). If stop 3a has been covered over by gully wash or we are running ahead of time, continue to stop 3b another 1.7 to 2 miles to the SSE. Drive SE past the turn-off to 17 Palms and turn right into a narrow track leading to Tule Wash. Whenever the road splits turn left or follow any signs to Tule Wash, and drive to the fault exposed at stop 3b. This smaller fault has a NE strike and is a left-oblique strike-slip fault. It is exciting because it is one of a large population of NE– to E-striking left-oblique faults that dominate the SW 40% of the Clark fault's damage zone in the Arroyo Salada and Tarantula Wash fault segment (Fig. 12). The deep structure beneath these left-oblique faults is completely different, however, and consists of a 6-13 km deep planar fault, which is called the Tule Wash fault (Belgarde, 2007)(Fig. 17 and 18). The Tule Wash fault dips steeply NE and passes beneath the shallow and subvertical NE-striking faults exposed at the surface. A decollement surface must separate the incompatible structures at the shallow and deep levels. We envision a left-oblique fault array on an "overpass" and a steeply NE-dipping dextral fault on an "underpass" (Janecke and Belgarde, 2007, 2008)(Figs. 12, 17, 18). Decollements and pitchfork fault structures, like those modeled by Le Guerroué and Cobbold in Figure 19 E, may facilitate this behavior.

Crossing strike-slip faults also interfere with one another at the same structural level in other parts of

the field area (Fig. 11). Mutual interference and mutual bending developed in these situations.

Turn around and return to pavement. Drive west on the Borrego-Salton Seaway Highway for about 5.5 miles. Turn SW (left) into Fonts Wash and follow the signs and track up to Fonts Point in the south.

Stop 4: Fonts Point (33° 15.454' N, 116° 13.958' W). The view looking south from Fonts Point provides a breath-taking vista of the Borrego and Ocotillo formations exposed in the southern Borrego Badlands, as well as other features including Borrego Mountain which is cut by strands of the Coyote Creek fault, the complexly faulted eastern of the Peninsular Ranges, and low-lying sedimentary rocks of the western Salton Trough. Here we are standing at the top of a precipitous erosional escarpment that is currently retreating to the north as a result of ongoing uplift and erosion in the Borrego Badlands. Figure A11.

The Ocotillo Formation is exposed beneath and east of Fonts Point in the erosional escarpment. Using magnetostratigraphy calibrated with the 0.76-Ma Bishop Ash, the sharp base of the Ocotillo Formation was dated at 1.05 ± 0.03 Ma (Lutz, 2005; Lutz et al., 2006). This contact records abrupt expansion of alluvial-fan and fluvial systems that prograded rapidly into and across the former Borrego lake depocenter at this time. Paleocurrent data show that coarse sediment entered the basin from multiple newly emergent sources located south and SW (Vallecito Mts.), west and NW (San Ysidro Mts.), north (Coyote Mt.), and NE (southern Santa Rosa Mts.) of the Borrego Badlands depocenter (Lutz et al., 2006). A systematic up-section increase in C-suite sandstone clasts recycled from the Arroyo Diablo Formation provides evidence for uplift and exhumation of the former hangingwall basin of the WSDF (ibid). Isopach and facies patterns record syn-basinal titling to the NE in response to growth of the San Felipe anticline and oblique slip on the Clark fault (ibid). Based on this and companion studies by Kirby et al. (2007) and Steely et al. (in press), we conclude that rapid progradation of the Ocotillo and Brawley formations across the western Salton Trough was driven by a dramatic increase in sediment flux from the eastern Peninsular Ranges at ~1.1 Ma. This marks a major, tectonically controlled basin reorganization that resulted from initiation of the San Jacinto and San Felipe fault zones and related onset of uplift and erosion in the former hangingwall of the Late Cenozoic West Salton detachment fault.

The Fonts Point Sandstone (FPS) is a thin, well-cemented, widespread sandstone characterized by a stripped calcic paleosol with deep calcite-filled fissures, which in this area rests on the Ocotillo Formation. Lutz et al. (2006) inferred that deposition of the FPS began at ~0.60 ± .02 Ma based on: (1) presence of the 740-ka Thermal Canyon ash in the upper Ocotillo Formation, 49 m below the contact with the FPS; (2) a likely range of sediment-accumulation rates based on correlation to the nearby, well dated Beckman Wash section; and (3) detailed mapping and visual inspection of the contact which indicate that the Ocotillo-FPS contact in this area (from Fonts Point to Inspiration Point) is concordant and conformable. Subsequent mapping by Dorsey around Inspiration Point supports this interpretation. Farther to the north and south, the base of the FPS is clearly an angular unconformity that truncates early folds and faults in the western Borrego Badlands. Our preferred age for the FPS is not 100% confident and deserves to be further tested. Recent dating of nearby Quaternary terraces and pediment deposits using cosmogenic isotopes (Le et al, this volume) and OSL (T. Rittenour, Janecke and Belgarde) reveals that many terrace deposits that superficially resemble the mesa-capping FPS have much younger ages ranging from about 20 to 60 Ka. Although the deep, stripped nature of calcic paleosols in the FPS suggests that it probably is much older than most of the Late Quaternary pediment deposits, we cannot be certain there was no break between deposition of the uppermost Ocotillo Formation and the basal FPS, even where the contact is concordant and appears conformable. New data are needed to resolve existing uncertainty in the age of the FPS and the depositional - deformational events that it brackets.

Return to pavement and drive past Borrego Springs to the Yaqui Narrows area. Turn east into Nude Wash north of the Narrows. Park where the wash is no longer drivable and hike SW along the wash for about 0.3 miles. Admire the exceptional exposures of pseudotachylyte and fault rocks

(Kairouz, 2005, Steely, 2006; Janecke et al. (2008)) on the way to an overlook at Stop 5.

Stop 5: Overview of San Felipe fault zone (33° 7.962' N, 116° 17.264' W). This stop (which is based on Steely, 2006 and Steely et al., in press) illustrates the typical relationship between Pleistocene to Recent strike slip faults and Ocotillo Formation. We are located within a double contractional stepover of the San Felipe fault zone. This relatively unknown dextral strike slip fault reaches from the NW Elsinore fault to the SE part of the San Jacinto fault zone. It is about 60 km long from end to end. In the Yaqui Ridge area there is a cross-cutting relationships between the San Felipe fault zone and the older West Salton detachment fault, as well as syntectonic deposits shed from the nascent San Felipe fault zone. Structurally, the San Felipe fault zone steps left from the large fault on the N side of the Fish Creek Mountains and Vallecito Mountains (the Fish Creek Mountains fault) to the San Felipe fault. The San Felipe fault is south of here under San Felipe Wash and at the base of Yaqui Ridge. A small fault called the Sunset fault is parallel to these two larger structures and lies a couple hundred meters NE of our stop. Slip steps from the Fish Creek Mountains fault to the Sunset fault and then SW to the San Felipe fault. A thick section of folded and faulted conglomerate is north of the Sunset fault, whereas the folded West Salton detachment, mylonite and other crystalline rocks lie south of the Sunset fault. See Steely et al. (in press) for an overly long structural discussion of this stepover.

Our purpose today is to illustrate the stratigraphic and sedimentary record of initial slip in the San Felipe fault zone. The conglomerates that we can see from here, on the NE side of Sunset Wash, were correlated to the Pliocene Canebrake Conglomerate by Dibblee (1954). Detailed mapping and analysis by Steely et al. (in press) shows that this conglomerate correlates instead to the early to middle Pleistocene Ocotillo Formation. The Canebrake is derived from the footwall of the West Salton detachment fault (Axen and Fletcher, 1998; Kairouz, 2005; Steely, 2006). The conglomerate along Sunset Wash does not contain a single clast of mylonite derived from the footwall of the detachment fault, despite being located as little a 300 m NE of the detachment fault. Its provenance was exclusively in the hanging wall of the detachment fault and most of the sediment was shed from displaced and uplifted plutonic rocks immediately SW of the Sunset fault (See figures in Steely et al., in press). Paleocurrents show dispersal to the NE, grain size decreases in that direction, and the composition and grain size are perfectly concordant with those in the Ocotillo formation nearby. Boulders up to 4 m across near the Sunset fault attest to active tectonism within the San Felipe fault zone and across the Sunset fault during deposition of the conglomerate. An angular unconformity, missing units beneath the Ocotillo Formation about a km SE of here, and the presence of recycled sandstone clasts derived from the Pliocene Arroyo Diablo Formation further support our interpretation.

Very similar relationships exist adjacent to the San Jacinto fault zone, and show that the Ocotillo formation, and its finer lateral equivalent, the Brawley Formation, were deposited in a new sedimentary basin ringed by brand new dextral oblique strike slip faults. The Ocotillo formation thickens by a factor of ~2 NE toward the Clark fault from a condensed section near Font's Point (Stop 4)(Lutz et al., 2007). The Ocotillo Formation coarsens in that direction and contains distinctive clasts shed from the NE side of the Clark fault. Paleocurrents indicate southward flow. Westward thickening and coarsening, and eastward paleocurrent show that the East Coyote Mountain fault was an active structure within the San Jacinto fault zone starting about 1.05 Ma (Lutz et al., 2006). A disconformity and angular unconformity separate the Ocotillo and Brawley formation from the underlying basin fill, and mark the change from syndetachment to syn-strike slip deposition.

Concluding remarks: Many lines of evidence now show that the San Felipe and San Jacinto fault zone are early Pleistocene dextral faults with high lifetime slip rates. Refined and new displacement estimates, combined with magnetostratigraphic dating of the Borrego/Ocotillo contact are the main constraint on this. In addition, the San Jacinto fault zone is far more complex and broad than generally thought. This is especially true where the fault deforms mud-rich sedimentary rocks but dispersed faults are also developed in the crystalline damage zone adjacent to the central part of the fault zone.

We believe that this dispersed deformation partly explains the lower slip rates determined in neotectonic studies (e.g. Le et al., this volume) when compared to slip rates inverted from GPS data and calculated using offset bedrock features (Fig. 8, tables 1 and 2)(Janecke et al., in prep.).
Very similar relationships exist adjacent to the San Jacinto fault zone, and show that the Ocotillo formation, and its finer lateral equivalent, the

Day 3 - November 16th (Sunday) Paleo-erosion rates, Elsinore fault, Lake Cahuilla

Today we head south to the Fish Creek Badlands, the Coyote Mountains, and end near Interstate 8.

From camp, head west on highway **78** about **7.5 miles** to Scissors crossing and turn **left** (south) on highway **S2**. Drive south for **~26** miles to Canebrake. You will drive through Earthquake Valley (renamed Shalter Valley by developers) along the Old (Great southern) Overland Stage Road (S2). Drive past Blair Valley and the Mormon Battalion monument in Box Canyon, through Mason Valley (look to your left - the Elsinore fault is clearly visible as scarps and channel deflections), down through Vallecito Valley, past the Tierra Blanca Mountains, and cross Carrizo Wash (the Elsinore fault is just to your left at this point). We will turn off the highway and head northeast through Badlands Wash to stop 1 **(Figure 7).**

Stop 1. Fish Creek-Vallecito Basin
We will turn **left** off the highway onto a **dirt road (Figure 7)**. The road is **Old Vallecito Overland Stage Creek Route**, there may or may not be a sign. From the road, you will drive ~ **0.5** miles, until you reach the intersection with **View of the Badlands Rd (another dirt road).** Drive for approximately **~0.5** miles and park along the road. The outcrop is **1.0** miles from the intersection of the two dirt roads. We will have a short hike to STOP 1 to view the Upper Hueso Formation.

At Stop 1, we will discuss the extraction of paleo-erosion rates from the sedimentary rocks deposited in Fish Creek-Vallecito Basin. We integrate stratigraphy, paleomagnetic data, and detrital ^{10}Be concentrations to extract an archive of paleo-erosion rates from 3 Ma to present. Please see field book for details.

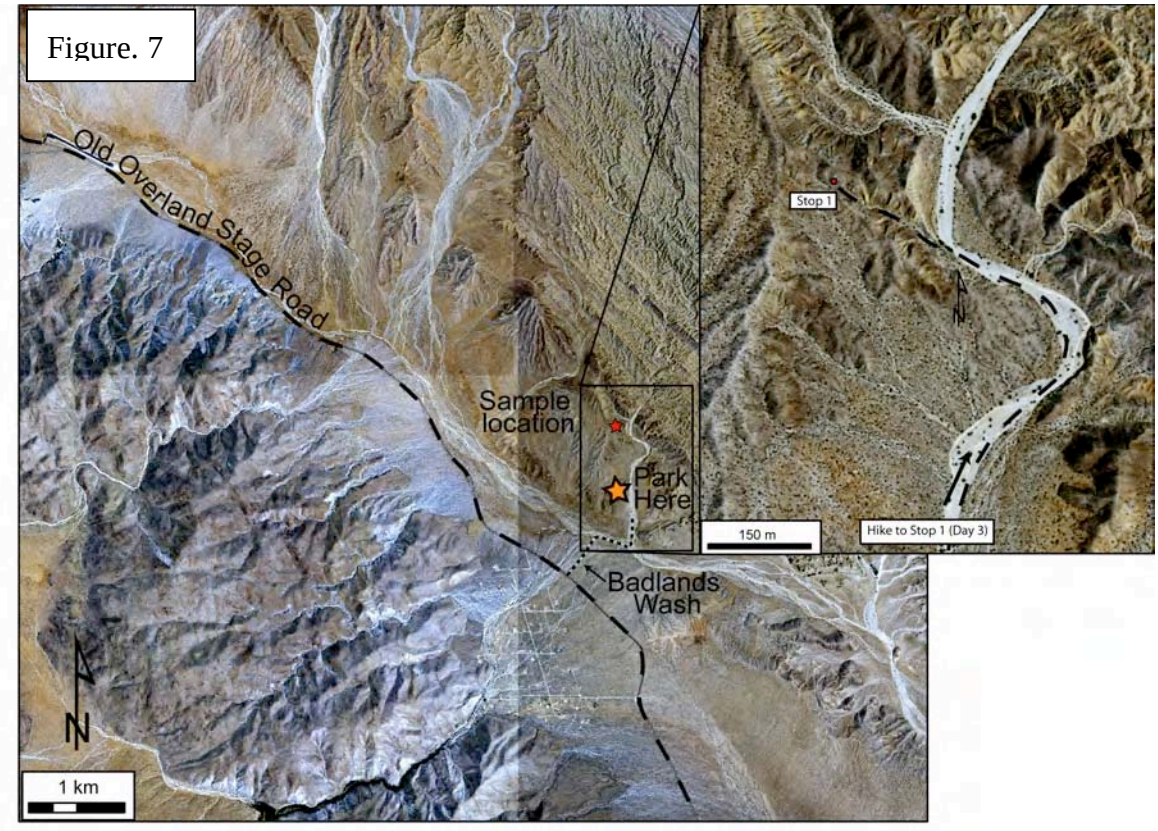

From stop 1, head back up to highway S2 and continue south on S2 along the Coyote Mountains (to your left) for about **12** miles to Fossil Canyon Road at the stop sign. Turn left and head up towards the Coyote Mountains. The pave road makes several bends and crosses the fault - we will turn off the paved road to head towards Fossil Canyon just before the road heads into the quarry, about **2.2** miles from highway S2 (so we essentially go straight onto the dirt). From here, we continue on dirt for about **0.8** miles and park ALONG the road before it enters the gorge into Fossil Canyon. From here we strike out on foot to **STOP 2**.

STOP 2: Elsinore fault

We will walk about 1-1.5 miles total. The first stop is just a few hundred yards from where we park.

Here we will examine evidence for late Holocene displacement along the Elsinore fault for about 1.5 m of displacement in the most recent event. We will also see several ~5 m displacements that are interpreted as the result of three events. Then, we will look at soil pits dug into late Pleistocene deposits that are offset about 80 m, and from which we collected CRN samples and U-series samples. Here we debate the various geochronologic methods, their results, and their implications for slip rate determinations. See Fletcher et al. (this volume) for a complete discussion of the data and age comparisons. We will walk to other displaced deposits that we dated with U-series and discuss the local slip rate variations that appear to have occurred during the late Pleistocene.

After lunch, we head to our final stop of the fieldtrip. Return to pavement and back to highway S2. Turn left at the 4-way stop sign onto highway S2 and proceed 1.3 miles through the town of Ocotillo to old highway 80 (Evan Hewes Highway), immediately before the interstate 8. Turn left on old highway 80 and proceed about 11 miles through Plaster City to the late Holocene shoreline of Lake Cahuilla.

STOP 3: Lake Cahuilla Shoreline

Here we will discuss the Holocene history of the lake and OSL dating of shoreline berm deposits. See Lippincott et al. (this guidebook) for a discussion of this technique as applied to Lake Cahuilla deposits.

This ends the official part of the field trip. If there is still time, we will head back through Plaster City and examine some Pleistocene beach deposits of "Lake Cahuilla" - these are essentially the shoreline deposits for the upper Brawley Formation sediments.